Determination of agonist intrinsic efficacies at the dopamine D2 receptor

Lisa Alice Stott, BSc.

Thesis submitted to the University of Nottingham for the degree of Doctor of Philosophy

August 2016

Abstract

G protein coupled receptor agonists can be described by two parameters; affinity (ability to bind a receptor) and efficacy (ability to activate a receptor once bound). While affinity is now an accessible parameter through binding studies, agonist efficacies have historically been difficult to determine. This is due to the significant system dependence of agonist responses and is particularly true of traditional maximal response and potency measurements.

The Black and Leff operational model determines agonist affinity and efficacy estimations directly from functional data. Its measure of efficacy (τ) offers improvement over maximal response determinations but remains a system dependent parameter. More recently, the Slack and Hall operational model has been described. This model uses receptor constitutive activity to estimate the system contribution to agonist responses to derive system independent measures of intrinsic agonist efficacy. This thesis explores the use of operational models in the analysis of agonist functional responses at the dopamine D2 receptor. This receptor is an important therapeutic target in the treatment of schizophrenia and Parkinson's disease, and has well documented receptor constitutive activity.

Maximal responses and potencies in two representative functional assays, CRE-SPAP reporter gene and receptor internalisation, were determined for a panel of ligands at the D2L receptor. In the receptor internalisation assay, agonist maximal responses and potencies were decreased, consistent with an assay of reduced receptor reserve. Applying the Black and Leff operational model to the responses of four representative agonists, in the absence and presence of the irreversible antagonist phenoxybenzamine, yielded affinity and efficacy estimations consistent with the known pharmacology of the compounds. However, experiments did not provide evidence for the receptor constitutive activity necessary to apply the Slack and Hall operational model.

As such, site-directed mutagenesis was performed to generate a constitutively active D2L receptor. T6.34R mutation increased agonist potencies and relative

maximal responses consistent with a receptor more likely to adopt the active state; however, potencies of the ergo-derived compounds were selectively decreased. Mutagenesis of three key binding site serine residues examined the mode of agonist binding in both wild type (WT) and T6.34R backgrounds. Each serine mutation had differential effects on the responses of structurally distinct agonists, suggesting agonists engage specific serine residues; while S5.42 and S5.46 were required for catechol agonist responses, S5.46 was essential for the responses of the ergo-derived compounds, bromocriptine and dihydroergocristine. It was unknown whether these specific modes of binding would generate functionally similar active conformations. Generally, the differences between the effects on CRE-SPAP reporter gene and receptor internalisation assay responses were sufficiently explained by differences in receptor reserve. However, there were differential effects of serine mutations on WT and T6.34R D2L receptors, particularly the opposing effect of S5.42A on quinpirole potencies in the CRE-SPAP reporter gene assay. This suggests that WT and T6.34R D2L receptors adopt different conformations.

Finally, we have described a method to determine agonist affinity and efficacy from [^{35}S]-GTPγS binding assays using operational models, which does not rely on irreversible antagonist treatments. Buffer Na^+ substitution revealed consistent constitutive activation of the D2S receptor, but not of the D2L or D2L T6.34R receptors. Agonist responses at the D2S receptor, in the presence and absence of buffer Na^+, were analysed with the Black and Leff and Slack and Hall operational models respectively, generating agonist affinity and efficacy estimations. A novel operational model, written specifically for the analysis of [^{35}S]-GTPγS binding assays, was also examined. This model provided similar affinity derivations to the Black and Leff operational model but provided a τ value that may have reduced system dependency. Although there may be compromises in the associated experimental conditions and which receptors can be investigated, the Slack and Hall operational model can be applied to constitutively active systems to provide system independent measures of agonist intrinsic efficacy.

Acknowledgements

First and foremost, I would like to send the biggest thanks to my supervisors, Dr Nicholas Holliday, Dr David Hall and Professor Steve Hill for all their guidance and support these past 4 years (and apologise profusely for leaving it so late to get those last chapters to you!) Special thanks to Nick, who has borne the brunt of my whinging (and my refusal to start writing and leave the lab) but has always had an open door whenever I needed help or advice. Thank you for everything, especially your trust in letting me supervise students and all of your encouragement to present at both national and international conferences, all of which have been invaluable experiences. I would also like to thank the BBSRC and GSK for funding my studentship.

I also want to say a massive thank you to everyone in the Cell Signalling Research Group in Nottingham for making the last 4 years an incredible, cake, laughter, Sporcle and Game of Thrones theories filled experience. It's been like being part of an amazing, if slightly dysfunctional, family; you all make coming to work a pleasure every day and I will miss you all greatly. Special mentions and thanks first to Dr Laura Kilpatrick, for showing me the ways of the Holliday lab when I first started and for always being there when I needed to chat about anything from a dodgy experiment to why Wesley is the best character of the Whedon-verse. I also want to thank Dr Leigh Stoddart, surrogate supervisor to all us PhD students, for always being around to help with any question great or small (when not away having beautiful babies). A massive thank you to Penny Ensor for letting me use her D2S cell line without which my modelling chapter would not have been possible, and for being my dopamine buddy these past few years. To my fellow final year student Joanne Carter, for giving me some of the weirdest conversations I have ever had but for always being there for support throughout this whole process. To Nicola Dijon, for being an amazing student and helping me make and profile the serine mutants. To David Sykes, for teaching me how to use the 96-well harvester and for all the interesting D2-related conversations. To Seema Rajani, for all her help with the Ultra and not getting fed up with me asking

her to restart the analysis PC every other week. To Richard Proudman, for all his help with sorting out the radiation work and finally, to Marleen Groenen and June McCulloch for keeping the lab and tissue culture cleaned and well stocked.

I would also like to thank Phillip Hardwicke, Nisha Bhudia and Dr Robert Slack for all their help during my placement at GSK.

Lastly, I want to thank my family for all of their support. To my mum, Linda Stott, for all her encouragement over the years, despite not having a clue what I was talking about and an initial “aren’t there any PhDs in Dundee?” To my partner, Ronan Muir, without whom I would have seriously struggled to get through this process at times. Your support and belief kept me strong despite my mild/mad “I’m running out of weeks to finish this thing” panic. Having both of us writing up at the same time has been a bit of a nightmare at times but we’ve made it through!

Finally, I would like to dedicate my thesis to my granda, Lewis Stott, who passed away at the end of my first year in Nottingham. You were always so proud of me and it’s one of my biggest regrets that you will not be here to see me graduate.

Nicola Dijon contributed replicates to the CRE-SPAP reporter gene and receptor internalisation data for the S5.43A and S5.43A T6.34R cell lines in **Figure 4.14**, **Figure 4.18** and **Figure 4.19**.

Ben Thomson and Catherine Seymour generated the internalisation data for S5.43A cell line in **Figure 4.17** and **Figure 4.19**.

Abbreviations

(-)-3-PPP	(S)-(−)-3-(3-Hydroxyphenyl)-N-propylpiperidine; preclamol
(+)-3-PPP	R(+)-3-(3-Hydroxyphenyl)-N-propylpiperidine
AC	Adenylyl cyclase
B_{max}	Maximum binding; expression level
BSA	Bovine serum albumin
cAMP	Adenosine-3',5' cyclic monophosphate
CHO	Chinese hamster ovary
CPM	Counts per minute
CRE	cAMP-linked response element
D2L	Dopamine D2 receptor (long isoform)
D2S	Dopamine D2 receptor (short isoform)
DMEM/F12	Dulbecco's Modified Eagle's Medium: Nutrient Mixture F-12
DMSO	Dimethyl sulphoxide
DPM	Disintegrations per minute
EC_{50}	Concentration of ligand which produces 50% of its maximal response; potency
ECL	Extracellular loop
EEDQ	N-Ethoxycarbonyl-2-ethoxy-1,2-dihydroquinoline
E_{max}	Maximum system response
ERK1/2	Extracellular regulated kinase 1 and 2
FCS	Foetal calf serum
GDP	Guanosine 5'-diphosphate
GPCR	G protein coupled receptor
GRK	G protein coupled receptor kinase
GTP	Guanosine 5'-triphosphate
GTPγS	Guanosine 5'-[γ-thio]triphosphate
HBSS	Hepes buffered saline solution
ICL	Intracellular loop
MAPK	Mitogen activated protein kinase
NSB	Non-specific binding

PBS	Phosphate buffered saline
PBz	Phenoxybenzamine
PCR	Polymerase chain reaction
PKA	Protein kinase A
PKC	Protein kinase C
PTx	Pertussis toxin
R_{max}	Maximal ligand response
SFM	Serum free media
SPAP	Secreted placental alkaline phosphatase
TB	Total binding
TM	Transmembrane domain
WT	Wild type
β2AR	β2-adrenoceptor

Chapter One : Introduction **1**

1.1 G Protein Coupled Receptors 1

1.2 Dopamine 4

1.3 Dopamine D2 receptors and disease 7

1.4 GPCR Signalling 13

1.5 'Switching off' GPCR signalling 22

1.6 β-arrestin mediated signalling of GPCRs 26

1.7 Receptor theory 32

1.8 Quantifying ligand parameters from functional data 36

1.9 Aims of the thesis 47

Chapter Two : Materials and Methods **49**

2.1 Materials 49

2.2 Molecular biology 50

2.3 Cell Culture 63

2.4 Generation of new cell lines 65

2.5 Membrane preparation 67

2.6 Binding assays 68

2.7 Functional assays 71

2.8 Data analysis 76

Chapter Three : Estimation of dopamine D2L receptor agonist efficacy in reporter gene and internalisation assays, and use of irreversible antagonists to establish the receptor depletion method for operational modelling **82**

3.1 Introduction 83

3.2 Results 90

3.3 Discussion 123

3.4 Conclusions 138

Chapter Four : Differential roles of transmembrane 5 serine residues in agonist binding to wild type and constitutively active D2L receptors: evidence for multiple activated receptor conformations **139**

4.1 Introduction 140

4.2 Results 150

4.3 Discussion 199

4.4 Conclusions 216

Chapter Five : Exploration of novel operational model approaches to assess dopamine D2 agonist efficacy through [^{35}S]-GTPγS binding assays **217**

5.1 Introduction 218

5.2 Results 228

5.3 Discussion 278

5.4 Conclusions 293

Chapter Six : General Discussion **294**

Chapter Seven : References **302**

Chapter One: Introduction

1.1 G Protein Coupled Receptors

1.1.1 Introduction to GPCRs

G protein coupled receptors (GPCRs) are the largest family of cell surface receptors, with approximately 800 GPCR genes identified in the human genome. They act to relay an extracellular signal to a biological response through ligand-receptor interactions and the activation of a host of intracellular signalling pathways (Bjarnadottir *et al.*, 2006). GPCRs are a major drug target, with a recent analysis finding that 26% of currently clinically available drugs target this receptor superfamily (Garland, 2013). All GPCRs share a common, 7 transmembrane (TM) domain structural motif with the carboxy terminus located intracellularly and the amino terminus extracellularly (**Figure 1.1**). TM domains are connected by intracellular (ICL) and extracellular (ECL) loops and form a cylindrical bundle in the membrane, in an anticlockwise orientation (Lee *et al.*, 2015). GPCRs have been grouped according to sequence homology; the GRAFS system lists 5 distinct families: rhodopsin (also known as class A), secretin (class B), glutamate (class C), adhesion and frizzled/taste2 receptors (Bjarnadottir *et al.*, 2006; Fredriksson *et al.*, 2003).

Class A GPCRs are the largest sub family of GPCRs with almost 700 members, around 40% of which are classed as non-olfactory receptors (Bjarnadottir *et al.*, 2006; Fredriksson *et al.*, 2003). In addition to the usual 7TM domains, class A GPCRs often contain an additional 8th helix as part of the C terminus, which runs parallel to the membrane and is bounded by one or more sites for palmitoylation. Generally, the orthosteric ligand binding site is located in the extracellular half of the TM bundle although exact positions differ between receptors. However some class A GPCRs, such as the glycoprotein hormone receptors, have large extracellular domains which form the ligand binding site

(Lee *et al.*, 2015). Class A GPCRs also contain a number of highly conserved residues and motifs. The most conserved residues are highlighted in **Figure 1.1**; these residues are assigned the number 50 in the numbering scheme of Ballesteros-Weinstein (Ballesteros *et al.*, 1995). Highly conserved motifs include the E/DRY motif which comprises of residues E/D3.49, R3.50 and Y3.51 in TM3 and the NPxxY motif (where x represents any residue) in TM7 (discussed further in **1.4.3**) (Fredriksson *et al.*, 2003; Trzaskowski *et al.*, 2012).

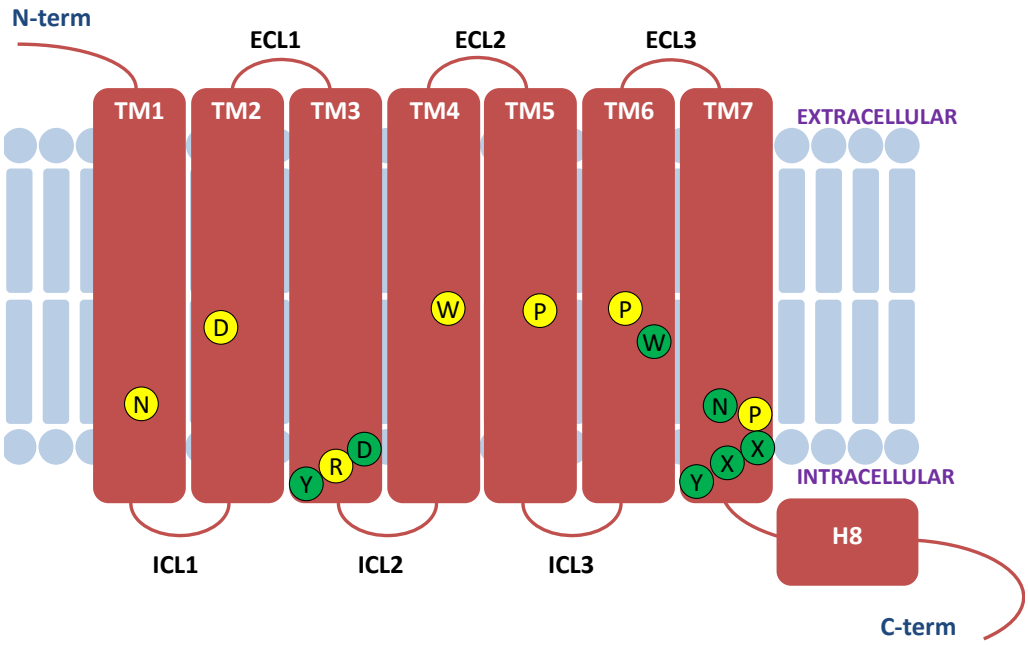


Figure 1.1: General structure of class A GPCRs and approximate location of conserved residues and motifs

The most conserved residues (the reference residue number 50 for Ballesteros-Weinstein numbering) for each TM domain are highlighted in yellow. In green are important motifs and residues in class A GPCRs that are discussed in the text: the E/DRY motif (E/D3.49, R3.50, Y3.51), the toggle switch (W6.48) and the NPxxY motif (N7.49, P7.50, Y7.53).

The class B family is a much smaller group of GPCRs containing 15 receptors, all of which bind peptide endocrine hormones (Bjarnadottir *et al.*, 2006; Fredriksson *et al.*, 2003). These GPCRs are characterised by an N terminal extracellular domain which forms an α-helix and four β-strands that are stabilised by conserved disulphide bridges. Peptides bind both to this region, which governs peptide selectivity and affinity, and within the TM bundle to activate the receptor (Fredriksson *et al.*, 2003; Lee *et al.*, 2015).

The class C GPCR family traditionally contains 15 GPCRs including metabotropic glutamate, γ-aminobutyric acid (GABA), calcium-sensing and some taste receptors; these receptors are activated by amino acids and ions (Fredriksson *et al.*, 2003). More recently, 7 orphan receptors (which have no known endogenous ligand) were added to this group to bring the total to 22 (Bjarnadóttir *et al.*, 2005). Like class B, class C receptors also have a large extracellular domain; however, this domain is much greater at around 600 amino acids. This two lobed structure, the so-called 'venus flytrap' domain, forms the ligand binding site (Bjarnadóttir *et al.*, 2005).

The adhesion group is a relatively new group which contains 33 GPCRs (Schiöth *et al.*, 2010). These GPCRs are poorly characterised and are mostly orphan receptors although there are reports of ligands identified for GPR56 (Luo *et al.*, 2011) and more recently, GPR126 (Küffer *et al.*, 2016). They are so-called because they contain motifs likely to participate in cell adhesion and are characterised by long and highly variable N termini that are rich in glycosylation sites (Fredriksson *et al.*, 2003; Trzaskowski *et al.*, 2012).

The frizzled/taste2 receptor family also consists of 24 GPCRs; it contains two types of receptors, frizzled and taste2, which have been grouped together due to the presence of consensus sequences not found in any of the other families (Fredriksson *et al.*, 2003). Little is known about the taste2 receptors however, more is understood about frizzled receptors. These receptors bind Wnt glycoproteins and are important in the control of cell fate, proliferation and polarity (Fredriksson *et al.*, 2003).

1.2 Dopamine

1.2.1 Dopamine

Dopamine is a catecholamine neurotransmitter, first discovered almost 60 years ago (Carlsson *et al.*, 1957). In presynaptic dopaminergic neurons, dopamine is synthesised from the amino acid tyrosine to its precursor L-3,4-dihydroxyphenylalanine (L-DOPA) through the action of the enzyme tyrosine hydroxylase. L-DOPA is then converted to dopamine through the action of aromatic acid decarboxylase (also known as DOPA-decarboxylase). It is stored in synaptic vesicles until its release into the synaptic cleft from where it can activate postsynaptic receptors. Dopamine transporters (DAT) reuptake dopamine into presynaptic terminals. Dopamine can be degraded by a number of enzymes including monoamine oxidase (MAO) and catechol-O-methyl transferase (COMT) (**Figure 1.2**) (Miyake *et al.*, 2011). Dopamine release and synthesis is subject to a negative feedback system through presynaptic D2 autoreceptors. Activation of D2 autoreceptors decreases tyrosine hydroxylase phosphorylation, inhibiting its activity and reducing dopamine synthesis (Lindgren *et al.*, 2003).

Dopamine receptors are expressed throughout both the central and peripheral nervous systems. Within the central nervous system, there are four main dopaminergic pathways: the nigrostriatal, mesolimbic, mesocortical and tuberoinfundibular pathways (Beaulieu *et al.*, 2011; Cho *et al.*, 2010a). The nigrostriatal pathway extends from the substantia nigra pars compacta to the striatum and is involved in motor control; loss of dopaminergic signalling in this pathway is implicated in Parkinson's Disease (**1.3.3**). The mesolimbic pathway extends from the ventral tegmental area (VTA) to the nucleus accumbens and is also known as the reward pathway. The mesocortical pathway extends from the VTA to the frontal cortex and is involved in the control of motivation and emotional responses. Together, these pathways are collectively known as the mesolimbocortical pathway; dysregulation of these pathways is associated with the symptoms of schizophrenia (**1.3.1**). The tuberoinfundibular pathway extends from the hypothalamus to the pituitary

and is involved in regulation of prolactin secretion; inhibition of this pathway is implicated in hyperprolactinemia (**1.3.4**) (Cho *et al.*, 2010a). In the periphery, dopamine is involved in the regulation of a number of processes including olfaction and the cardiovascular, immune and renal systems (Beaulieu *et al.*, 2011).

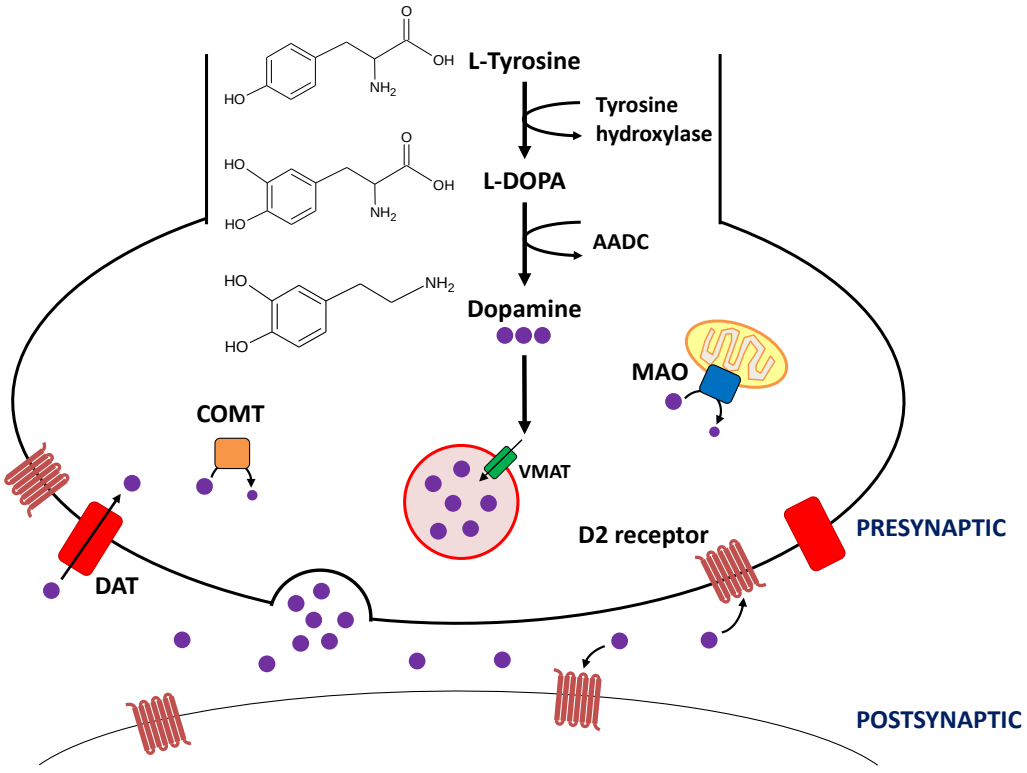


Figure 1.2: Synthesis, transport and degradation of dopamine at synapses
Dopamine is synthesised from L-tyrosine in a two-step reaction; L-tyrosine hydroxylase converts L-tyrosine to L-DOPA, which is then metabolised to dopamine by aromatic acid decarboxylase (AADC). Vesicular monoamine transporters (VMAT) uptake synthesised dopamine into vesicles ready for release. Monoamine oxidase (MAO) and catechol-O-methyl transferase (COMT) degrade dopamine while dopamine transporters (DAT) reuptake synaptic dopamine into the presynaptic terminal.

1.2.2 Dopamine Receptors

Dopamine receptors are members of the class A GPCR family. There are 5 dopamine receptor subtypes that are classed according to their G protein coupling: the D1-like receptors, D1 and D5, couple to $G\alpha_s$ to activate adenylyl cyclase to increase cellular cAMP levels whereas the D2-like receptors, D2, D3 and D4, inhibit adenylyl cyclase and decrease cAMP through activation of $G\alpha_{i/o}$ proteins (discussed further in **1.4.5**). While the D1 and D5 receptors share 80% homology in their TM domains, the D2-like family is less homologous; D2 and D3 receptors share 75% homology while D2 and D4 receptors are only 53% homologous in their TM domains (Beaulieu *et al.*, 2011).

Of these 5 receptor subtypes, the dopamine D2 receptor is the most widely studied as the main pharmacological target in the treatment of a number of diseases (discussed further in **1.3** below). The D2 receptor gene is located on chromosome 11 at q22-q23 (Cho *et al.*, 2010a). As described above, it couples primarily to inhibitory Gα proteins to decrease cellular cAMP (discussed further in **1.4**). Additionally, following receptor activation, Gβγ subunits can couple to ion channels to modulate neuronal activity; activation of the dopamine D2 receptor regulates the activity of both L- and N-type calcium channels to control intracellular calcium concentration. Furthermore, Gβγ subunits can also couple to G protein coupled inwardly rectifying potassium channels (GIRKs). Activation of the D2 receptor activates GIRKs to inhibit neuronal activity (Beaulieu *et al.*, 2011).

The D2 receptor exists in two splice variants, long (D2L) and short (D2S), which differ due to the deletion of twenty nine amino acids in ICL3 of the D2S receptor generated by alternative splicing (Giros *et al.*, 1989; Grandy *et al.*, 1989; Monsma *et al.*, 1989). It has been suggested that D2S is located presynaptically whereas D2L is located postsynaptically (Lindgren *et al.*, 2003; Usiello *et al.*, 2000). However, recent studies with virus mediated expression of D2L and D2S receptors in D2 receptor knockout mice have found little

difference in the ability of either isoform to restore presynaptic functions (Neve *et al.*, 2013).

1.3 Dopamine D2 receptors and disease

1.3.1 Schizophrenia

Schizophrenia is a complex psychiatric disorder characterised by a range of symptoms including positive (delusions, hallucinations), negative (lack of motivation and social interaction) and cognitive, with a worldwide prevalence of around 1%. It is associated with both environmental and genetic factors, with approximately a tenth of sufferers taking their own life (Karam *et al.*, 2010). As a disorder, schizophrenia is poorly understood, however dysfunction of dopaminergic signalling is thought to be a major cause of the symptoms; most effective antipsychotics are dopamine D2 receptor antagonists (Karam *et al.*, 2010) and early studies demonstrated a close correlation between dopamine D2 receptor occupancy and clinical efficacy (Creese *et al.*, 1976; Seeman *et al.*, 1975).

There have been a number of reformulations of the 'dopamine hypothesis of schizophrenia' over the years. Early work implicated that schizophrenia was caused solely by hyperdopaminergic signalling hence the effectiveness of D2 receptor antagonists in tackling positive symptoms (Snyder, 1976). However, this was incompatible with imaging and metabolite studies, which demonstrated that dopamine levels were not universally elevated. For example, early studies suggested reduced blood flow and glucose metabolism in the prefrontal cortex of schizophrenic patients (Buchsbaum *et al.*, 1982; Ingvar *et al.*, 1974) which is supported by later studies which demonstrate reduced D1 receptor binding in the prefrontal cortex (Okubo *et al.*, 1997), although this is not consistently observed (Karlsson *et al.*, 2002). It was therefore proposed that schizophrenia arose from regional specific changes in dopamine signalling; hypodopaminergia in the prefrontal cortex resulted in negative and cognitive symptoms whereas hyperdopaminergia in the mesolimbic system resulted in positive symptoms (Davis *et al.*, 1991). The

most recent reformulation of the hypothesis moves the focus away from D2 receptors specifically, to the control of dopamine signalling at the presynaptic level, with genetic and environmental inputs resulting in aberrant dopamine signalling (Howes *et al.*, 2009).

There is a range of evidence for the dysregulation of dopamine signalling in schizophrenia from pharmacological, imaging and genetic studies. For example, amphetamine administration, which increases extracellular dopamine concentrations, is associated with psychoses similar to those seen in schizophrenic patients (Angrist *et al.*, 1970). Positron emission topography (PET) scans of schizophrenic patients administered with radiolabelled L-DOPA, which provides an indication of dopamine synthesis and storage, have revealed increased striatal dopamine availability that correlates with reduced blood flow in the prefrontal cortex (Meyer-Lindenberg *et al.*, 2002). There have also been reports of a number of genes associated with schizophrenia, a number of which are directly linked to dopamine pathways (Howes *et al.*, 2009). These include single nucleotide polymorphisms (SNPs) of the dopamine D2 receptor (Arinami *et al.*, 1994; Glatt *et al.*, 2006; Schizophrenia Working Group of the Psychiatric Genomics, 2014). Of these, the S311C variant is widely studied (Arinami *et al.*, 1994; Glatt *et al.*, 2006; Itokawa *et al.*, 1996; Nickolls *et al.*, 2004). This mutation, located in ICL3, is associated with an increased risk of schizophrenia (Arinami *et al.*, 1994; Glatt *et al.*, 2006). Recent modelling studies have proposed this mutation leads to conformational rearrangements of the intracellular loops, which decreases the ability of $G\alpha_{i/o}$ proteins to bind by disrupting the hydrogen bond network between the G protein and receptor (Podder *et al.*, 2016). However, this contrasts earlier functional studies where co-expression of specific Gα protein subunits had no difference in the coupling of the D2S receptor to $G\alpha_o$, $G\alpha_{i1}$, $G\alpha_{i2}$ or $G\alpha_{i3}$ following S311C mutation (Nickolls *et al.*, 2004).

In addition to regulation of the dopamine system, there is now a growing appreciation that a number of other signalling systems may factor in schizophrenia, including the glutamatergic system (Karam *et al.*, 2010). Early

evidence for the role of N-methyl-D-aspartate (NMDA) receptors in schizophrenia came from studies with a transgenic mouse model in which the expression of the essential NMDA receptor subunit NR1 was reduced by 90-95%. These mice displayed schizophrenia-like behaviours, which could be ameliorated by treatment with the antipsychotic drugs haloperidol and clozapine (Mohn *et al.*, 1999). Both chronic and acute treatments with NMDA antagonists such as phencyclidine (PCP) can induce schizophrenia-like symptoms in both humans and animals, and exacerbate symptoms in schizophrenic patients (Bubeníková-Valešová *et al.*, 2008).

It has been proposed that acute inhibition of NMDA receptors can lead to activation of the mesolimbic dopamine system (**1.2.1**), associated with the positive symptoms of schizophrenia, as well as disinhibition and increases of extracellular levels of other monoamine neurotransmitters (Bubeníková-Valešová *et al.*, 2008). Furthermore, studies in primates demonstrate decreased dopamine utilisation in the dorsolateral prefrontal cortex following PCP treatment, suggesting decreased activation of the mesocortical pathway leading to cognitive deficits (Jentsch *et al.*, 1997). Thus, inhibition of NMDA receptor signalling may cause both the hyper- and hypo-dopaminergic signalling associated with schizophrenia. Further evidence for the role of NMDA receptors has been provided by genetic studies, which have linked SNPs in NMDA receptors to schizophrenia (Schizophrenia Working Group of the Psychiatric Genomics, 2014).

1.3.2 Antipsychotic drug action

There are a now a large number of antipsychotics in clinical use that share the common property of dopamine D2 receptor antagonism, though many have a diverse pharmacology against several monoamine receptor targets. They have been broadly split into two categories: typical (such as haloperidol or chlorpromazine) and atypical (such as clozapine or risperidone). While these classifications are largely superficial, with little pharmacological or structural basis to the groupings, atypical antipsychotics tend to be the more recently approved drugs associated with fewer extrapyramidal symptoms (EPS), higher

efficacy against negative symptoms, and affinity for other implicated receptors such as serotonin receptors (Mailman *et al.*, 2010). This classification is supported by meta-analyses of clinical trials which demonstrate that atypicals do tend to cause fewer EPS despite similarities in clinical efficacy (Geddes *et al.*, 2000; Leucht *et al.*, 2009).

EPS, such as dystonias and tardive dyskinesia, are caused by antagonism of the nigrostriatal pathway leading to motor symptoms similar to Parkinson's Disease (Mailman *et al.*, 2010). Typical antipsychotics tend to have a greater affinity for the D2 receptor than atypicals (Kapur *et al.*, 2001) and have a greater occupancy of D2 receptors at therapeutic doses (Nord *et al.*, 2011). It has been proposed that atypical antipsychotics occupy D2 receptors at such a level to be clinically effective, without going over the threshold for inducing EPS, which is induced at around 80% occupancy (Nord *et al.*, 2011). An alternative hypothesis has been proposed in which atypical antipsychotics have a reduced propensity to induce EPS due to a faster dissociation rate from the receptor; antagonism of the D2 receptor results in antipsychotic efficacy but the reduced residence time at the receptor limits the induction of EPS (Kapur *et al.*, 2001).

In addition to reduced propensity for EPS, atypical antipsychotics have affinity for a range of serotonin receptors (Meltzer *et al.*, 2011). Selectivity for the 5-HT_{2A} receptor over the D2 receptor is proposed to underlie the improved therapeutic profile of atypical antipsychotics (Meltzer *et al.*, 1989). The ability of antipsychotics to bind with relatively high affinity to a range of serotonin receptor subtypes has been explored extensively (Bruins Slot *et al.*, 2006; Lawler *et al.*, 1999; Newman-Tancredi *et al.*, 2011; Shapiro *et al.*, 2003). Atypical antipsychotics at clinically effective doses display antagonism of 5-HT_{2A} receptors and stimulation of 5-HT_{1A} receptors (either directly or indirectly), with some also displaying antagonism at 5-HT_6 and 5-HT_7 receptors (Meltzer *et al.*, 2011). 5-HT_{2A} receptors modulate dopaminergic signalling in a number of brain areas, with dual antagonism of 5-HT_{2A} and D2 receptors thought to preferentially activate the mesocortical pathway over

the nigrostriatal and mesolimbic pathway. This leads to increased efficacy for negative symptoms and a reduced propensity for EPS (Meltzer *et al.*, 2003). In contrast, 5-HT_{1A} receptors act as autoreceptors, inhibiting serotonergic signalling and leading to similar physiological outcomes as 5-HT_{2A} receptor antagonism. As such, 5-HT_{1A} agonism is also implicated in improving therapeutic profile of antipsychotics, as well as improvements in cognitive deficits (Meltzer *et al.*, 2003; Meltzer *et al.*, 2011). However, atypical antipsychotics are also associated with an increased propensity for weight gain (Geddes *et al.*, 2000; Leucht *et al.*, 2009) which has been associated with 5-HT_{2C} receptor antagonism (Meltzer *et al.*, 2011).

The recent introduction of aripiprazole into clinical use opened a new field of study into antipsychotics. Aripiprazole was originally classed as a dopamine D2 receptor partial agonist, hypothesised to inhibit dopamine hyperactivity in the mesolimbic pathway to limit the positive symptoms of the disease, while enhancing D2 receptor activation in the presence of low endogenous dopamine levels in the mesocortical pathway to alleviate the negative symptoms (Mailman *et al.*, 2010). Compared with both typical and atypical antipsychotics, aripiprazole has a reduced side effect profile whilst maintaining therapeutic efficacy (Stip *et al.*, 2010). Following the approval of aripiprazole into clinical use, there was a concerted pharmaceutical effort to license additional D2 receptor partial agonists for the treatment of schizophrenia, however many failed in clinical trials due to either efficacy or safety concerns (Mailman *et al.*, 2010). Recently, a second structurally related partial agonist, brexpiprazole, has been licensed for the treatment of schizophrenia (Eaves *et al.*, 2016).

Like the atypical antipsychotics, aripiprazole has a complex pharmacological profile; in addition to its partial agonism at the D2 receptor, it is a partial agonist of dopamine D3 and serotonin 5-HT_{1A} receptors, an antagonist of 5-HT_6 receptors and a weak partial agonist/antagonist of 5-HT_{2A} and 5-HT_7 receptors (Bruins Slot *et al.*, 2006; Maeda *et al.*, 2014; Shapiro *et al.*, 2003; Tadori *et al.*, 2011b). Similarly, brexpiprazole is a partial agonist at D2, D3 and

5-HT_{1A} receptors and an antagonist of 5-HT_{2A} and 5-HT_{2B} receptors (Maeda *et al.*, 2014). It is thought that this complex pharmacology is a key contributor to antipsychotic efficacy (Mailman *et al.*, 2010) although more recently, biased signalling has also been implicated (discussed further in **1.6.3** and **1.6.4**).

1.3.3 Parkinson's Disease

Parkinson's disease is a neurodegenerative disorder characterised by a significant decrease in the ability to control voluntary and involuntary movements. At a pathological level, it is caused by a substantial loss of dopaminergic neurons in the substantia nigra pars compacta, and is associated with the presence of Lewy bodies, which are aggregates of the protein α-synuclein (Lew, 2007). By the time the motor symptoms of the disease become apparent, a substantial loss of the dopaminergic neurons (at least 50%) has already occurred, meaning drug treatment is more palliative than disease curing. The principal treatment for Parkinson's disease is the dopamine precursor L-DOPA (**Figure 1.2**), which is effective initially at suppressing Parkinsonian symptoms but over time, induces dyskinesia (Iravani *et al.*, 2012). Alternative treatments are now more commonly being utilised to delay the induction of L-DOPA treatment. These include dopamine receptor agonists such as apomorphine and bromocriptine, as well as MAO and COMT inhibitors to prevent the degradation of dopamine (**Figure 1.2**) (Beaulieu *et al.*, 2011; Lew, 2007).

1.3.4 Other diseases targeted via the dopamine D2 receptor

While schizophrenia and Parkinson's disease are the main targets of D2 receptor therapeutics, there are a number of other conditions in which the D2 receptor has been targeted such as hyperprolactinemia, bipolar disorder, nausea and restless legs syndrome. Dysfunctional dopamine signalling has also been implicated in attention deficit hyperactivity disorder (ADHD) and Tourette's syndrome (Beaulieu *et al.*, 2011).

Prolactin is an anterior pituitary hormone that modulates a number of reproductive functions; its secretion is controlled by the hypothalamus. In hyperprolactinemia, there are elevated blood levels of prolactin resulting in a range of symptoms, including decreased menstruation, decreased libido and infertility. Hyperprolactinemia can be induced through a range of physiological and pathological conditions including pregnancy, prolactinomas (tumours of the pituitary gland) and systemic disorders such as hypothyroidism (Majumdar *et al.*, 2013). It is also a common side effect of many antipsychotics due to blockade of the tuberoinfundibular pathway (**1.2.1**) (Mailman *et al.*, 2010). Dopamine agonists inhibit prolactin secretion (Meller *et al.*, 1992; Meller *et al.*, 1991) and are the mainstay of treatment unless the elevated prolactin levels are a consequence of a systemic disorder (Majumdar *et al.*, 2013).

Many of the symptoms associated with bipolar disorder are shared with schizophrenia, however patients with bipolar disorder tend to have less negative and cognitive symptoms, and their psychosis is preceded by high levels of depression and mania (van Os *et al.*, 2009). This overlap in symptoms indicates the potential for some common mechanisms. Like schizophrenia, hyperdopaminergia has been implicated in mania whereas depression may be due to decreased dopamine signalling, potentially caused by a down-regulation following overstimulation the receptors (Berk *et al.*, 2007). A number of antipsychotics used in the treatment of schizophrenia are also clinically effective for the treatment of bipolar disorder (Berk *et al.*, 2007; Gao *et al.*, 2005).

1.4 GPCR Signalling

1.4.1 GPCR ligand pharmacology

GPCR ligands can be broadly categorised depending on where they bind and how they affect receptor signalling. Binding location determines whether the ligand is orthosteric (binds to the endogenous ligand binding site) or allosteric (binds to a binding site separate to the orthosteric site). Ligands are then

further described by two key parameters: affinity, the ability of the ligand to bind the receptor and efficacy, the ability of the ligand to activate (or inhibit) the receptor once bound (discussed further in **1.8**) (Kenakin *et al.*, 2014).

Orthosteric ligands are classed into 3 groups: agonists, antagonists and inverse agonists, according to their efficacy. Agonists are ligands that bind and activate the receptor to modulate downstream signalling, promoting the stabilisation of an active state of the receptor and so having 'positive efficacy'. Full agonists induce a maximal signalling response whereas partial agonists, even at full receptor occupancy, can never reach the response of a reference full agonist. Antagonists have no efficacy and are unable to activate the receptor themselves; however they can block the binding of other compounds (Kenakin *et al.*, 2014). Inverse agonists are a more recently discovered phenomenon and were identified along with the realisation that receptors can constitutively signal in the absence of agonist (Costa *et al.*, 1989). Inverse agonists act to block this receptor constitutive activity, stabilising the inactive state of the receptor and have 'negative efficacy' (Kenakin *et al.*, 2014) (discussed further in **1.7.3, Chapter Four**) (**Figure 1.3**). So-called 'superagonists' have also been described for a number of GPCRs (Schrage *et al.*, 2015). While still not an officially recognised term, these compounds are described as such due to their higher maximal responses than the endogenous ligand.

Allosteric ligands offer the promise to fine tune receptor signalling and act to modulate the activity of a ligand bound to the orthosteric binding site. They can be broadly classified as either positive or negative allosteric modulators depending on their ability to either enhance or reduce the binding and/or functional response of the orthosteric ligand. Neutral allosteric modulators are also possible; ligands which bind the allosteric site but do not affect the functional responses of the orthosteric ligand. Allosteric ligands may also have efficacy in their own right, acting as either agonists or inverse agonists. Allosteric modulators are described by not only their own affinity and

efficacy, but also cooperativity factors that govern the degree and direction of the orthosteric ligand modulation (Christopoulos, 2014; Keov *et al.*, 2011).

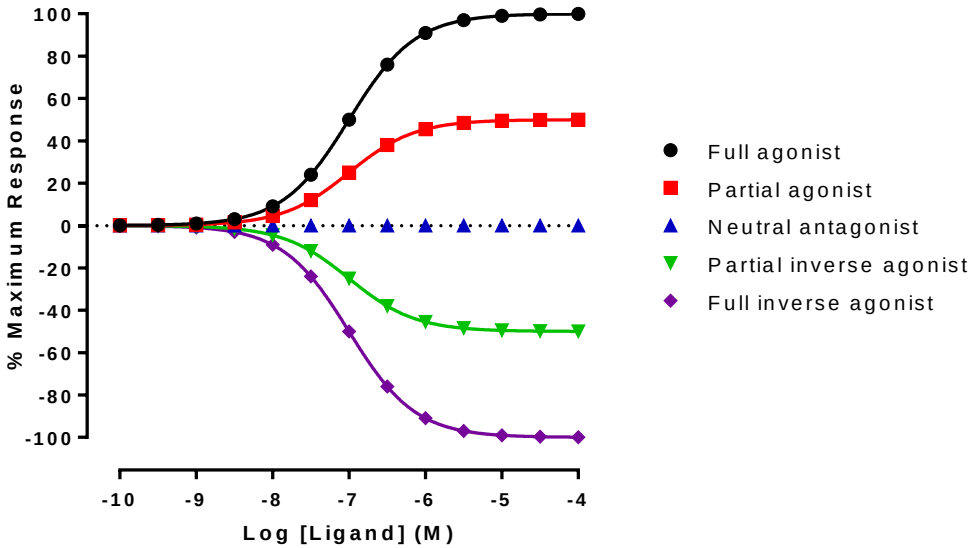


Figure 1.3: Orthosteric ligand classification

Ligands are classified according to their ability to induce a functional response. Agonists act to increase intracellular signalling upon ligand binding and can be further classified as either full or partial agonists depending on their efficacy. Neutral antagonists are able to bind receptors but induce no response themselves. They can however inhibit the binding of other ligands as they bind at the same site as agonists. Inverse agonists have negative efficacy; they act to inhibit the constitutive signalling of the receptor thus reducing the signalling response. Like agonists, these can be classified as full or partial depending on their efficacy.

1.4.2 Ligand binding and activation of GPCRs

The orthosteric ligand binding site of class A GPCRs is generally located in the extracellular half of GPCR and is formed mainly by TMs 3, 6 and 7. Specific contacting residues differ between receptors and many receptors have important contacts in other TMs (e.g. TM5 for monoamine receptors, see **Chapter Four**) (Lee *et al.*, 2015). For monoamine receptors, agonist binding promotes the inward movement of the extracellular ends of TM5 and TM6 to contract the ligand binding pocket and stabilise the active conformation of the receptor (Dror *et al.*, 2011; Kling *et al.*, 2014; Rasmussen *et al.*, 2011b; Warne *et al.*, 2011). Furthermore, NMR studies have correlated agonist induced movements in the TM5 backbone with ligand efficacy (Isogai *et al.*, 2016). The highly conserved proline residues in TMs 5, 6 and 7 result in kinks in the TM domains, creating a pivot around which the intracellular and extracellular halves of these TMs can move and rotate upon ligand binding and receptor activation (Schwartz *et al.*, 2006).

The 'global toggle switch' model proposed that agonist binding results in a see-saw movement of TM6 around the conserved proline (P6.50). This movement closes the extracellular part of TM6 around the ligand and opens the intracellular end of TM6 to facilitate G protein binding (Schwartz *et al.*, 2006). This is supported by crystal structures of the active β2-adrenoceptor (β2AR)-G protein and adenosine A2A-G protein complexes, both of which display a large outward movement of cytoplasmic end of TM6 relative to the inactive state structures (Carpenter *et al.*, 2016; Rasmussen *et al.*, 2011a). This movement of TM6 has also been associated with the highly conserved W6.48 that is part of the CWxP motif with P6.50. It has been suggested that rotation of this residue upon receptor activation releases steric constraints upon the receptor conformation, allowing the inward movement of the extracellular half of TM6 (Schwartz *et al.*, 2006). W6.48 has also been indicated in stabilising interhelical interactions between TM3 and TM6 (Tehan *et al.*, 2014).

The overall result of these conformational changes is a substantial rearrangement of the TM domains, particularly their intracellular face, which facilitates the binding of effector molecules such as G proteins. These rearrangements also break a series of interhelical contacts which are proposed to stabilise the inactive state of the receptor (such as the E/DRY motif; **1.4.3**) and lead to rearrangements of hydrogen bond networks to propagate ligand binding to G protein activation.

1.4.3 Role of conserved motifs in receptor activation

The crystal structure of rhodopsin (Palczewski *et al.*, 2000), the first GPCR to be crystallised, provided the first evidence for the mechanisms of receptor activation in GPCRs. In this seminal paper, it was noted that E3.49 and R3.50 of the highly conserved E/DRY motif were connected to E6.30 and T6.34 of TM6. The salt bridge between R3.50 and E6.30 has become known as the 'ionic lock', and was the focus of much investigation using mutagenesis for its role in receptor activation (Ballesteros *et al.*, 2001; Feng *et al.*, 2003; Kim *et al.*, 2008; Rasmussen *et al.*, 1999; Scheer *et al.*, 1996). It was postulated that this interaction between TM3 and TM6 may act to stabilise the receptor in an inactive state, so that breaking this interaction would lead to receptor activation. This supported mutagenesis studies in which constitutively active receptors were generated through mutations of these residues in a number of GPCRs including the β2AR (Ballesteros *et al.*, 2001; Rasmussen *et al.*, 1999) and the α_{1B}-adrenoceptor (Scheer *et al.*, 1996).

However, most class A GPCRs cannot form an ionic lock; only 27% of receptors contain an acidic residue at position 6.30, suggesting this interaction is not as key to receptor activation as was first proposed. This is supported by its general absence in the inactive state GPCR crystal structures solved thus far (Tehan *et al.*, 2014). Furthermore, for some receptors, such as the dopamine D2 and cannabinoid receptor type 2 (CB2), R3.50 mutations actually abolish G protein-dependent signalling (Feng *et al.*, 2003; Kim *et al.*, 2008). This indicates that R3.50 may be involved in G protein coupling as well as stabilising specific receptor states. The crystal structures of the active

β2AR-G protein and adenosine A2A receptor-G protein complexes show an interaction between R3.50 and the α5 helix of the G protein (Carpenter *et al.*, 2016; Rasmussen *et al.*, 2011a). This supports molecular dynamic simulations of the dopamine D2 receptor which demonstrate the presence of an ionic interaction between R3.50 and D350 of the $G\alpha_i$ protein when dopamine is bound to the receptor (Kling *et al.*, 2016).

Another important motif implicated in receptor activation is the NPxxY motif at the base of TM7, which is separated from the E/DRY motif by a hydrophobic barrier in the inactive receptor state. The hydrophobic barrier consists of six conserved residues in TMs 2, 3 and 6 (L2.43, L2.46, L3.43, L3.46, M6.36 and M6.40). Upon receptor activation, rotation of W6.48 disrupts the hydrophobic barrier, inducing conformational rearrangements of Y7.53 of the NPxxY motif and Y5.58. This promotes the formation of a hydrogen bonding water network from the CWxP motif to the E/DRY motif and the G protein (Trzaskowski *et al.*, 2012).

1.4.4 G protein dependent signalling

The mainstay of GPCR signalling is through activation and subsequent dissociation of heterotrimeric G proteins. G proteins exist in a trimer of α, β and γ subunits; in humans, there are 21 Gα subunits, 6 Gβ and 12 Gγ subunits (Oldham *et al.*, 2008). Of those, the α subunit largely governs downstream signalling events with 4 main families identified. $G\alpha_s$ activates adenylyl cyclase to increase cellular cAMP levels and $G\alpha_{i/o}$ inhibits adenylyl cyclase to decrease cellular cAMP (discussed further in **1.4.5**). $G\alpha_{q/11}$ couples to phospholipase Cβ to increase inositol 1,4,5-trisphosphate (IP_3) production and subsequently intracellular calcium levels, and $G\alpha_{12/13}$ couples to Rho GTPase nucleotide exchange factors (RhoGEFs) to modulate signalling of the Rho-ROCK pathway (Milligan *et al.*, 2006; Siehler, 2009). The β and γ subunits form a constitutive dimer which can also regulate downstream signalling, for example through GIRKs (Milligan *et al.*, 2006).

In the presence of an inactivated receptor, the Gα subunit is GDP bound and associated with the βγ dimer. Crystal structures of G protein heterotrimers show that GDP binds within the α subunit, sandwiched between the Ras and helical domains of Gα (Lambright *et al.*, 1996; Wall *et al.*, 1995). Recently however, molecular dynamic simulations have shown that these domains can spontaneously separate (Dror *et al.*, 2015) which supported earlier biophysical studies that demonstrated substantial flexibility in these domains (Van Eps *et al.*, 2011; Westfield *et al.*, 2011). While this domain separation alone is not sufficient to promote GDP release from the G protein, it is necessary for guanine nucleotide exchange (Dror *et al.*, 2015; Van Eps *et al.*, 2011).

Upon receptor activation, either spontaneously (constitutive activity) or as a consequence of ligand binding, the GPCR associates with the G protein complex and acts as a guanine nucleotide exchange factor to promote GDP/GTP exchange. Receptor activation induces conformational changes in the bound Gα protein, rotating and displacing its α5 helix away from GDP, weakening the interactions between Gα and GDP (Dror *et al.*, 2015). This movement was clearly observed in the β2AR-G protein crystal structure, whereby the α5 helix in the activated G protein is displaced towards the receptor, projecting into the TM bundle at the base of the β2AR (Rasmussen *et al.*, 2011a). This reduction in affinity of GDP for the G proteins allows the release of GDP upon spontaneous separation of the Ras and helical domains. The open conformation then allows the spontaneous binding of GTP to the guanine nucleotide binding site (Dror *et al.*, 2015).

Binding of guanine nucleotide, such as GTP, destabilises the GPCR-G protein complex resulting in the dissociation of the G protein from the receptor (Westfield *et al.*, 2011). This dissociation from the GPCR, and subsequent dissociation of the G protein subunits, frees the Gα-GTP and Gβγ subunits to bind and regulate downstream effectors. The inherent GTPase activity of the Gα subunit results in the hydrolysis of GTP to GDP; this may be catalysed by regulators of G protein signalling (RGS) proteins. This releases inorganic

phosphate, and the cycle is free to begin again (**Figure 1.4**) (Oldham *et al.*, 2008).

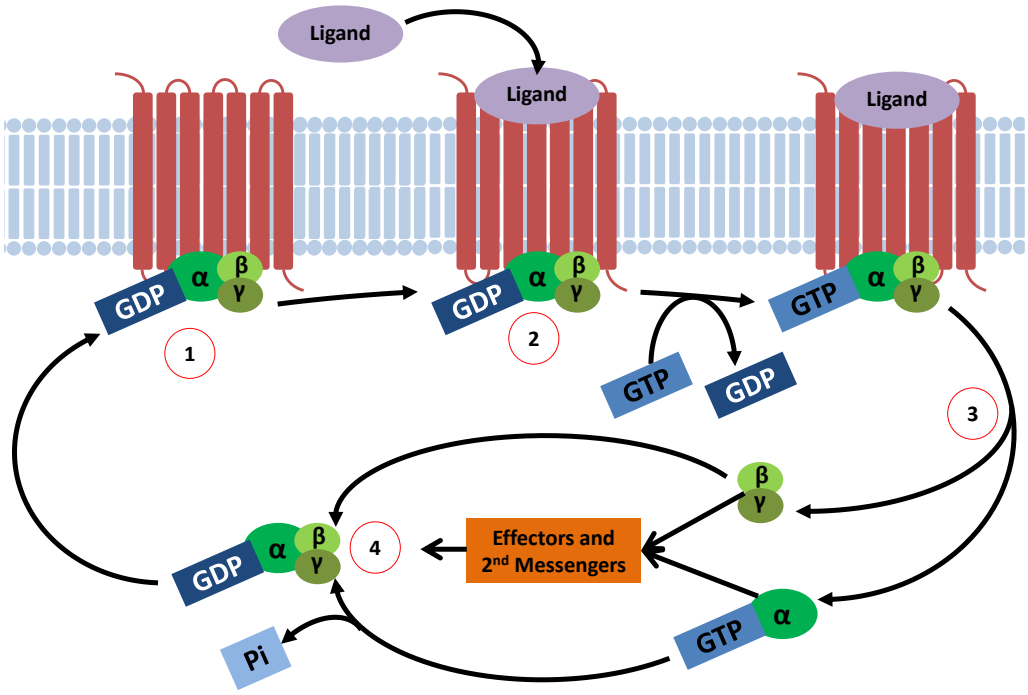


Figure 1.4: The G protein cycle

Inactive heterotrimeric G proteins are bound to GDP (1). Ligand binding and receptor activation (2) induces a conformational change in the receptor that facilitates the exchange of GTP for GDP on the Gα subunit. This causes the G protein to dissociate from the receptor resulting in dissociation of the G protein subunits (3). These are now free to initiate intracellular signalling pathways. The inherent GTPase activity of the Gα subunit hydrolyses the GTP to GDP, releasing inorganic phosphate (4). The heterotrimeric complex is reforms, binds a GPCR and the cycle begins again.

1.4.5 Downstream effectors of G protein signalling: cAMP and PKA

One of the primary second messengers linked to GPCR activation is cAMP, which is synthesised by the enzyme adenylyl cyclase (AC) and degraded by phosphodiesterases (Steegborn, 2014). AC catalyses the cyclisation of ATP to cAMP, releasing pyrophosphate, with its activity modulated by activation of $G\alpha_s$ and $G\alpha_{i/o}$ proteins. There are 9 isoforms of transmembrane AC named AC1-AC9 which are grouped according to their other regulatory properties: Group 1 (AC1, 3 and 8) are stimulated by Ca^{2+}; Group 2 (AC 2, 4 and 7) are stimulated by Gβγ subunits; Group 3 are inhibited by $G\alpha_i/Ca^{2+}$ (AC 5 and 6) and Group 4 (AC9) is insensitive to forskolin. All AC isoforms are stimulated by $G\alpha_s$ (Sadana *et al.*, 2009; Steegborn, 2014). Each isoform of AC has a specific distribution pattern and associated physiological functions; for example, AC1 is predominantly expressed in the brain and has a role in learning and memory whereas AC5 and 6 are expressed in the heart and involved in cardiac contraction (Sadana *et al.*, 2009).

Activation of the dopamine D2 receptor is associated with inhibition of AC isoforms 1, 5, 6 and 8 (Nevo *et al.*, 1998; Robinson *et al.*, 1997). AC5 is the predominant AC isoform in the striatum. AC5 knockout mice display Parkinsonian-like motor dysfunction and substantial attenuation of AC regulation by both dopamine D1 ($G\alpha_s$ coupled) and D2 ($G\alpha_i$ coupled) receptors. These models have suggested a role of AC5 in dopamine mediated motor activity and the neuroleptic effects of antipsychotics (Iwamoto *et al.*, 2003; Lee *et al.*, 2002).

An increase in cellular cAMP levels leads to activation of protein kinase A (PKA). PKA is a prototypical protein kinase composed of two regulatory and two catalytic subunits (Taylor *et al.*, 2012). cAMP binds to the regulatory subunits (Brostrom *et al.*, 1971), resulting in their dissociation; this frees the catalytic domains to regulate downstream signalling. PKA has a wealth of downstream targets, both cytoplasmic and nuclear, and can be targeted to

specific sub-cellular locations through A kinase anchoring proteins (Taylor *et al.*, 2012). PKA, and protein kinase C (PKC), can also act to regulate AC activity. While PKA phosphorylates and inactivates AC5 and 6 (Iwami *et al.*, 1995), PKC regulation can be either inhibitory or stimulatory depending on the AC isoform, the PKC isoform and the mode of AC stimulation e.g. $G\alpha_s$ or forskolin (Sadana *et al.*, 2009).

Modulation of PKA activity through dopamine receptors regulates the activity of dopamine and cAMP-regulated phosphoprotein-32kD (DARPP-32). DARPP-32 is a highly conserved protein, predominantly expressed in medium spiny neurons that plays a central role in many neurotransmitter pathways, including dopamine. Upon phosphorylation of threonine residue 34 by PKA, DARPP-32 becomes a potent protein phosphatase-1 (PP1) inhibitor (Beaulieu *et al.*, 2011). DARPP-32 knockout mice show significant reduction, or complete inhibition, of their molecular, physiological and behavioural responses to both dopamine and dopamine receptor ligands (Greengard, 2001).

1.5 'Switching off' GPCR signalling

1.5.1 Arrestins and GRKs

Following receptor activation, GPCRs can be desensitised and internalised in order to regulate signalling and prevent prolonged responses. This is mediated by two key protein families: G protein coupled receptor kinases (GRKs) and β-arrestins. There are 7 GRKs which have been grouped into 3 families; GRK1-like kinases (GRK1 and 7) are localised to the retina and regulate rod and cone opsins; GRK2-like kinases (GRK 2 and 3) are ubiquitously expressed and contain binding domains for phosphatidyl inositol bisphosphate (PIP_2) and Gβγ that mediate plasma membrane recruitment; and GRK4-like kinases (GRK4, 5 and 6) which use PIP_2 and/or covalent lipid modification to maintain their plasma membrane location. While GRK5 and 6 are expressed throughout the body, GRK4 is restricted mostly to the testes. GRKs are serine/threonine kinases that phosphorylate these residues on the

carboxy terminus and ICL3 of activated GPCRs. This phosphorylation leads to β-arrestin binding and subsequent receptor desensitisation and internalisation (Black *et al.*, 2016; Premont *et al.*, 2007).

The arrestin family of scaffolding proteins contains 4 members: arrestin-1 and arrestin-4 are found solely in the retina while arrestin-2 (β-arrestin1) and arrestin-3 (β-arrestin2) are ubiquitously expressed (Black *et al.*, 2016; Premont *et al.*, 2007). While both β-arrestin isoforms can interact with activated receptors, they differ in their cell localisation; both are found in the cytoplasm but only β-arrestin1 is located in the nucleus. Furthermore, they can differentially modulate downstream GPCR signalling, although this is often cell type and receptor specific (Smith *et al.*, 2016). β-arrestins were first identified for their role in receptor desensitisation (Lohse *et al.*, 1990; Wilden *et al.*, 1986) (**1.5.2**), however it is now appreciated they are required for clathrin-dependent receptor internalisation (Smith *et al.*, 2016) (**1.5.3**) as well as signalling partners in their own right (discussed further in **1.6**).

1.5.2 Desensitisation

Desensitisation modulates GPCR coupling to downstream pathways over short periods of time, usually seconds to minutes. This is in contrast to downregulation, which is a more long-term adaptation to decrease receptor signalling over hours. In both cases, receptors become less sensitive to further stimulation (Smith *et al.*, 2016). Two types of desensitisation have been described – homologous and heterologous.

Homologous desensitisation is selectively targeted at the activated population of receptors; agonist stimulation leads to phosphorylation of the activated receptor by GRKs, facilitating β-arrestin binding and uncoupling the G protein from the receptor (Cho *et al.*, 2013). GRK phosphorylation increases the affinity of β-arrestin for the receptor, promoting its binding (Violin *et al.*, 2006). β-arrestin binding inhibits receptor-G protein coupling by sterically blocking the receptor interacting with the G protein. The crystal structure of the rhodopsin-arrestin complex shows that arrestin binds to a similar region

of the GPCR as the G protein, thus preventing G protein binding. However the contact region is greater, involving TMs 5,6 and 7, helix 8 and the intracellular loops, although the surface area buried at the interface is smaller than in the β2AR-G protein complex (Kang *et al.*, 2015; Rasmussen *et al.*, 2011a). Once bound, β-arrestin undergoes receptor-specific conformational changes that can promote specific downstream signalling and regulatory responses before dissociating from the receptor (Lee *et al.*, 2016; Nuber *et al.*, 2016).

In contrast, heterologous desensitisation is not specific to active receptors and involves the phosphorylation of multiple receptors, whether or not they are occupied by ligand, throughout the cell by second messenger protein kinases such as PKA or PKC (Cho *et al.*, 2013). These phosphorylation sites are distinct from those which are involved in GRK-mediated phosphorylation and can result in progression down different regulatory pathways such as recycling or degradation (Cho *et al.*, 2013; Tran *et al.*, 2004).

While the dopamine D2 receptor is reported to undergo GRK-mediated phosphorylation and β-arrestin recruitment, studies have indicated that it does not undergo agonist-induced desensitisation following pre-treatment with maximal concentrations of dopamine (Cho *et al.*, 2010b; Cho *et al.*, 2013). Desensitisation of the D2 receptor appears instead to be mediated by PKC (Cho *et al.*, 2013; Morris *et al.*, 2007; Namkung *et al.*, 2004). Treatment with the PKC activators phorbol 12-myristate 13-acetate (PMA) or 12-*O*-tetradecanoyl 4β-phorbol 13α-acetate (TPA) leads to receptor desensitisation that is attenuated in the presence of a specific PKC inhibitor. PKC phosphorylation sites have been mapped to ICL2 and ICL3 (Cho *et al.*, 2013; Morris *et al.*, 2007; Namkung *et al.*, 2004). It has also been proposed that there are differences in receptor desensitisation between the D2 receptor splice variants; the D2S receptor is more sensitive to PKC-mediated desensitisation than D2L. This might be due to the presence of a PKC pseudosubstrate site in the ICL3 insertion in the D2L receptor that inhibits PKC activity (Morris *et al.*, 2007).

For GPCRs, this classical view of desensitisation focusses on the attenuation of G protein signalling events. However, it is now appreciated that β-arrestin bound GPCRs are not necessarily desensitised and can continue to signal through β-arrestin mediated pathways (discussed further **1.6**).

1.5.3 Internalisation

Following the binding of β-arrestin, most GPCRs are internalised from the cell surface. β-arrestins act as adaptor proteins, scaffolding to AP-2 and clathrin to mediate receptor internalisation via clathrin-coated pits. These clathrin-coated pits pinch off from the membrane in a process mediated by the GTPase dynamin, forming intracellular vesicles which are sorted into either recycling or degradation pathways (Smith *et al.*, 2016; Sorkin *et al.*, 2009). While classically internalisation was thought to attenuate signalling by physically removing GPCRs from the cell surface, there is increasing evidence that GPCRs can continue to signal from endosomal compartments (Ellisdon *et al.*, 2016). This signalling is often temporally distinct depending on the sub-cellular location; for example, neurokinin 1 (NK1) receptor cytosolic extracellular regulated kinase 1 and 2 (ERK1/2) signalling is transient, peaking after 5min before returning to baseline after 20min whereas nuclear ERK1/2 signalling slowly increases over time and is sustained for 20min (Jensen *et al.*, 2014).

Of the receptors which internalise in a clathrin-dependent manner, two classes of GPCRs were identified depending on the presence or absence of conserved serine and threonine residues on the carboxy terminal of the receptor, and their ability to bind the different arrestin isoforms. Class A receptors lack this cluster, transiently binding β-arrestin2 and internalising without it whereas class B receptors bind both β-arrestin1 and 2, internalising in a complex with the arrestin (Oakley *et al.*, 2001; Oakley *et al.*, 2000). However, subsequent studies have suggested more complexity than this broad definition; for example, studies with the purinergic P2Y2 receptors have demonstrated that the recruitment of β-arrestin isoforms is differentially regulated by agonists (Hoffmann *et al.*, 2008). Furthermore, the

absence of the serine and threonine cluster in the short carboxy terminus of the dopamine D2 receptor classifies it as class A, therefore β-arrestin is not expected to complex and internalise with the receptor (Quan *et al.*, 2008). However microscopy studies have shown that both β-arrestin1 and β-arrestin2 internalise with D2L and D2S receptors (Kim *et al.*, 2004).

Studies with both dopamine D2 receptor isoforms indicate the importance of GRK phosphorylation and β-arrestin recruitment to the internalisation of the receptor. Receptor activation leads to GRK-dependent receptor phosphorylation and recruitment of β-arrestins to the membrane (Ito *et al.*, 1999; Kim *et al.*, 2001; Kim *et al.*, 2004). Co-expression of a dominant-negative form of β-arrestin, which blocks receptor internalisation by preventing interactions with clathrin, prevented both D2L and D2S receptor internalisation (Kim *et al.*, 2004). Furthermore, alanine substitution of ICL3 residues 212-215 abolishes recruitment of β-arrestin2 and receptor internalisation (Lan *et al.*, 2009). However, mutation of only 3 of these 4 residues maintains β-arrestin2 recruitment but still prevents receptor internalisation suggesting β-arrestin recruitment is necessary but not sufficient for D2 receptor internalisation (Clayton *et al.*, 2014). Interestingly, the two splice variants appear to have distinct mechanisms of internalisation. While D2S internalisation appears dependent on dynamin, suggesting a clathrin-mediated mechanism, D2L receptor internalisation is independent of dynamin (Kim *et al.*, 2001; Kim *et al.*, 2004). This corroborated an earlier study which also demonstrated dynamin-independent D2 receptor internalisation (Vickery *et al.*, 1999).

1.6 β-arrestin mediated signalling of GPCRs

1.6.1 G protein independent signalling

It is now well established that GPCRs can also signal independently of heterotrimeric G proteins through the β-arrestin family of scaffolding proteins. Traditionally known for their role in receptor internalisation and desensitisation as previously discussed, β-arrestins can scaffold to cellular

signalling partners such as ERK1/2 and c-Jun N-terminal kinase (JNK) to modulate cellular signalling (Smith *et al.*, 2016). It has been suggested that β-arrestin mediated signalling is spatially and temporally distinct from G protein dependent signalling; for example, generally G protein mediated activation of ERK1/2 is rapid, transient and results in nuclear translocation whereas β-arrestin mediated ERK1/2 activation is slower, sustained and cytoplasmic (Ahn *et al.*, 2004; Shenoy *et al.*, 2006). However this does not apply to all GPCRs; α_{1D}-adrenoceptor mediated ERK1/2 phosphorylation is transient, cytoplasmic and independent of both PKC and β-arrestin (Perez-Aso *et al.*, 2013) suggesting each GPCR may have its own profile of downstream signalling.

Recent studies have shown GPCRs can induce distinct β-arrestin conformations that can be related to their downstream signalling profiles. Even for a given receptor, different ligands can induce specific β-arrestin conformations (Lee *et al.*, 2016; Nuber *et al.*, 2016). If β-arrestin conformational changes can be associated with distinct intracellular signalling profiles, this offers the opportunity to design ligands based on these conformational changes. This is particularly relevant to the investigation of ligand bias (discussed below, **1.6.3**).

1.6.2 β-arrestin mediated signalling of the dopamine D2 receptor

One of the major emerging signalling pathways mediated through dopamine D2 receptors is a β-arrestin mediated pathway through Akt and glycogen synthase kinase-3 (GSK3). There is increasing evidence that GSK3 activation through dopamine D2 receptors involves a G protein-independent, β-arrestin dependent pathway involving a complex of the serine/threonine kinase Akt, protein phosphatase 2A (PP2A) and β-arrestin2. It was first reported during an *in vivo* study into the effects of lithium using a DAT knockout mice model. In this model, there are persistently elevated extracellular dopamine levels which cause prolonged dopamine D2 receptor activation (Beaulieu *et al.*,

2004). DAT knockout mice demonstrated dephosphorylation of Akt, effects that were matched through treatment of wild type mice with both dopamine agonists and amphetamine, which acts to indirectly increase dopamine levels. Dephosphorylation of Akt reduces its kinase activity which in turn, increases activation of GSK3α and GSK3β. Treatment of the knockout mice with the D2/D3 receptor antagonist raclopride increased phosphorylation of Akt and both GSK3 isoforms which was independent of PKA and calcineurin, suggesting a cAMP independent pathway (Beaulieu *et al.*, 2004). A subsequent study revealed the importance of β-arrestin2 and PP2A in this pathway. β-arrestin2 knockout mice display no change in Akt phosphorylation upon administration of dopamine direct and indirect agonists. Glutathione S-transferase (GST) pull down assays confirmed that β-arrestin2, Akt and PP2A directly interact, and that this interaction was absent in β-arrestin2 knockout mice, suggesting β-arrestin2 is an essential scaffolding protein in this interaction (Beaulieu *et al.*, 2005). In vitro studies have confirmed that dopamine D2 receptor activation influences the Akt/GSK3 pathway however, in contrast to the *in vivo* studies, dopamine D2 receptor activation in a transfected D2L CHO line increased Akt and GSK3 phosphorylation in a G protein dependent manner. Administration of the D2/3 agonist quinelorane to rats increased Akt and GSK3β phosphorylation. The authors suggest that the conflicting reports are caused by short-term and long-term distinct signalling routes, as the previous *in vivo* studies used a longer drug exposure time. This may reveal differential G protein and β-arrestin modulation of this pathway (Mannoury la Cour *et al.*, 2011).

1.6.3 Biased Signalling

The knowledge of G protein independent signalling offers the potential for ligands to signal down specific intracellular signalling pathways. This phenomenon has been given a number of names over the years, most commonly functional selectivity or biased signalling. While most examples of biased signalling have concentrated on G protein versus β-arrestin mediated signalling (reviewed in (Kenakin, 2012; Rajagopal *et al.*, 2010; Urban *et al.*,

2007a; Violin *et al.*, 2014)), there are examples of ligands preferentially activating specific subsets of G proteins (Gazi *et al.*, 2003; Griffin *et al.*, 2007; Lane *et al.*, 2007; Thompson *et al.*, 2016). More recently, studies have looked at a wider range of signalling endpoints outside of the typical β-arrestin versus G protein mediated signalling, comparing a whole host of both functional and regulatory responses (Klein Herenbrink *et al.*, 2016; Thompson *et al.*, 2015).

Biased ligands offer the opportunity to improve therapeutics by preferentially activating the signalling pathways which mediate the therapeutic response rather than those which mediate side effects (Violin *et al.*, 2014). This has been exemplified by a number of biased ligands in current clinical trials, which promise reduced side effects over traditional ligands. One such example is the reported G protein biased agonist of the μ-opioid receptor, TRV130. In recombinant cell line functional assays, this compound can only moderately recruit β-arrestin while maintaining a full agonist profile at G protein signalling. *In vivo*, this compound produces analgesia with reduced respiratory depression compared to the gold standard analgesic, morphine (DeWire *et al.*, 2013). As such, it has been postulated that analgesia at the μ-opioid receptor is mediated by G protein dependent signalling whereas respiratory depression and constipation are mediated through β-arrestin mediated signalling. Phase 1 clinical trials have shown that this improved therapeutic effect has translated into human subjects, with those treated with TRV130 demonstrating analgesia with a reduced propensity for respiratory depression and nausea than morphine (Soergel *et al.*, 2014).

Biased signalling is thought to arise from ligands stabilising distinct receptor conformations, leading to the preferential activation of specific intracellular signalling pathways. This has been supported by a number of biophysical, mutagenesis and energy transfer studies which have demonstrated the presence of multiple ligand induced receptor states (Fowler *et al.*, 2012; Ghanouni *et al.*, 2001; Kofuku *et al.*, 2012; Manglik *et al.*, 2015; Staus *et al.*, 2016; Swaminath *et al.*, 2005; Wiens *et al.*, 1998; Zürn *et al.*, 2009). The β2AR

is the most widely studied receptor with respect to this; early spectroscopic studies revealed that the partial agonists salbutamol and dobutamine were stabilising an active state distinct to that of the full agonist isoproterenol (Ghanouni *et al.*, 2001). The use of Förster resonance energy transfer (FRET) based biosensors in the α_{2A}-adrenoceptor has revealed at least 4 ligand-specific receptor conformations, based on movements of ICL3 for a range of weak partial to full agonists (Zürn *et al.*, 2009). These ligand specific conformations are not restricted to agonists; recent ^{19}F-NMR spectroscopy studies have revealed the presence of two β2AR inactive states, corresponding to an intact and broken ionic lock (Manglik *et al.*, 2015; Staus *et al.*, 2016). This supports an earlier report of multiple β1AR crystal structures bound to 4 different antagonists that also demonstrated two distinct conformations of TM6, one of which was stabilised by an intact ionic lock (Moukhametzianov *et al.*, 2011). These distinct ligand induced receptor conformations appear to arise as a consequence of ligands interacting differently with receptor binding sites. Structurally distinct ligands disrupt different intramolecular interactions stabilising receptor states, thus promoting different conformational states and activation mechanisms upon ligand binding (Swaminath *et al.*, 2005).

Along with ligand bias, there is also system and observational bias to consider; neither can be exploited therapeutically as effects are common to all ligands, but they must be considered in studies of ligand bias (Kenakin *et al.*, 2013b). System bias arises from differential coupling of the system to different effector pathways whereas observational bias depends on the sensitivities of the signalling assays under measure, and is dependent on assay conditions such as temperature and buffer conditions (Kenakin *et al.*, 2013b). Observational bias is particularly pronounced in traditional studies of G protein versus β-arrestin biased ligands; β-arrestin recruitment assays have low levels of signal amplification in comparison to conventional G protein dependent assays such as second messenger and reporter gene assays. This may result in low efficacy agonists appearing G protein biased due to a lack of

response in a β-arrestin recruitment assay when in fact the assay is not sensitive enough to detect their restricted responses (Stott *et al.*, 2016).

1.6.4 Biased signalling of the dopamine D2 receptors

There are now a wealth of studies which provide evidence for biased signalling at the dopamine D2 receptor (Brust *et al.*, 2015a; Brust *et al.*, 2015b; Kilts *et al.*, 2002; Klein Herenbrink *et al.*, 2016; Lane *et al.*, 2007; Mottola *et al.*, 2002; Shonberg *et al.*, 2013; Szabo *et al.*, 2014; Tschammer *et al.*, 2011; Urban *et al.*, 2007a; Urban *et al.*, 2007b). Early reports of ligand bias concentrated on the dopamine D1/D2 receptor agonist dihydrexidine (DHX). DHX was reported to act as an agonist at postsynaptic dopamine D2 receptors, inhibiting AC and prolactin secretion; however it appeared to antagonise, or have no effect, on other dopamine D2 receptor presynaptic receptor functions such as the control of dopamine synthesis, cell firing and release (Kilts *et al.*, 2002; Mottola *et al.*, 2002).

Bias at the dopamine D2 receptor may also have significant therapeutic benefit; one compound that highlights this is the partial agonist aripiprazole. As described in **1.3.2**, aripiprazole was hypothesised to act as a 'dopamine stabiliser' and has demonstrated a reduced side effect profile whilst maintaining therapeutic efficacy as an antipsychotic (Stip *et al.*, 2010). Studies have suggested that aripiprazole may also be a biased ligand, which may contribute to these characteristics (Brust *et al.*, 2015a; Brust *et al.*, 2015b; Szabo *et al.*, 2014; Urban *et al.*, 2007b). *In vivo* studies with β-arrestin biased aripiprazole derivatives have shown antipsychotic action with markedly reduced EPS. In β-arrestin knockout mice, this antipsychotic efficacy was attenuated (Allen *et al.*, 2011). However, there are conflicting lines of evidence for the importance of inhibiting of β-arrestin mediated signalling in antipsychotic efficacy. An early study demonstrated that clinically used antipsychotics, including aripiprazole, could not recruit β-arrestin and inhibited quinpirole-induced β-arrestin recruitment (Masri *et al.*, 2008). Furthermore, activation of the dopamine D2 receptor induces G protein independent signalling through a β-arrestin2-Akt-PP2A complex leading to the

dephosphorylation and activation of GSK3 (**1.6.2**). However antipsychotics lead to an increase in GSK3β phosphorylation (Emamian *et al.*, 2004; Li *et al.*, 2007) and reduced GSK3β phosphorylation has been demonstrated in schizophrenic patients (Emamian *et al.*, 2004). Together, these results suggest that inhibiting β-arrestin mediated signalling may be beneficial in the treatment of schizophrenia.

1.7 Receptor theory

1.7.1 Occupancy theory

The roots of quantitative pharmacological theory can be traced back to the early 1900s, when AV Hill derived the Hill-Langmuir equation from the law of mass action (Hill, 1909; Hill, 1910). This equation describes the formation of the agonist-receptor complex ([AR]) at equilibrium as a function of total receptor concentration (R_T), concentration of agonist ([A]) and agonist dissociation constant (K_A), the concentration of agonist required to occupy 50% of the receptors.

$$[AR] = \frac{R_T[A]}{[A] + K_A} \quad (1)$$

This equation forms the basis of the sigmoidal log concentration occupancy curve, in which the ligand concentration at the midpoint, K_A, represents half-maximal receptor occupancy. Thus, the equilibrium dissociation constant K_A became a standard representation of ligand affinity for the target receptor. Clark was the first to apply this equation in concentration response relationships to relate ligand binding to a functional response (Clark, 1926b). His proposed occupancy theory assumed functional response was directly related to the proportion of occupied receptors (Clark, 1933).

1.7.2 Measuring antagonist affinity

While the Hill-Langmuir equation provided a framework to analyse the functional responses of agonists, alternative methods of analysis were required to analyse antagonist responses. Early studies by both Clark and Gaddum had demonstrated rightward shifts in agonist response curves in the

presence of a competitive antagonist (Clark, 1926a; Gaddum, 1926) although it was not until later that Gaddum published a mathematical relationship. He was the first to explicitly write an equation to relate the proportional receptor occupancy of an agonist (ρ_A) in presence of agonist [A] and antagonist [B], where K_A is the equilibrium dissociation constant of the agonist and K_B is the equilibrium dissociation constant of the antagonist (Gaddum, 1937).

$$\rho_A = \frac{[A]/\,K_A}{[A]/\,K_A + [B]/\,K_B + 1} \quad (2)$$

However, this equation only described ligand binding at equilibrium and was not related to functional responses. Furthermore, the relationship between binding and functional response was not known. This was circumvented by Schild (Arunlakshana *et al.*, 1959; Schild, 1949) by using a null method approach, comparing conditions that generate the same system response (with the assumption that in each case, this was generated by an unknown, but equal, level of agonist-receptor occupancy). Schild examined the increase in agonist concentration necessary to generate the same level of response in the presence of antagonist. His measure of antagonist affinity was pA_2, the negative log concentration of antagonist that produces a two-fold shift in the agonist concentration response curve. It is calculated from the concentration ratio (CR), the ratio of the concentration of agonist required to generate an equal response in the absence and presence of antagonist, and the concentration of antagonist ([B]). This simplified the Gaddum equation to:

$$K_B = \frac{[B]}{CR-1} \quad (3)$$

Schild expanded on Gaddum's work, rewriting the equation in log form:

$$pK_B = log\ (CR - 1) - log\ [B] \quad (4)$$

Plotting log (CR-1) against log [B] generates a linear regression whereby the x intercept provides a pA_2 value. If the slope of the line, the Schild slope, is equal to unity, then the antagonist is truly competitive and the pA_2 provides a measure of antagonist affinity, pK_B (Kenakin, 2014b).

1.7.3 Efficacy and mechanistic models

While the Schild method allowed the calculation of antagonist parameters, measurements of agonist parameters were more difficult. Furthermore, the discovery of partial agonism (Ariens *et al.*, 1954; Stephenson, 1956) demonstrated Clark's occupancy theory did not hold true and ligand responses were not directly proportional to receptor occupancy. Therefore, the concentration of agonist that produced a half maximal response on a concentration-response curve (EC_{50}) could not be assumed to be equivalent to its affinity for the receptor, as measured by K_A. To account for partial agonism, Stephenson defined efficacy as the ability of a ligand to produce a functional response, and separated this parameter from agonist binding affinity (Stephenson, 1956). This provided a theoretical framework to explain why partial agonists, despite full receptor occupancy, produced sub-maximal responses. Stephenson described ligand responses as a function of the 'stimulus' given to the tissue, the product of ligand efficacy (e) and proportion of occupied receptors – however this function was left numerically undefined.

The subsequent description of the two-state model by Del Castillo and Katz (Del Castillo *et al.*, 1957) provided a firmer description of efficacy. While it was originally described for ion channels, it was thought it could also provide a simple model for GPCRs:

$$A + R \underset{}{\overset{K_A}{\rightleftharpoons}} AR \overset{e}{\rightleftharpoons} AR^*$$

Under this model, the receptor transitions from an inactive (R) to active (R*) state. Affinity can be described by the initial binding of agonist (A) to the inactive receptor and efficacy is described by its ability to induce the R* state once bound. This empirical separation of affinity and efficacy has however been criticised (Colquhoun, 1998). As previously described (**1.4.2**), it is now appreciated that receptor activation involves conformational changes within the GPCR and the binding of G proteins. Ideally, affinity measurements would just determine the ability of ligand to bind to the receptor in its inactive state, with no change in receptor conformation. While some have argued that

addition of guanine nucleotide to binding experiments in GPCRs uncouples the receptor and thus provides a better measure of ligand affinity (Strange, 2008), this cannot exclude the receptor conformational changes induced following ligand binding. Instead, experimentally derived affinity (and efficacy) values are a function of all the underlying microscopic rate constants – not only the ability of the ligand to bind to the receptor, but the rate constants that govern the conformational changes within the receptor following ligand binding. Thus, ligand affinity and efficacy are intrinsically linked; most measurements of affinity will incorporate a degree of efficacy, with the affinity measurement encapsulating a range of receptor activation states. For more efficacious agonists, it is likely the contribution of efficacy to affinity measurements will be even greater (Colquhoun, 1998; Strange, 2008). However, these microscopic rate constants that govern the transitions between receptor states are not accessible experimentally and as such, cannot provide measures of ligand parameters.

Furthermore, for GPCRs, there is not only the receptor to consider but also the G protein. This led to the development of the ternary complex model (De Lean *et al.*, 1980) which incorporated the effect of G protein on the system. In this model, agonists promote the stabilisation of a ternary complex of agonist, receptor and G protein (ARG) which represents the activated receptor.

$$A + R \rightleftharpoons AR + G \rightleftharpoons ARG$$

However the discovery of constitutive activity (Costa *et al.*, 1989) revealed that receptors could adopt an active state in the absence of agonist. This lead to a reformulation of the model, known as the extended ternary complex model, to incorporate this phenomenon (Samama *et al.*, 1993).

$$\begin{array}{ccccc} \mathbf{AR + G} & \rightleftharpoons & \mathbf{AR^* + G} & \rightleftharpoons & \mathbf{AR^* G} \\ \Updownarrow & & \Updownarrow & & \Updownarrow \\ \mathbf{A + R + G} & \rightleftharpoons & \mathbf{A + R^* + G} & \rightleftharpoons & \mathbf{A + R^* G} \end{array}$$

Under this model, agonists promote stabilisation of the active, R* state whereas inverse agonists move the equilibrium towards the inactive, R state.

However, this model is thermodynamically incomplete, without fully describing the relationship between receptor and G proteins. In the extended ternary complex model, only activated receptors could interact with G proteins – but this interaction is also theoretically possible for inactive receptors. This is accounted for in the cubic ternary complex model (**Figure 1.5**) (Weiss *et al.*, 1996), which in theory allows inverse agonists to stabilise inactive ternary complexes, removing G proteins from the cellular pool and inhibiting the signalling of other active GPCRs. However this model also introduces further microscopic binding constants which cannot be measured experimentally, and thus limits practical application (Kenakin, 2014b). Furthermore, the subsequent discovery that receptors can adopt multiple active and inactive states (**1.6.3**) indicates that even the cubic ternary complex model is an incomplete model of receptor activation.

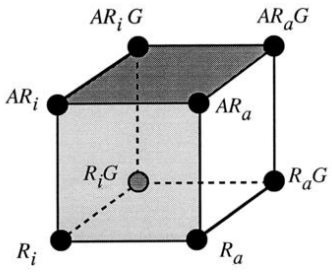


Figure 1.5: Cubic ternary complex model

In the cubic ternary complex model, the receptor can exist in 8 distinct receptor species, active (R_a) or inactive (R_i), bound to either ligand (A) or G protein (G) or both. *From (Weiss et al., 1996).*

1.8 Quantifying ligand parameters from functional data

1.8.1 Basic concentration response analysis

As previously discussed (**1.4.1**), receptor ligands are described by two key properties: affinity and efficacy. While binding experiments have made

affinity measurements accessible in the form of K_i values (the concentration of ligand which inhibits 50% of binding), quantifying efficacy has historically proven difficult. In theory, intrinsic efficacy (as introduced by Furchgott (Furchgott, 1966)) is a property of the ligand itself, a measure of its ability to activate a receptor, and should be independent of the system under measure. However what is actually measured as efficacy in functional assays is a more system dependent term, defining the overall ability of the ligand-receptor complex to initiate downstream signalling (Stott *et al.*, 2016). This makes deriving ligand parameters from functional data more complicated.

Ligand parameters are often derived through concentration response curve analysis from which the most basic and widely quoted values are the ligand maximum response (R_{max}) and potency (EC_{50}) (**Figure 1.6**). R_{max} is defined as the plateau of the ligand concentration response curve while EC_{50} is the concentration of ligand which produces a half maximal response, also known as potency (this and subsequent equations assume a unit Hill slope) (Strange, 2008).

$$E = \frac{R_{max}\,[A]}{[A] + EC_{50}} \tag{5}$$

Although these parameters can be useful for comparing ligands at a single signalling endpoint, they are highly system dependent and as such, do not provide good measures of agonist efficacy and affinity. Cell parameters such as cell type, receptor expression levels, accessory proteins and point in the signalling cascade significantly contribute to functional response and as such, comparisons across different assay systems must be done with care (Stott *et al.*, 2016). For high efficacy agonists especially, the system under measure can often limit their response, meaning that R_{max} is achieved with less than full receptor occupancy (known as receptor reserve). This can make a number of ligands appear equally efficacious (in terms of the system response generated) despite differing intrinsic efficacies, and can lead to the overestimation of partial agonist efficacy (Stott *et al.*, 2016; Strange, 2008). In reporter gene assays, and others with high receptor reserve (discussed

further in **Chapter Three**), low efficacy agonists may achieve the same maximum response as high efficacy agonists, by occupying proportionately more receptors such that they appear equally efficacious (Hill *et al.*, 2001; Stott *et al.*, 2016).

Ligand potency is an even more convolved parameter than R_{max}, dependent on the system parameters described above as well ligand efficacy and affinity. For highly efficacious agonists, and for highly coupled systems, agonist potencies can be far removed from their affinities. However, for assays with no receptor reserve, potency can be a good measure of ligand affinity. Under these conditions, it is assumed that the agonist response follows the proportional occupancy of the receptor (Stott *et al.*, 2016). In principle, β-arrestin recruitment assays, which rely on a 1:1 interaction between the receptor and β-arrestin, lack signal amplification. Studies with the μ-opioid receptor have shown that agonist EC_{50}s are well correlated with binding affinities calculated through both traditional radioligand competition binding assays and operational model fitting (discussed in **1.8.3**) (Nickolls *et al.*, 2011).

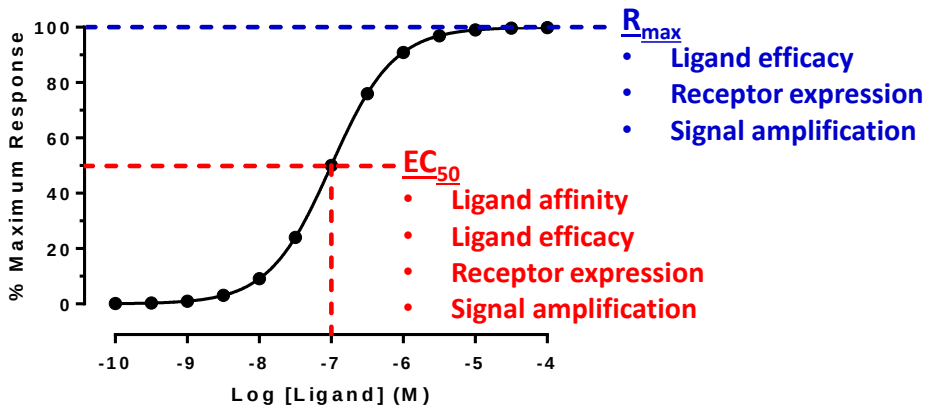


Figure 1.6: Basic concentration response curve analysis: ligand R_{max} and EC_{50} determinations

Basic concentration response curve analysis derives ligand maximal response (R_{max}) from the upper asymptote of the graph and potency (EC_{50}) values from the concentration of ligand that produces a half-maximal response. However, as shown above, these parameters are dependent on both ligand and system dependent properties.

1.8.2 The method of Furchgott to determine agonist affinity

Building on the work of Stephenson, Furchgott further developed the notion of efficacy. In Stephenson's original definition of efficacy, it was dependent on both the system and ligand. Furchgott described that efficacy is the product of ligand intrinsic efficacy, a property of the ligand itself, and total receptor concentration. He described a method to estimate agonist dissociation constants from functional data (Furchgott, 1966). This method involved generating agonist concentration response curves in the presence and absence of an irreversible antagonist, and plotting a double reciprocal plot of equiactive concentrations i.e. concentrations of agonist in absence and presence of irreversible antagonist which produced equal responses. He described the following relationship:

$$\frac{[A]}{[A]+K_A} = q\left(\frac{[A\prime]}{[A\prime]+K_A}\right) \quad (6)$$

Where [A] and [A'] are the equiactive concentrations of agonist in the absence and presence of irreversible antagonist respectively and q is the fraction of occupied receptors remaining after irreversible antagonist treatment. Rearranging this equation for a reciprocal plot gives:

$$\frac{1}{[A]} = \frac{1}{[A']} \text{ x } \frac{1}{q} + \frac{1}{K_A} \text{ x} \frac{1-q}{q} \quad (7)$$

From a linear plot of 1/[A] against 1/[A'], the K_A can be calculated as:

$$K_A = \frac{Slope-1}{y\ intercept} \quad (8)$$

Where the slope is equal to 1/q. While this method provided agonist dissociation constants, the necessary double reciprocal plot could magnify any errors in the data. More recently, analysis packages such as GraphPad Prism have allowed the use of non-linear regression to determine agonist parameters, which improves their accuracy (Dennis *et al.*, 1992; Morey *et al.*, 1998). However, while Furchgott provided a definition of intrinsic efficacy, his method still did not provide its measurement.

1.8.3 The Black and Leff operational model

In order to address the problem of quantifying agonist efficacy and affinity from functional concentration response data, a new type of analysis was required. Introduced in the 1980's, the Black and Leff operational model (Black *et al.*, 1983; Black *et al.*, 1985) built on traditional pharmacological theory to derive a new model that could better describe agonist parameters. Like traditional models, Black and Leff assumed that agonists bound to receptors according to the law of mass action, with the concentration of occupied receptors dependent on the total concentration of receptors (R_T) and agonist affinity (K_A) and concentration ([A]).

$$[AR] = \frac{R_T[A]}{K_A+[A]} \tag{9}$$

However, reports of partial agonists (Ariens *et al.*, 1954; Stephenson, 1956) and experiments with irreversible antagonists (Furchgott, 1966) demonstrated that were was a disconnect between receptor occupancy and response. Thus, a function was required which could translate this receptor occupancy into a pharmacological effect; it assumed this relationship was hyperbolic and as such, the relationship between agonist effect and occupied receptors was described:

$$E = \frac{E_{max}[AR]}{K_E + [AR]} \tag{10}$$

Agonist responses were dependent on the system maximal response (E_{max}), concentration of agonist occupied receptors ([AR]) and the concentration of agonist-receptor complex required to generate a half maximal response (K_E), a measure of how well coupled the system is.

Combining equations 9 and 10, and defining the transduction function, τ, as equal to R_T/K_E generates the operational model equation:

$$E = \frac{E_{max}\tau[A]}{K_A+[A](1+\tau)} \tag{11}$$

In this model, τ acts as a measure of efficacy, however it still remains an inherently system dependent parameter (Black *et al.*, 1983; Black *et al.*, 1985). Nonetheless, τ is progress from conventional R_{max} or EC_{50} comparisons as it should distinguish agonist efficacies even in a highly coupled system.

The operational model has 5 parameters, unlike the 4 parameters of standard concentration response analysis. This means they cannot be unambiguously defined by the fit to a single curve (Hall *et al.*, 2010). As such, data sets must be globally fit under conditions which vary τ. This is usually achieved by varying the receptor concentration, usually through treatment with irreversible antagonists in a method akin to the earlier work of Furchgott (Furchgott, 1966) (**Figure 1.7**). It has been shown that application of the operational model to agonist data in the presence and absence of an irreversible antagonist generates agonist dissociation constants comparable with the method of Furchgott. However, it also provides previously unobtainable efficacy estimations (Black *et al.*, 1985). Under these conditions, receptor alkylation removes receptor reserve, resulting in ligand potency equating to affinity. The definition of potency in the operational model is:

$$EC_{50} = \frac{K_A}{1+\tau} \tag{12}$$

Thus, when τ < 1 i.e. for low efficacy agonists or for full agonists whereby τ has been reduced due to a significant reduction in R_T, ligand potencies approach the equilibrium dissociation constant. This allows the model to solve for the remaining parameters. Furthermore, ligand maximal responses are defined by:

$$R_{max} = \frac{E_{max}\tau}{1+\tau} \tag{13}$$

Where τ is very large, agonist maximal responses approximate to the system maximal response. However when τ is very low i.e. for very low efficacy agonists (or poorly coupled systems – see **1.8.1**), R_{max} becomes proportional to τ and thus provides a measure of ligand efficacy.

Further work also modified the model to calculate the affinity and efficacy of partial agonists through global fitting with a full agonist. In this situation, the full agonist defines the system maximal response from which τ and K_A values for partial agonists can be derived (Leff *et al.*, 1993).

Despite the improvement from traditional R_{max} comparisons, τ is still an inherently system dependent parameter. Thus, there is still a need for quantitative approaches to derive ligand intrinsic efficacies (discussed further in **Chapter Five**). However, the operational model still provides a useful framework to derive agonist affinity and efficacy estimates, and in the determination of ligand bias, discussed below.

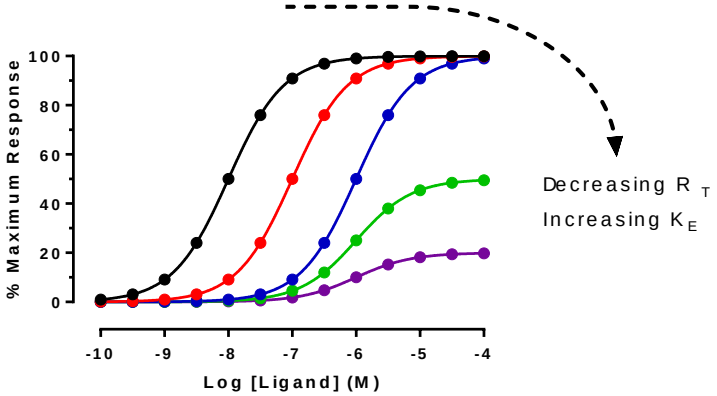


Figure 1.7: Example curve series required for modelling

Due to the number of parameters, operational models require global fitting of multiple data sets in order to derive parameters. Treatment with increasing concentrations of irreversible antagonist causes a successive decrease in available receptors, causing both a reduction in potency and decrease in maximal response. If there is no receptor reserve then there is no potency shift. The same effect can be achieved by increasing the concentration of GDP in a [^{35}S]-GTPγS binding assay (see **Chapter Five**). GDP competes with [^{35}S]-GTPγS for binding to G protein, reducing the signal coupling efficiency of the system and increasing the concentration of agonist-receptor complex required to produce a half maximal effect.

1.8.4 Expanding the use of the operational model: quantifying ligand bias

The identification of ligand bias (**1.6.3**) has highlighted the need to more accurately determine ligand efficacies for specific signalling pathways. The problem with identifying biased ligands is determining whether there are genuine variations in ligand efficacy between pathways, or if the observed differences are due to system dependent influences on signalling pathways. Two methods based on the operational model have been described to identify and quantify ligand bias; transduction ratios based on τ/K_A ratios (Kenakin *et al.*, 2010; Kenakin *et al.*, 2011) and bias factors from differences in effective signalling, based on τ ratios (Rajagopal *et al.*, 2011). However, the system dependency of τ previously described (**1.8.3**) still remains. As such, these ratiometric methods compare results to a reference ligand to normalise the system contributions.

In the bias factors (β) method (Rajagopal *et al.*, 2011), ligand τ values are derived from operational model fits whereby the K_A values have been fixed from separately conducted binding experiments. Effective signalling (σ) ratios are calculated for two signalling pathways (path1 and path2) as below, to calculate β; β significantly different from zero indicates bias.

$$\sigma_{lig} = \log\left(\frac{\tau_{lig}}{\tau_{ref}}\right) \quad (14)$$

$$\beta_{lig} = \left(\frac{\sigma_{lig}^{path1} - \sigma_{lig}^{path2}}{\sqrt{2}}\right) \quad (15)$$

For the transduction coefficients method (Kenakin *et al.*, 2010; Kenakin *et al.*, 2011), ligand bias is calculated from both τ and K_A values determined from operational modelling of the data. These are normalised against a reference ligand before the difference between two pathways is calculated. Transduction coefficients significantly different from zero indicate ligand bias.

$$\Delta log(\tau/K_A) = log(\tau/K_A)_{lig} - log(\tau/K_A)_{ref} \quad (16)$$

$$\Delta\Delta log(\tau/K_A)_{path1-path2} = \Delta log(\tau/K_A)_{path1} - \Delta log(\tau/K_A)_{path2} \quad (17)$$

$$bias = 10^{\Delta\Delta log(\tau/K_A)_{path1-path2}} \quad (18)$$

While both of these methods utilise the Black and Leff operational model, with responses normalised against reference agonist responses to reduce system influences, there is a key difference in the determination of the ligand affinity component. While the transduction ratios method directly determines ligand affinities from functional data, the bias factors method constrains the K_A of the operational model to the K_i from separately conduced binding experiments. These binding experiments are performed under conditions which limit the formation of the ternary complex thus allowing the empirical separation of efficacy and affinity parameters (Rajagopal *et al.*, 2011). This constraining of operational model fits has been widely discussed in the literature (Kenakin *et al.*, 2013a; Kenakin *et al.*, 2013b; Rajagopal, 2013). There are multiple potential issues with this approach; first, there is a need to match binding and functional experimental conditions in order to provide more accurate affinity determinations (Stott *et al.*, 2016). Furthermore, it has been demonstrated that a single ligand affinity value cannot always describe ligand behaviour; it has been postulated that the coupling of receptors to different effector proteins can alter the affinity of the ligand for the receptor (Kenakin, 2014a). Thus, it has been argued that ligand bias calculations should consider both efficacy and affinity as is described in the transduction ratios method (Kenakin, 2014a; Kenakin *et al.*, 2013a; Kenakin *et al.*, 2013b).

1.9 Aims of the thesis

The Black and Leff operational model is a well-established method to estimate agonist efficacy and affinity parameters; however, these estimations remain highly system dependent. More recently, the Slack and Hall modification of the operational model (Slack *et al.*, 2012) describes a model which in theory, allows the separation of system and ligand dependent parameters under conditions of measureable receptor constitutive activity. In this thesis, we explore the use of different operational models in the estimation of agonist parameters at the dopamine D2 receptor, with the aim to derive system independent measures of intrinsic agonist efficacy.

Chapter Three explores the pharmacology of a panel of dopamine D2 ligands at a SNAP-tagged D2L receptor. Agonist potencies and relative maximal responses are determined in two representative functional assays, receptor internalisation and CRE-SPAP reporter gene, which display differing levels of receptor reserve. The use of the receptor depletion method of the operational model is then explored, with an irreversible antagonist of the D2 receptor identified.

As receptor constitutive activity is needed for application of the Slack and Hall operational model, attempts are made to generate a constitutively active D2L receptor in **Chapter Four**. This mutant displays agonist-specific effects on functional potencies, hypothesised to result from distinct modes of binding to the D2L receptor. This is explored through mutagenesis of key binding site serine residues in both wild type and mutant backgrounds, to examine the mode of binding of a panel of agonists. This chapter also begins to address a key question surrounding whether mutant receptors can adopt the same active conformation as the wild type receptor.

Finally, **Chapter Five** explores the use of operational models to analyse [^{35}S]-GTPγS binding assay data, and the applicability of the Slack and Hall operational model to generate agonist affinities and intrinsic efficacies. Substitution of buffer Na^+ generates two assay systems in which constitutive

activity is either present or absent, which allows the application of the Slack and Hall and Black and Leff operational models respectively. A novel operational model derived specifically for the analysis of [^{35}S]-GTPγS binding is also explored. Affinity estimates generated are compared with those from traditional radioligand techniques and global fitting of data is discussed in regards to fitting data in two software packages: GraphPad Prism and Microsoft Excel.

Chapter Two: Materials and Methods

2.1 Materials

CHO-K1 cells stably expressing a CRE-SPAP reporter gene (CHO CRE-SPAP) were a kind gift from Professor Jillian Baker (University of Nottingham, UK). All tissue culture reagents were from Sigma-Aldrich (Gillingham, UK) except foetal calf serum (FCS) which was from PAA laboratories (Pasching, Austria). Tissue culture plastic ware was from Fischer Scientific (Loughborough, UK) while pcDNA 3.1(+)zeo vector, optiMEM, lipofectamine and zeocin were from Invitrogen (Paisley, UK). Buffer components and experimental reagents were purchased from Sigma-Aldrich, except boric acid (Fisher Scientific, Loughborough, UK). SNAP-Surface Alexa Fluor 488 was obtained from New England Biolabs (NEB; Ipswich, MA, USA).

Dopamine ligands were obtained from Tocris Bioscience (Bristol, UK) except for aripiprazole (Abcam, Cambridge, UK) and the following compounds from Sigma-Aldrich: N-Ethoxycarbonyl-2-ethoxy-1,2-dihydroquinoline (EEDQ), phenoxybenzamine (PBz), (S)-(−)-3-(3-Hydroxyphenyl)-N-propylpiperidine hydrochloride ((-)-3-PPP), R(+)-3-(3-Hydroxyphenyl)-N-propylpiperidine hydrochloride ((+)-3-PPP), (-)-butaclamol hydrochloride, (+)-butaclamol hydrochloride, R(−)-propylnorapomorphine hydrochloride (RNPA) and pergolide mesylate. Generally, compounds were stored as single-use aliquots, diluted in dimethyl suphoxide (DMSO) at -20°C except for (+)-butaclamol and (-)-butaclamol which were diluted in double distilled water (ddH_2O). Dopamine and RNPA stocks were freshly diluted on experiment day in ddH_2O containing w/v 0.1% ascorbic acid.

[^{3}H]-spiperone (73Ci mmol^{-1}) and [^{35}S]-GTPγS (1250Ci mmol^{-1}) were from PerkinElmer (Waltham, MA, USA). GF/B filter plates and back seals were from Millipore (U.K.) Limited (Watford, UK). Deep 1ml 96 well plates and black

sided, clear bottomed black plates (655090; imaging plates) were from Greiner Bio-one (Stonehouse, UK).

2.2 Molecular biology

The human dopamine D2L receptor cDNA (Genbank NM_000795) or human dopamine D2S receptor cDNA (Genbank NM_016574) were placed into an already made pcDNA3.1 (+) zeo vector containing the SNAP coding region (NEB). The pcDNA3.1 (+) zeo vector contains a human cytomegalovirus immediate-early (CMV) promoter for high expression in mammalian cells and a bovine growth hormone (BGH) polyadenylation signal for transcription termination and polyadenylation of mRNA. It also contains resistance genes for the antibiotics ampicillin and zeocin for selection in *E.coli* and mammalian cells respectively as well as the T7 and BGH reverse promoters for sequencing. The SNAP tag was placed into the multiple cloning site of this vector between the KpnI and BamHI restriction sites with the 5-HT_3 receptor signal sequence (amino acids MRLCIPQVLLALFLSMLTGPGEGSRK) placed upstream to facilitate membrane integration. The dopamine D2L or D2S receptors, both lacking their start codons, were placed downstream of the SNAP tag, between BamHI and XbaI restriction sites. The pcDNA3.1 (+) zeo SNAP and pcDNA3.1 (+) zeo SNAP-D2L constructs were made by Dr Nicholas Holliday (University of Nottingham; see **Figure 2.1** for plasmid map) and the pcDNA3.1 (+) zeo SNAP-D2S construct was made by Penny Ensor (University of Nottingham).

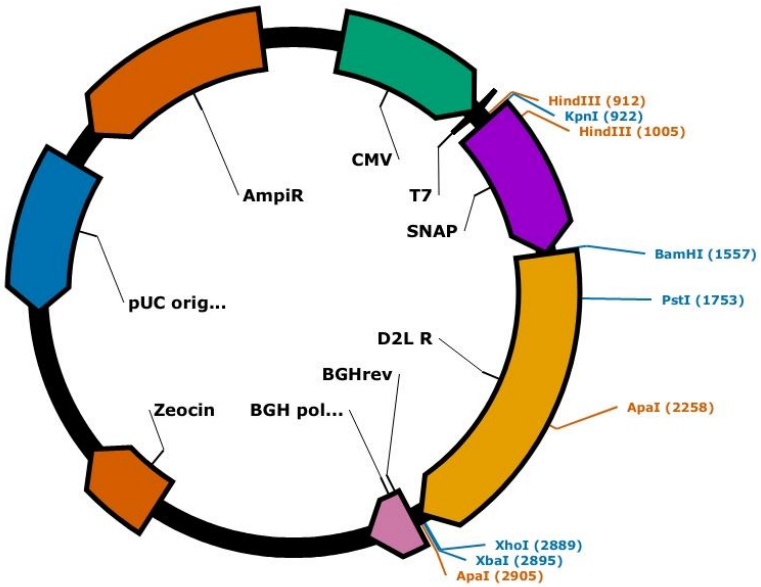


Figure 2.1: Plasmid map of pcDNA3.1 (+) zeo SNAP-D2L vector

In this vector, the dopamine D2L receptor (yellow) was placed into the multiple cloning site of a pcDNA3.1 (+) zeo vector between the BamHI and XbaI restriction sites. This vector also contained a SNAP tag (purple) upstream of the receptor, between KpnI and BamHI restriction sites. Other notable vector features, such as antibiotic resistance genes (orange) are shown.

2.2.1 Site-directed mutagenesis of the dopamine D2L receptor

To construct amino acid point mutations within the binding site or intracellular domains of the D2L receptor, a polymerase chain reaction (PCR) based mutagenesis approach was used. The principle of this technique is outlined in **Figure 2.2**. The entire vector was amplified using paired primers containing each desired mutation (primer sequences in **Table 2.1**). The template DNA was then digested using the enzyme DpnI, which selectively degrades methylated DNA. Only the template DNA, which had been isolated from a *dam* positive strain of *E.coli*, is methylated and thus degraded by DpnI. This leaves only the non-methylated, mutated plasmid DNA generated by PCR for transformation

Experimental and negative control PCR reactions contained (in a volume of 50µl): 50ng template DNA (pcDNA 3.1 (+) zeo SNAP-D2L), 125ng of both forward and reverse primers (custom synthesised by Eurogentec, Southampton, UK; **Table 2.1**), 5µl accuzyme buffer (final concentration: 60mM Tris-Cl, 6mM $(NH_4)_2SO_4$, 10mM KCl, 2mM $MgSO_4$, pH 8.3) and 200µM deoxynucleotides (dATP, dCTP, dGTP and dTTP). A Hotstart protocol heated reactions to 95^oC for 2min before being held at 60^oC to allow specific annealing of the primers prior to addition of Accuzyme (proof reading DNA polymerase; Bioline, London, UK) to the experimental PCR reaction. Subsequent PCR employed 16 cycles of denaturation (95^oC, 30sec), primer annealing (60^oC, 1min) and polymerase extension (68^oC, 11min) (**Figure 2.2**).

20µl PCR product was treated with 1µl DpnI (Thermo Fisher, Paisley, UK) for 2h at 37^oC to remove all methylated, parent DNA. 5µl of the digested reaction was used to transform competent cells as described in **2.2.2**. Successful amplification was confirmed by the presence of colonies from the experimental reaction, and the absence of transformed colonies on the negative control plate. Initially, two positive colonies were picked and grown as described in **2.2.3**. The presence of plasmid DNA was confirmed by

restriction digest and agarose gel electrophoresis (**2.2.4**, **2.2.6**). The presence of the mutation was identified with DNA sequencing (University of Nottingham sequencing facility) (**Figure 2.3**).

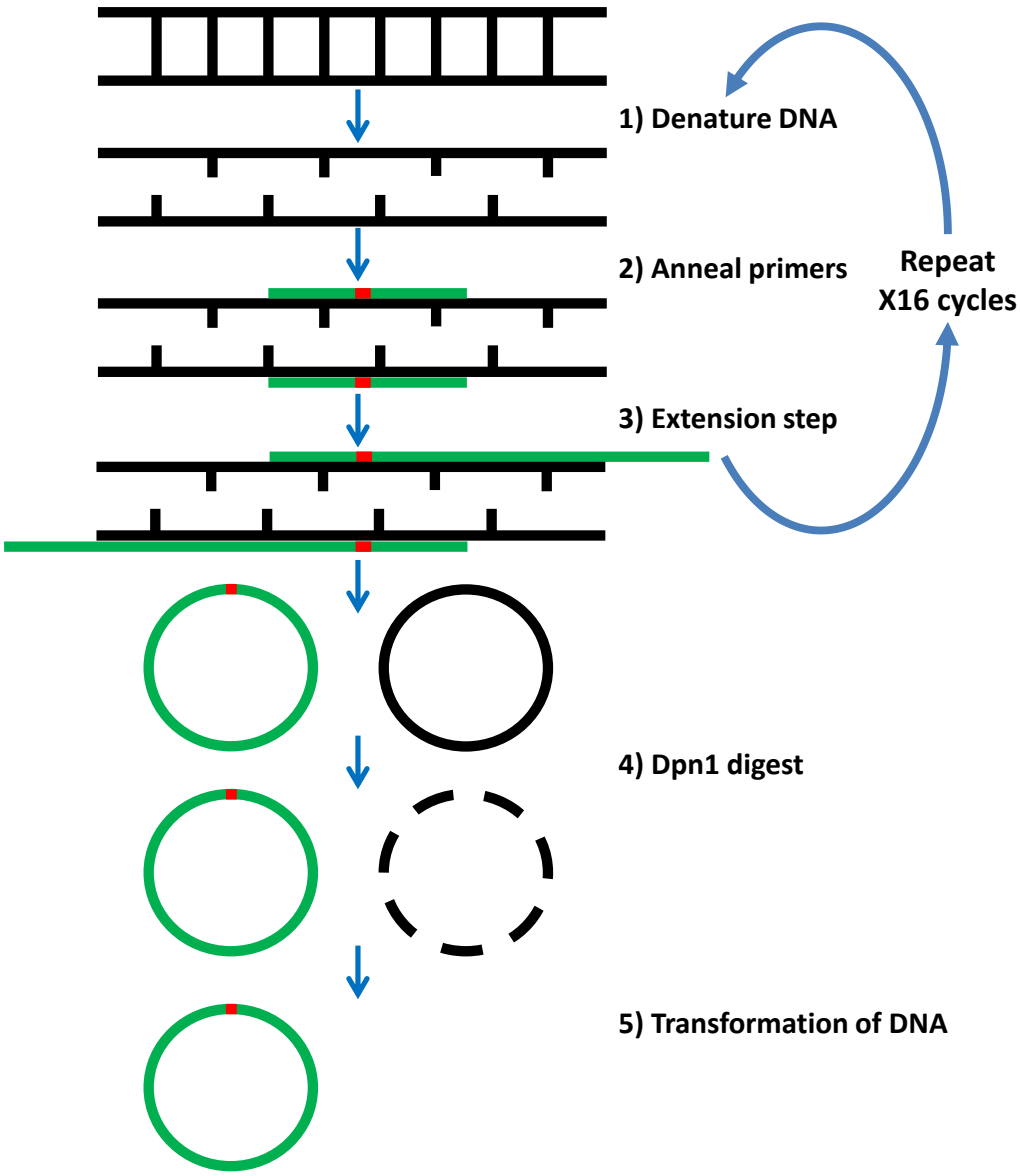


Figure 2.2: Site directed mutagenesis

To introduce point mutations in the D2L receptor, a PCR-based mutagenesis approach was utilised. The entire vector was amplified using paired primers containing the desired mutation. Methylated template DNA was then selectively digested using the enzyme DpnI, leaving intact the non-methylated amplified mutated plasmid DNA for transformation

Mutation	Primer	Sequence
T6.34R	Forward	5′ – GCAGAAGGAGAAGAAAGCC**AGG**CAGATGCTCGCCATTGTTCTCG
	Reverse	5′ – CGAGAACAATGGCGAGCATCTG**CCT**GGCTTTCTTCTCCTTCTGC
S5.42A	Forward	5′– GCCTTCGTGGTCTAC**GCC**TCCATCGTCTCCTTC
	Reverse	5′– GAAGGAGACGATGGA**GGC**GTAGACCACGAAGGC
S5.43A	Forward	5′– CCTTCGTGGTCTACTCC**GCC**ATCGTCTCCTTCTAC
	Reverse	5′– GTAGAAGGAGACGATGG**CGG**AGTAGACCACGAAGG
S5.46A	Forward	5′– GGTCTACTCCTCCATCGTC**GCC**TTCTACGTGCCCTTC
	Reverse	5′– GAAGGGCACGTAGAA**GGC**GACGATGGAGGAGTAGACC

Table 2.1: Summary of primer sequences for site-directed mutagenesis of the D2L receptor

Primer sequence summary, with mutations highlighted. Primers were complementary to the D2L sequence and designed to have the mutation central to the sequence, with 15-18 nucleotides either side and if possible, 2 G's or C's at the end to aid priming of the PCR polymerase. Mutation codon sequence was chosen for being the most common sequence in humans for that amino acid.

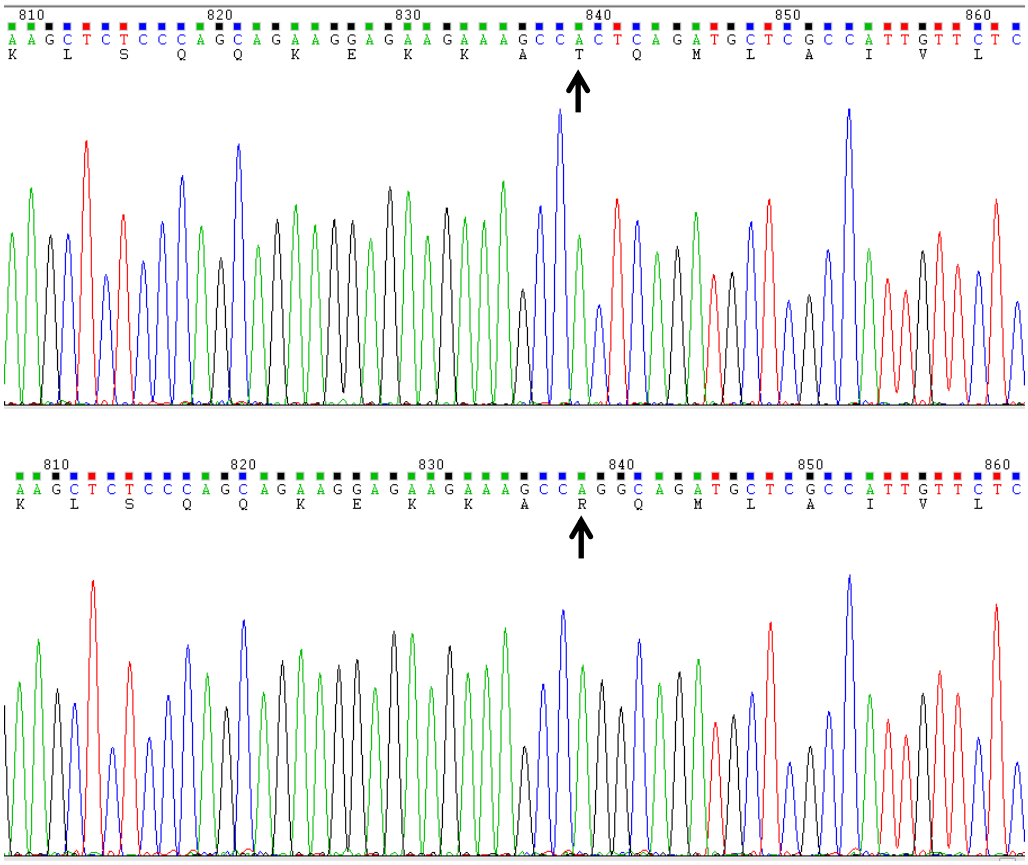


Figure 2.3: Example sequencing chromatogram files for D2L T6.34R mutation

Chromatogram files showing D2L sequence (residues 362-379) in both WT (top) and T6.34R (bottom) backgrounds with the mutation highlighted.

2.2.2 Bacterial transformation

Chemically competent cells from *E. Coli* strain XL-1 were prepared by Marleen Groenen (University of Nottingham) and stored in 500µl aliquots at -80°C until required for use.

Competent cells were defrosted on ice and 100µl cells added to the appropriate number of 1.5ml labelled microcentrifuge tubes on ice. 1.5µl of 1.43M β-mercaptoethanol solution was added to cells for 10min on ice. 5µl of DNA (either PCR reaction or ligation product) was then added to each tube of cells for 30min on ice. Following this, cells were heat-shocked for 45sec at 42°C to increase cellular DNA uptake. 400µl of sterile LB broth (20g l^{-1}) was added to each tube and cells incubated in a shaking incubator for 1h at 37°C. 150µl of cells were then spread onto LB agar (35mg ml^{-1}) plates containing antibiotic (75µg ml^{-1} ampicillin) and left to grow overnight at 37°C. Resistant colonies were then identified, derived from bacterial cells that had successfully taken up vector DNA containing the antibiotic resistance gene.

2.2.3 Miniprep

Resistant colonies were picked using a 200µl sterile pipette tip, which was then expelled into a universal containing 5ml LB broth containing 100µg ml^{-1} ampicillin. Miniprep cultures were then grown overnight in a shaking incubator at 37°C.

Minipreps were performed using a GenElute™ Plasmid Miniprep Kit (Sigma-Aldrich) according to the manufacturer's instructions. 3ml from the overnight bacterial culture was first pelleted by centrifugation at 3000rpm for 5min, with the remaining culture stored at 4°C. After removal of the supernatant, the pellet was resuspended in chilled 'resuspension solution' containing RNase to remove any RNA from the preparation. Alkaline lysis was performed with 'lysis solution' (NaOH / SDS), gently inverted to mix without shearing genomic DNA then 'neutralisation/binding solution' (potassium acetate) was added to precipitate cell debris and genomic DNA, while maintaining solubility of the plasmid DNA. After centrifugation (10min; 14,000rpm), the supernatant

was centrifuged through silica binding columns prepared with column preparation solution (12,000rpm; 30sec) discarding the eluate. 750µl of diluted 'wash solution' (80% v/v ethanol) was then added to the column and centrifuged (12,000rpm; 30sec), discarding the eluate, to remove residual salts and other contaminants. The binding column was centrifuged again (12,000rpm; 2min) to remove any remaining ethanol. The binding column was transferred to a new microcentrifuge tube, 100µl sterile ddH_2O added and then the column centrifuged (12,000rpm; 1min) to elute the plasmid DNA.

A small sample of DNA was sent off to the University of Nottingham sequencing facility to confirm the presence of the mutation (**Figure 2.3**).

2.2.4 Restriction digest of DNA

Once the presence of the mutation was confirmed, receptor DNA was transferred to a fresh pcDNA 3.1(+)zeo vector in case the PCR process had introduced any undesired mutations in the unsequenced vector.

First, both mutated D2L receptor DNA (insert) and fresh pcDNA 3.1(+)zeo vector were double-digested using the same restriction enzymes flanking the D2L receptor cDNA sequence – BamHI and XbaI (Thermo Fisher, Paisley, UK). DNA digests in sterile 0.5ml microcentrifuge tubes contained 2µg DNA, 2µl fast digest buffer and 1µl of each restriction enzyme, made up to 20µl with ddH_2O. For the insert digests, green fast digest buffer was used as it includes glycerol and dyes to allow direct loading of agarose gels. Digests were incubated for 1h at 37^oC to allow the enzymes to digest the DNA then heated for 5min to 80^oC and then cooled to 65^oC for 20min to inactivate the enzymes.

2.2.5 Alkaline phosphatase treatment of vector

Digested vector DNA was treated with shrimp alkaline phosphatase to dephosphorylate the vector DNA sticky ends. This helps prevent vector fragments re-ligating and giving high background colonies. To the digested vector mix, 2µl fast alkaline phosphatase (AP) buffer (final concentration: 10mM Tris-HCl, 5mM $MgCl_2$, 100mM KCl, 0.02% Triton X-100. 0.1mg ml^{-1}

bovine serum albumin (BSA); pH 8.0) and 2µl fast AP was added and incubated for 1.5h at 37°C. The reaction mixture was then heated to 75°C for 10min to inactivate the enzymes.

The vector DNA was then purified using the GenElute™ PCR Clean-up kit (Sigma-Aldrich) according to the manufacturer's instructions. Briefly, a collection tube was prepared by inserting a mini spin column into a 2ml collection tube, 500µl of 'column preparation solution' added and centrifuged (30sec; 12,000rpm). The eluate was discarded. To 20µl digested vector mix, 100µl (5x volume) of 'binding solution' was added and mixed by pipetting before transferring to a binding column. This was centrifuged (1min; 12,000rpm) and the eluate discarded before addition of 500µl 'wash solution' (80% v/v ethanol) and further centrifugation (1min; 12,000rpm). The eluate was discarded. The column was then centrifuged again at 12,000rpm for 1min to remove any excess ethanol. The binding column was then transferred to a fresh 2ml collection tube and 40µl ddH_2O added to the centre of the column. This was incubated for 1min to allow the DNA to dissolve before centrifugation (1min; 12,000rpm) to elute the DNA.

2.2.6 Separation of DNA digest by agarose gel electrophoresis

Agarose gel electrophoresis allows the separation of DNA fragments by size. An electric current is applied to the gel, causing the negatively charged DNA fragments to migrate towards the positive electrode. The speed at which they migrate is dependent on fragment size.

A 1% agarose gel was prepared by dissolving 400mg of agarose in 40ml TBE buffer (89mM Tris base, 89mM boric acid, 2mM EDTA; pH 7.6) and heated in a microwave for a 2min to facilitate the agarose going into solution. Once cooled for a few min, ethidium bromide (0.125µg ml^{-1}) was added then gel was poured and allowed to set. Ethidium bromide intercalates into DNA and fluoresces when exposed to ultraviolet (UV) light allowing the visualisation of

DNA bands. Once set, the gel was placed in an electrophoresis tank and covered in TBE buffer.

The digested DNA insert was loaded into the gel alongside 5µl of 1kb DNA ladder (Promega, Madison, WI, USA). Once loaded, the gel was run for 35-40min at 80v. Following this, the gel was illuminated using UV light in order to visualise the DNA bands (**Figure 2.4**). Using the DNA ladder as a guide, the appropriate DNA band was cut from the gel using a scalpel (~1.3kbp for D2L) and placed into a pre-weighed 1.5ml microcentrifuge tube. This was done as quickly as possible to avoid the UV light damaging the DNA.

DNA was then extracted from the gel using the GenElute™ Gel Extraction Kit (Sigma-Aldrich) according to the manufacturer's instructions. Briefly, 3 gel volumes of gel solubilisation solution was added to the gel slice and incubated at 60°C for 10min with vortexing, or until the gel was completely dissolved. A binding column was prepared by placing a binding column into a 2ml collection tube, adding 500µl of column preparation solution and centrifuging for 1min at 12,000rpm. Once the gel slice had completely dissolved, 1 gel volume of isopropanol was added and vortexed. This solution was then added to the binding column and centrifuged for 1min at 12,000rpm. The column was then washed by addition of 500µl diluted wash solution (80% v/v EtOh) and centrifuged (1min; 12,000rpm). The eluate was discarded, the binding column replaced in the collection tube and centrifuged again (1min; 12,000rpm) to remove any remaining ethanol. The binding column was transferred to a new collection tube, 40µl ddH_2O added to centre of the membrane and left to incubate for 1min. The DNA was then eluted by centrifugation (1min; 12,000rpm).

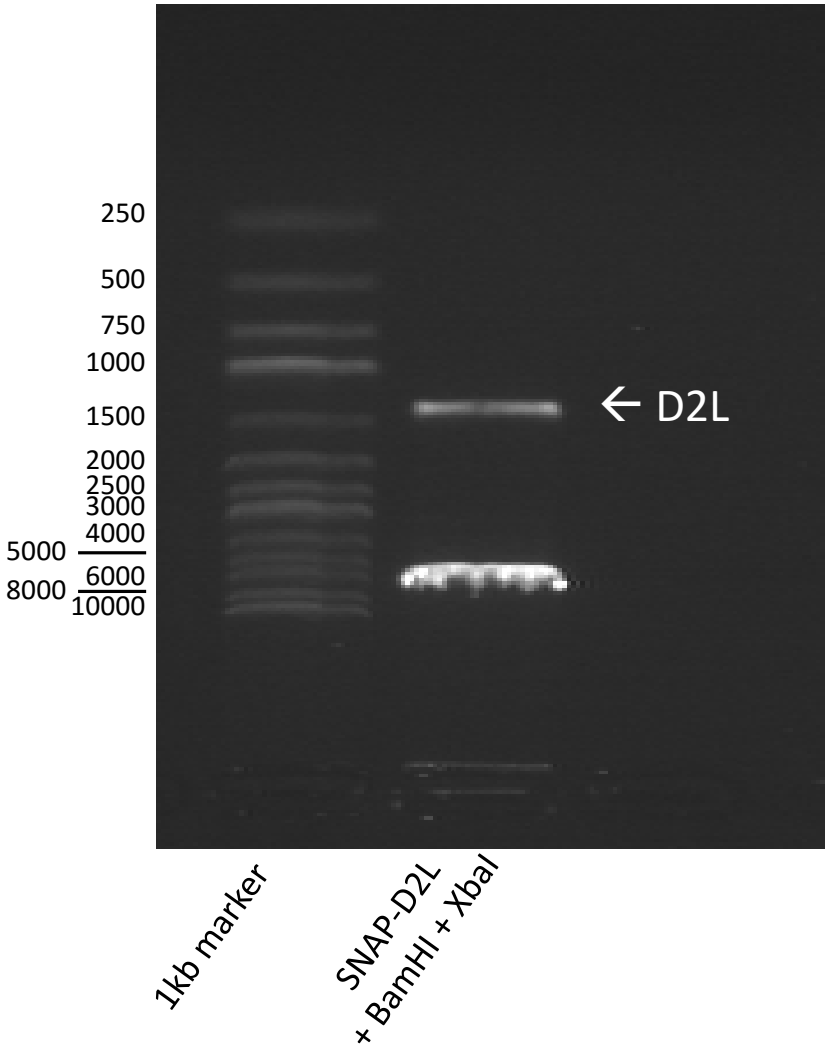


Figure 2.4: Representative example agarose gel showing digest of pcDNA3.1 (+) zeo SNAP-D2L

pcDNA3.1 (+) zeo vector containing the SNAP-tagged D2L (2µg) was digested with BamHI and XbaI (1h; 37°C) prior to inactivation of the enzymes. This treatment released the D2L fragment (~1.3kbp) as shown on the gel. The left hand lane contains the 1kb marker containing known fragment sizes that can be used to estimate the size of unknown fragments.

2.2.7 Ligation reactions

Once both insert and vector DNA were extracted and purified, overnight ligation reactions were set up to ligate the DNA. To increase ligation efficiency, the molar ratio of vector:insert was 1:3.

The volume of DNA required for each reaction was calculated as follows, assuming 80% yield of DNA from extractions and purification steps with 50ng vector in reactions deemed optimal:

$$Vector\ or\ insert\ DNA\ concentration = 2\mu g\ x\ \left(\frac{vector\ or\ insert\ size}{total\ original\ plasmid\ size}\right) x\ 0.8$$

$$Insert\ required\ (ng) = 3\ x\ \left(\frac{50}{\left(\frac{vector\ size}{insert\ size}\right)}\right)$$

The actual volumes of vector and insert required for each reaction were then calculated based on their concentrations and their required amount in reactions.

Positive and negative ligation reactions were set up containing appropriate volume of both vector and insert (negative reaction contained no insert), 1µl ligase buffer (final concentration: 40mM Tris-HCl, 10mM $MgCl_2$, 10mM dithiothreitol, 0.5mM ATP; pH 7.8), 1µl T4 DNA ligase, made up to a total of volume of 10µl with ddH_2O. Reactions were then incubated at 16°C for 16h.

Once completed, ligations were transformed (**2.2.2**) and positive clones picked, grown and miniprepped (**2.2.3**). To select a positive clone for maxipreps, restriction digests were performed on minipreps using the same restriction enzymes as before (BamHI and XbaI). Positive clones were identified by the presence of the D2L band using gel electrophoresis (**2.2.4**).

2.2.8 Maxiprep

In order to increase DNA yields for subsequent transfections, 200µl of stored miniprep culture containing the desired D2L plasmid DNA was grown for ~7h in 5ml LB broth containing 100µg ml^{-1} ampicillin in a shaking incubator at 37°C

to initiate the exponential phase of bacterial growth. Following this growth period, bacteria were transferred to 120ml LB broth containing 100µg ml^{-1} ampicillin and were grown overnight (12–16h) in a shaking incubator at 37°C.

The next day, bacteria were pelleted by centrifugation (4000g; 15min), the supernatant discarded and the pellet air dried. DNA was then extracted using GenElute™ Plasmid Maxiprep Kit (Sigma-Aldrich) according to the manufacturer's instructions, the principles of the method being the same as for miniprep isolation (**2.2.3**). 12ml of 'resuspension solution' containing RNAse A solution was added and the cells vortexed. Cells were lysed by addition of 12ml of 'lysis solution' and the contents immediately mixed. The mixture was left for 3-5min until it became clear and viscous but was not left longer than 5min to prevent damage to the DNA. Lysed cells were then neutralised with 12ml chilled 'neutralisation solution' and gently inverted causing a white aggregate to form. 9ml of 'binding solution', containing a chaotropic salt to promote DNA binding to silica, was added and the cells inverted twice before pouring the solution into a pre-prepared filter syringe. This was left to allow the aggregate to float to the top. 12ml of 'column preparation solution' was added to a binding column in a 50ml collection tube to increase DNA yield and centrifuged (2min; 3000rpm). Once the aggregate was floating, the cell lysate was filtered into the binding column and centrifuged (2min; 3000rpm), discarding the eluate. The column was washed with 12ml of 'wash solution 1' and centrifuged (2min; 3000rpm), discarding the eluate. It was then washed again with 12ml of 'wash solution 2' (80% v/v ethanol) and centrifuged (2min; 3000rpm), discarding the eluate. The centrifugation step was repeated with no wash solution to remove any remaining ethanol. The binding column was transferred to a fresh 50ml tube, 3ml elution solution added and centrifuged (5min; 4000rpm).

A further ethanol purification step was used to resuspend the vector DNA at the desired concentration (1µg $µl^{-1}$). The 3ml eluate was mixed with 7ml 100% ethanol and 300µl 3M sodium acetate (pH 5.2) and the precipitated DNA pelleted by centrifugation (10min; 4000rpm). The pellet was then washed by

addition of 2.5ml 70% ethanol and centrifuged (5min; 4000g). The ethanol was then removed and the pellet left to dry. The pellet was resuspended in TE buffer (10mM Tris base, 1mM EDTA; pH 8 with HCl) before calculation of the DNA concentration and sample purity (**2.2.9**). If the DNA was considered relatively free of contamination, its concentration was adjusted to 1µg μl^{-1} and stored at -20°C until required. A sample was sent to the University of Nottingham sequencing facility. When sequencing maxipreps where the DNA would be used to generate new cell lines, the DNA was fully sequenced using both forward and reverse primer sites flanking the vector multiple cloning site. For pcDNA 3.1(+)zeo SNAP-D2L vectors, these primer sites were T7 promoter (forward) and BGH reverse (reverse).

2.2.9 Calculation of DNA concentration and purity with UV spectrophotometry

DNA concentration was determined by measuring sample absorbance with a UV spectrophotometer at 260nm. At 260nm, the absorbance of 50ng ml^{-1} double stranded DNA will equal 1 AU, allowing the calculation of DNA concentration. Furthermore, the ratio of absorbances at 260nm and 280nm ($A_{260/280}$) provides information on sample purity because RNA also has a high absorbance at 260nm and the aromatic amino acids in proteins absorb strongly at 280nm. An $A_{260/280}$ ratio of 1.8 is considered optimal, with ratios of 1.7-1.9 accepted as being relatively free of contamination. A ratio of less than 1.7 indicates high protein contamination whereas a ratio of greater than 1.9 indicates high RNA contamination.

2.3 Cell Culture

2.3.1 Passaging

Cells were passaged at 80-100% confluency with split ratios of 1:2 – 1:20 depending on when they were required. Media (Dulbecco's Modified Eagle's Medium: Nutrient Mixture F-12 containing 10% v/v FCS and 2mM L-glutamine; DMEM/F12) was removed before cells were washed with sterile phosphate buffered saline (PBS). 1ml of trypsin-EDTA solution (Sigma-Aldrich)

was added and cells incubated for 3-5min at 37°C before knocking the flask to remove them from the plastic. The flask surface was washed with 10ml DMEM/F12 to dislodge any remaining cells, which were then collected and placed in a 30ml universal. Cells were pelleted by centrifugation (1000rpm; 5min) then the supernatant discarded. The cell pellet was then resuspended in 10ml of DMEM/F12 and split accordingly between required flasks or counted if the cells were being plated (see **2.3.2**).

2.3.2 Seeding

Cells were seeded a day in advance, except if a serum-starvation step was required (i.e. CRE-SPAP assay) where they were plated 2 days in advance. Cells were removed from flasks and centrifuged as above before resuspending in 20ml of DMEM/F12. A sample was then transferred to a haemocytometer to count the cells in a 5x5 1 mm^2 grid, with a depth of 0.1mm. The cell count within this volume (0.1µl) was multiplied by 10^4 to give the number of cells per ml i.e. 50 cells counted = $50x10^4$ cells ml^{-1}. When seeding 100µl into 96 well plates, seeding density (e.g. 20,000 ($20x10^3$) cells per well) is multiplied by 10 to give the number of cells per ml required (e.g. $20x10^4$ cells ml^{-1}).

The volume of cell suspension required was then calculated as below:

$$Volume\ of\ cell\ suspension\ required = \frac{No.of\ cells\ per\ ml\ required\ x\ volume\ required\ (ml)}{No.of\ cells\ counted}$$

The calculated cell suspension volume was then diluted in the final volume required to give the necessary seeding density. 100µl of the diluted cell suspension was then added to each well of a clear 96 well plate (for CRE-SPAP assays) or the inner 60 wells of an imaging plate (for receptor internalisation).

2.3.3 Freezing and thawing of cells

To freeze down, cells were removed from the flask and pelleted as previously described (**2.3.1**). Once pelleted, cells were resuspended in freezing media

(FCS containing 10% (v/v) DMSO), 2ml per 75cm^2 tissue culture flask (T75) and divided between two cryovials. Cells were placed in a freezing container (Nalgene® Mr. Frosty) containing isopropyl alcohol which, when placed in the -80°C freezer, cools the cells by 1°C per minute preventing cell damage from crystallisation. Following at least 24h at -80°C, cells were moved to liquid nitrogen dewars for long term storage.

Cells were defrosted from liquid nitrogen by warming cryovial in hand until the freezing mix had melted. Cells were then transferred into a T75 flask and left to grow overnight. The next morning, media was replaced with fresh DMEM/F12 to remove any DMSO and cells grown until confluent when they could be passaged as normal.

2.4 Generation of new cell lines

2.4.1 Transfection

CHO-K1 CRE-SPAP cells were grown to 50-60% confluence in 25cm^2 tissue culture flasks (T25). 2µg of DNA was added to 200µl optiMEM in a sterile 1.5ml microcentrifuge tube. This was added to a second microcentrifuge tube containing 200µl optiMEM with 9x DNA volume of lipofectamine (for example: DNA stock at 1µg ml^{-1} gives 2µl DNA with 18µl lipofectamine) and mixed by pipetting. These were combined for 45min at room temperature to allow the DNA and lipofectamine to form complexes. T25s were washed with 1ml optiMEM and media replaced with 1.2ml optiMEM. Following 45min incubation, 800µl of optiMEM was added to the 400 µl DNA:lipofectamine suspension, mixed by pipetting, and then the contents added to the cell media. Cells were grown overnight at 37°C/5% CO_2 to allow cells to take up DNA lipid complexes.

The next day, optiMEM was replaced by DMEM/F12 containing selection antibiotic (200µg ml^{-1} zeocin). Selection was continued for 2 weeks. Cells that have not taken up the vector DNA will not contain antibiotic resistance gene and should die off over the selection period. The media was replaced every few days to remove dead cells.

2.4.2 Dilution cloning

Following 2 weeks of selection pressure, cells were pelleted as described previously (**2.3.1**) and counted using a haemocytometer (**2.3.2**). Cells were then diluted to 10,000 cells ml^{-1} in media before further dilution in 20ml of selection-containing DMEM/F12 to 200 cells ml^{-1} and 20 cells ml^{-1}. 100µl of these dilutions were then added to each well of a clear bottomed 96 well plate to give 4 plates of cells. Following a week of growth, wells in which single individual colonies could be identified were marked and the media replaced. Once confluent in the 96 well plates, individual colonies of cells were washed with 100µl PBS, removed from the plate with 50µl trypsin-EDTA solution and added to individually marked wells of a 24 well plate containing 2ml of selection antibiotic-containing DMEM/F12 (50µg ml^{-1} zeocin). At this point, cell samples (2 x 100µl samples) were also transferred to imaging plates.

2.4.3 Clone screening and selection

Once confluent, imaging plates from dilution cloning were screened for receptor expression by monitoring SNAP-surface labelling. Cells were labelled in DMEM/F12 for 30min with 0.1µM SNAP-surface benzyl guanine AF488 prior to treatment with vehicle or 10µM quinpirole for 1h. Cells were then fixed, washed, stained and imaged as in **2.7.2**.

Of the cells which displayed positive SNAP labelling, 4 were picked which showed homogenous SNAP labelling (suggesting a clonal population) and an appropriate morphology. These clones were grown in T75s and re-screened for activity in the CRE-SPAP reporter gene assay (**2.7.1**) to determine if they also showed robust intracellular signalling. Of these, the clone with the best cell surface expression and signalling characteristics was chosen for further experiments. Other positive clones were frozen down when confluent either in the 24 well plate or from T75 flasks to be re-visited if necessary (as described in **2.3.3**).

2.5 Membrane preparation

2.5.1 Preparation of membranes

Cells were grown to confluence on 500cm^2 square trays (Corning 431110; NY, USA) and washed with PBS before scraping into 10ml of chilled membrane prep buffer (50mM HEPES, 1mM EDTA, 0.1mM 4-(2-Aminoethyl) benzenesulphonyl fluoride hydrochloride (AEBSF); pH 7.4 with KOH). Cells were centrifuged (1500g; 10min; 4°C) to pellet the cells and the supernatants discarded. Cell pellets were frozen at -80°C until membranes were prepared.

For the membrane preparation, all samples were kept on ice between steps to help prevent protein degradation. Membranes were prepared by first thawing the cell pellet before resuspending it in 15ml of chilled membrane prep buffer. Cell suspensions were homogenised using an Ultra-Turrax in 8x 2sec bursts. The homogenised suspensions were centrifuged (1500g; 20min; 4°C) to pellet nuclei and unbroken cells. The supernatants were then transferred to high-speed centrifuge tubes and centrifuged (41,500g; 30min; 4°C) to isolate cell membranes. The supernatant was discarded and the membrane pellet resuspended in membrane prep buffer in a volume approximately 4x volume of the original cell pellet. Pellets were resuspended by first pipetting with a 1ml pipette to both lift the pellet from the centrifuge tube and begin to break it up before transferring to a glass tube. The membranes were then resuspended by 20 strokes of a dounce homogeniser. Membrane concentration was calculated (**2.5.2**) before membranes were aliquoted into microcentrifuge tubes and stored at -80°C until required.

2.5.2 Protein concentration determination

Protein concentration was determined using the Pierce^{TM} BCA (Bicinchoninic acid) Protein Assay Kit according to the manufacturer's instructions using BSA as a standard. In the BCA assay, Cu^{2+} is reduced to Cu^{+} by peptide bonds under alkaline conditions, with the amount of Cu^{+} produced proportional to the protein concentration. Cu^{+} chelates with BCA to form a purple complex which strongly absorbs light at 562nm (Smith *et al.*, 1985).

BSA standards were diluted in membrane prep buffer to give a concentration range of 0.125mg ml^{-1} – 2mg ml^{-1} to generate the standard curve and 25µl of each standard added, in triplicate, to a clear 96 well plate. Membranes were then diluted 1:3 and 1:5 before being added to the plate in triplicate alongside an undiluted sample. BCA working reagent was then prepared by mixing 50 parts of BCA Reagent A with 1 part of BCA Reagent B and 200µl of this added to each well. The plate was then incubated for 30min at 37°C before measuring absorbance at 562nm on a MRX plate reader (Dynatech Labs, Chantilly, VA).

The absorbance values for the standards were plotted to give a standard curve from which membrane protein concentrations could be interpolated from their absorbance values. Absorbance values out with the range of the standard curve were not used.

2.6 Binding assays

2.6.1 [^{3}H]-spiperone binding – saturation

Membranes were diluted down to 5-10µg protein per well (**Table 2.2**) in [^{3}H]-spiperone binding assay buffer. D2L and D2L T6.34R binding assays were conducted in sodium free buffer (20mM HEPES, 1mM EDTA, 1mM EGTA, 6mM $MgCl_2$; pH 7.4 with KOH to prevent addition of Na^{+} to assay buffer). D2S binding assays were conducted in either sodium containing (20mM HEPES, 1mM EDTA, 1mM EGTA, 6mM $MgCl_2$, 100mM NaCl; pH 7.4 with NaOH) or NMDG-containing (20mM HEPES, 1mM EDTA, 1mM EGTA, 6mM $MgCl_2$, 100mM NMDG; pH 7.4 with HCl) [^{3}H]-spiperone binding assay buffer. Membranes were added to deep well 96 well plates containing ~15pM-1500pM [^{3}H]-spiperone, in the absence or presence of 3µM (+)-butaclamol to determine total and non-specific binding (NSB). Following a 3h incubation at room temperature (~21°C) with shaking, plates were filtered using PerkinElmer FilterMate Harvester onto 96 well GF/B filter plates followed by a 2ml cold PBS wash. Plates were allowed to dry before addition of 40µl scintillation fluid (MicroScint-20; PerkinElmer) to each well. Top and back

seals were applied before plates were read on a TopCount Scintillation counter on a [^{3}H]-isotope protocol.

Actual concentrations of spiperone were determined by adding an equal volume of [^{3}H]-spiperone to scintillation vials with 5ml of scintillation fluid (Ultima Gold XR; PerkinElmer) and counting on TriCarb on a [^{3}H] protocol. Radiation counts in disintegrations per minute (dpm) were converted to give the concentration of radioligand using the specific activity (SA) of the radioligand according to the following formula:

$$Moles\ radioligand\ added = \frac{Counts\ (dpm)}{\left(\frac{SA(Ci\ mmol^{-1})}{2.2\ x\ 10^{12}} x\ 1000\right)}$$

2.6.2 [^{3}H]-spiperone binding – competition

Membranes were diluted down to 10-20µg protein per well (**Table 2.2**) in [^{3}H]-spiperone binding assay buffer (D2L, D2L T6.34R - sodium free; D2S - both sodium and NMDG containing) and added to deep well 96 well plates containing increasing concentrations of ligand and ~100pM [^{3}H]-spiperone. Here, and in all subsequent assays, dopamine, RNPA and apomorphine dilutions were conducted in the presence of 0.1% ascorbic acid to prevent oxidation of the compounds. NSB binding was determined in the presence of 3µM (+)-butaclamol. Plates were incubated with shaking for 3h at room temperature and filtered, washed and read as in **2.6.1**.

2.6.3 [^{35}S]-GTPγS binding assays

Membranes were diluted down to 10µg protein per well in either sodium containing (20mM HEPES, 10mM $MgCl_2$, 100mM NaCl; pH 7.4 with NaOH) or NMDG containing (20mM HEPES, 10mM $MgCl_2$, 100mM NMDG; pH 7.4 with HCl) [^{35}S]-GTPγS buffer as indicated. They were added to deep well 96 well plates containing increasing concentrations of ligand for 1h at room temperature. Following 1h incubation, [^{35}S]-GTPγS was added to give a final concentration of 200pM. The volume of [^{35}S]-GTPγS added was altered to

account for the decay of the radioisotope with the SA on experiment day calculated according to the following equations:

$$D_F = 10^{-\frac{(assay\ date - reference\ date) x\ 0.693}{half\ life}}$$

$$SA = \frac{D_F}{\frac{1}{SA\ cal} - \frac{(1 - D_F)}{SA\ Theo}}$$

Where D_F is the fraction of radioactivity remaining, SA is the specific activity expressed as Ci mmol^{-1}, SA cal is the SA on calibration date, SA Theo is the theoretical specific activity of carrier free ^{35}S which is equal to 1498Ci mmol^{-1}.

Following a further 20min incubation at room temperature, plates were filtered, washed and read as in **2.6.1** except that plates were read using the available ^{14}C protocol, equivalent in emission energy to ^{35}S protocol.

Cell line	Saturation Binding	Competition Binding
CHOcs ssD2L	5µg	7.5µg
CHOcs ssD2L T6.34R	10µg	20µg
CHOcs ssD2S	5µg	10µg

Table 2.2: Membrane concentrations used in [^{3}H]-spiperone binding assays
Summary of the membrane concentrations used for each cell line for both saturation and competition [^{3}H]-spiperone binding experiments. CHOcs ssD2L T6.34R membranes were added at higher concentrations to maintain signal window with the reduced receptor expression.

2.7 Functional assays

2.7.1 CRE-SPAP reporter gene assay

The CRE-SPAP reporter gene assay is a downstream measure of cAMP production (as described in **3.1.1**). Cells were seeded at 25,000 cells per well 2 days before experiment on clear 96-well plates and serum starved in DMEM/F12 containing 2mM L-glutamine without FCS (SFM) 20h prior to experiment. For pertussis toxin (PTx) experiments, cells were serum starved for 20h in PTx-containing (100ng ml^{-1}) SFM.

On experiment day, media was replaced with fresh SFM. Cells were ligand treated in SFM for 1h at required concentrations and incubated at 37°C/5% CO_2 prior to addition of 3µM forskolin unless otherwise indicated. Where used, antagonist was added for 30min prior to a 30min agonist and antagonist co-incubation unless stated otherwise. For PBz and EEDQ irreversibility experiments, paired plates were treated with either 10µM EEDQ or 3µM PBz for 10min, 30min or 60min. Following this pre-incubation, one of the paired plates for each antagonist was washed to remove antagonist prior to quinpirole and subsequent forskolin treatments.

Following a 5h co-incubation of ligand and forskolin, media was replaced with 40µl fresh SFM and incubated at 37°C/5% CO_2 for a further hour. Plates were then incubated at 65°C for 30min to destroy any endogenous phosphatases. 100µl of 5mM *para*-nitrophenol phosphate (PNPP) in diethanolamine (DEA) buffer (10% v/v DEA, 280mM NaCl, 0.5mM $MgCl_2$; pH 9.85 with HCl) was then added to each well for 20min at 37°C/0% CO_2. SPAP activity was measured through the colour change induced by the hydrolysis of PNPP to yellow *para*-nitrophenol (PNP); this was quantified by measuring absorbance at 405nm on a Dynatech MRX plate reader.

2.7.2 Receptor internalisation

Receptor internalisation was measured using the SNAP-tag system (described in **3.1.2**). Cells were seeded on imaging plates at 20,000 cells per well the day before the experiment. On experiment day, cells were incubated for 30min in

0.1µM membrane impermeant SNAP-surface benzyl guanine-AF 488 in complete media at 37°C/5% CO_2. Plates were washed with HEPES buffered saline solution (HBSS: 10mM HEPES, 2mM sodium pyruvate, 146mM NaCl, 5mM KCl, 1mM $MgSO_4$, 1.7mM $CaCl_2$, 1.5mM $NaHCO_3$, 5mM D-glucose; pH 7.45 with NaOH) before addition of ligand at required concentrations and incubated for 1h at 37°C/0% CO_2. Where used, antagonists were added for 30min prior to ligand incubation. For time course experiments, ligands were added at decreasing time points as indicated prior to fixation.

Cells were fixed for 15min with 100µl 3% paraformaldehyde in PBS at room temperature before washing with 100µl PBS. They were then incubated at room temperature with 100µl 2µg ml^{-1} Hoechst 33342 (H33342: nuclear stain) for 15min and then the solutions replaced with 100µl PBS. Plates were then imaged at 4 sites per well using an IX Ultra confocal plate reader (Molecular Devices, San Diego, CA, U.S.A.) equipped with a Plan Fluor 40x NA0.6 extra-long working distance objective and 405/488 nm laser for H33342 and SNAP fluorophore excitation respectively.

2.7.3 Quantification of receptor internalisation with granularity algorithm

Receptor internalisation was quantified through an automated granularity algorithm (MetaXpress 5.01, Molecular Devices) which identified fluorescent internal cell 'granules' of internalised receptor fluorescence of diameter 6-10µm (**Figure 2.5**). Granules were identified based on a set area of pixel brightness above a specified threshold grey level count. Thresholds were set on each experiment individually using positive (10µM quinpirole) and negative controls (vehicle) to maximise signal window. This algorithm also identified nuclei of 7-12µm in diameter which allowed the analysis to generate a granule count per cell. Each individual experimental data point represents a mean granule count of at least 8 images (4 sites per well in duplicate or triplicate). For pooled data sets, granule count was normalised to 10µM quinpirole (100%) and vehicle (0%) controls.

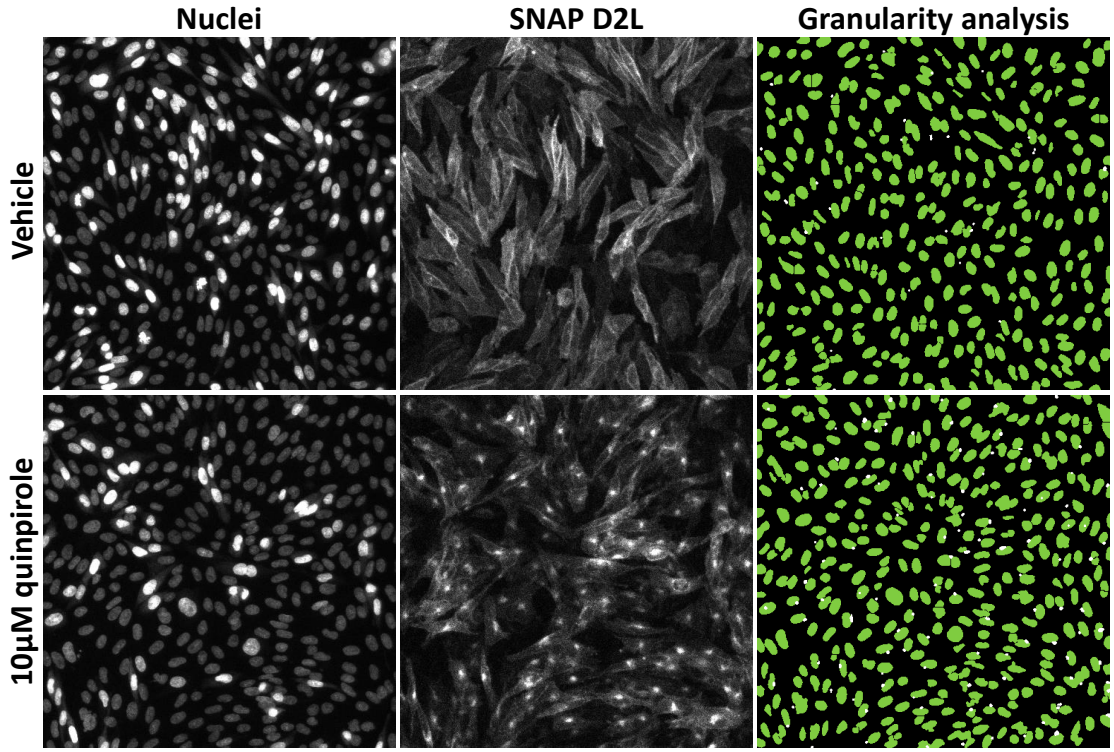


Figure 2.5: Representative granularity analysis images
Representative images of vehicle and 10µM quinpirole treated (1h, 37°C) CHOcs ssD2L cells. The left hand panel shows H33342 stained nuclei, the middle panel labelled SNAP-tagged D2L fluorescence and right hand panel the associated granularity analysis; nuclei are in green and internalised receptor spots of 6-10µm in white. Thresholds were set to maximise signal window between vehicle and 10µM quinpirole, minimising the detection of plasma membrane localised fluorescence as granules (some examples of this present in the vehicle analysis). Treatment with 10µM quinpirole markedly increases the number of white spots associated with internalised receptor, predominantly present in perinuclear compartments, allowing the quantification of receptor internalisation.

E_{max}	Maximum system response
R_{max}	Maximum ligand response
EC_{50}	Concentration of ligand which produces half maximal response; potency
n	Hill slope
K_A/ K_B/ K_D/ K_i	Equilibrium dissociation constant of the ligand-receptor complex; concentration which occupies half the receptors
IC_{50}	Concentration of ligand which produces half maximal inhibition
[A]/[L]/[B]	Concentration of agonist / ligand / antagonist
K_E	Concentration of agonist–receptor complex required for half maximal response; stimulus coupling efficiency
R_T	Total receptor concentration
τ	Transducer function
ε	Ligand intrinsic efficacy
χ	System coupling efficiency
K_{GDP}	Apparent affinity of GDP
[GDP]	Concentration of GDP
CR	Concentration ratio; the ratio of the concentrations of agonist required to give an equi-efficacious response in the absence and presence of antagonist

Table 2.3: Definition of equation parameters

List of the most commonly used parameters in data analysis section.

2.8 Data analysis

All data were analysed using GraphPad Prism v6.04 (GraphPad software, San Diego CA, U.S.A) using pre-programmed equations, except for the Slack and Hall and GDP dependence operational models which were coded as custom equations in the program. Microsoft Excel was used to re-analyse Slack and Hall and GDP dependence operational model data as described in **2.8.10**. Parameters used in the equations below are summarised in **Table 2.3**.

Operational models were fit with n constrained to one as a result of GraphPad Prism co-variance analysis showing high co-variance between parameters in Slack and Hall operational model fits. This high co-variance could be markedly reduced by constraining n to 1.

2.8.1 Agonist concentration response analysis

Concentration response curves were analysed according to the following equation:

$$Response = \frac{R_{max}\,[A]^n}{[A]^n + {EC_{50}}^n}$$

Where R_{max} is the maximal agonist response, [A] is the concentration of agonist, EC_{50} is the concentration of agonist which produces a half maximal effect and n is the Hill slope.

For SPAP data, individual experiment data were normalised to 3μM forskolin (100%) and vehicle (0%) responses. For internalisation data, data were normalised to a 10μM quinpirole (100%) and vehicle (0%) responses.

2.8.2 Gaddum equation

Where agonist concentration response curves were generated in the presence of a single concentration of antagonist, the Gaddum equation (Gaddum, 1937) was used to determine the antagonist affinity (K_D):

$$CR = \frac{[A']}{[A]}$$

$$K_D = \frac{[B]}{CR - 1}$$

Where [B] is the concentration of antagonist used and CR is the concentration ratio; the ratio of the concentration of agonist required to give an equi-efficacious response in the absence ([A]), and presence ([A']) of antagonist (see **Figure 2.6**).

2.8.3 Schild analysis

When agonist concentration responses curves were generated in the presence of multiple concentrations of antagonist, Schild analysis (Arunlakshana *et al.*, 1959) was used to determine the antagonist affinity. For Schild analysis, graphs of log [B] against CR-1 were plotted and log K_D determined from the x-intercept of the graph. The slope of the line, the Schild slope, should equal unity if the assumptions of competitive reversible antagonism at equilibrium are met.

$$pK_D = Log\ (CR - 1) - Log\ [B]$$

2.8.4 Competitive method for partial agonists

In the instances where partial agonism was observed, in ligands that also antagonised a full agonist response, the affinity of the partial agonist was estimated with the method of Stephenson (Stephenson, 1956).

$$Y = \frac{[A2] - [A1]}{[A3]}$$

$$K_D = \frac{Y\ [P]}{1 - Y}$$

Where [A1] is the concentration of full agonist where the CRCs of the full agonist alone and the full agonist in the presence of the partial agonist intersect; [A2] is the concentration of full agonist alone which produces a given response; [A3] is the agonist concentration which produces a given response (equivalent to A2) in the presence of a fixed concentration of partial agonist (see **Figure 2.7**) and [P] is the partial agonist concentration.

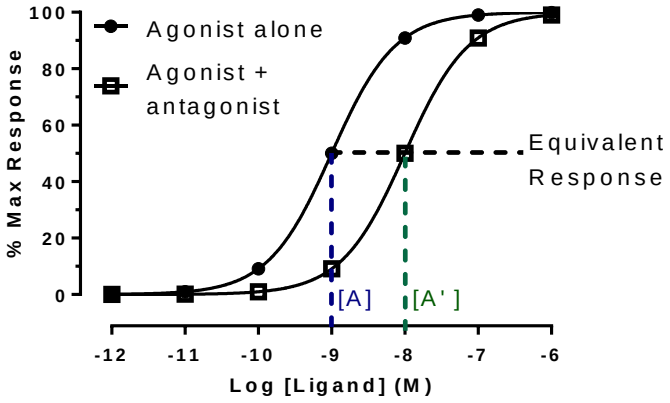


Figure 2.6: Representation of parameters for Gaddum and Schild analysis

The simulated dataset above demonstrates how the dose ratio ([A']/[A]) can be calculated from equivalent responses.

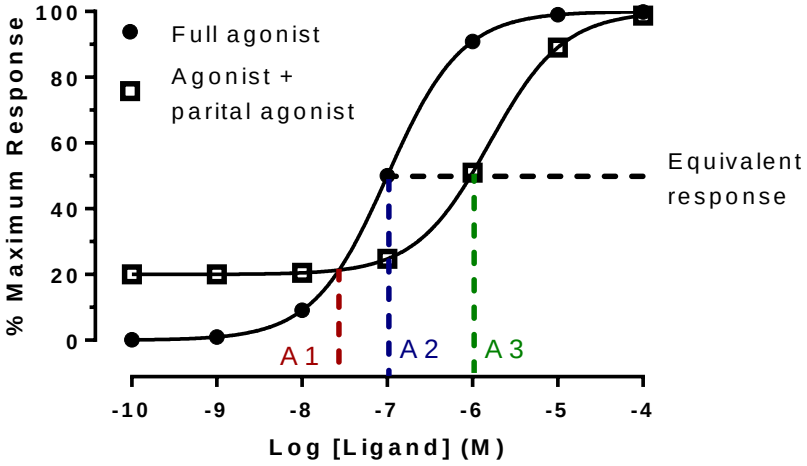


Figure 2.7: Representation of parameters for Stephenson analysis

The above simulated dataset demonstrates how the [A1], [A2] and [A3] are derived from agonist CRCs.

2.8.5 Saturation binding data analysis

Saturation binding data were globally fit to the following two equations:

$$Total\ Binding = \left(\frac{B_{max}[L]}{[L] + K_D}\right) + (NS\ [L]) + Background$$

$$Non - Specific\ Binding = (NS\ [L]) + Background$$

Where B_{max} is the maximal specific binding, [L] is concentration of radioligand, NS is the slope of the linear non-specific binding and background represents the counts in the absence of radioligand.

B_{max} was converted to a receptor concentration in pmol mg^{-1} using the known SA of the radioligand and the following equations. The counts in dpm from the data fits were converted to Bq by dividing by 60 (1Bq = 60 dpm).

$$Moles\ radioligand = \frac{\frac{B_{max}(dpm)}{60}}{S.A.\ (GBq\ mmol^{-1})}$$

$$Receptor\ concentration = \frac{moles\ radioligand}{protein\ added}$$

2.8.6 Competition binding data analysis

Specific [^{3}H]-spiperone binding was determined by normalising counts using NSB as 0% and total binding as 100%. Data were fitted to either one-site or two-site binding models depending on the absence or presence of both high and low affinity binding sites. Models were compared using an extra sum of squares F-test in GraphPad Prism to determine the most suitable fit. IC_{50}s from these fits were converted to ligand pK_is using the Cheng-Prusoff correction (Cheng *et al.*, 1973):

$$K_i = \frac{IC_{50}}{1 + \frac{[L]}{K_D}}$$

Where K_i is the affinity of the test ligand, IC_{50} is the concentration of test compound which inhibits 50% of [^{3}H]-spiperone binding, [L] is the concentration of [^{3}H]-spiperone (calculated as described in **2.6.1**) and K_D is the affinity of [^{3}H]-spiperone as calculated by saturation binding.

2.8.7 The Black and Leff operational model

To derive ligand affinity (K_A) and efficacy (τ) estimations, data were fitted to the Black and Leff operational model (**1.8.3**) (Black *et al.*, 1983; Black *et al.*, 1985):

$$E = \frac{E_{max}\tau[A]}{K_A + [A](1 + \tau)}$$

$$\tau = \frac{R_T}{K_E}$$

Where τ is the transducer function, [A] is the concentration of agonist, K_A is the agonist dissociation constant, R_T the total receptor concentration and K_E the concentration of agonist–receptor complex required for half maximal response. The inbuilt equation was modified to globally fit all data sets with E_{max} and basal shared across all data sets, K_A shared within each agonist data set and τ allowed to vary freely.

2.8.8 The Slack and Hall operational model

For the analysis of a constitutively active system, the Slack and Hall operational model was applied (**5.1.4**) (Slack *et al.*, 2012).

$$E = \frac{E_{max}\chi(K_A + \varepsilon[A])}{(K_A + [A]) + \chi(K_A + \varepsilon[A])} + basal$$

Where χ is the system coupling efficiency, ε is the agonist intrinsic efficacy and basal is the constitutive receptor signal in the absence of agonist. When analysing the [^{35}S]-GTPγS binding data sets, the equation was set up to globally fit the data sets as follows; E_{max} and basal were shared across all data sets, K_A and ε within agonist data sets and χ shared across GDP concentrations

2.8.9 GDP Dependence operational model

In order to reduce the system dependence from the τ parameter, [^{35}S]-GTPγS binding assays were conducted in the presence of multiple concentrations of GDP and fit to a novel GDP dependence operational model (**5.1.4**):

$$E = \frac{E_{max}\tau_0[A]}{(K_A + [A])\left(\left(1 + \frac{[GDP]}{K_{GDP}}\right)^s\right) + \tau_0[A]}$$

Where τ_0 is the transducer ratio in the presence of no GDP, [GDP] is the assay concentration of GDP, K_{GDP} is the apparent affinity of GDP for the receptor, s is the slope of this response and other parameters are as previously described. The data were globally fit with parameters shared as follows; E_{max} was shared across all data sets, τ_o and K_A shared within agonist data sets and K_{GDP} and s constrained to the EC_{50} and hill slope of a concurrently performed GDP concentration response curve.

2.8.10 Microsoft Excel analysis

Operational models were written into Microsoft Excel (David Hall, GSK) and non-linear regression performed by minimising the sum of squared residuals using the Microsoft Excel Solver add-in. All equation parameters except for E_{max} and basal were varied using their log values to account for their likely log-normal distribution (Slack *et al.*, 2012).

2.8.11 Statistical analysis

All statistical comparisons between results were conducted in GraphPad Prism with $P<0.05$ deemed significant. For comparisons between two groups, Student's unpaired t tests were conducted. For comparisons between multiple groups, One-way ANOVA followed by Dunnett's post hoc analysis was conducted when comparisons were being made to a control group, however if all groups were being compared to each other, Tukey's post hoc analysis was used.

All pooled data (except where indicated) are expressed as mean ± standard error of the mean (SEM) from at least 3 independent experiments performed in duplicate or triplicate as described. Independent experiments were individually fit and derived parameters pooled and expressed as mean ± SEM. Where n=2, data are expressed at mean ± range.

Chapter Three: Estimation of dopamine D2L receptor agonist efficacy in reporter gene and internalisation assays, and use of irreversible antagonists to establish the receptor depletion method for operational modelling

3.1 Introduction

3.1.1 Assessing GPCR signalling with reporter gene assays

As a $G\alpha_{i/o}$-coupled receptor, the dopamine D2 receptor is negatively coupled to the production of cAMP. There are a number of methods to measure cAMP accumulation, including direct measurement of [^{3}H]-cAMP accumulation, a number of commercially available cAMP kits which utilise fluorescent or luminescent technologies, FRET-based biosensors and cAMP-dependent reporter genes (Hill *et al.*, 2010). While measuring [^{3}H]-cAMP accumulation provides the most direct method to monitor cAMP levels and has a large signal-to-noise ratio, it is low throughput and has the associated safety concerns of using radioactive isotopes. In contrast, commercially available kits are more amenable to high throughput screening but can have issues around signal detection; the relationship between cAMP production and assay signal is not linear which can lead to issues in ligand potency and relative efficacy determinations depending on how measurements are analysed (Allen *et al.*, 2002; Hill *et al.*, 2010). FRET-based biosensors are now a popular method to monitor cellular cAMP levels. Early studies utilised a fluorescent protein FRET pair tagged to the catalytic and regulatory domains of PKA (Zaccolo *et al.*, 2000) however due to complex nature of PKA activation, a simpler sensor was developed based on the exchange protein directly activated by cAMP (Epac) which showed a higher signal window and faster signal kinetics (Nikolaev *et al.*, 2004). In this sensor, cyan fluorescent protein (CFP) and yellow fluorescent protein (YFP) are fused to either end of the Epac protein which, upon cAMP binding, undergoes a conformational change that decreases the FRET signal between the fluorescent proteins (Nikolaev *et al.*, 2004). While cAMP biosensors can provide spatial and temporal resolution to cAMP signals, their dynamic range is much lower than other techniques, causing problems with detection of low concentrations of cAMP and signal saturation at higher concentrations (Hill *et al.*, 2010). Alternatively, cAMP-dependent reporter genes have the advantage of being highly sensitive, amenable to

high throughput screening and have lower associated costs than most alternatives (Hill *et al.*, 2001).

Reporter genes are DNA sequences that encode quantifiable protein products under the control of specific promoter regions. These promoters bind transcription factors which can be activated by intracellular signalling pathways (Hill *et al.*, 2001). For example, for monitoring cellular cAMP levels, cAMP response element (CRE)-linked reporters are utilised and can be linked to a number of transcription products such as secreted placental alkaline phosphatase (SPAP) or luciferase. These have been used to investigate the pharmacology of a wide range of GPCRs, with examples including the β-adrenoceptor family (Baker *et al.*, 2011; Baker *et al.*, 2002; Baker *et al.*, 2004), dopamine D2 receptor (George *et al.*, 1998; Kemp *et al.*, 1999), melanocortin MC_3 and MC_4 receptors (Simon *et al.*, 2009) and serotonin 5-HT_{1B} and calcitonin C1a receptors (George *et al.*, 1997).

SPAP is a thermostable alkaline phosphatase, modified from its endogenous membrane-bound state to be constitutively secreted by cells (Cullen *et al.*, 1992). It is unusual in that it is very thermo-stable, withstanding much higher temperatures than other members of its family. This unusual thermostability allows measurement of the reporter specific enzyme activity by heating the cells to 65°C to denature endogenous phosphatases. The samples are then cooled before addition of a substrate (p-nitrophenol phosphate; PNPP), which produces a coloured product. By linking this reporter gene to the CRE promoter, changes in cAMP production and protein kinase A (PKA) activation are reflected in changes in SPAP production. Thus, stimuli that reduce cAMP, decrease PKA, and reduce CRE binding protein phosphorylation, decreasing the transcription of the CRE-mediated SPAP gene (summarised in **Figure 3.1**).

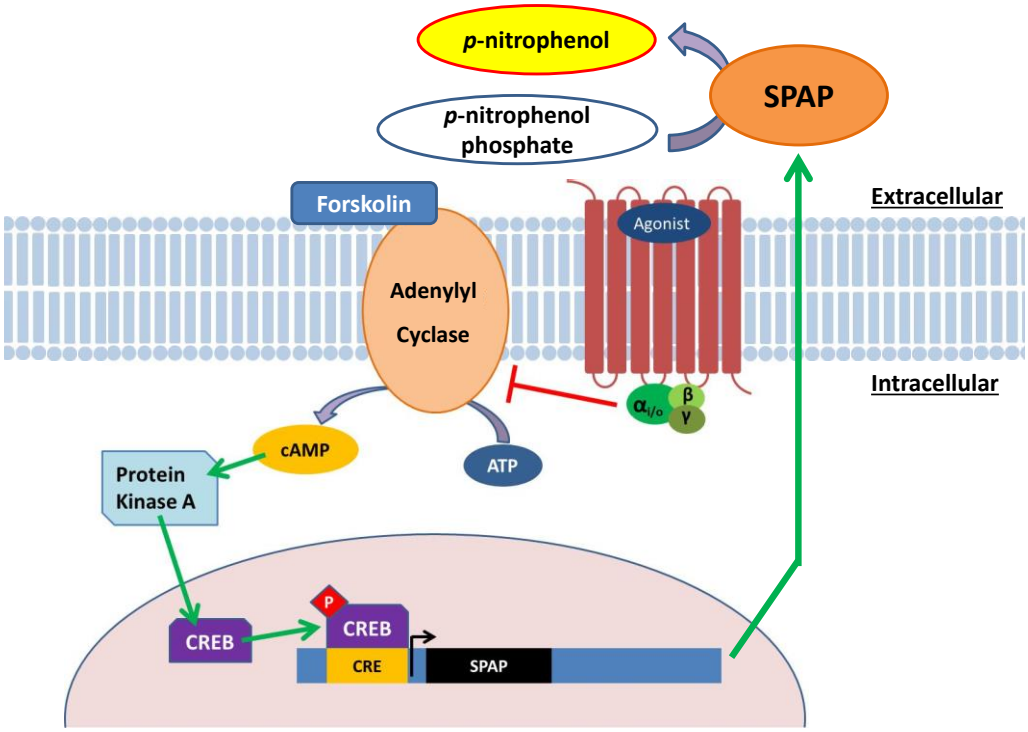


Figure 3.1: The CRE-SPAP reporter gene assay

The CRE-SPAP reporter gene assay is an indirect method to measure cAMP accumulation in cells. Forskolin acts as a direct activator of adenylyl cyclase to increase cellular cAMP levels. cAMP activates protein kinase A, freeing its catalytic domains to move into the nucleus and phosphorylate CREB. Phosphorylated CREB can then bind CRE, initiating SPAP gene transcription. Activation of the dopamine D2 receptor activates inhibitory heterotrimeric G-proteins that inhibit adenylyl cyclase, thus reducing the cellular concentration of cAMP and subsequent SPAP gene transcription. Once transcribed, SPAP is secreted from the cells. SPAP activity is then determined by the addition of PNPP to assay media; SPAP catalyses the hydrolysis of PNPP to the yellow product *p*-nitrophenol, the production of which can be assessed by measuring plate absorbance at 405nm.

Reporter gene assays have a number of advantages over more direct measurements of intracellular signalling events. They are very sensitive; the high level of signal amplification allows the detection of even very weak partial agonists (Baker *et al.*, 2003; Hill *et al.*, 2001; Kemp *et al.*, 1999). However, this amplification can also be problematic; the high levels of receptor reserve can increase relative maximal responses, making a range of agonists appear highly efficacious despite a low intrinsic efficacy. This often results in partial agonists appearing as efficacious as full agonists due to the response of the full agonists being limited by the system under measure (Hill *et al.*, 2001).

3.1.2 Fluorescence-based labelling techniques for receptor detection in whole cells

In order to follow the internalisation of a receptor of interest, it is necessary to first label the protein. There are a number of approaches available to fluorescently label proteins, including a number of variants of green fluorescent protein (GFP). GFP was discovered in the 1960's (Johnson *et al.*, 1962; Shimomura *et al.*, 1962) when it was isolated from the jellyfish *Aequorea victoria* alongside the Ca^{2+}-dependent bioluminescent protein, aequorin. The cloning of the GFP gene, a number of years later, accelerated its now widespread exploitation as a gene expression marker and protein tag (Sample *et al.*, 2009). Mutations have been introduced to improve GFP stability and folding, and to tune the emission and excitation spectra. As such, fluorescent proteins are now available in a wide variety of colours, both through mutations of the original GFP gene (reviewed in (Tsien, 1998)) as well as subsequent isolations of fluorescent proteins from other marine species (Fradkov *et al.*, 2000; Matz *et al.*, 1999). While there are now a wide range of fluorescent proteins available, many have issues with low brightness and bleaching (Sample *et al.*, 2009).

An alternative to fluorescent proteins is to use a protein tag than can be irreversibly labelled with a reactive fluorophore. There are a number of

approaches to do this including the Halo-, FlAsH and SNAP-tags. The HaloTag system utilises a modified bacterial haloalkane dehalogenase that has been modified to covalently bind fluorescent ligands (Los *et al.*, 2008). In contrast, FlAsH (fluorescein arsenical hairpin binder) is based on the binding of a short tetracysteine peptide sequence to a small fluorescein derivative (FlAsH) in complex with ethanedithiol that only fluoresces upon peptide binding (Griffin *et al.*, 1998; Hoffmann *et al.*, 2010). The SNAP-tag technology exploits the ability of the DNA repair enzyme, O^6-alkylguanine-DNA alkyltransferase (hAGT), to accept O^6-benzylguanine (BG) derivatives as substrates (Keppler *et al.*, 2003) (**Figure 3.2**). These BG-derivatives can be fused to a wide variety of fluorescent probes to irreversibly label the protein of interest, by transferring the fluorophore to the thiol group of the enzyme active site. By fusing the SNAP-tag to the N-terminus of the GPCR, the use of membrane impermeable dyes allows selective labelling of cell surface receptors, preventing labelling of pre-internalised or improperly translocated receptors which remain visible in GFP fusions (Keppler *et al.*, 2003; Keppler *et al.*, 2004). Unlike fluorescent proteins, which have fixed excitation and emission spectra, the availability of multiple BG-derivatives allows this versatile technology to couple different fluorophores to the tagged protein depending on experimental needs. This flexibility allows the SNAP-tag to be combined with other fluorescent based tags, such as GFP variants, to image multiple protein populations. For example, this has been used to examine dimerisation of neuropeptide Y1 and Y5 receptors by combining the SNAP-tag technology with biomolecular fluorescence complementation (BiFC) where two halves of YFP re-complement to form functional YFP (Kilpatrick *et al.*, 2015).

Furthermore, by introducing 8 point mutations into the SNAP-tag, Gautier *et al* generated the CLIP-tag, which has altered substrate specificity (Gautier *et al.*, 2008). Unlike the SNAP-tag, the CLIP-tag accepts O^2-benzylcytosine derivatives, which, like the SNAP-tags BG-derivative substrates, can be coupled to multiple fluorophores. Combining these two technologies allows the simultaneous coupling of two-tagged proteins with different fluorophores

and has been used in FRET studies to examine GPCR oligomerisation (Maurel *et al.*, 2008; Pou *et al.*, 2012). SNAP-tags are also increasingly being used in combination with fluorescent ligands for ligand binding assays as an alternative to traditional radioligand binding techniques (Klein Herenbrink *et al.*, 2016; Zwier *et al.*, 2010).

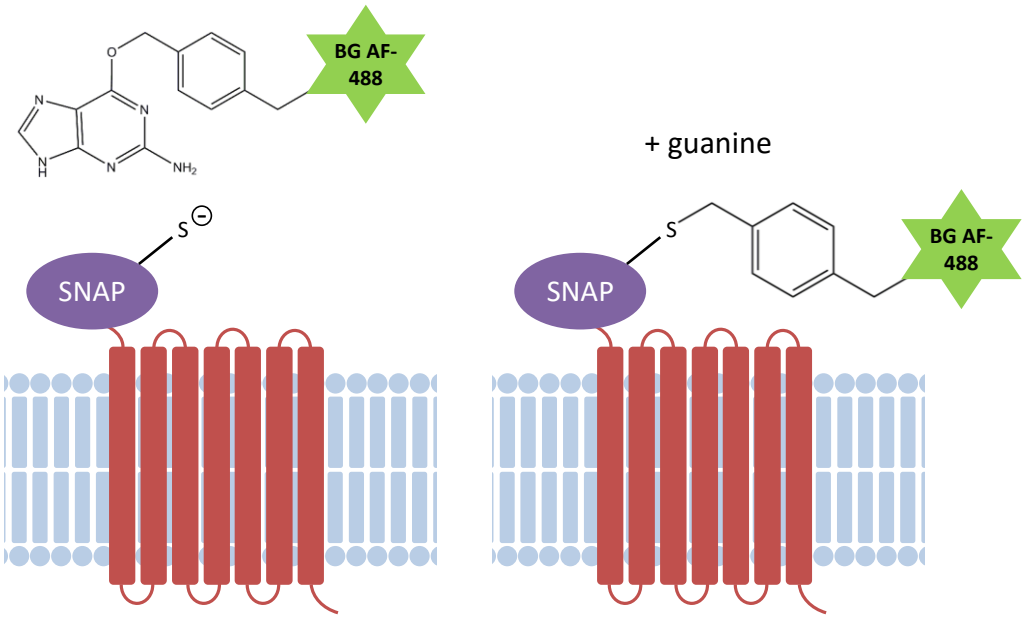


Figure 3.2: SNAP-tag for labelling cells

The SNAP-tag can be expressed on the N-terminal of GPCRs. Addition of a BG derivative linked to a fluorophore (e.g. AlexaFluor 488) fluorescently labels the receptor as the BG substrate reacts irreversibly with the SNAP-tag, leading to a covalently bound benzyl fluorophore and the release of guanine.

3.1.3 Chapter aims

In this chapter, we aimed to characterise the newly generated CHO-K1 CRE-SPAP SNAP-tagged D2L (CHOcs ssD2L) cell line for different functional readouts including a cAMP-dependent reporter gene, receptor internalisation and radioligand binding assay to ensure that the SNAP-tag receptor modification did not alter the expected functional responses of the D2L receptor. After establishing the behaviour of representative ligands of different structural classes in each assay, we then investigated two reported irreversible antagonists of the D2L, EEDQ (Hamblin *et al.*, 1983) and PBz (Hamblin *et al.*, 1982), to determine which would be appropriate for future operational modelling of data and completed an initial modelling experiment on D2L SPAP responses for four ligands.

3.2 Results

3.2.1 Generation of clonal CHOcs ssD2L cell line

In this construct, the human D2L cDNA lacking its start codon, was placed downstream of a 5-HT_3 signal sequence (20 amino acids) and the SNAP-tag coding region ("ss", 180 amino acids), within the pcDNA3.1 (+) zeo mammalian expression vector, as described in **2.2.** Following transfection of the CHO-K1 CRE-SPAP (cs) reporter gene cell line and antibiotic selection, dilution cloning was performed to isolate cell lines with more homogeneous levels of receptor expression. Clones were examined for their cell surface expression through SNAP-labelling and positive clones further screened for their responses in the SPAP assay to ensure both expression and functionality. From 4 clones with equivalent SNAP labelling and functional characteristics in the SPAP assay, a single clone (CHOcs ssD2L) was identified as the focus for all subsequent experiments.

3.2.2 Initial characterisation of dopamine D2L receptor responses in the CRE-SPAP reporter gene assay

We initially determined whether the CRE-SPAP assay, as an indirect measure of receptor-induced changes in cAMP accumulation, could be used to monitor dopamine D2L receptor ligand responses. Forskolin, a direct activator of adenylyl cyclase (Seamon *et al.*, 1981), was used to stimulate CRE-SPAP production to allow detection of the expected inhibitory $G\alpha_{i/o}$ signalling of the dopamine D2L receptor. Concentration response curves to forskolin were initially generated in CHOcs ssD2L cells in the presence of vehicle, the D2L agonist quinpirole (10µM), and the antagonists haloperidol or PBz, both at 10µM (**Figure 3.3**). The pEC_{50} of forskolin alone was 5.94 ± 0.09, while 10µM quinpirole induced a 25.5 ± 3.8-fold rightward shift in the forskolin concentration response curve. However, neither haloperidol nor PBz had any effect on the forskolin pEC_{50} value (**Table 3.1**). The moderate increases in maximum forskolin response, in the presence of either haloperidol or PBz, were not statistically significant (One-way ANOVA followed by Dunnett's post-

hoc analysis). For detection of D2L agonism, the greatest signal window between vehicle and 10µM quinpirole responses was observed at 3µM forskolin (88.5 ± 2.7 % inhibition, n=4). This optimal concentration of forskolin was then chosen for all subsequent experiments, unless otherwise stated.

In order to ensure D2L mediated SPAP responses were a product of receptor coupling to $G\alpha_{i/o}$ proteins, cells were pre-treated with pertussis toxin (PTx; 100ng ml^{-1}) prior to assay. PTx is a bacterial protein secreted by *Bordetella pertussis* which ADP-ribosylates the cysteine residue 4 residues from the carboxy terminus of $G\alpha_{i/o}$ G proteins, locking the protein in its inactive state and preventing $G\alpha_{i/o}$ mediated signalling (Mangmool *et al.*, 2011). As shown in **Figure 3.4**, pre-treatment with PTx abolished ligand-induced reductions in SPAP production to maximal concentrations of quinpirole and three other agonists (dopamine, aripiprazole and bromocriptine; see **3.2.3**).

Furthermore, to ensure CRE-SPAP mediated responses were due to ligand effects at the dopamine D2 receptor, 6 ligands were examined for their ability to modulate forskolin-stimulated SPAP production in non-transfected CHO CRE-SPAP cells (**Figure 3.5**). No concentration-dependent effects of any ligand were seen at up to 10µM, the maximal concentration used for most compounds in this assay. There was no effect of dopamine at up to 100µM whereas other compounds had effects at 10-100µM. Only the bromocriptine data could be unambiguously fit to a ligand concentration response curve (pEC_{50} 5.56 ± 0.01, E_{max} 93.4 ± 5.4% inhibition of 3µM forskolin response). To examine whether this response was due to activation of endogenous 5-HT_{1B} receptors in the CHO cells (George *et al.*, 1997), cells were pre-treated with the selective 5-HT_{1B} receptor antagonist SB 224289 (100nM). This treatment however did not inhibit the bromocriptine response (n=2; **Figure 3.6**).

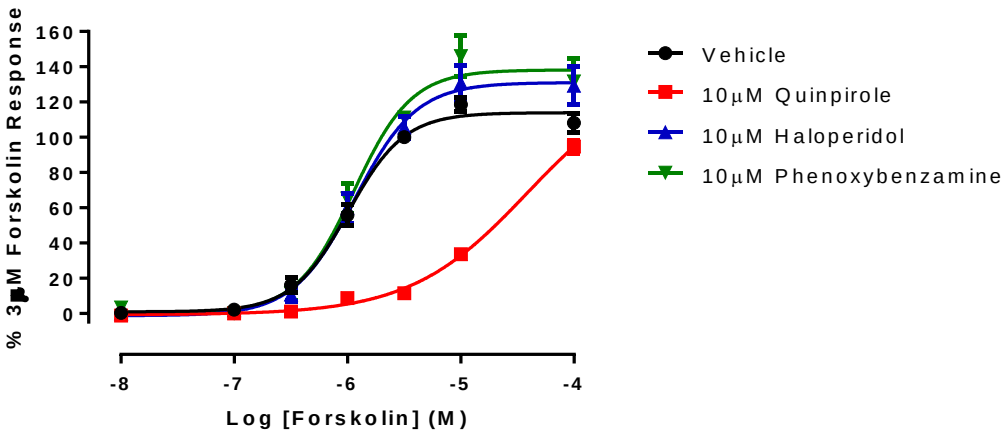


Figure 3.3: Forskolin concentration response curves in the CRE-SPAP reporter gene assay in the absence and presence of dopamine D2 receptor ligands

Cells were treated with 10μM dopamine D2 receptor ligands for 1h prior to 5h stimulation with increasing concentrations of forskolin. Data represent pooled data (mean ± SEM) of 4 independent experiments performed in triplicate, normalised to vehicle (0%) and 3μM forskolin response (100%) with pEC_{50} and R_{max} values given in **Table 3.1**.

Treatment	pEC_{50}	R_{max}
Vehicle	5.98 ± 0.08	114.0 ± 4.4
10μM Quinpirole	4.63 ± 0.13*	121.4 ± 12.9
10μM Haloperidol	5.95 ± 0.09	131.5 ± 9.8
10μM PBz	5.98 ± 0.07	139.1 ± 12.2

Table 3.1: Summary of forskolin concentration response curves in the absence and presence of D2L ligands

Summary of parameters derived from the forskolin concentration response curves shown in **Figure 3.3**. Data are pooled (mean ± SEM) of 4 independent experiments performed in triplicate with R_{max} expressed as % 3μM forskolin response. *P<0.05 compared to vehicle treatment (One way ANOVA followed by Dunnett's post hoc analysis).

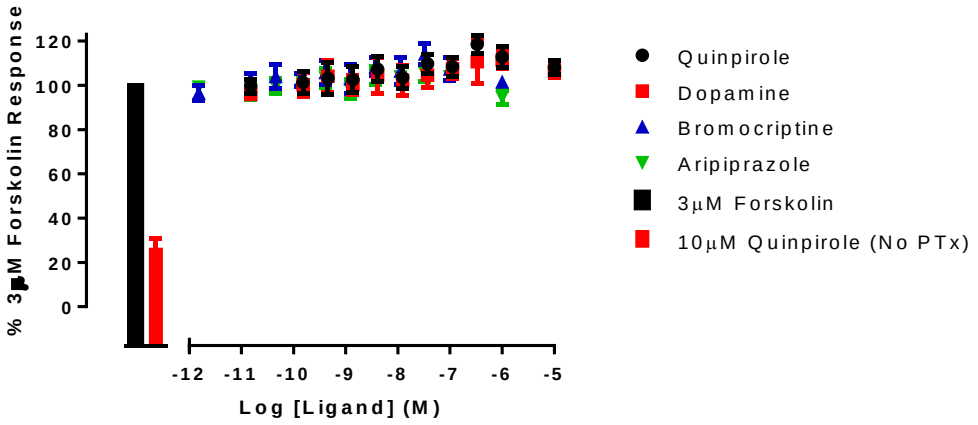


Figure 3.4: Effects of PTx treatment on SPAP responses in CHOcs ssD2L cells

Cells were pre-treated with PTx (100ng ml^{-1}) for 20h prior to assay. Data represent pooled data (mean ± SEM) of 3 independent experiments performed in duplicate, normalised to non-PTx treated 3μM forskolin (100%) and vehicle (0%) controls.

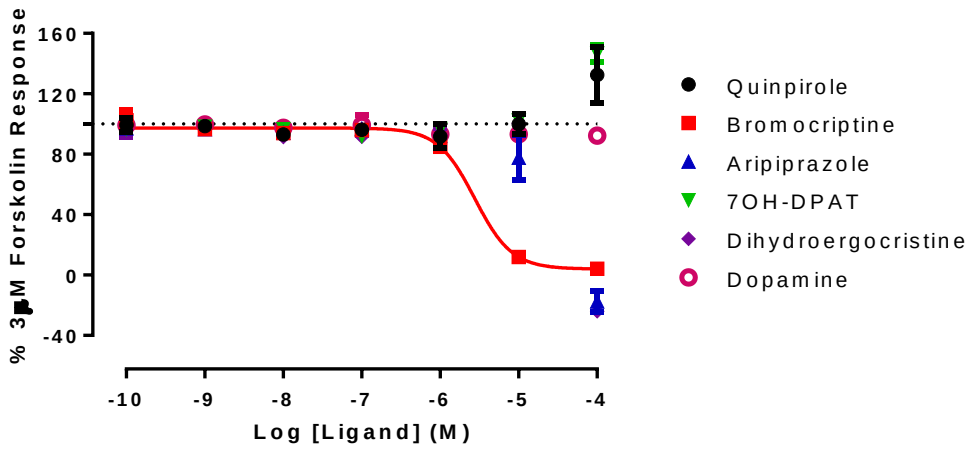


Figure 3.5: Effect of representative D2 ligands on untransfected CHO CRE-SPAP cells

6 dopamine ligands were examined for their ability to inhibit forskolin-stimulated SPAP production in untransfected CHO CRE-SPAP cells, under the same assay conditions as **Figure 3.7**. Data represent pooled (mean ± SEM) of 4 independent experiments performed in duplicate, normalised to 3μM forskolin controls (100%) and vehicle (0%) controls.

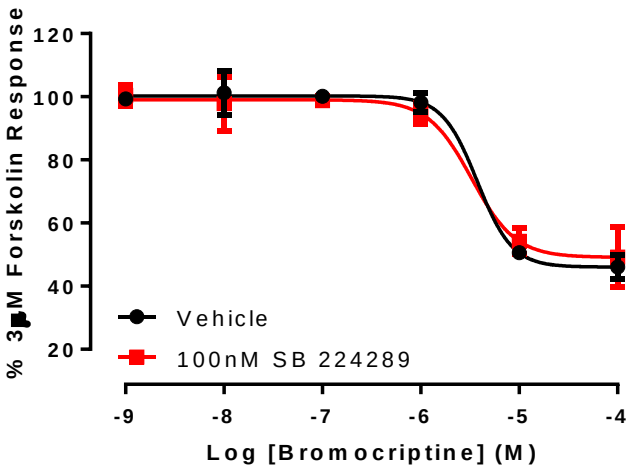


Figure 3.6: Effect of SB 224289 on bromocriptine responses in untransfected CHO CRE-SPAP cells

CHO CRE-SPAP cells were preincubated for 30min in the presence or absence of 100nM of the selective 5-HT_{1B} receptor antagonist SB 224289 prior to 30min incubation with increasing concentrations of bromocriptine and 5h 3µM forskolin treatment. Data represent pooled data (mean ± range) of 2 independent experiments performed in triplicate, normalised to 3µM forskolin (100%) and vehicle (0%) controls.

3.2.3 Characterisation of agonist and antagonist responses in the CRE-SPAP reporter gene assay

A range of dopamine D2 receptor ligands were then tested for their inhibitory effects on CHOcs ssD2L SPAP production (**Figure 3.7, Table 3.2**), referenced to quinpirole responses (pEC_{50} 7.78 ± 0.25). Dopamine is the endogenous ligand for the dopamine D2 receptor and appeared both equi-potent and equi-efficacious compared to quinpirole, as did 7OH-DPAT. RNPA and apomorphine were both full agonists but with higher potency than quinpirole. Two ligands, aripiprazole and (-)-3-PPP were partial agonists whereas (+)-3-PPP was a full agonist. The ergo-derived compounds all had higher potency than quinpirole and were full agonists relative to quinpirole except for dihydroergocristine. The overall rank order of potency was RNPA > bromocriptine = cabergoline > dihydroergocristine > pergolide = apomorphine > 7OH-DPAT = aripiprazole = quinpirole = dopamine > (-)-3-PPP = (+)-3-PPP. The order of efficacy of the partial agonists was dihydroergocristine > (-)-3-PPP > aripiprazole (**Table 3.2**).

None of the antagonists in this study demonstrated any effects on forskolin-stimulated SPAP production (**Figure 3.7**). As such, their ability to inhibit quinpirole-induced inhibition of forskolin-stimulated SPAP production was determined. Increasing concentrations of both haloperidol and sulpiride produced parallel rightward shifts in quinpirole concentration response curves, allowing the calculation of haloperidol and sulpiride affinities in the form of pA_2s from Schild analysis (Schild, 1949) (**Figure 3.8**). The pA_2s of haloperidol and sulpiride were calculated as 9.06 ± 0.18 and 8.68 ± 0.19 (**Table 3.5**), with Schild slopes of 1.66 ± 0.15 and 0.90 ± 0.07 respectively (n=4). The Schild slope calculated from the haloperidol data (but not that of sulpiride), was significantly different from unity ($P<0.05$; One sample t-test with reference to theoretical value of one). Like haloperidol and sulpiride, (+)-butaclamol induced a rightward shift in quinpirole concentration response curves however increasing concentrations also caused a reduction in quinpirole R_{max} (**Figure 3.9**).

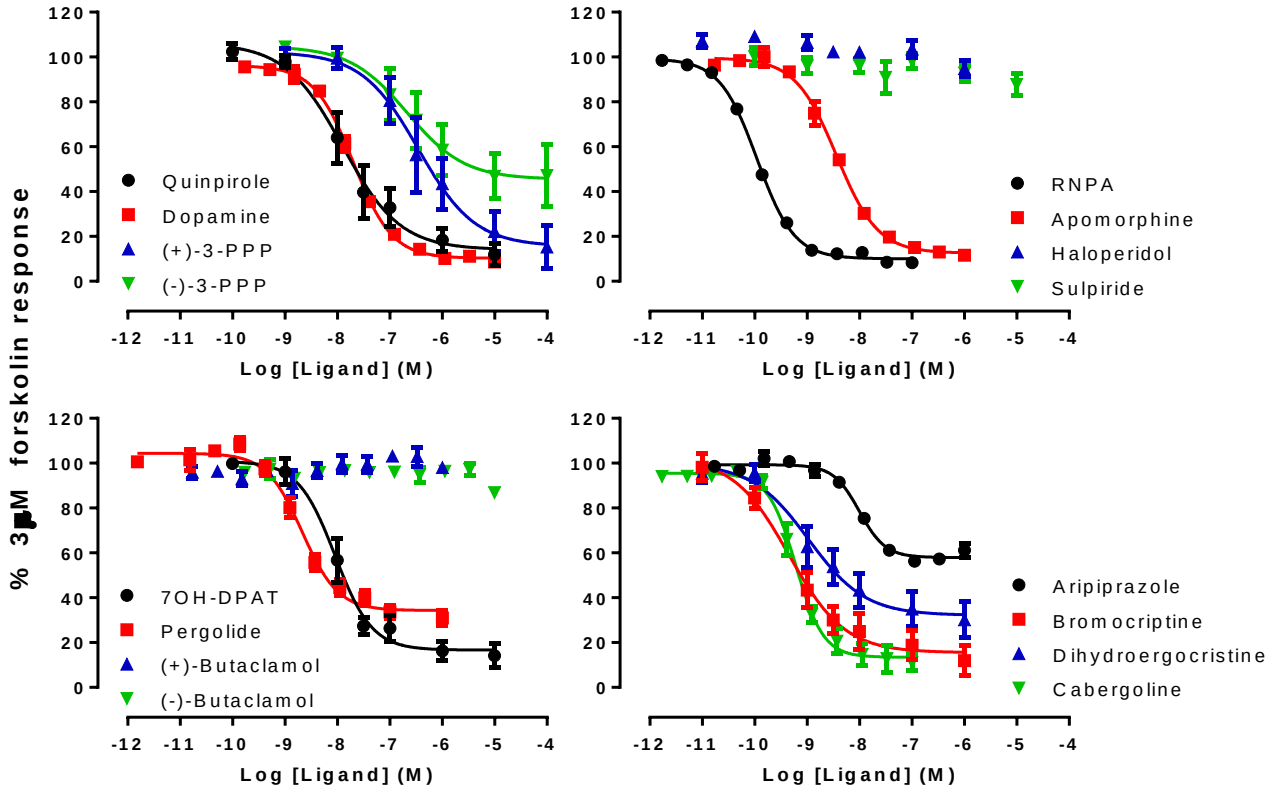


Figure 3.7: The ability of dopamine D2 receptor ligands to inhibit forskolin-stimulated SPAP production.

Cells were treated with increasing concentrations of dopamine D2 receptor ligands for 1h prior to 5h 3µM forskolin stimulation. Data represent pooled data (mean ± SEM) from 4 independent experiments performed in duplicate or triplicate, normalised to 3µM forskolin (100%) and vehicle (0%) controls, with data summarised in **Table 3.2**.

Ligand	pEC_{50}	R_{max}
Quinpirole	7.80 ± 0.23	99.3 ± 1.1
Dopamine	7.70 ± 0.04	102.9 ± 2.0
(+)-3-PPP	6.37 ± 0.29	100.3 ± 6.2
(-)-3-PPP	6.63 ± 0.24	63.3 ± 10.7*
RNPA	9.96 ± 0.02	103.4 ± 1.6
Apomorphine	8.45 ± 0.04	100.3 ± 1.6
Haloperidol	NE	NE
Sulpiride	NE	NE
7OH-DPAT	8.04 ± 0.16	100.7 ± 1.1
Pergolide	8.67 ± 0.09	96.7 ± 3.1
(+)-Butaclamol	NE	NE
(-)-Butaclamol	NE	NE
Aripiprazole	8.02 ± 0.08	48.1 ± 0.5*
Bromocriptine	9.31 ± 0.12	99.5 ± 4.1
Dihydroergocristine	8.97 ± 0.15	81.4 ± 3.7*
Cabergoline	9.24 ± 0.08	103.8 ± 3.9

Table 3.2: Summary of maximal responses and pEC_{50}s from CRE-SPAP reporter gene assays in the CHOcs ssD2L cell line

Data were derived from the ligand concentration response curves in **Figure 3.7**. Data are pooled (mean ± SEM) of 4 independent experiments performed in duplicate or triplicate, with R_{max} expressed as a percentage of 10µM quinpirole response. NE = no effect; *P<0.05 compared to quinpirole response (One-way ANOVA followed Dunnett's post-hoc analysis).

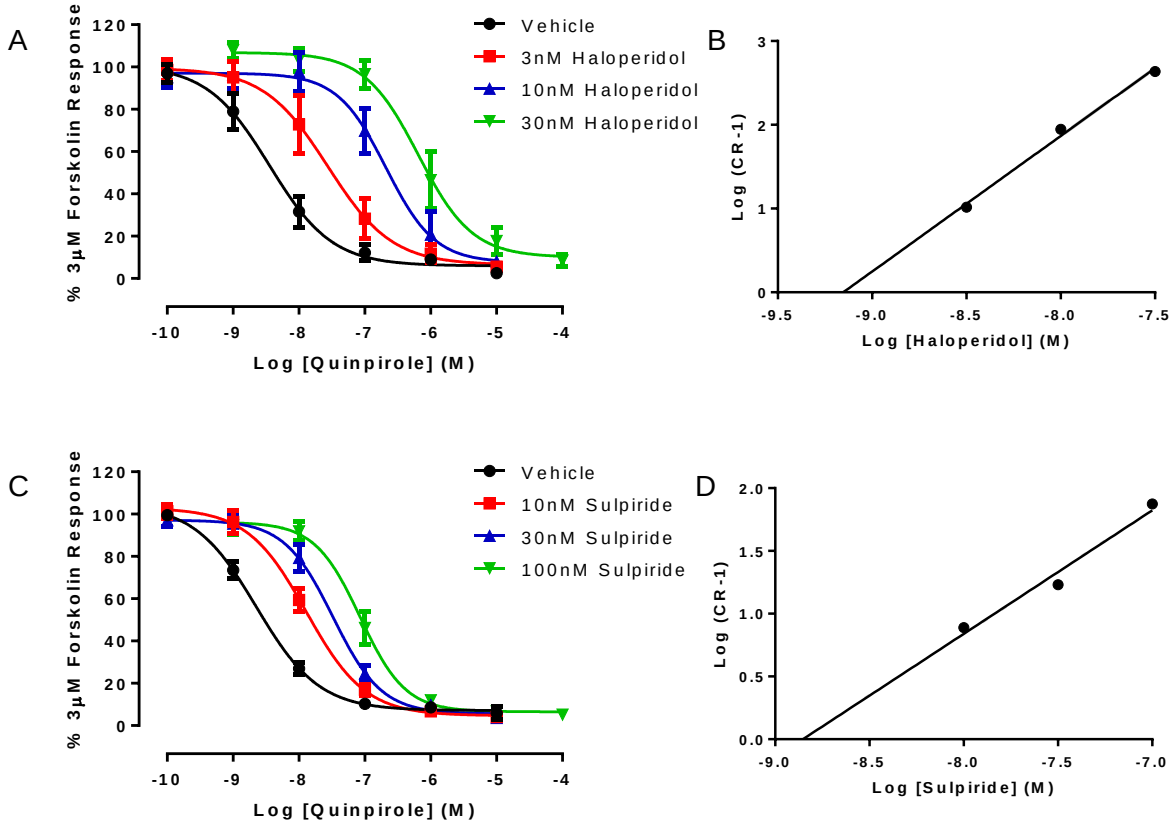


Figure 3.8: Determination of antagonist affinities by Schild analysis in the CHOcs ssD2L cell line

Cells were pre-treated with 3-30nM haloperidol (**A**) or 10-100nM sulpiride (**C**) for 30min prior to 30min quinpirole treatment and subsequent 5h 3µM forskolin stimulation. Data represent pooled data (mean ± SEM) of 4 independent experiments performed in triplicate, normalised to 3µM forskolin (100%) and vehicle (0%) controls. From these data, concentration ratios (CR) were calculated and Schild plots constructed (see example **B,D**) to calculate pA_2 values for haloperidol of 9.06 ± 0.18 and sulpiride of 8.68 ± 0.19.

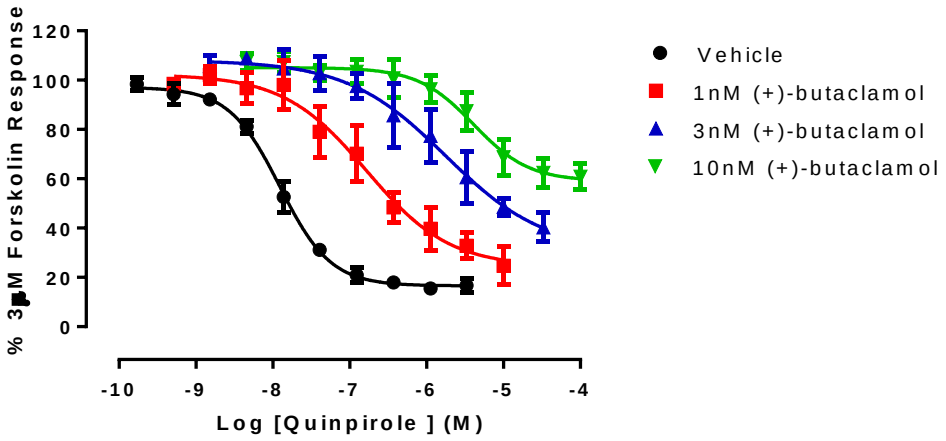


Figure 3.9: Investigation of the antagonism of (+)-butaclamol in the CRE-SPAP reporter assay

Cells were incubated with 1-10nM (+)-butaclamol for 30min prior to 30min quinpirole treatment and subsequent 5h 3µM forskolin treatment. Data represent pooled data (mean ± SEM) of 3 independent experiments performed in duplicate, normalised to 3µM forskolin (100%) and vehicle (0%) controls.

3.2.4 Monitoring agonist-promoted internalisation of the dopamine D2L receptor

An alternative method to measure receptor activation is to examine receptor internalisation, which occurs following ligand stimulation of many GPCRs as a regulatory mechanism (Sorkin *et al.*, 2009). To investigate this in CHOcs ssD2L cells, SNAP-tagged receptors were first labelled with membrane impermeant fluorophore (SNAP-surface AF488), prior to treatment with vehicle or different D2 receptor ligands. Cells were then fixed and receptors visualised using an IX Ultra imaging plate-reader (**2.7.2**). Following labelling of the SNAP-tagged receptor, the receptor was localised predominantly to the plasma membrane under control conditions and internalised following 1h agonist treatment (**Figure 3.10**). Time courses demonstrated a 20min delay in receptor internalisation following ligand stimulation whereby receptors seemed to initially cluster on the membrane prior to internalisation. Receptor internalisation following 10μM quinpirole treatment was maximal after 100min with a half time of 51.3 ± 5.8min (n=4; **Figure 3.11**).

Internalised labelled receptors gathered particularly in perinuclear intracellular compartments; the number and intensity of these fluorescent spots was detected by an automated granularity analysis (compartment size of 6–10μm diameter) as a measure of ligand-promoted internalisation. All 16 dopamine D2 receptor ligands were examined for their ability to internalise the receptor following 1h ligand stimulation (**Figure 3.12** and **Figure 3.13**). 1h was chosen as a time point with significant receptor internalisation without leaving the cells in HBSS for an extended period. **Figure 3.13** illustrates that D2 receptor ligands displayed differing abilities to internalise the receptor compared to the reference agonist quinpirole, with a much wider range of maximal responses than the SPAP assay (summarised in **Table 3.3**). Only quinpirole, dopamine and RNPA were full agonists, while (-)-3-PPP, dihydroergocristine and aripiprazole were unable to induce receptor internalisation at the highest concentrations tested (1-100μM). All other agonists were partial agonists with maximal responses ranging from 43.5-

82.9% of 10µM quinpirole internalisation. Agonist potencies in this assay were around 10-fold lower than the SPAP assay (for example: quinpirole pEC_{50} 6.51 ± 0.18 compared with 7.78 ± 0.25). However the rank order of potency was similar in both assays (for internalisation: RNPA > bromocriptine = cabergoline > pergolide = apomorphine > 7OH-DPAT > quinpirole = dopamine > (+)-3-PPP). Interestingly, the antagonist haloperidol displayed a weak ability to internalise the D2L receptor (pEC_{50} 8.18 ± 0.32; R_{max}¬ 19.7 ± 4.0% efficacy 10µM quinpirole) whereas the other antagonists sulpiride and (+)-butaclamol had no effect.

The ability of haloperidol (10nM) and sulpiride (30nM) to antagonise quinpirole-induced receptor internalisation was also investigated (**Figure 3.14**). Both produced parallel rightward shifts in the quinpirole curves allowing the calculation of antagonist affinities. However, the observed partial agonism of haloperidol necessitated two different types of analysis. The sulpiride data were fitted with the Gaddum equation, assuming simple competitive antagonism (Gaddum, 1937). For the haloperidol data, the method of Stephenson allowed the ligand's partial agonism to be taken into account (Stephenson, 1956). This calculates pK_Ds of 8.37 ± 0.04 for sulpiride and 9.20 ± 0.20 for haloperidol, comparable with the calculated affinities from the Schild analysis of the SPAP data (see **Table 3.5**).

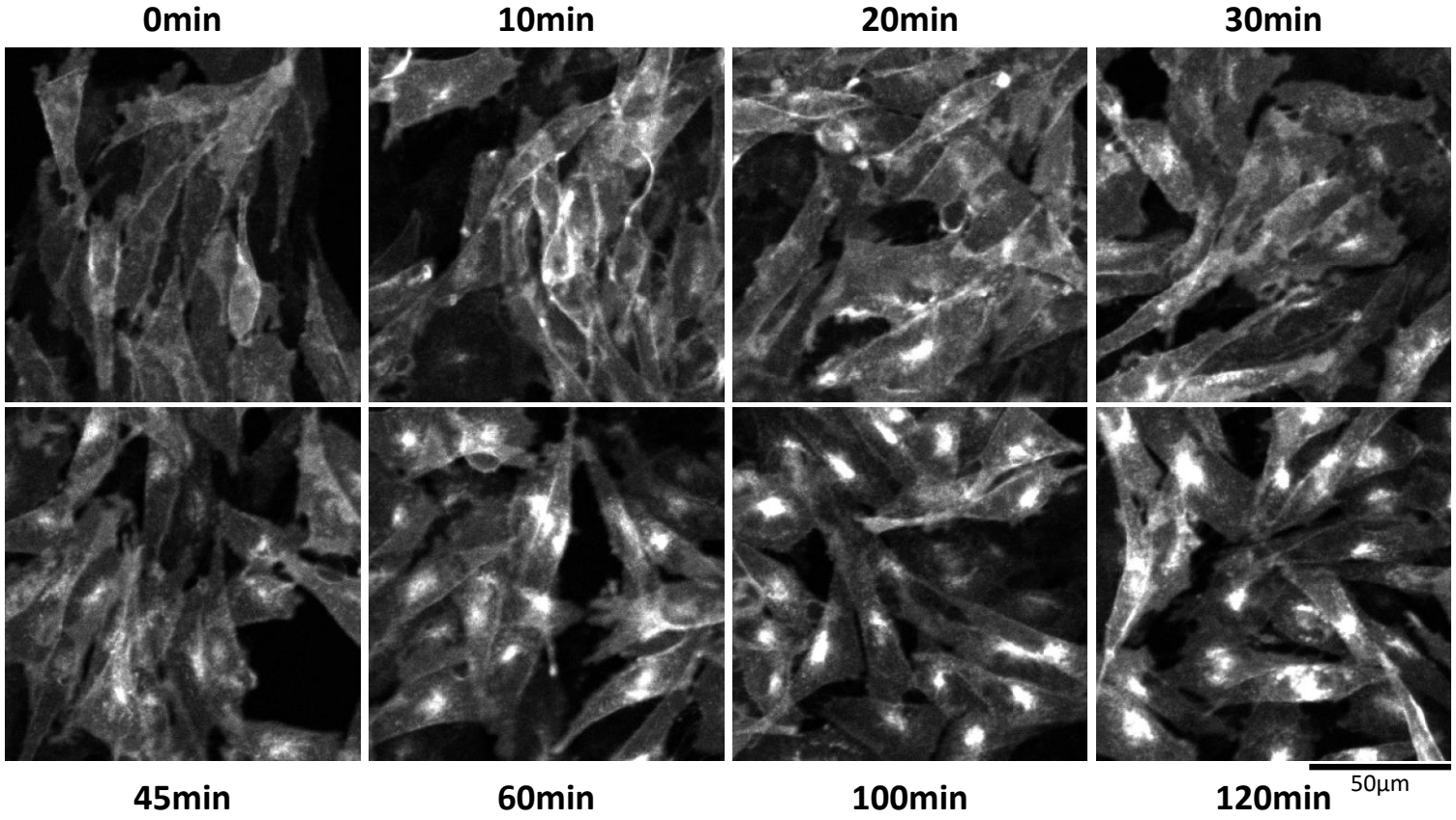


Figure 3.10: Time course of quinpirole induced receptor internalisation

Representative images of SNAP-D2L following treatment with 10µM quinpirole for increasing time points. For clarity, the images above were cropped to 120µm x 120µm from the original 400µm x 400µm image used for analysis. Data are quantified in **Figure 3.11**.

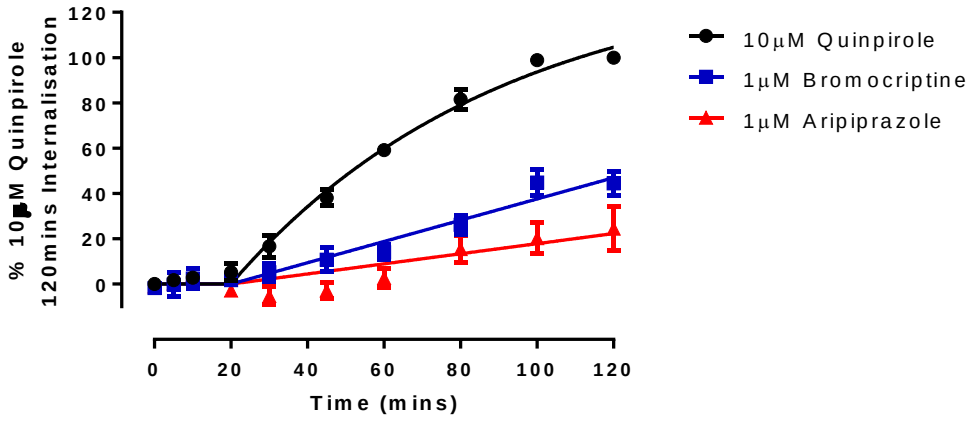


Figure 3.11: Time course of SNAP-tagged D2L receptor internalisation

CHOcs ssD2L cells were SNAP-labelled for 30min prior to treatment with 10µM quinpirole, 1µM bromocriptine and 1µM aripiprazole for increasing times in HBSS (example images in **Figure 3.10**). Data shown are pooled (mean ± SEM) for 4 independent experiments performed in duplicate, normalised to vehicle (0%) and 10µM, 120min quinpirole internalisation (100%).

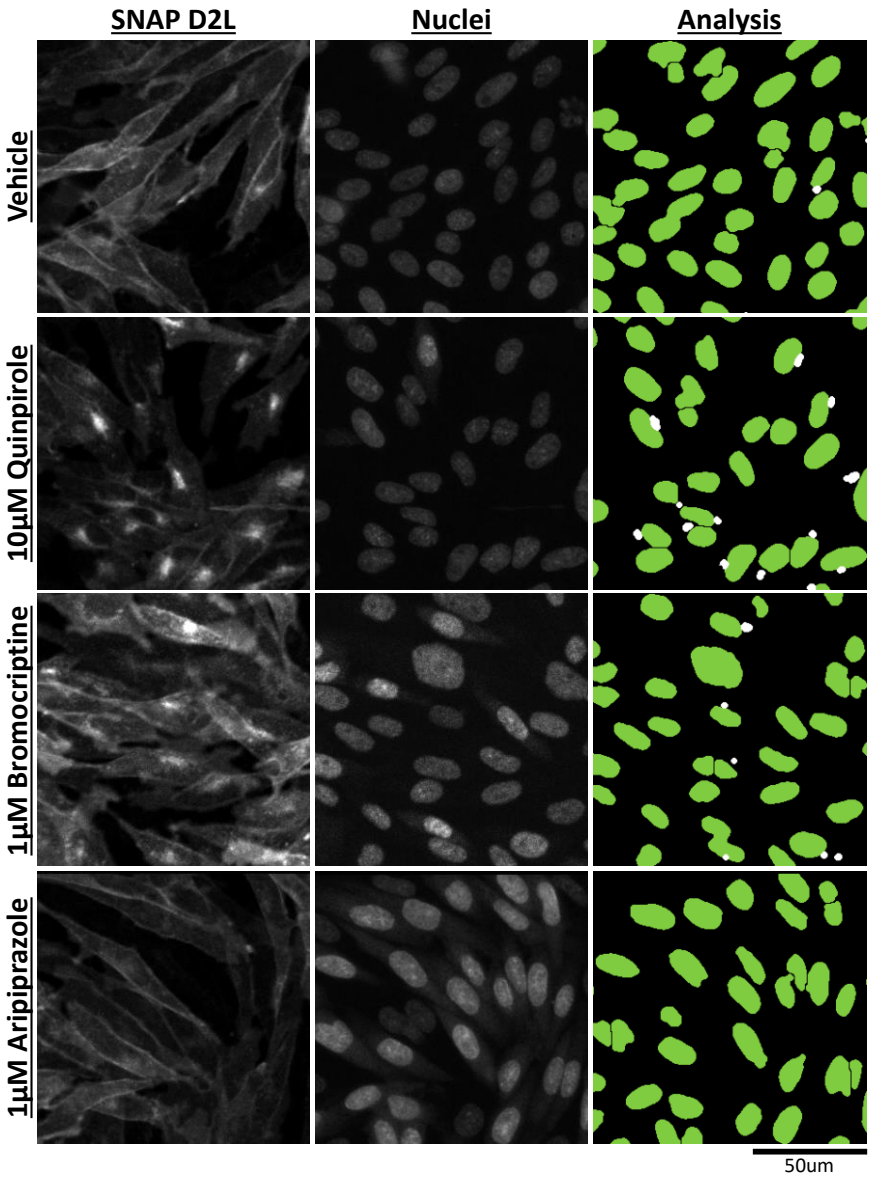


Figure 3.12: Internalisation of the SNAP-tagged dopamine D2L receptor in response to ligand stimulation

Cells were SNAP-labelled then treated with increasing concentrations of ligands for 1h prior to fixation. Representative images show cells treated with vehicle, reference full agonist (10µM quinpirole), representative partial agonist (1µM bromocriptine) and a compound displaying no ability to internalise the receptor (1µM aripiprazole). For clarity, the images above were cropped to 120µm x 120µm from the original 400µm x 400µm image used for analysis. The panels show the SNAP-tagged D2L (left), H33342 stained nuclei (middle) and associated granularity analysis (right), with nuclei in green and receptor containing granules of 6-10µm diameter in white. The internalisation of 16 D2 ligands was determined and quantified (**Figure 3.13**).

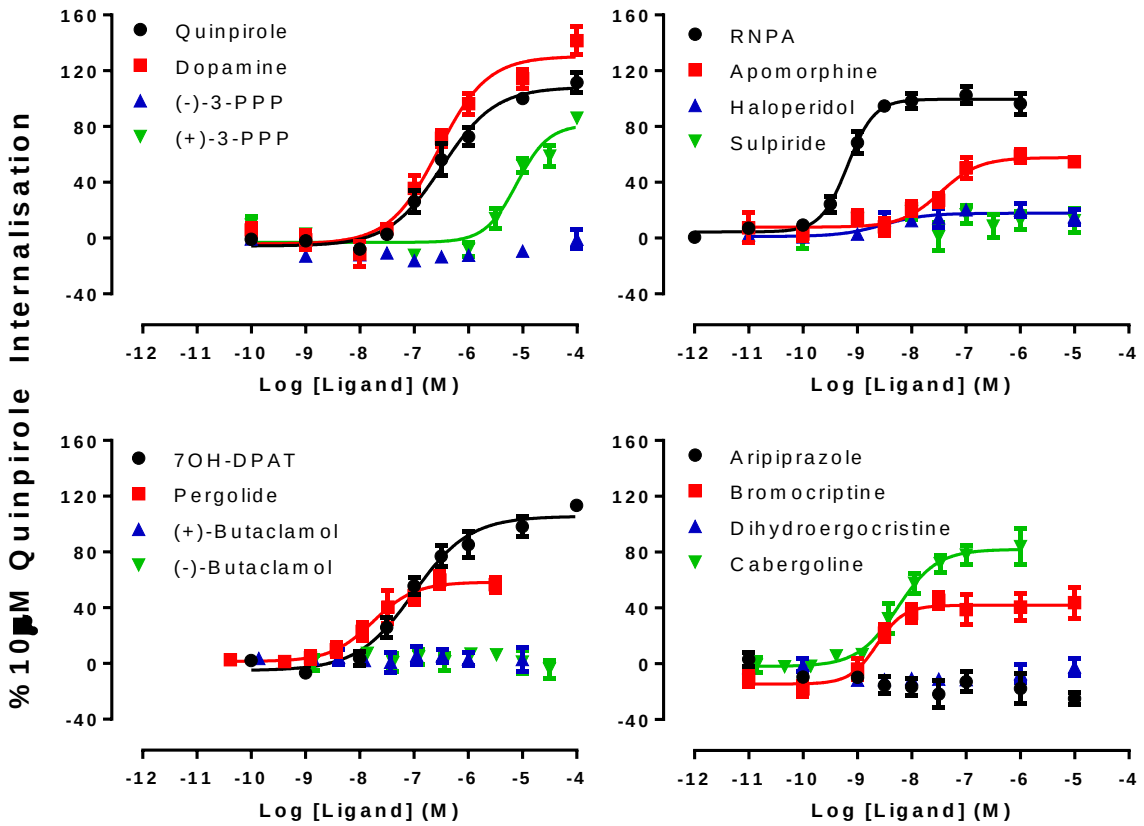


Figure 3.13: Quantification of dopamine D2L receptor internalisation in response to treatment with a panel of dopamine D2 receptor ligands

Receptor internalisation following 1h ligand stimulation was quantified by an automated granularity algorithm identifying the number of granules per cell for a range of D2 receptor ligands (see example images in **Figure 3.12**). Data points represent pooled data (mean ± SEM) of 4 independent experiments performed in duplicate or triplicate, normalised to 10μM quinpirole (100%) and vehicle (0%) controls with data summarised in **Table 3.3.**

Ligand	pEC_{50}	R_{max}
Quinpirole	6.51 ± 0.18	107.3 ± 5.0
Dopamine	6.58 ± 0.08	129.9 ± 8.4
(+)-3-PPP	5.14 ± 0.12	82.9 ± 7.7
(-)-3-PPP	NE	NE
RNPA	9.18 ± 0.04	99.7 ± 6.0
Apomorphine	7.52 ± 0.15	58.3 ± 2.6*
Haloperidol	8.18 ± 0.32	19.7 ± 4.0*
Sulpiride	NE	NE
7OH-DPAT	6.96 ± 0.17	108.1 ± 3.7
Pergolide	7.83 ± 0.27	59.1 ± 4.6*
(+)-Butaclamol	NE	NE
(-)-Butaclamol	NE	NE
Aripiprazole	NE	NE
Bromocriptine	8.65 ± 0.07	43.5 ± 9.6*
Dihydroergocristine	NE	NE
Cabergoline	8.36 ± 0.21	78.2 ± 5.3*

Table 3.3: Summary of maximal responses and pEC_{50}s from internalisation assays in the CHOcs ssD2L cell line

Data were derived from the ligand concentration response curves in **Figure 3.13**. Data are pooled (mean ± SEM) of 4 independent experiments performed in duplicate or triplicate, with R_{max} expressed as a percentage of 10μM quinpirole response. NE = no effect; *P<0.05 compared to quinpirole response (One-way ANOVA followed Dunnett's post-hoc analysis).

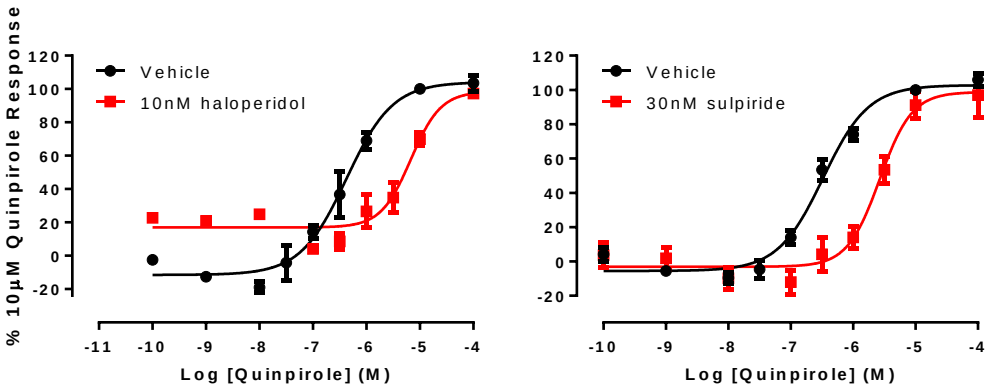


Figure 3.14: Haloperidol and sulpiride antagonise quinpirole induced dopamine D2L receptor internalisation

Both haloperidol (10nM) and sulpiride (30nM) inhibit quinpirole-induced receptor internalisation, as quantified by granularity analysis. However, as seen in **Figure 3.13**, haloperidol at 10nM alone induced some receptor internalisation. Data are pooled (mean ± SEM) from 4 independent experiments performed in triplicate and normalised to 10µM quinpirole (100%) and vehicle (0%) controls.

3.2.5 Determination of ligand affinities at the SNAP-tagged dopamine D2L receptor

The ability of all ligands to compete with [^{3}H]-spiperone for binding to the SNAP-tagged D2L receptor was examined to allow the calculation of ligand affinities. This was performed on membrane preparations in a sodium-free binding buffer as sodium is a known allosteric modulator of the dopamine D2 receptor (Neve, 1991). Saturation binding experiments were initially conducted (**Figure 3.15**); data were best fit to a single site model with B_{max} determined as 2.67 ± 0.33pmol mg^{-1} with [^{3}H]-spiperone pK_D as 10.42 ± 0.10 (n=4). Competition binding experiments were then completed for a panel of ligands (**Figure 3.16**), and in each case, selection of the most appropriate one site or two site model was determined by an extra sum of squares F-test. Most agonist competition curves were best fit to a two-site binding model, with the exceptions being aripiprazole and the ergo-derived compounds bromocriptine, cabergoline and dihydroergocristine (described sufficiently by one-site binding). All antagonists were also best fit to a single site model. IC_{50} values from these experiments were converted to pK_is using the Cheng-Prusoff correction (Cheng *et al.*, 1973), with data summarised in **Table 3.4**. The pK_i value for (-)-butaclamol could not be determined.

The pK_i for haloperidol of 9.18 ± 0.05 was very similar to the functionally derived pK_Ds however the sulpiride pK_i of 7.03 ± 0.09 was statistically different from both the SPAP (8.68 ± 0.19) and internalisation (8.37 ± 0.04) calculated pK_Ds ($P<0.05$; One way ANOVA followed by Dunnett's multiple comparisons test) (**Table 3.5**).

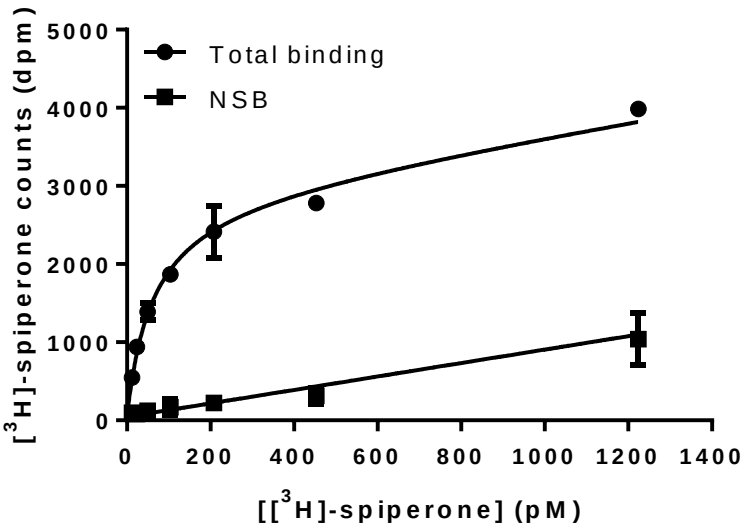


Figure 3.15: Determination of D2L receptor concentration and [^{3}H]-spiperone pK_D through saturation binding analysis

CHOcs ssD2L membranes were incubated with increasing concentrations of [^{3}H]-spiperone for 3h at room temperature prior to filtration. Non-specific binding (NSB) was determined in the presence of 3µM (+)-butaclamol. Data shown are a representative example (mean ± range) from 4 independent experiments performed in duplicate.

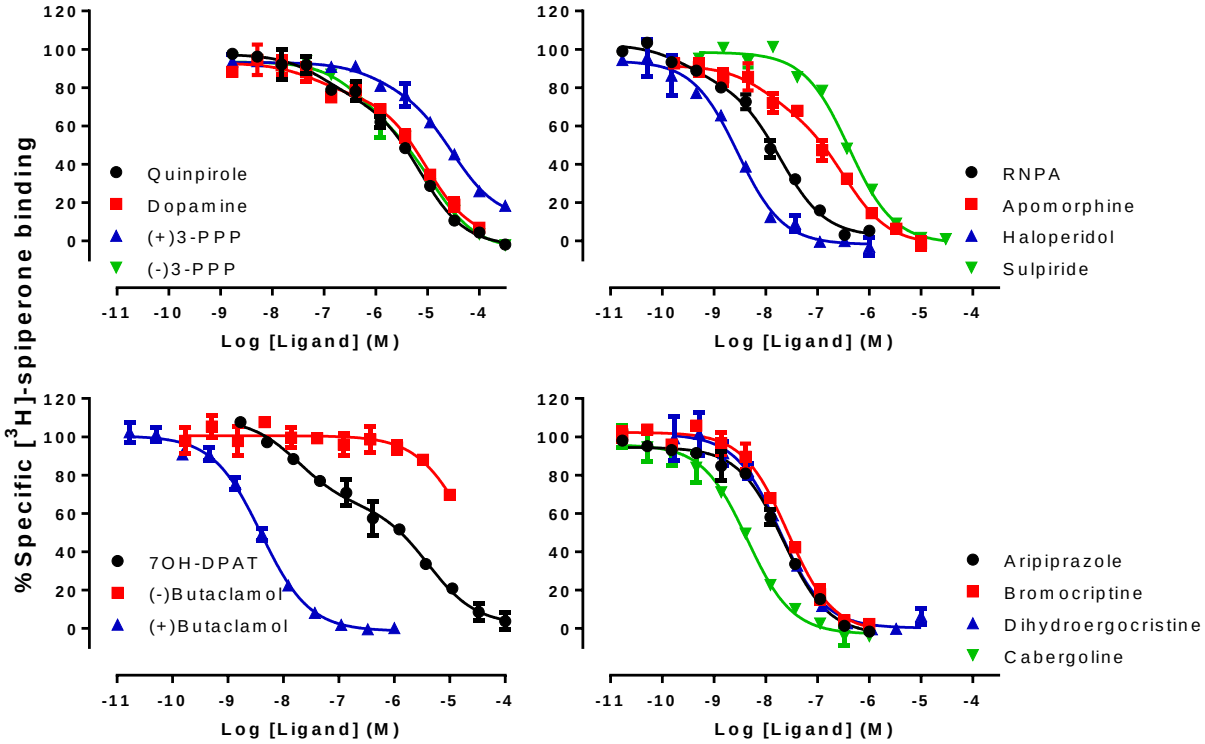


Figure 3.16: Determination of ligand affinities at the SNAP-tagged dopamine D2L receptor by [^{3}H]-spiperone competition binding

CHOcs ssD2L membranes were incubated with 70-130pM [^{3}H]-spiperone and competing ligand for 3h before filtration. Using the Cheng-Prusoff correction, these data were used to calculate the pK_is for all ligands (see **Table 3.4**). Data were fit to both one and two-site binding models as determined by an extra sum of squares F-test. Data shown are a representative example (mean ± range) from 4 independent experiments performed in duplicate, normalised to total binding (100%) and non-specific binding (0%) controls.

Ligand	pK_i High	pK_i Low	%High
Quinpirole	7.37 ± 0.11	5.69 ± 0.03	32.3 ± 5.2
Dopamine	7.68 ± 0.05	5.66 ± 0.07	23.1 ± 2.5
(+)-3-PPP	6.65 ± 0.05	4.98 ± 0.09	26.3 ± 4.4
(-)-3-PPP	7.16 ± 0.25	5.56 ± 0.10	38.7 ± 7.9
RNPA	9.56 ± 0.17	8.13 ± 0.08	38.8 ± 6.9
Apomorphine	8.46 ± 0.18	7.00 ± 0.08	26.2 ± 3.6
Haloperidol*	-	9.18 ± 0.05	-
Sulpiride*	-	7.03 ± 0.09	-
7OH-DPAT	8.11 ± 0.20	5.94 ± 0.23	30.1 ± 4.2
(+)-Butaclamol	-	8.82 ± 0.10	-
(-)-Butaclamol	ND	ND	ND
Aripiprazole*	-	8.46 ± 0.08	-
Bromocriptine*	-	8.17 ± 0.12	-
Dihydroergocristine*	-	8.26 ± 0.11	-
Cabergoline*	-	8.95 ± 0.03	-

Table 3.4: Summary of ligand affinities for the dopamine D2L receptor

Using the Cheng-Prusoff correction and the pK_D for [^{3}H]-spiperone determined from saturation binding analysis, ligand IC_{50}s from competition binding experiments (**Figure 3.16**) were converted to pK_i values using GraphPad Prism. Data were fit to either one-site(*) and or two-site binding models, as selected by an extra sum of squares F-test. Data represent pooled data (mean ± SEM) of 4 independent experiments performed in duplicate; ND = No displacement.

Ligand	pK_i binding	pA_2 SPAP	pK_D internalisation
Haloperidol	9.18 ± 0.05	9.06 ± 0.18	9.20 ± 0.20
Sulpiride	7.03 ± 0.09	8.68 ± 0.19*	8.37 ± 0.04*

Table 3.5: Comparison of calculated affinities for haloperidol and sulpiride

Summary of the calculated affinities for haloperidol and sulpiride from both functional and binding data. Data represent pooled data (mean ± SEM) of 4 independent experiments performed in duplicate or triplicate. *P<0.05 compared to pK_i (One-way ANOVA followed by Dunnett's post hoc analysis).

3.2.6 Investigation of the antagonism of EEDQ and PBz

Receptor depletion by irreversible antagonists is one method by which to obtain families of agonist concentration response curves suitable for operational model analysis (Black *et al.*, 1985). Two irreversible antagonists for the dopamine D2 receptor have been previously described that are potentially suitable for this method; EEDQ (Hamblin *et al.*, 1983) and PBz (Hamblin *et al.*, 1982). It was first necessary to determine the characteristics of each antagonist in the CHOcs ssD2L system and determine which was most appropriate for operational modelling. Initial experiments determined the concentration dependence for each compound to inhibit quinpirole induced responses in the SPAP assay (**Figure 3.17**). Both compounds (1-10µM, 30min pre-treatment) inhibited quinpirole responses, inducing right ward concentration response curve shifts. However, under these conditions, EEDQ behaved like competitive antagonist, while the actions of PBz appeared non-competitive, particularly at the highest concentration. As shown in **Figure 3.17**, while EEDQ and PBz treatments had no effect on responses in the absence of forskolin, they did cause small, concentration-dependent increases in forskolin-stimulated SPAP production. This was only significant for 3µM and 10µM EEDQ ($P<0.05$; One-way ANOVA followed by Dunnett's post hoc analysis).

Both ligands were also examined for their ability to inhibit quinpirole-induced receptor internalisation following 30min antagonist pre-treatment. Treatment with either antagonist had no effect on vehicle treated cells, with the receptor remaining on the cell surface (**Figure 3.18**). 1µM EEDQ did not have a significant effect on the quinpirole curve R_{max} (96.1 ± 5.3%) or pEC_{50} (6.06 ± 0.05) compared to control (R_{max} 104.8 ± 2.4%, pEC_{50} 6.42 ± 0.07). However at 10µM EEDQ, there was a significant reduction in R_{max} to 55.1 ± 10.5% 10µM quinpirole response and pEC_{50} to 5.01 ± 0.20 (One way ANOVA followed by Dunnett's post hoc analysis). In contrast, PBz completely abolished quinpirole dependent internalisation following preincubation at 1µM. However, at

100nM, it caused a reduction in quinpirole R_{max} to 70.0 ± 13.1 with no change in pEC_{50} (6.48 ± 0.05; n=2) (**Figure 3.18** and **Figure 3.19**).

For suitability in the operational model receptor depletion method, the antagonists used should be truly irreversible, at least within the time frame of the experiment. Thus, the reversibility of EEDQ and PBz was examined in paired experiments. Cells were pre-treated with maximal effective concentrations of EEDQ (10µM) and PBz (3µM) for increasing times. Following pre-treatment, one set of plates was washed to remove the antagonist before addition of the agonist and subsequent forskolin incubation. As seen in **Figure 3.20**, EEDQ inhibition showed no time dependent inhibition, and its effects on quinpirole SPAP responses were completely reversible with washout. In contrast, PBz inhibition increased with antagonist incubation time and persisted following washout.

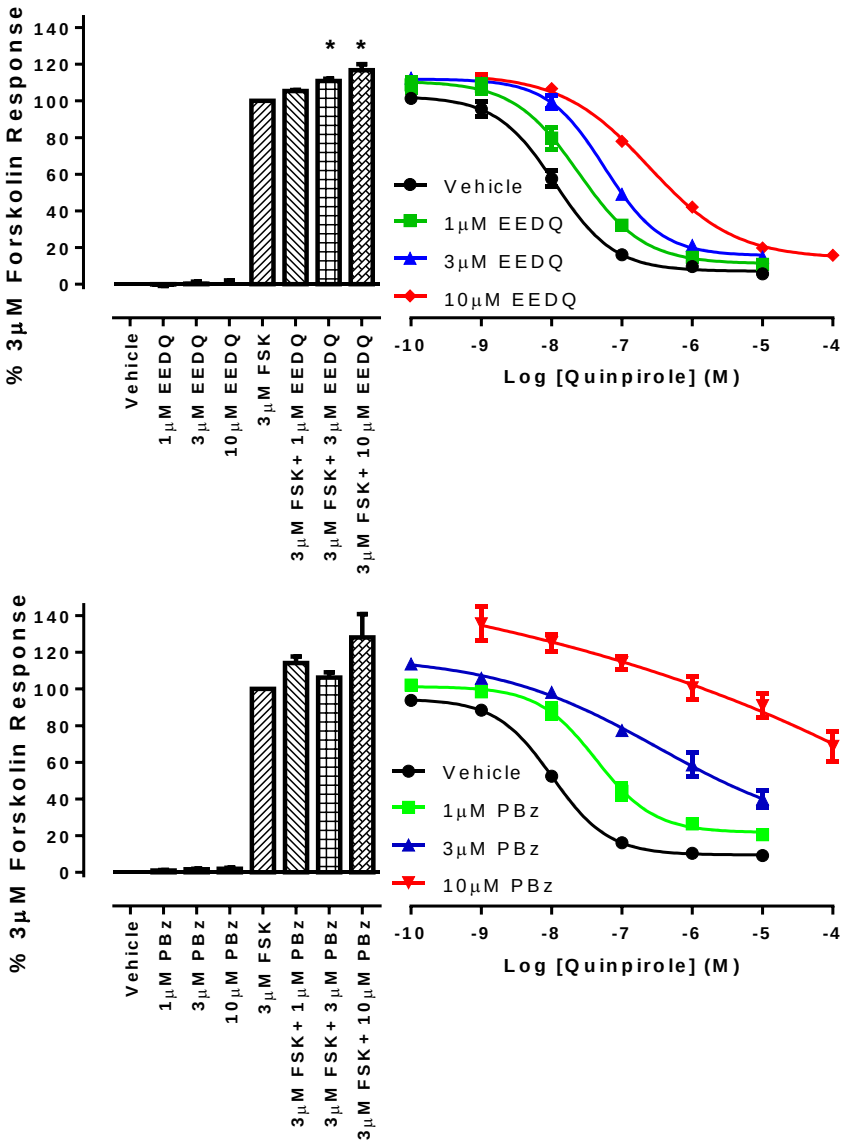


Figure 3.17: EEDQ and PBz inhibit quinpirole responses in the CRE-SPAP reporter gene assay in CHOcs ssD2L cells

CHOcs ssD2L cells were treated with 1-10µM EEDQ or PBz for 30mins prior to 30min incubation of increasing concentrations of quinpirole and 5h 3µM forskolin stimulation. Data represent pooled data (mean ± SEM) of 3 independent experiments performed in triplicate, normalised to 3µM forskolin (100%) and vehicle (0%) controls. *P<0.05 compared to 3µM forskolin (FSK) alone (One-way ANOVA followed by Dunnett's post hoc analysis).

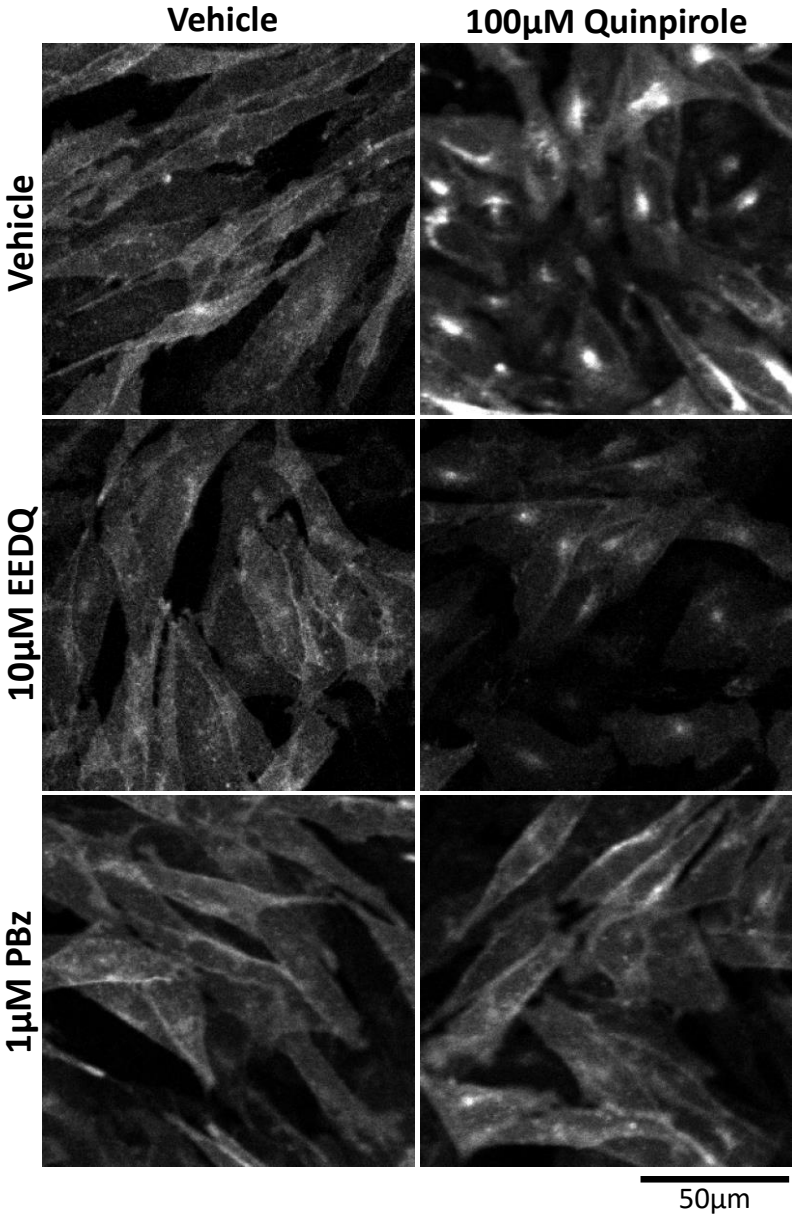


Figure 3.18: EEDQ and PBz inhibit quinpirole induced dopamine D2L receptor internalisation

CHOcs ssD2L cells were SNAP labelled, treated with either vehicle, 10µM EEDQ or 1µM PBz for 30min prior to 1h quinpirole stimulation and fixation. The panel above shows representative images of cells treated with either vehicle or 100µM quinpirole alone or following EEDQ or PBz pre-treatment. For clarity, the images above were cropped to 120µm x 120µm from the original 400µm x 400µm image used for analysis. This internalisation was quantified in **Figure 3.19**.

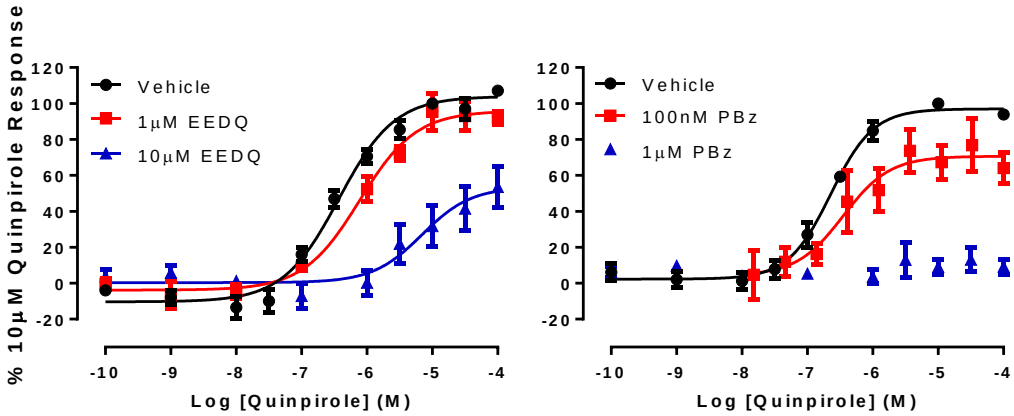


Figure 3.19: Quantification of EEDQ and PBz inhibition of quinpirole-induced D2L receptor internalisation

Cells were pre-treated with EEDQ (1-10µM) and PBz (100nM-1µM) for 30min prior to 1h quinpirole treatment and fixation. Both EEDQ and PBz antagonised quinpirole-induced receptor internalisation, as quantified by granularity analysis. Data points represent pooled data (mean ± SEM) from 4 independent experiments (except for 100nM PBz where n=2, expressed as mean ± range) performed in triplicate normalised to 10µM quinpirole (100%) and vehicle (0%) controls.

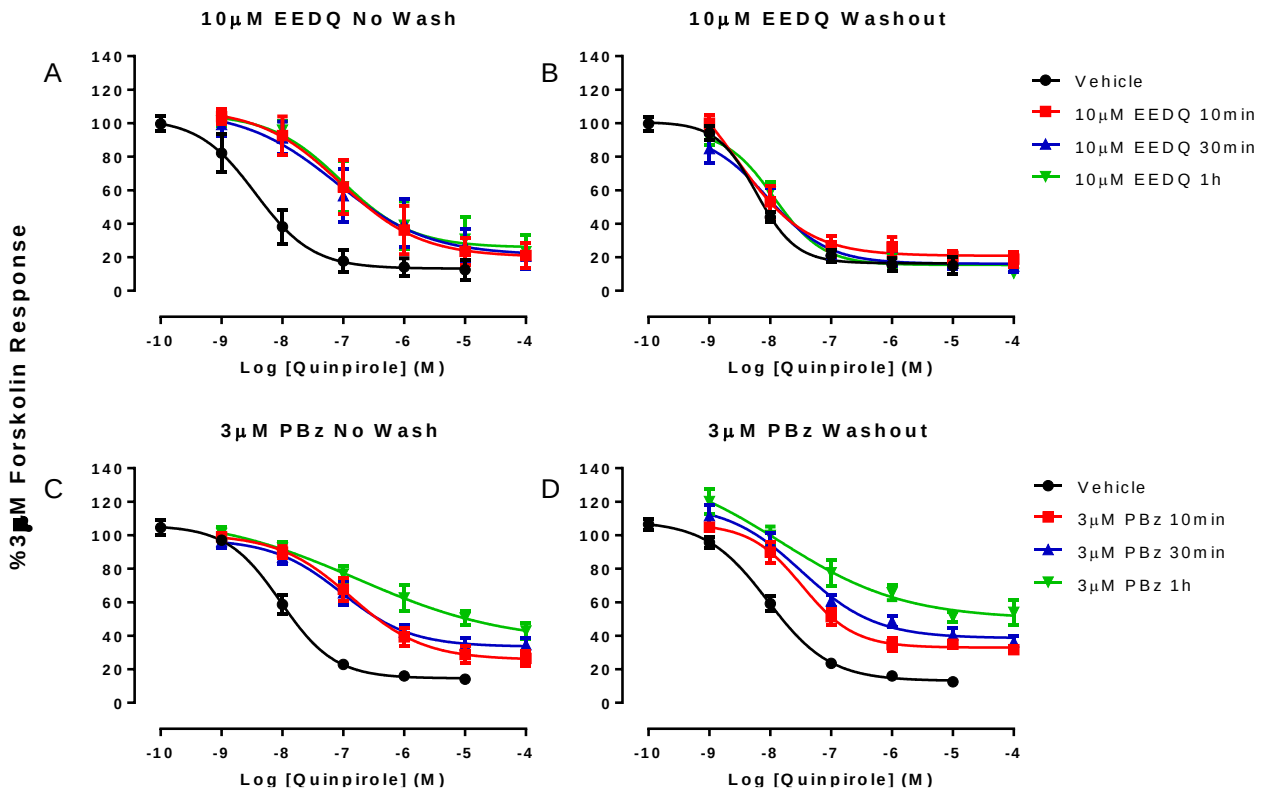


Figure 3.20: Effect of preincubation time and wash out on the irreversibility of PBz and EEDQ

10µM EEDQ (**A,B**) and 3µM PBz (**C,D**) were applied to quinpirole concentration response curves for increasing incubation times. In paired experiments, one plate was washed to remove the antagonist (**B,D**) following its preincubation and the other not (**A,C**) prior to addition of quinpirole and 3µM forskolin. Data represent pooled data (mean ± SEM) from 4 independent experiments performed in triplicate, normalised to 3µM forskolin (100%) and vehicle (0%) controls.

3.2.7 Operational modelling of agonist CRE-SPAP reporter gene assay responses

Based on experiments in **3.2.6**, PBz was deemed the most appropriate ligand for operational modelling of ligand responses. Four agonists of predicted differing efficacy, quinpirole, dopamine, aripiprazole and bromocriptine, were chosen for initial modelling experiments using the CRE-SPAP reporter gene assay. Concentration response curves were constructed following pre-incubation (30min) with increasing concentrations of PBz and the data globally fit to the operational model (**Figure 3.21**; **2.8.7**). As summarised in **Table 3.6**, fitting the operational model gave an order of efficacy (as defined by the logτ values) of quinpirole = dopamine > bromocriptine > aripiprazole and an order of affinity (pK_A) of bromocriptine = aripiprazole > quinpirole = dopamine. As expected by the decreased receptor number through receptor depletion, the logτ values decreased with increasing PBz concentration. The derived pK_A values for dopamine and aripiprazole were not significantly different to the radioligand binding derived pK_i low. This difference was significant however for both quinpirole and bromocriptine (**Table 3.7**, $P<0.05$; Student's unpaired t-test).

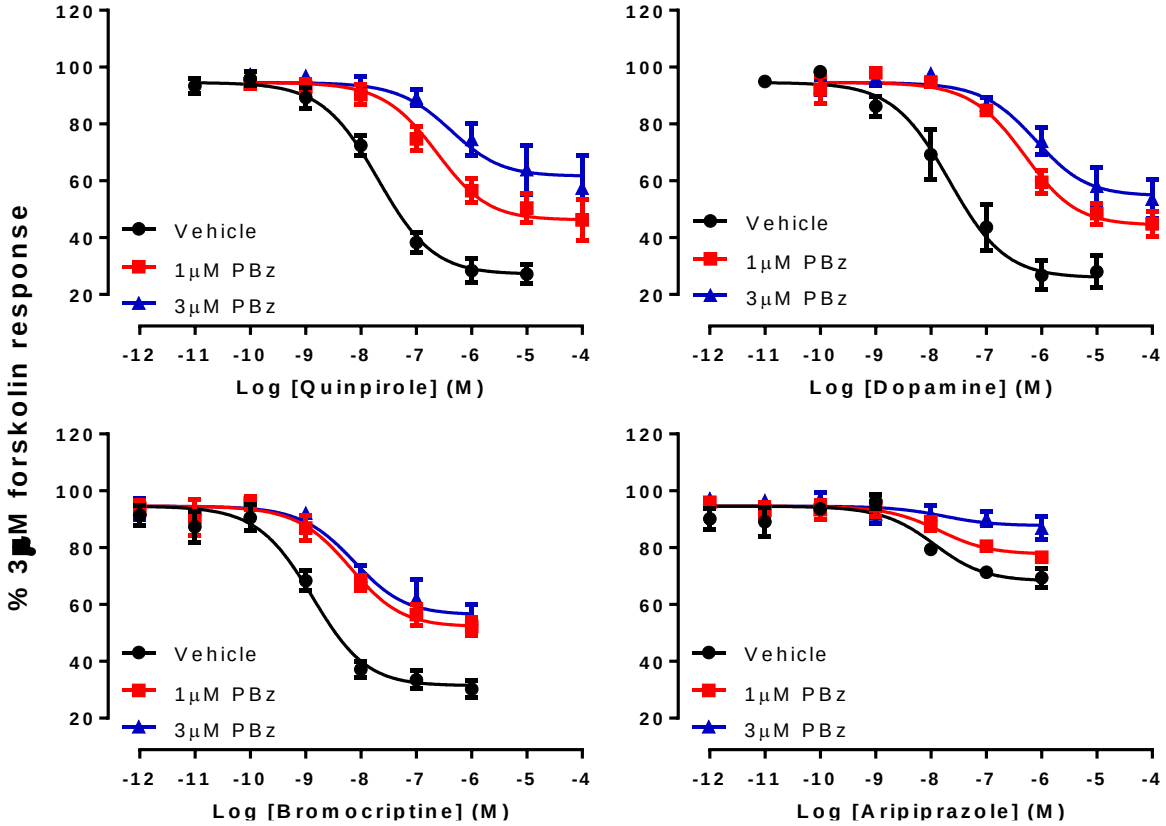


Figure 3.21: Operational modelling of agonist responses in the absence and presence of PBz Individual families of quinpirole, dopamine, bromocriptine and aripiprazole concentration response curves in the presence of vehicle, 1µM and 3µM PBz were globally fit to the operational model as described, with data summarised in **Table 3.6**. Data represent pooled data (mean ± SEM) from 4 independent experiments performed in triplicate, normalised to 3µM forskolin (100%) and vehicle (0%) controls.

Ligand	pK_A	Log τ (vehicle)	Log τ1 (1μM PBz)	Log τ3 (3μM PBz)
Quinpirole	6.53 ± 0.22	1.30 ± 0.17	0.16 ± 0.12	-0.22 ± 0.24
Dopamine	5.90 ± 0.21	1.35 ± 0.25	0.27 ± 0.09	-0.01 ± 0.16
Bromocriptine	7.78 ± 0.07	0.94 ± 0.13	0.10 ± 0.06	-0.11 ± 0.16
Aripiprazole	7.95 ± 0.23	-0.28 ± 0.22	-0.71 ± 0.15	-0.98 ± 0.24

Table 3.6: Summary of operational modelling of SPAP data

Agonist dissociation constants (pK_A) and efficacy estimates (τ) were determined from global fitting of the operational model to the SPAP data shown in **Figure 3.21.** Increasing PBz concentration decreased logτ values in line with the reduction in the receptor concentration following receptor depletion by irreversible antagonism. Data shown are pooled (mean ± SEM) of 4 independent experiments performed in triplicate.

Ligand	pK_A	pK_i low	Fold-difference
Quinpirole	6.53 ± 0.22*	5.69 ± 0.03	6.9
Dopamine	5.90 ± 0.21	5.66 ± 0.07	1.7
Bromocriptine	7.78 ± 0.07*	8.17 ± 0.12	2.5
Aripiprazole	7.95 ± 0.23	8.46 ± 0.08	3.2

Table 3.7: Comparison of affinities derived through operational modelling and competition binding experiments

Comparison of ligand affinities derived through operational modelling and [^{3}H]-spiperone competition binding experiments. Data are pooled (mean ± SEM) of 4 independent experiments performed in duplicate or triplicate. *$P<0.05$ c.f. pK_i low; Student's unpaired t-test.

3.3 Discussion

Here, we utilised a CHO cell line stably expressing both an N-terminal SNAP-tagged D2L receptor and a CRE-SPAP reporter gene to examine the pharmacology of a panel of dopamine D2 receptor ligands belonging to multiple classes of compounds. Ligands were assessed using two signalling readouts, CRE-SPAP reporter gene and receptor internalisation assays, to obtain orders of agonist potency and relative maximal responses. These were consistent with the levels of receptor reserve across the two assays and demonstrated that the SNAP-tag modification did not affect receptor functionality. In addition, antagonist affinity estimations were derived from functional data and were broadly consistent with [^{3}H]-spiperone competition binding data. Furthermore, PBz was identified as a suitable irreversible antagonist to allow fitting the standard operational model of agonism using the receptor depletion method to derive agonist affinity and efficacy estimations.

3.3.1 CRE-SPAP responses in the CHOcs ssD2L cell line are dependent on D2 receptor activation and $G\alpha_{i/o}$ mediated signalling

This study used the CRE-SPAP reporter gene assay as an indirect readout of cAMP accumulation. As the dopamine D2L receptor is known to couple to the $G\alpha_{i/o}$ family of G-proteins (Beaulieu *et al.*, 2011), it was necessary to artificially increase cellular cAMP using forskolin, a direct activator of adenylyl cyclase (Seamon *et al.*, 1981), in order to observe the inhibitory response. Initial experiments determined 3µM forskolin as the optimal assay concentration for future studies (**Figure 3.3**).

As the reporter gene is much further downstream in the signalling cascade than the initial second messenger signalling, there can also be issues regarding interference from other signalling cascades. When examining CRE-dependent reporter gene activity, it is essential to serum starve cells overnight prior to experimentation to reduce background from serum

induced modulation of CRE (Hill *et al.*, 2001). Furthermore, it is important to acknowledge that CRE-dependent reporter gene activity may not be solely dependent on cellular cAMP concentration. It has been shown at the β2AR that propranolol is an inverse agonist when measuring [^{3}H]-cAMP accumulation but an agonist when measuring CRE-mediated reporter gene transcription, which is not consistent with a singular, linear signalling cascade. The use of a U0126, an inhibitor of dual specificity mitogen-activated protein kinase kinase 1 (MEK-1) and MEK-2, attenuated propranolol responses, demonstrating the involvement of the MAPK pathway in CRE-dependent reporter gene activity at the β2AR (Baker *et al.*, 2003). At the dopamine D2 receptor, PTx treatment abolished ligand CRE-SPAP responses (**Figure 3.4**), demonstrating that CRE-dependent reporter gene activity in this cell line is dependent on the activation of $G\alpha_{i/o}$ proteins although input from other signalling cascades other than cAMP cannot be excluded.

In order to check that the responses measured were due to dopamine D2L receptor signalling, 6 ligands were examined for their responses in untransfected CHO CRE-SPAP cells. It has been previously demonstrated in a CHO cell line expressing a CRE-dependent reporter gene, that there are no endogenous dopamine responses in the presence or absence of forskolin, suggesting a lack of any endogenously expressed dopamine receptors (George *et al.*, 1997). Of the ligands tested, only bromocriptine was able to generate a concentration-dependent response (**Figure 3.5**). It was thought that this was due to activation of serotonin 5-HT_{1B} receptors endogenously expressed in CHO cells (George *et al.*, 1997) as bromocriptine has been shown to have moderate affinity for this receptor (Millan *et al.*, 2002). However, treatment with a 5-HT_{1B} inhibitor had no effect on the bromocriptine response (**Figure 3.6**). Furthermore, dihydroergocristine had no effect in this cell line despite being shown to be a partial agonist at 5-HT_{1B} receptors (Kemp *et al.*, 1999), suggesting this receptor is not involved in the response. However, as all ligands were only able to modulate forskolin-stimulated SPAP responses at concentrations above the concentration range used routinely, it was accepted

that the responses measured in the CHOcs ssD2L cell line were due to dopamine D2L receptor mediated signalling.

3.3.2 Dopamine D2 receptor agonists inhibit CRE-SPAP reporter gene activity

A panel of dopamine D2 receptor ligands were screened for their ability to inhibit forskolin-stimulated SPAP production (**Figure 3.7**). All agonists screened were full agonists except (-)-3-PPP, aripiprazole and dihydroergocristine. Given the amplification apparent in reporter gene assays (Hill *et al.*, 2001), it is no surprise that most agonists appeared equally efficacious in this assay. Aripiprazole and (-)-3-PPP are very weak partial agonists, with their agonism often only detectable following experimental manipulation such as changing buffer composition (Lin *et al.*, 2006) or increasing receptor expression levels (Koener *et al.*, 2012; Tadori *et al.*, 2011a; Tadori *et al.*, 2005). In the CHOcs ssD2L system, the increased signal amplification with a reporter gene assay also allowed detection of significant agonism with these compounds.

Few *in vitro* studies have examined dopamine D2L responses in cAMP-dependent reporter gene assays. Using a CRE-mediated luciferase reporter gene, Kemp *et al* reported that both dopamine and bromocriptine were full agonists with pEC_{50}s of 6.42 ± 0.09 and 6.79 ± 0.10 respectively, much lower than the pEC_{50}s of 7.70 ± 0.04 (dopamine) and 9.33 ± 0.12 (bromocriptine) reported here. In a subsequent study using the same cell line, further agonists and antagonists were analysed including RNPA, apomorphine, quinpirole and dopamine, all of which were full agonists with pEC_{50}s around 10-fold lower than reported here. However, this cell line reports much lower receptor expression (100fmol mg^{-1}) than the CHOcs ssD2L line and the cells were not serum starved prior to experiment, both of which may account for the reduced potencies compared with the data presented here. Furthermore, this study used a rat D2L receptor rather than human isoform, which also may account for differences.

The SNAP-tag is a 20 kDa protein fused to the N-terminus of the receptor (Keppler *et al.*, 2003; Keppler *et al.*, 2004) and as such, may prevent proper folding or trafficking of the receptor. However, previous reports with SNAP-labelled GPCRs have shown that they maintain cell surface expression and are functional (Keppler *et al.*, 2004; Kilpatrick *et al.*, 2015; Watson *et al.*, 2012). In general, agonist pEC_{50}s and relative maximal responses (including relative order of potencies) reported here for the SNAP-tagged D2L receptor are similar to published cAMP accumulation results at the D2L receptor (Hall *et al.*, 1999). This similarity indicates that modification of the N terminus with the SNAP-tag protein does not adversely affect D2L receptor function, a conclusion reinforced by cell surface expression and [^{3}H]-spiperone binding data discussed later (**3.3.6**).

3.3.3 Antagonism in the CRE-SPAP reporter gene assay – lack of evidence for receptor constitutive activity

None of the antagonists/inverse agonists screened showed any response, both in terms of inhibiting or potentiating SPAP production. A number of antagonists at the dopamine D2L receptor are reported to be inverse agonists at the dopamine D2S receptor (Hall *et al.*, 1997; Roberts *et al.*, 2005) however a constitutively active system is necessary to detect such responses.

Small increases in forskolin-stimulated SPAP production may be suggestive of constitutive activity by blocking a constitutive inhibition of forskolin-stimulated SPAP production. While small increases were observed in the presence of haloperidol and PBz (**Figure 3.3**), these were not consistently seen and were not significant. Furthermore, there was little evidence for potentiation of 3µM forskolin-stimulated SPAP responses in the presence of either of the reported irreversible antagonists, EEDQ and PBz. While 3-10µM EEDQ did cause a small, significant increase in SPAP production, there was no significant effect with PBz, which further experiments showed was a truly irreversible antagonist (**Figure 3.17,** discussed in **3.3.7**). Together, these

results suggest that the dopamine D2L receptor shows negligible, if any, constitutive activity in this assay.

The actions of haloperidol and sulpiride as antagonists were also assessed by Schild analysis (Arunlakshana *et al.*, 1959) (**Figure 3.8**). Schild plots also offer extra information regarding the nature of the antagonism with a Schild slope of one indicative of competitive antagonism. The haloperidol pA_2 was very similar to both the radioligand pK_i and internalisation derived pK_D (**Table 3.5**) however, the Schild slope of 1.66 ± 0.15 was significantly different from unity suggesting something other than simple competitive antagonism. Haloperidol here has been shown as a weak partial agonist in receptor internalisation assays (**3.2.4**) and therefore it is possible that over the assay timeframe, receptor sequestration could be affecting the resulting analysis – for example, by disrupting equilibrium conditions required for such method. In contrast, the unit Schild slope for sulpiride was consistent with competitive, reversible antagonism with the pA_2 and pK_D from the SPAP and internalisation assays consistent (**Table 3.5**) although the pA_2 was 51-fold greater than the radioligand pK_i (discussed further in **3.3.6**).

Unlike haloperidol and sulpiride, (+)-butaclamol treatment caused a depression in quinpirole R_{max} normally associated with non-competitive antagonism (**Figure 3.9**) precluding the application of Schild analysis to determine affinity. There is little evidence for (+)-butaclamol behaving as an irreversible antagonist at this receptor, although there are many reports it is a strong inverse agonist (Hall *et al.*, 1997; Roberts *et al.*, 2004; Roberts *et al.*, 2005) which may contribute to this reduction in response. Although, as discussed above, there is little evidence for receptor constitutive activity in this assay. Another explanation surrounds the kinetics of (+)-butaclamol; (+)-butaclamol has much slower kinetics than both haloperidol and sulpiride (DA Sykes, personal communication) which may cause the appearance of non-competitive antagonism. It is possible that despite the long assay incubation time, (+)-butaclamol and quinpirole were not reaching equilibrium leading to the appearance of non-competitive antagonism.

3.3.4 Estimation of dopamine D2L receptor agonist efficacy using receptor internalisation assays

The CRE-SPAP reporter gene assay predominantly reflects G protein-dependent signalling in response to dopamine D2L receptor activation, in which a high degree of signal amplification supports high relative maximal responses for agonists reported to exhibit low efficacy (Hill *et al.*, 2001). To examine an alternative signalling pathway expected to have lower receptor reserve, we established an automated imaging method to quantify receptor internalisation responses. This unique method of examining internalisation allows the collection of both quantitative and qualitative data in a single experiment and has been successfully used by others in the group to quantify the internalisation of the adenosine A_1 and neuropeptide Y receptors (Kilpatrick *et al.*, 2010; Stoddart *et al.*, 2014).

The markedly reduced receptor reserve in the internalisation assay leads to significant decreases in agonist potencies as well as a greater range of relative maximal responses compared with the reporter gene assay results. This reduction in receptor reserve is further reflected in the inhibition of quinpirole responses by the irreversible antagonist PBz (**3.3.7**); while 1μM PBz only reduces agonist R_{max} and pEC_{50} in the CRE-SPAP reporter gene assay (**Figure 3.21**), it abolishes quinpirole induced receptor internalisation (**Figure 3.18**). Furthermore, preliminary data with a reduced PBz concentration demonstrated no potency shift in the quinpirole concentration response curve despite the reduced R_{max} following receptor alkylation. Taken together, these results indicate that there is minimal receptor reserve in this assay, which is expected because it measures an event at the level of the receptor. While there was a potency shift with EEDQ treatment in the internalisation assay (**Figure 3.18**), later experiments have shown this antagonist is not irreversible and as such, has a different mechanism of action to PBz (discussed further in **3.3.7**). It has been suggested that for assays with no receptor reserve, R_{max} is a good measure of relative ligand efficacy (Stott *et al.*, 2016) however the lack of signal amplification also presents problems

with the identification of weak partial agonists. If internalisation R_{max} alone were used to determine dopamine D2 receptor agonist efficacy, the three compounds unable to internalise the receptor would be classed as antagonists, which is not supported by their agonism in amplified systems.

In this assay, only dopamine, quinpirole, RNPA and 7OH-DPAT were full agonists, with (+)-3-PPP, apomorphine, bromocriptine, pergolide and cabergoline partial agonists. Aripiprazole, (-)-3-PPP and dihydroergocristine were unable to internalise the receptor (**Figure 3.13**). This is in agreement with previously published work that showed neither aripiprazole nor (-)-3-PPP could internalise FLAG-tagged D2L receptors expressed in HEK293 cells (Urban *et al.*, 2007b) and supports the order of efficacy from operational modelling (discussed later in **3.3.8**).

Early studies of dopamine D2 receptor internalisation utilised [^{3}H]-sulpiride, a hydrophilic antagonist radioligand which should only label cell surface receptors, to determine receptor internalisation by relating this to a loss of plasma membrane radioligand binding sites after agonist stimulation. The potency of dopamine-induced receptor internalisation for both the dopamine D2L and D2S receptors matches the pEC_{50} reported here for our SNAP-tagged D2L (Itokawa *et al.*, 1996). While offering some insight into potential mechanisms, use of radioligands naturally does not allow cell imaging and therefore the potential to monitor intracellular receptor locations. Goggi *et al* (2007) attempted to address this by detailing a method using region of interest analysis on confocal images of CHO D2S cells stained with fluorescently-conjugated secondary antibodies. They were able to quantify total internalisation following treatment with maximal concentrations of dopamine, bromocriptine and sulpiride, with bromocriptine a partial agonist relative to dopamine-induced internalisation and sulpiride treatment inhibiting agonist-induced internalisation in agreement with the results here (Goggi *et al.*, 2007). This confocal imaging method however is low throughput and did not generate concentration responses curves. Heusler *et al* used an indirect ELISA-based assay to examine the ability of ligands to internalise N-

terminal hemaglutinin (HA) tagged D2S and 5-HT_{1A} receptors. In this method, HA-tagged receptors were stimulated with ligand for 2h prior to fixation then receptor internalisation quantified through immunological detection with an anti-HA antibody. It was found that quinpirole could only induce a 20% loss in cell surface receptors following 2h incubation with aripiprazole internalisation negligible; however this could be markedly increased with co-expression of GRK2 and β-arrestin2 (Heusler *et al.*, 2008). Under those conditions, agonist concentration response curves for a number of compounds were derived. The pEC_{50}s are comparable with those presented here however relative maximal responses for some compounds were higher (bromocriptine full agonist; aripiprazole and (-)-3-PPP partial agonists), perhaps due to the over-expression of β-arrestin2 and GRK2, and the use of the D2S rather than D2L receptor isoform (Heusler *et al.*, 2008).

While comparisons with the above studies generally agree with the data presented here, most have used the D2S receptor rather than the D2L receptor. There is evidence that these receptors can internalise through different mechanisms (Kim *et al.*, 2004) (**1.5.3**) and as such, these comparisons must be made with care. The main advantage of the internalisation method used here is the ability to directly label and visualise receptors prior to and following ligand stimulation, unlike many of the indirect methods described above which use a loss of signal to infer receptor internalisation. Furthermore, the use of membrane impermeable SNAP-labels ensures only cell surface receptors are initially labelled and subsequently monitored, which can be confirmed through imaging. This approach however does involve receptor modification unlike for example, the radiolabelling approach, but evidence suggests this has not affected the receptors pharmacology (**3.3.2**). Moreover, the analysis described only picks up receptor accumulation in large intracellular compartments. As such, it is not only quantifying the receptor internalising from the membrane, but also subsequent intracellular trafficking.

3.3.5 Antagonist responses in the internalisation assay

Most of the antagonists examined failed to internalise D2L receptors (**Figure 3.13**) but could antagonise quinpirole-induced receptor internalisation with an equivalent affinity to that derived from Schild analysis of the CRE-SPAP reporter gene assay data (

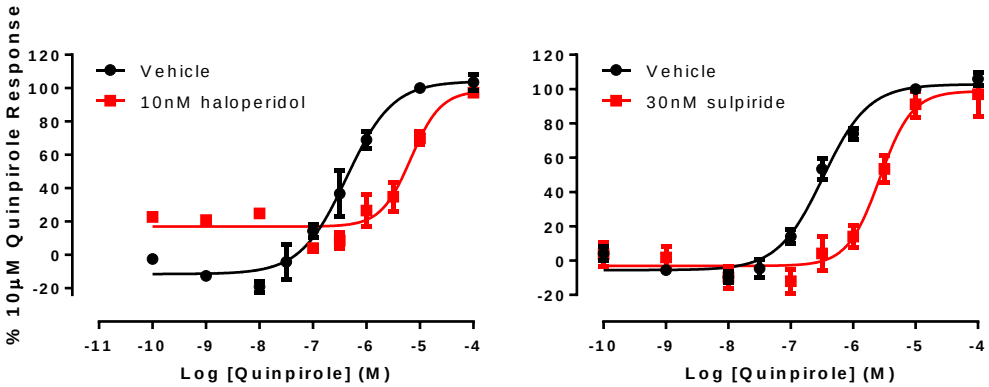


Figure 3.14). Interestingly, haloperidol was able to produce a modest internalisation response. There are examples in the literature of antagonists producing an internalisation response, for example at the cholecystokinin receptor (Roettger *et al.*, 1997), chemokine receptor CCR4 (Ajram *et al.*, 2014) and serotonin 5-HT_{2A} receptor (Raote *et al.*, 2013); however, haloperidol-induced D2 receptor internalisation has not been reported, even following co-expression of GRK2 and β-arrestin2 (Heusler *et al.*, 2008). While it is possible this is a non-specific effect, which could be examined by attempting to inhibit the response with other D2 receptor selective antagonists, the potency is close to the affinity measurements suggesting it is a ligand-mediated response. Another explanation could be that haloperidol is a biased ligand (**1.6.3**), selectively engaging β-arrestin-mediated pathways over $G\alpha_{i/o}$ signalling. However, there is evidence that in HEK293 cells expressing the dopamine D2L receptor, haloperidol does not recruit β-arrestin2 (Masri *et al.*, 2008) which is thought to be important in the internalisation of the D2 receptor (**1.5.3**).

β-arrestin independent internalisation has been reported for a number of GPCRs such as the metabotropic glutamate receptor 1 and the prostacyclin

receptor, with suggestions of an alternative adaptor protein, or the GRKs interacting with clathrin, to drive internalisation (van Koppen *et al.*, 2004). Furthermore, there have been reports that PKC activation alone is sufficient to drive receptor internalisation in 5-HT_{2A} receptors (Bhattacharyya *et al.*, 2002) with evidence for ligand-dependent mechanisms of internalisation, both dependent and independent of PKC at this receptor (Raote *et al.*, 2013). The PKC activator PMA can induce D2S receptor internalisation, which can be blocked by the specific PKC inhibitor Gö6976 (Cho *et al.*, 2013) suggesting a potential role for PKC in D2 receptor internalisation. Thus, it is possible that haloperidol (and potentially other ligands) can internalise the receptor in such a manner.

3.3.6 Determination of ligand affinities at the SNAP-tagged dopamine D2L receptor

Radioligand binding was performed to determine ligand affinities at the SNAP D2L receptor (**Figure 3.16**). The calculated affinities were within range of those reported in the literature for both the dopamine D2L and D2S receptors (Gardner *et al.*, 1998; Roberts *et al.*, 2004), providing further evidence that the SNAP-tag did not modify the pharmacological properties of this receptor. As sodium is a known allosteric modulator of the D2 receptor with its presence inducing significant changes in the binding affinities for a number of ligands (Neve, 1991; Neve *et al.*, 1991; Neve *et al.*, 2001), a sodium-free buffer, previously used in the literature (Gazi *et al.*, 2003; Lane *et al.*, 2007; Wilson *et al.*, 2001) was used for this assay.

The absence of Na^+ from the buffer increases the presence of two-site binding for agonists; however, this was only obtained for a subset of agonists. The ergo-derived compounds, bromocriptine, cabergoline and dihydroergocristine, along with the partial agonist aripiprazole, only displayed a single binding site (**Figure 3.16**). Bromocriptine has been previously reported to only display a single-site binding in a Na^+-free buffer when other agonists profiled displayed two sites. The authors there suggested that

bromocriptine may produce a different active state than other agonists (discussed further in **Chapter Four**) (Roberts *et al.*, 2004). It has been suggested that ergo-derived compounds engage the D2 receptor binding site by a different mechanism than traditional D2 receptor ligands, many of which have a number of hydroxyl groups which engage serine residues in the binding site. It has been proposed that the ergo-derived compounds bind preferentially to S5.46 whereas hydroxyl-containing agonists engage more with S5.42, which sits one turn of an alpha helix higher on TM5 (Krogsgaard-Larsen *et al.*, 2014) (**4.1.3**).

There was a large discrepancy between the functional and radioligand derived affinities for sulpiride (**Table 3.5**). The binding derived pK_i closely matches literature reports of sulpiride affinity in NaCl-free assay buffers (Roberts *et al.*, 2005; Wilson *et al.*, 2001) whereas the functional affinities were at least 22-fold higher. This large difference in derived affinities could be due to the differing experimental conditions between whole cell and membranes, and the resulting differences in buffer composition. Whole cell experiments, such as the CRE-SPAP reporter gene and internalisation assays were conducted in SFM and HBSS respectively, both of which contain physiological concentrations of NaCl. It has been demonstrated that some D2 receptor ligands, including sulpiride, are sodium sensitive with regard to their receptor binding. Literature reports have demonstrated a 10-44 fold increases in sulpiride affinity with the inclusion of NaCl in the assay buffer (Neve, 1991; Neve *et al.*, 2001). It is believed that the dopamine D2 receptor contains a sodium binding pocket, formed by interactions with residues in TM1, 2, 3 and 7 (Neve *et al.*, 2001; Selent *et al.*, 2010). Mutation of the conserved TM2 aspartate residue (D2.50) to alanine or glutamate induced marked decreases in ligand affinities for a number of compounds, and reduced the impact of NaCl removal from the buffer (Neve *et al.*, 1991).

3.3.7 PBz, but not EEDQ, is an irreversible antagonist of the dopamine D2 receptor

Both EEDQ and PBz are reported as irreversible antagonists of the D2 receptor (Hamblin *et al.*, 1983; Hamblin *et al.*, 1982) and have both been previously used as alkylating agents to reduce the D2 receptor population in both *in vitro* and *in vivo* studies (Burris *et al.*, 2002; Meller *et al.*, 1992; Meller *et al.*, 1991). PBz is an example of a β-haloalkylamine, which is reported to bind irreversibly to a number of monoamine receptors including the α-adrenoceptor family and histamine H_1 (Frang *et al.*, 2001; Jenkinson, 2003) as well as to the D2 receptor. Once in solution, it is thought to cyclise and form an ethyleneiminium ion that can open in the binding site to form a reactive intermediate. This intermediate is then free to covalently bind the receptor, binding irreversibly to side chains such as –SH, -OH, =NH and –COOH (Jenkinson, 2003). PBz irreversibility at the β2AR and α_{2A}-adrenoceptor is dependent on the presence of a TM3 cysteine (C3.36) in the binding site, located one alpha helix turn down from the conserved aspartate (D3.32). Mutation of C3.32 in the α_{2A}-adrenoceptor prevents the irreversible blockade by PBz while introducing this residue into the β2AR, which has a valine in the corresponding site and is largely resistant to PBz treatment, creates a receptor more susceptible to PBz blockade. Together, this suggests this residue is a target for alkylation (Frang *et al.*, 2001). In the dopamine D2 receptor, the corresponding residue is also a cysteine and like the α_{2A}-adrenoceptor, this residue is exposed in the binding site (Javitch *et al.*, 1995), suggesting it may be the target for PBz binding. All 3 receptors also have the highly conserved TM3 aspartate (D3.32) in the binding site which contains a side chain amenable to PBz binding but the relative lack of efficacy of PBz at the β2AR suggests this residue is not the main target for binding (Frang *et al.*, 2001). It has been shown that PBz in its parent form has very little reactivity at the α-adrenoceptors expressed in rat vas deferens, and that is only the ethyleneiminium ion reactive intermediates which form rapidly (within 3min)

in solution that are responsible for the irreversible blockade (Henkel *et al.*, 1976).

EEDQ is thought to act in a different manner to PBz. Studies on α-adrenoceptors expressed in rabbit aorta have suggested EEDQ acts at two distinct sites at this receptor; one which it shares with PBz and a second where EEDQ binding can be potentiated by binding of amines (Kalsner, 1973). Its mechanism of binding is thought to involve the generation of a reactive intermediate containing a carboxyl group, which leads to cross-linking and receptor inactivation (Belleau *et al.*, 1969; Kalsner, 1973).

The fitting of both the Black and Leff (Black *et al.*, 1983; Black *et al.*, 1985), and Slack and Hall (Slack *et al.*, 2012), operational models to functional data requires data sets in which the system coupling efficiency has been varied; this is often achieved through receptor depletion by irreversible antagonists (**1.8.3**). It was important to establish appropriate PBz and EEDQ concentrations that reduce cell surface receptor density, and critical to confirm that they acted irreversibly within the time frame of the assay so that any subsequent modelling was completed appropriately. In order to validate their irreversibility, both compounds were examined in washout experiments in which antagonist preincubation time was varied (**Figure 3.20**). If an antagonist is irreversible, in theory extending the incubation time should increase the level of antagonism by decreasing the number of binding sites accessible to agonist (Kalsner, 1973). It was found that the actions of EEDQ, but not those of PBz, were reversible upon ligand washout. Previous studies have demonstrated that a 1h incubation with 1μM or 10μM EEDQ can cause 50% and 80% receptor depletion respectively, as determined by radioligand binding (Burris *et al.*, 2002). The discrepancy around the reversibility of EEDQ could be that the total incubation time of the SPAP assay (at least 6h) is much longer than the previously conducted radioligand binding assays. Thus, it is possible that EEDQ is acting as a reversible antagonist but with slow dissociation kinetics, which within a shorter timeframe gives the appearance of irreversible antagonism.

3.3.8 Determination of ligand efficacy and affinity through application of the Black and Leff operational model

As PBz antagonism persisted following washout, PBz was used in subsequent studies as the irreversible antagonist to allow operational modelling of data. As described previously (**3.3.1**), a reporter gene is far downstream of the receptor and thus there is the potential for interference from other signalling pathways. In addition to the irreversible antagonism of a number of monoamine receptors, PBz is an irreversible antagonist of the Ca^{2+} binding protein calmodulin (Cimino *et al.*, 1988). Binding of Ca^{2+} to calmodulin increases the affinity of calmodulin for calmodulin kinases (CaMKs), leading to the activation of calcium/calmodulin-dependent kinase kinase 2 (CaMKK2) which then modulates further CaMKs to regulate downstream signalling pathways. Additionally, the activity of CaMKK2 can be inhibited by PKA, a downstream target of cAMP (Racioppi *et al.*, 2012). Thus, there is the potential that PBz is modulating CRE-SPAP activity through not only inhibition of dopamine D2 receptor mediated signalling, but through modulation of calmodulin signalling. However, as shown in **Figure 3.17**, there was no effect of PBz on CRE-SPAP responses alone or in the presence of forskolin, suggesting its main action in this system was to inhibit dopamine D2 receptor mediated responses.

In the absence of measureable constitutive activity, the Black and Leff operational model was fitted to the data to derive ligand τ and pK_A estimates. Global fitting of data (in this case across 12 data sets - 4 agonists, vehicle and 2 PBz concentrations) reduces variability of derived parameter estimations because of the increased number of data points in the fit, thus giving the model more information on the system under measure (Hall *et al.*, 2010). This is especially true when fitting partial agonist data, where a full agonist is required to define the E_{max} (Leff *et al.*, 1993). Thus, it was especially important for fitting the aripiprazole data that the other data sets could provide the model with an appropriate value for E_{max} to allow a better estimate of its τ value.

In theory, functionally derived pK_As should match pK_i low values. It is thought that the high-affinity binding site corresponds to the binding of the receptor-G protein complex and is guanine-nucleotide sensitive, whereas the low affinity state corresponds to binding of the uncoupled receptor in its inactive state (Roberts *et al.*, 2004). As the pK_A values derived from modelling are from functional, whole cell data, the low affinity site is predicted to predominate because of the high cellular GTP concentration. Despite significant differences in the conditions associated with each assay have been conducted, generally, there was a good agreement between the pK_i low and pK_A values for the 4 ligands examined although the differences were significant for quinpirole and bromocriptine (**Table 3.7**).

There have been suggestions that reporter gene assays are unsuitable data sets for operational modelling (Leff *et al.*, 1989; Nickolls *et al.*, 2011). The basis of this criticism is that the operational model can overestimate agonist affinity and provide inaccurate τ estimates under conditions in which the transducer is far in excess of the receptor concentration e.g. for a highly amplified signalling endpoint (Leff *et al.*, 1989). As only the quinpirole pK_A was greater than 3-fold different to the pK_i low, it suggests in general that our pK_A values have not been overestimated.

As τ is a convolved parameter, equal to the ratio of receptor concentration (R_T) and stimulus coupling efficiency (which is itself dependent on both ligand intrinsic efficacy and system coupling efficiency; **1.8.3**), it cannot provide a ligand efficacy estimation which can be compared across multiple systems. However, a rank order of agonist τ values, within the same assay system, should still indicate an appropriate order of intrinsic efficacy. For the four agonists studied, the order of τ values of quinpirole = dopamine > bromocriptine > aripiprazole is in agreement with both the known pharmacology of these ligands at the dopamine D2L receptor and the results presented within this chapter. Both quinpirole and dopamine are full agonists at this receptor in both assays examined and as such would be expected to have similar τ values. Equally, the very low τ value for aripiprazole is

consistent with both sets of assay data and its low efficacy reported elsewhere (Lin *et al.*, 2006; Urban *et al.*, 2007b). Despite being a full agonist in the high receptor reserve CRE-SPAP reporter gene assay, the lower τ value for bromocriptine is consistent with its revealed partial agonism in the internalisation assay. This is also in agreement with previous studies which have bromocriptine as a full agonist in similar reporter gene assays (Kemp *et al.*, 1999) and a partial agonist in functional readouts less downstream of the receptor, such as [^{35}S]-GTPγS binding (Gardner *et al.*, 1998). Thus, even where agonists have similar R_{max} responses within an assay format, the application of the operational model can allow the distinction between agonists of differing intrinsic efficacy.

3.4 Conclusions

This chapter established two methods to determine agonist efficacy at the SNAP-tagged dopamine D2L receptor – the CRE-SPAP reporter gene assay as a downstream measure of cAMP production and receptor internalisation assays. The variations in ligand response between the two assays were consistent with the increased receptor reserve in the highly amplified reporter gene assay. As maximal responses are often a poor indicator of relative ligand efficacy (**1.8.1**), we moved to identify assay conditions that would allow the application of operational models. PBz was identified as a suitable irreversible antagonist for application of the receptor depletion method of the Black and Leff operational model. This allowed the derivation of agonist affinity (K_A) and efficacy (τ) estimations for 4 representative agonists which were consistent with the functional and binding data presented both within the chapter and the literature. However, the lack of constitutive activity in the cell line precluded the use of the Slack and Hall operational model. As such, a number of ways to generate constitutive activity at the dopamine D2 receptor was then investigated, including the generation of a constitutively active D2L receptor (T6.34R; **Chapter Four**), the use of the dopamine D2S receptor and alternative assays such as [^{35}S]-GTPγS binding assays (**Chapter Five**).

Chapter Four: Differential roles of transmembrane 5 serine residues in agonist binding to wild type and constitutively active D2L receptors: evidence for multiple activated receptor conformations

4.1 Introduction

Initial characterisation of the CHOcs ssD2L cell line provided little evidence for the receptor constitutive activity necessary to apply the Slack and Hall operational model. Thus, it was decided to examine whether a constitutively active D2L receptor could be generated through receptor mutagenesis. Constitutive activity has been identified at a wide range of GPCRs (Seifert *et al.*, 2002). While there are some examples of receptor constitutive activity at physiological expression levels (Meye *et al.*, 2014; Seifert *et al.*, 2002), it has mostly been identified either through increasing receptor concentration or introducing mutations (Seifert *et al.*, 2002; Smit *et al.*, 2007). Constitutively active mutant (CAM) receptors have been described for a wide number of receptors. These receptors are proposed to favour receptor activation by shifting the receptor equilibrium to the R* state (as described by the two state model (**1.7.3**)). This leads to increases in agonist affinity, efficacy and an increased ability to detect constitutive activity (Seifert *et al.*, 2002). A number of receptor regions have been targeted to generate CAMs, such as the DRY motif (**1.4.3**) and the BBXXB motif.

4.1.1 The role of the BBXXB motif in receptor activation

The BBXXB motif (where B represents a basic residue and X a non-basic), is located at the junction between ICL3 and TM6 and has been reported to be important in receptor activation. Mutations to this motif have generated constitutive activity in a number of GPCRs, particularly class A monoamine receptors and μ-opioid receptors (Huang *et al.*, 2001; Kjelsberg *et al.*, 1992; Pauwels *et al.*, 1999; Purohit *et al.*, 2003; Ren *et al.*, 1993; Spalding *et al.*, 1997). It has therefore been proposed that this region may be important conformationally in holding the receptor in an inactive state or facilitating G protein binding (Pauwels *et al.*, 1999). Wilson *et al* investigated the role of this region in the dopamine D2 receptor, mutating T6.34 (BBX**X**B) of the D2S receptor to lysine, arginine and serine, with the greatest increase in constitutive activity seen with the arginine mutation. Generally, the mutation

increased agonist affinities and functional potencies, and increased receptor constitutive activity (Wilson *et al.*, 2001).

As previously described (**1.4.2**), receptor activation of class A GPCRs is associated with substantial rearrangements of the TM domains, in particular, an outward movement of the intracellular end of TM6 (Dror *et al.*, 2011; Rasmussen *et al.*, 2011a). While most studies have focussed on the interaction between R3.50 and E6.30 (the so-called 'ionic lock' (Rovati *et al.*, 2007) (**1.4.3**)), it is evident in the inactive crystal structures of rhodopsin and μ-opioid receptor that R3.50 also interacts with T6.34 (Manglik *et al.*, 2012; Palczewski *et al.*, 2000). This interaction is proposed to hold the receptor in an inactive state, and is broken in the active state structure of the μ-opioid receptor (Huang *et al.*, 2015). In a study at the rat μ-opioid receptor, T6.34 was mutated to lysine, generating a CAM receptor. When this receptor was modelled computationally, the amino acid substitution generated a repulsive force which favoured the movement of TM6 away from TM3, thus promoting the active state of the receptor (Huang *et al.*, 2001).

In a subsequent study, L6.30 of the rat μ-opioid receptor was mutated to glutamate in the T6.34K background to mirror constitutively activating mutations at monoamine receptors. This double mutant had reduced constitutive activity compared to the T6.34K receptor, which appeared to contradict studies with CAMs of monoamine receptors. Computational analysis suggested that the inclusion of the glutamate stabilised interactions between TM3 and TM6, reducing the propensity of the receptor to adopt the active state (Huang *et al.*, 2002). Modelling of the μ-opioid and α_{1B}-adrenoceptors revealed that the μ-opioid receptor has bulkier side chains in the cytoplasmic ends of TM5 and TM6 that creates a larger space to tolerate mutations at position 6.34. In contrast, the shorter distance between the corresponding side chains in the α_{1B}-adrenoceptor results in mutations of this residue being poorly tolerated. This is especially true when this residue (most commonly the smallest amino acids glycine or alanine in monoamine receptors) is replaced with those containing larger side chains. This creates

steric clashes, leading to conformational rearrangements of TM5 and TM6 to relieve the clashes which promotes the active state of the receptor (Huang *et al.*, 2002). This is supported by an early mutagenesis study at the α_{1B}-adrenoceptor whereby A6.34 was mutated to all other possible 19 amino acids with every mutation inducing some degree of receptor constitutive activity. The greatest effects were seen with some of the largest, and charged, amino acids, arginine, lysine and glutamate, supporting the notion that introducing steric clashes in TM6 may promote receptor activation (Kjelsberg *et al.*, 1992).

Thus, it is hypothesised for the dopamine D2 receptor that the replacement of T6.34 with larger, charged residues will induce receptor constitutive activity by introducing steric clashes in TM6 that promote the conformational rearrangements required for adoption of the active state. Constitutive D2 receptor activation may also be achieved by mutations of the ionic lock residues. While this interaction is absent from many of the inactive state GPCR crystal structures, it is present in the dopamine D3 crystal structure (Chien *et al.*, 2010) and homology modelling suggests it is also present in the inactive D2 receptor structure (Platania *et al.*, 2012).

4.1.2 Binding site of the dopamine D2 receptor

The binding site of the dopamine D2 receptor has been extensively probed through both mutagenesis studies (Coley *et al.*, 2000; Fowler *et al.*, 2012; Javitch *et al.*, 1995; Mansour *et al.*, 1992; Wiens *et al.*, 1998) and molecular modelling (Kalani *et al.*, 2004; Kling *et al.*, 2013; Kling *et al.*, 2014; Krogsgaard-Larsen *et al.*, 2014; Sukalovic *et al.*, 2013); key interactions between the endogenous ligand dopamine and the D2 receptor are highlighted in **Figure 4.1**. While the dopamine D2 receptor crystal structure is not yet available, the dopamine D3 receptor crystal structure was solved in 2010 (Chien *et al.*, 2010). Of the 18 contacts proposed between the D2/D3 receptor antagonist eticlopride and the receptor, 17 are identical in the dopamine D2 receptor, which suggests it has a very similar binding site. This is supported by homology modelling, although it was found that the D2L receptor had a larger

binding site than the D3 receptor (Platania *et al.*, 2012). In the D3 receptor crystal structure, residues in TMs 2, 3, 5, 6 and 7 are proposed the form the eticlopride binding site with ligand-receptor interactions with highly conserved residues D3.32, H6.55 and TM5 serines observed. Across the monoamine receptor family, there is a completely conserved TM3 aspartic acid (D3.32) (Shi *et al.*, 2002). This residue is proposed to form a salt bridge with amine groups common to the majority of agonist and antagonist ligands, as observed in the crystal structures of the dopamine D3 (Chien *et al.*, 2010), β1-adrengeric (Warne *et al.*, 2011), serotonin 5-HT_{1B} and 5-HT_{2B} (Wang *et al.*, 2013) and muscarinic M_3 acetylcholine receptors (Kruse *et al.*, 2012), and proposed in several modelling studies of the dopamine D2 receptor (Kling *et al.*, 2014; Krogsgaard-Larsen *et al.*, 2014; Sukalovic *et al.*, 2013). Functionally, early mutagenesis of D3.32 resulted in a complete loss of [^{3}H]-2-(N-propyl-N-2-thienylethylamino)-5-hydroxytetralin (N-0437) binding. This compound, which contains an amine, revealed the absolute necessity of D3.32 for the binding of amine containing compounds to the dopamine D2 receptor (Mansour *et al.*, 1992). Modelling studies also identify H6.55 as an important residue for ligand binding (Sukalovic *et al.*, 2013). This is supported by mutagenesis studies which demonstrate decreased agonist affinities following H6.55 mutation, although for some partial agonists and antagonists, H6.55 mutation increased affinity (Tschammer *et al.*, 2011). Additionally, molecular dynamics simulations have proposed that H6.55 can exist in two positions, with the side chain pointing either intracellularly or extracellularly. It is thought that some ligands may exert steric pressures on this residue, locking into a specific position which may influence ligand binding and lead to activation of specific intracellular signalling pathways (Kling *et al.*, 2013). This supports mutagenesis studies that have suggested that this residue may contribute to D2 receptor signalling bias. In an investigation of cAMP and ERK1/2 signalling at the dopamine D2L receptor, FAUC321 (*N*-[3-[4-(2-methoxyphenyl)piperazin-1-yl]propyl]pyrazolo-[1,5-a]pyridine-3-carboxamide) was indicated as biased towards ERK1/2 signalling over cAMP. In addition, FAUC350 ({3-[4-(2, 3-dihydro-benzofuran-7-yl)-piperazin-1-yl]-

propyl}ac-pyrazol[1,5-a]pyridine-3-carboxamide) and CPD1 (*N*-(4-(4-(2-methoxyphenyl)piper-azin-1-yl)butyl)biphenyl-4-carboxamide) had no response in cAMP but were partial agonists in ERK1/2 signalling indicating they may also be biased towards ERK1/2 (Tschammer *et al.*, 2011), although this may be an artefact of signal amplification. However, following H6.55A mutation, all ligands could inhibit cAMP accumulation and ERK1/2 maximal responses increased. This mutation removed the apparent bias of FAUC350 and FAUC321 and reversed the bias CPD1. Furthermore, dopamine now appeared biased towards cAMP over ERK1/2 phosphorylation (Tschammer *et al.*, 2011).

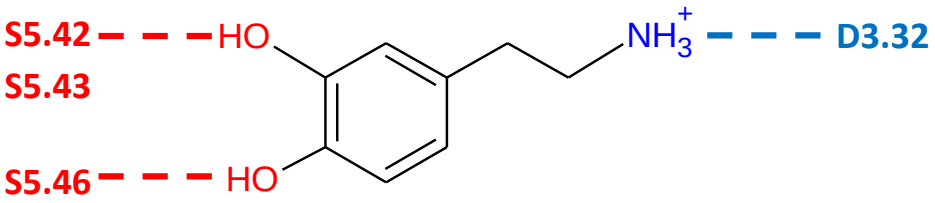


Figure 4.1: Structure of dopamine with key interactions with the dopamine D2 receptor binding site highlighted

Dopamine binding to the D2 receptor is stabilised by key interactions with binding site residues. The hydroxyl groups of the catechol have hydrogen bond interactions with TM5 serine residues. Furthermore, the highly conserved TM3 aspartic acid forms a salt bridge with the protonated amine common to the majority of monoamine receptor ligands.

4.1.3 The role of serine residues in ligand binding and receptor activation of the dopamine D2 receptor

Across the catecholamine family of class A GPCRs, there are a number of highly conserved serine residues in TM5 which line the ligand binding site (Shi *et al.*, 2002). These residues are critical to ligand binding as compound hydroxyl groups (or other suitable polar side chains) can form hydrogen bonds with these serine residues to stabilise the ligand-receptor complex. Both mutagenesis and modelling studies support their importance for binding across the receptor family (Coley *et al.*, 2000; Ebersole *et al.*, 2003; Fowler *et al.*, 2012; Liapakis *et al.*, 2000; Mansour *et al.*, 1992; Sato *et al.*, 2015; Strader *et al.*, 1989; Warne *et al.*, 2011; Wiens *et al.*, 1998). For the dopamine D2 receptor, a number of studies have examined the role of TM5 serine residues in ligand binding (Coley *et al.*, 2000; Fowler *et al.*, 2012; Mansour *et al.*, 1992; Wiens *et al.*, 1998) although most have only examined a small subset of ligands. The binding of the endogenous agonist dopamine, as shown in **Figure 4.1**, is thought to be governed by hydrogen bond interactions with S5.42 and S5.46 (Kling *et al.*, 2014) which is supported by mutagenesis studies (Coley *et al.*, 2000; Fowler *et al.*, 2012; Mansour *et al.*, 1992). Studies with multiple serine mutations have also proposed that dopamine requires interactions with at least two serine residues to maintain high affinity binding; while single S5.42A, S5.43A or S5.46A mutants retained two-site binding, multiple serine mutations displayed only single site binding (Coley *et al.*, 2000).

Furthermore, mutagenesis studies have revealed ligand specific differences in receptor binding and signalling following serine point mutations (Fowler *et al.*, 2012; Wiens *et al.*, 1998). This suggests distinct subsets of ligands engage differently with the dopamine D2 receptor binding site. Examinations of the structurally related 2-dipropylaminotetralin family (which includes 7OH-DPAT), have offered insights into this. In this series, the position of a hydroxyl group substitution is moved between 4 carbon positions on the benzene ring (see 7OH-DPAT structure in **Figure 4.3**). Furthermore, the presence of a chiral carbon (highlighted in **Figure 4.3**) generates both *R*- and *S*- stereoisomers.

When compared to their non-hydroxylated parent compounds, the addition of a hydroxyl group increased affinity 10-fold, but only for *S*-5OH-DPAT and *R*-7OH-DPAT. For the corresponding stereoisomers, this effect was either significantly reduced or lost. This indicates that specific positioning of ligand hydroxyls can significantly influence the ability of compounds to interact with TM5 serines (Payne *et al.*, 2002). When these compounds were examined in their racemic form in earlier mutagenesis studies, differential effects of serine mutations were derived, depending on the location of the hydroxyl group. When the enantiomers of 5OH-DPAT were examined in double serine mutants, it was clear that the binding of *R*-5OH-DPAT was dependent S5.46 whereas *S*-5OH-DPAT was dependent on S5.43 which is consistent with the specific location of the ligand hydroxyl group governing the hydrogen bond network between ligand and receptor (Coley *et al.*, 2000). Earlier studies on the hamster β2AR proposed a similar mode of binding for catechol adrenergic agonists, where S5.43 formed hydrogen bonds with the meta-hydroxyl group and S5.46 with the para-hydroxyl group (Strader *et al.*, 1989).

There is also evidence that TM5 serines play an important role in agonist promoted receptor activation (Dror *et al.*, 2011; Kling *et al.*, 2014; Sato *et al.*, 2015; Warne *et al.*, 2011). For example, it has been suggested that the number of ligand contacts with TM5 serines of the β1AR governs ligand efficacy; while full agonists contact both S5.42 and S5.46, partial agonists only contact S5.42. This stronger interaction between full agonists and TM5 serines promotes stronger interactions between ligand, TM5 and TM6 and contraction of the ligand binding pocket. This may aid the global conformation changes that increase the likelihood of the receptor adopting the active state (Sato *et al.*, 2015; Warne *et al.*, 2011). This is supported by molecular dynamics studies at the β2AR whereby receptor activation leads to movement of TM5 towards TM6, promoting hydrogen bond interactions between the ligand and S5.46 to stabilise the active state (Dror *et al.*, 2011).

A similar mechanism has been proposed for the dopamine D2 receptor, whereby modelling studies reveal that dopamine has hydrogen bond

interactions with both S5.42 and S5.46, which are not present with the partial agonist aripiprazole. When compared with the dopamine bound structure, this caused an outward movement of the extracellular half of TM6 away from TM5 which may inhibit receptor activation (Kling *et al.*, 2014).

4.1.4 Chapter Aims

This chapter aimed to generate and characterise a constitutively active mutant of the dopamine D2L receptor through mutation of the T6.34 residue. We then explored the mode of binding of different agonists at WT and T6.34R receptors through mutations of TM5 serine residues. In these experiments, we sought to establish whether the 'active' conformation of T6.34R mutated receptor was functionally the same as the agonist occupied WT receptor. Furthermore, we examined whether the behaviour of different agonist classes at the mutant receptors would provide evidence of agonist-selective D2L receptor conformations.

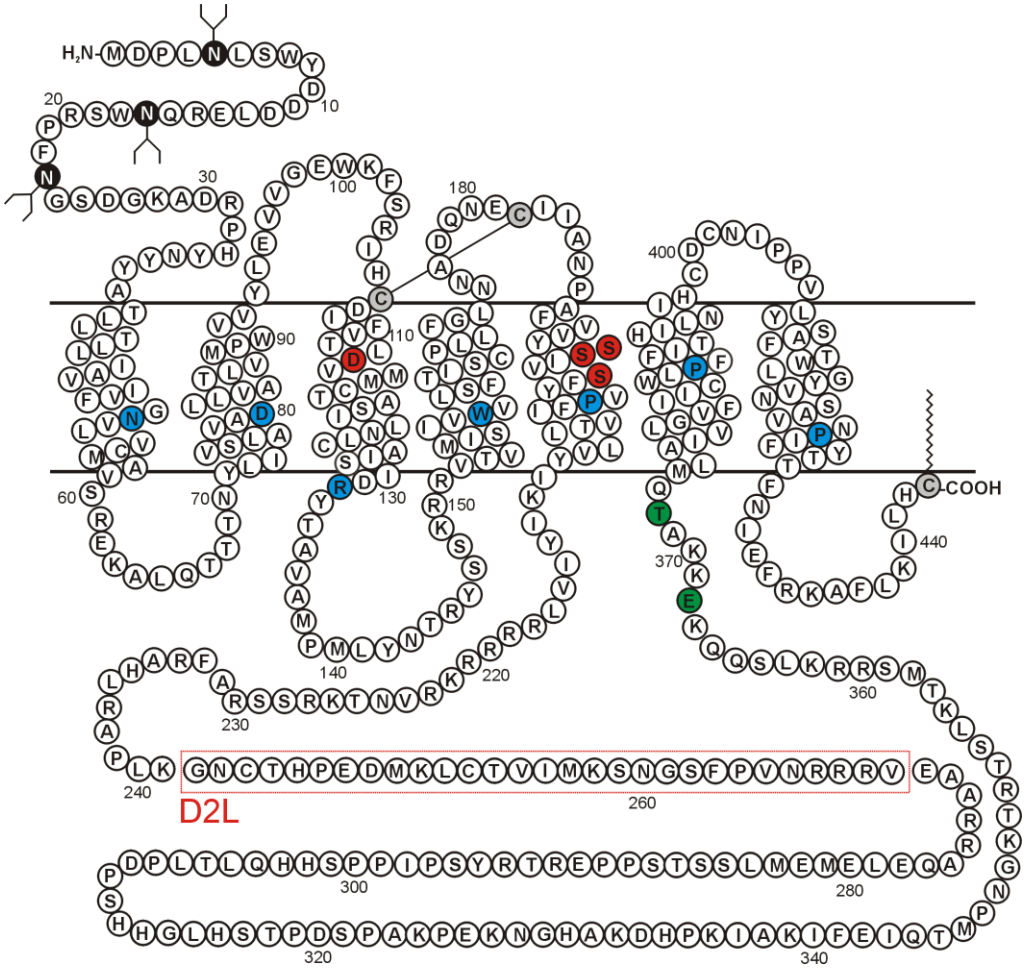


Figure 4.2: Diagram of the D2L receptor with key residues highlighted

Snake plot of the D2L receptor sequence with amino acids numbered according to the cDNA sequence. The location of the deletion of the D2S receptor in highlighted in the box. The most conserved residues (denoted 50 in the Ballesteros-Weinstein numbering scheme) are highlighted in blue. Residues critical to ligand binding (D3.32, S5.42, S5.43 and S5.46) are highlighted in red while mutation of residues in green (T6.34 and E6.30) is implicated in generating constitutive activity.

Figure provided by Dr Nicholas Holliday.

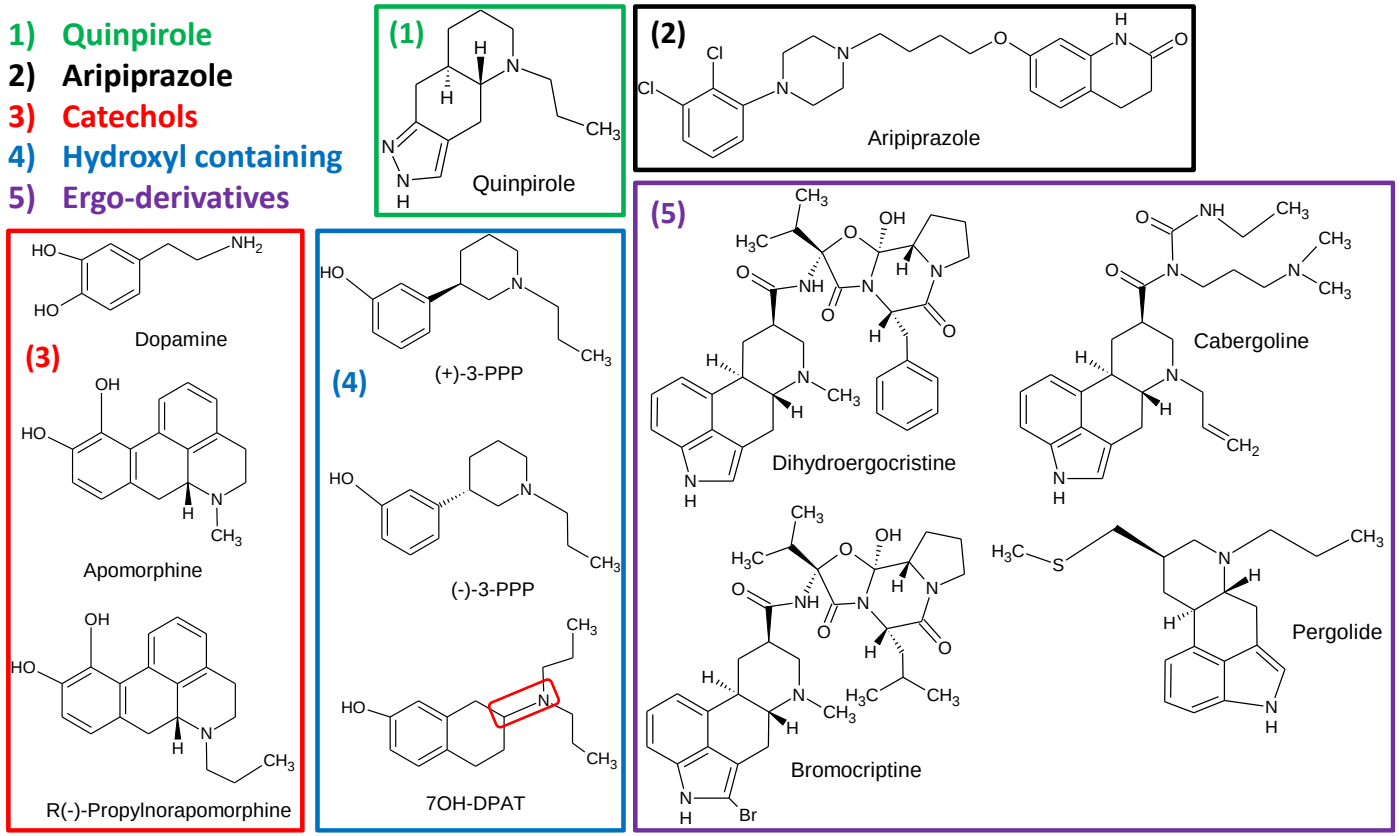


Figure 4.3: Structure of the compounds used in this study

Structure of the 12 agonists used in this study, grouped according to their structural class. The chiral bond of 7OH-DPAT is highlighted.

4.2 Results

4.2.1 Generation of constitutively active receptors

Previously in the lab, E6.30A, T6.34K and T6.34R SNAP-D2L mutants were constructed and expressed clonally in the CHO CRE-SPAP background. Of these three mutants, E6.30A and T6.34K demonstrated low receptor expression levels as visualised by SNAP-labelling and a high degree of constitutive receptor internalisation. Furthermore, both of these cell lines had limited agonist responses (data not shown). In contrast, the T6.34R mutant displayed greater cell surface expression and membrane localisation following SNAP-labelling. Moreover, there was a reproducible window in functional assays which allowed the determination of ligand responses. As such, this mutation was further explored to assess the effects of constitutive activity on D2L ligand responses.

4.2.2 The effect of T6.34R mutation on ligand binding at the D2L receptor

To examine how this mutation affected dopamine D2L receptor signalling, radioligand binding, CRE-SPAP reporter gene and receptor internalisation assays were conducted. Saturation radioligand binding experiments initially determined B_{max} for the D2L T6.34R cell line of 0.93 ± 0.31 pmol mg^{-1} with a [^{3}H]-spiperone pK_D of 9.98 ± 0.21 (n=4; **Figure 4.4**). While there was no significant difference in the pK_D for [^{3}H]-spiperone between WT and T6.34R D2L receptors, the B_{max} of the T6.34R cell line was significantly reduced at only 35% expression of the WT receptor ($P<0.05$; Student's unpaired t-test).

[^{3}H]-spiperone competition binding assays were then performed to determine ligand affinities at the mutant receptor (**Figure 4.5**). Data were fit to either one- or two-site binding models, as determined by an extra sum of squares F-test in GraphPad Prism. Quinpirole, dopamine, (-)-3-PPP, apomorphine and 7OH-DPAT were best described by a two-site binding model (yielding both pK_i high and pK_i low affinity estimates), whereas all other ligands were adequately described by a single site model (giving pK_i low) (**Table 4.1**). Single

site binding of (+)-3-PPP and RNPA to the D2L T6.34R receptor was observed, in contrast to the two-site binding observed in D2L WT, leading to an increased pK_i low for these compounds. There was also a significant increase in pK_i low affinity for quinpirole, and the percentage of high affinity binding sites for dopamine, apomorphine and 7OH-DPAT was significantly increased. Furthermore, there were small, significant decreases in affinity for haloperidol, (+)-butaclamol and bromocriptine ($P<0.05$, Student's unpaired t test; **Table 4.1**).

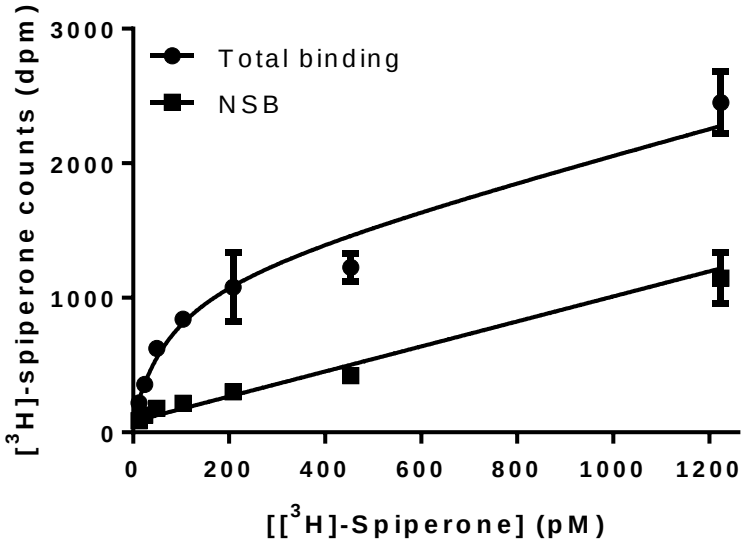


Figure 4.4: Determination of D2L T6.34R receptor expression and pK_D of [^{3}H]-spiperone by saturation binding analysis

CHOcs ssD2L T6.34R membranes were incubated for 3h at room temperature with increasing concentrations of [^{3}H]-spiperone prior to filtration. Non-specific binding (NSB) was determined in the presence of 3µM (+)-butaclamol. Data are from a single experiment (mean ± range), representative of 4 independent experiments performed in duplicate.

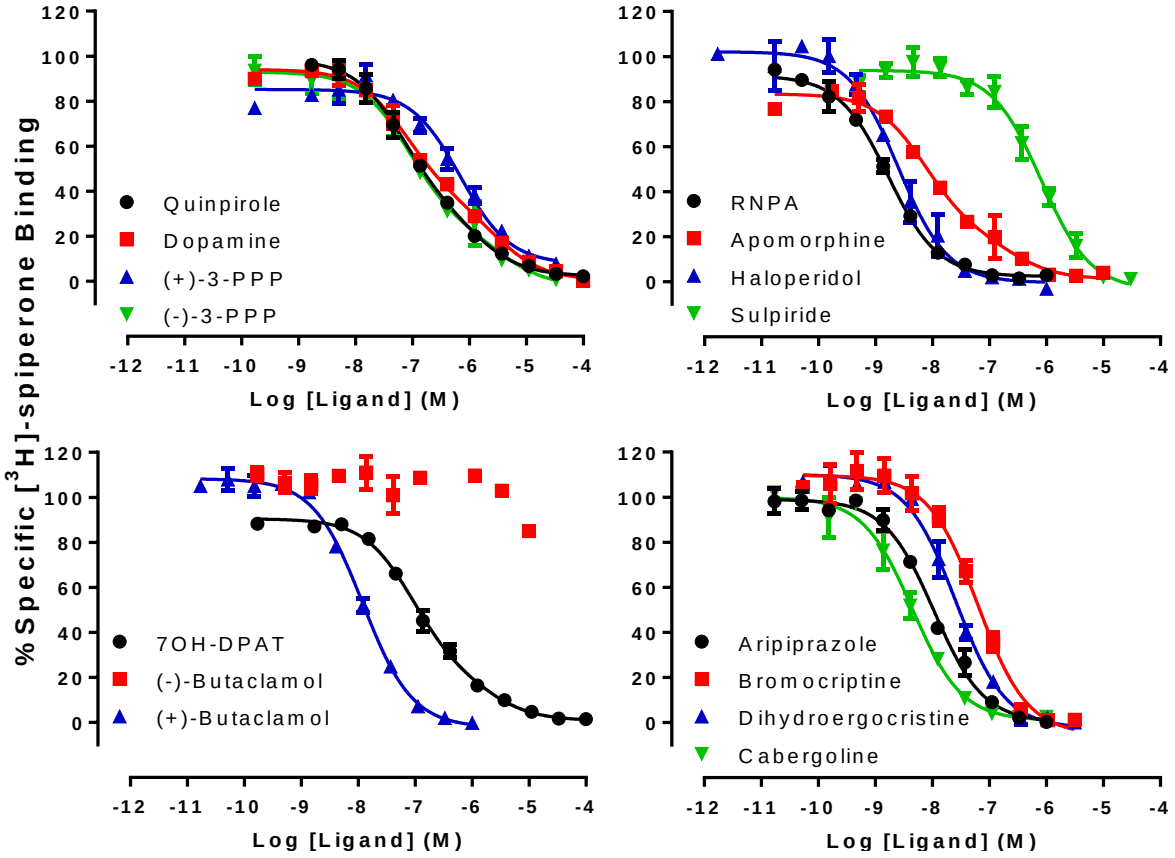


Figure 4.5: Determination of ligand affinities at the SNAP-tagged D2L T6.34R receptor using [^{3}H]-spiperone competition binding

CHOcs ssD2L T6.34R membranes were incubated for 3h with dopamine receptor ligands and 70-130pM [^{3}H]-spiperone for 3h prior to filtration. Data were fit to either one- or two-site binding models, as determined by an extra sum of squares F-test in GraphPad Prism. Ligand IC_{50}s were converted to pK_is according to the Cheng-Prussoff equation, with data summarised in **Table 4.1**. Data shown are from a single experiment (mean ± range), representative of 4 independent experiments performed in duplicate, normalised to total (100%) and non-specific binding (0%) as determined by 3µM (+)-butaclamol.

Ligand	T6.34R			WT		
	pK_i High	pK_i Low	%High	pK_i High	pK_i Low	%High
Quinpirole	7.92 ± 0.20	6.35 ± 0.09*	46.0 ± 10.0	7.37 ± 0.11	5.69 ± 0.03	32.3 ± 5.2
Dopamine	7.76 ± 0.17	6.02 ± 0.12	58.4 ± 1.8*	7.68 ± 0.05	5.66 ± 0.07	23.1 ± 2.5
(+)-3-PPP[†]	-	6.16 ± 0.12*	-	6.65 ± 0.05	4.98 ± 0.09	26.3 ± 4.4
(-)-3-PPP	7.01 ± 0.14	5.62 ± 0.18	59.0 ± 12.5	7.16 ± 0.25	5.56 ± 0.10	38.7 ± 7.9
RNPA[†]	-	9.34 ± 0.10*	-	9.56 ± 0.17	8.13 ± 0.08	38.8 ± 6.9
Apomorphine	8.72 ± 0.21	7.11 ± 0.21	63.6 ± 10.2*	8.46 ± 0.18	7.00 ± 0.08	26.2 ± 3.6
Haloperidol[†#]	-	8.93 ± 0.07*	-	-	9.18 ± 0.05	-
Sulpiride[†#]	-	6.81 ± 0.19	-	-	7.03 ± 0.09	-
7OH-DPAT	7.64 ± 0.16	6.24 ± 0.13	59.9 ± 6.6*	8.11 ± 0.20	5.94 ± 0.23	30.1 ± 4.2
(+)-Butaclamol[†#]		8.26 ± 0.07*		-	8.82 ± 0.10	-
(-)-Butaclamol	ND	ND	ND	ND	ND	ND
Aripiprazole[†#]	-	8.17 ± 0.13	-	-	8.46 ± 0.08	-
Bromocriptine[†#]	-	7.68 ± 0.10*	-	-	8.17 ± 0.12	-
Dihydroergocristine[†#]	-	7.98 ± 0.09	-	-	8.26 ± 0.11	-
Cabergoline[†#]	-	8.81 ± 0.09	-	-	8.95 ± 0.03	-

Table 4.1: Summary of ligand affinities for WT and T6.34R dopamine D2L receptors

Summary of binding affinities derived in both WT and T6.34R D2L receptor expressing cell membranes. Data were fit to either one-site ([†]T6.34R; [#]WT) or two-site binding models, as selected by an extra sum of squares F-test. Data are pooled (mean ± SEM) from 4 independent experiments performed in duplicate. ND: No displacement at 3μM (-)-butaclamol; *P<0.05 cf WT (Student's unpaired t-test).

4.2.3 The effect of T6.34R mutation on ligand pharmacology in the CRE-SPAP reporter gene assay

Next, CRE-SPAP reporter gene assays determined the effect of the mutation on $G\alpha_{i/o}$-mediated signalling. Forskolin concentration response curves determined the optimum forskolin concentration for future experiments (**Figure 4.6, Table 4.2**). The pEC_{50} of forskolin alone was 5.93 ± 0.08, with 10μM quinpirole treatment causing a 4.2 ± 0.8 fold decrease in pEC_{50} (n=4). Neither 10μM haloperidol nor 3μM PBz treatment significantly changed the pEC_{50} or R_{max}. The greatest signal window was observed at 3μM forskolin, where 10μM quinpirole induced 38.9 ± 8.1% inhibition of forskolin-stimulated SPAP production. The assay signal window was much smaller for this cell line compared to WT, in which 10μM quinpirole induced 88.5 ± 2.7% inhibition of 3μM forskolin stimulated SPAP production (**Figure 3.3**).

A panel of dopamine D2 receptor ligands were then examined for their ability to inhibit forskolin-stimulated SPAP production in CHO D2L T6.34R cells, referenced to quinpirole responses (pEC_{50} 7.85 ± 0.20, n=4; **Figure 4.7**). All agonists were full agonists relative to quinpirole, with significant increases in relative R_{max} for (-)-3-PPP, aripiprazole, dihydroergocristine and cabergoline compared to WT responses (**Figure 3.7**). However the ergo-derived compounds, bromocriptine, dihydroergocristine and cabergoline all had significantly decreased potency in this cell line compared to WT D2L receptor ($P<0.05$, Student's unpaired t-test; **Table 4.3**). The order of potency was RNPA > cabergoline = pergolide = apomorphine > aripiprazole > bromocriptine = 7OH-DPAT = dihydroergocristine > dopamine = quinpirole > (-)-3-PPP > (+)-3-PPP. Due to the markedly reduced signal window in this assay for this cell line, attempts to perform Schild analysis to determine haloperidol and sulpiride affinities to compare to WT results were unsuccessful (data not shown).

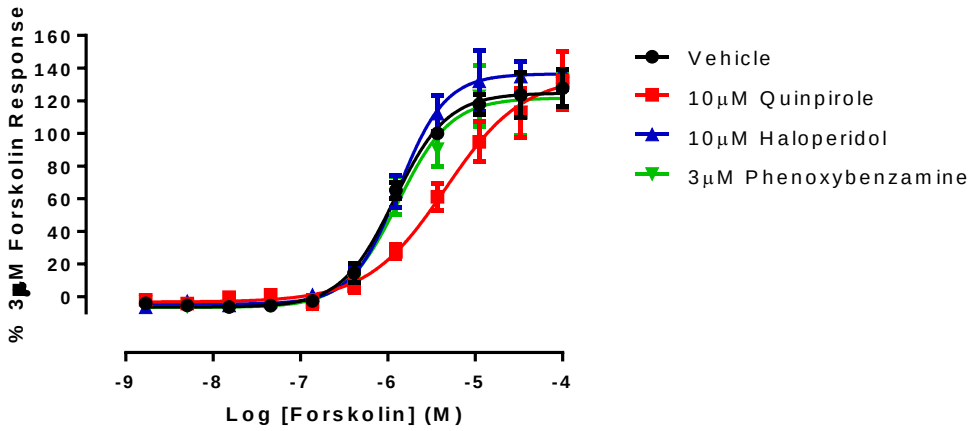


Figure 4.6: Forskolin concentration response curves in the CRE-SPAP reporter gene assay in the absence and presence of dopamine D2 receptor ligands, in CHOcs ssD2L T6.34R cells

Cells were treated with vehicle, 10µM quinpirole, 10µM haloperidol or 3µM PBz for 1h prior to 5h stimulation with increasing concentrations of forskolin. Data are pooled (mean ± SEM) of 4 independent experiments performed in duplicate, normalised to 3µM forskolin (100%) and vehicle (0%) controls. Data are summarised in **Table 4.2** below.

Treatment	pEC_{50}	R_{max}
Vehicle	5.93 ± 0.08	137.5 ± 18.1
10µM Quinpirole	5.33 ± 0.04*	130.0 ± 12.7
10µM Haloperidol	5.85 ± 0.09	137.0 ± 9.7
3µM PBz	5.86 ± 0.09	119.6 ± 10.4

Table 4.2: Summary of forskolin concentration response curves in CHOcs ssD2L T6.34R cells in the absence and presence of D2L ligands

Summary of the parameters derived from the forskolin concentration response curves in **Figure 4.6**. Data are pooled (mean ±SEM) of 4 independent experiments performed in duplicate with R_{max} expressed as a percentage of 3µM forskolin response. *P<0.05 cf. vehicle pEC_{50} (One-way ANOVA followed by Dunnett's post hoc analysis).

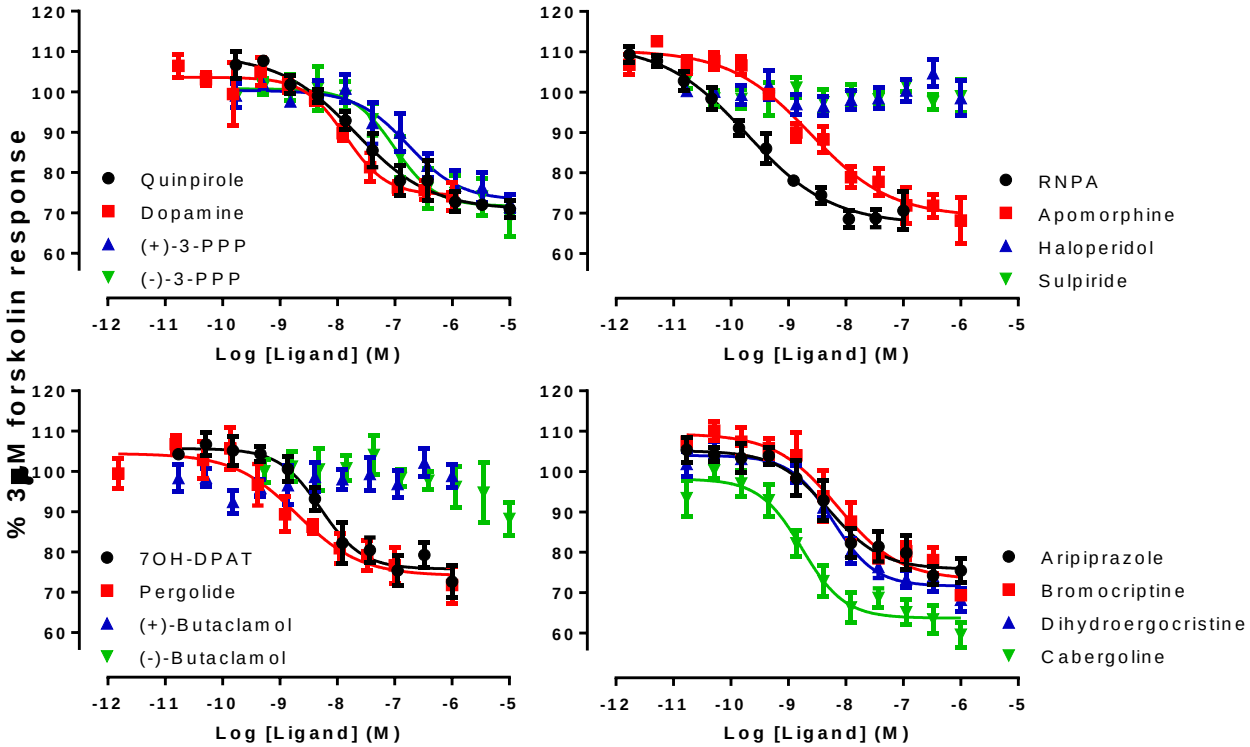


Figure 4.7: Dopamine D2 agonists inhibit forskolin-stimulated SPAP production in CHOcs ssD2L T6.34R cells.

Cells were treated with increasing concentrations of dopamine D2 receptor ligands for 1h prior to 5h 3µM forskolin stimulation. Data represent pooled data (mean ± SEM) of 4 independent experiments performed in duplicate, normalised to 3µM forskolin (100%) and vehicle (0%) controls. Data are summarised in **Table 4.3.**

Ligand	T6.34R		WT		Fold change in potency (EC_{50} ratio)
	pEC_{50}	R_{max}	pEC_{50}	R_{max}	
Quinpirole	7.84 ± 0.20	95.6 ± 4.8	7.80 ± 0.23	99.3 ± 1.1	+1.1
Dopamine	7.85 ± 0.10	102.3 ± 11.9	7.70 ± 0.04	102.9 ± 2.0	+1.4
(+)-3-PPP	6.76 ± 0.16	106.0 ± 9.3	6.37 ± 0.29	100.3 ± 6.2	+2.5
(-)-3-PPP	7.00 ± 0.09	109.4 ± 8.1*	6.63 ± 0.24	63.3 ± 10.7	+2.3
RNPA	9.69 ± 0.19	137.7 ± 24.9	9.96 ± 0.02	103.4 ± 1.6	-1.9
Apomorphine	8.66 ± 0.08	116.3 ± 13.2	8.45 ± 0.04	100.3 ± 1.6	+1.6
Haloperidol	NE	NE	NE	NE	-
Sulpiride	NE	NE	NE	NE	-
7OH-DPAT	8.24 ± 0.10	88.9 ± 7.7	8.04 ± 0.16	100.7 ± 1.1	+1.6
Pergolide	8.67 ± 0.09	96.7 ± 3.1	8.90 ± 0.26	87.4 ± 12.4	-1.7
(+)-Butaclamol	NE	NE	NE	NE	-
(-)-Butaclamol	NE	NE	NE	NE	-
Aripiprazole	8.53 ± 0.20	93.3 ± 11.5*	8.02 ± 0.08	48.1 ± 0.5	+3.2
Bromocriptine	8.27 ± 0.18*	98.2 ± 6.5	9.33 ± 0.12	96.4 ± 3.6	-11.5
Dihydroergocristine	8.23 ± 0.04*	111.7 ± 4.4*	8.97 ± 0.15	81.4 ± 3.7	-5.5
Cabergoline	8.74 ± 0.15*	137.6 ± 6.2*	9.24 ± 0.08	103.8 ± 3.9	-3.2

Table 4.3: Comparison of ligand responses in WT and T6.34R D2L receptors in the CRE-SPAP reporter gene assay

Summary of ligand responses in **Figure 4.7**, compared with WT responses (**Figure 3.7**). Data are pooled (mean ± SEM) from 4 independent experiments performed in duplicate or triplicate with R_{max} expressed as a percentage of 10µM quinpirole response. NE = no effect, *P<0.05 cf. WT (Student's unpaired t-test). The EC_{50} ratio indicates the increased (+) or decreased (-) fold change in agonist potencies in T6.34R compared to WT.

4.2.4 The effect of T6.34R mutation on ligand pharmacology in D2L receptor internalisation assays

Next, CHOcs ssD2L T6.34R cells were examined for their ability to induce receptor internalisation. As previously described in **3.2.4**, the use of a membrane impermeant SNAP fluorophore allowed selective labelling of cell surface receptors. This demonstrated that the CHO ssD2L T6.34R receptors were located predominantly on the plasma membrane, with 1h agonist treatment promoting receptor internalisation to intracellular compartments (**Figure 4.9**).

Time course experiments (**Figure 4.8**) derived the half time for receptor internalisation of 31.0 ± 3.1min for 10μM quinpirole and 30.1 ± 5.4min for 1μM bromocriptine (n=5). The half time for aripiprazole internalisation could not be reliably estimated over the 2h time course. Unlike the WT D2L receptor (**Figure 3.11**), there was no evidence of a delay in receptor internalisation following ligand stimulation. Furthermore, the half time for quinpirole internalisation was significantly decreased compared with WT receptor half time of 51.3 ± 5.8min ($P<0.05$; Student's unpaired t-test).

All agonists were able to induce receptor internalisation in the CHOcs ssD2L T6.34R cell line (**Figure 4.9**, **Figure 4.10**), unlike our previous characterisation of WT D2L receptors in which a number of weak partial agonists were unable to internalise the receptor (**Figure 3.13**). All agonists, except for (-)-3-PPP, aripiprazole and dihydroergocristine, were full agonists relative to quinpirole in this assay. Thus, T6.34R mutation significantly increased the relative maximal responses of (+)-3-PPP, (-)-3-PPP, apomorphine, aripiprazole, bromocriptine, dihydroergocristine and cabergoline compared to WT ($P<0.05$, Student's unpaired t test; **Table 4.4**). There were also significant increases in potency for dopamine, (+)-3-PPP, RNPA, apomorphine and 7OH-DPAT compared with WT responses. However bromocriptine potency decreased 34.7-fold ($P<0.05$; Student's unpaired t-test; **Table 4.4**), although there was no significant change in potency for the other ergot derivatives tested.

Compared to the CRE-SPAP reporter gene assay results, the potency changes following T6.34R mutation were greater in the internalisation assay (**Figure 4.11**). The overall order of potency for this assay was RNPA > apomorphine > cabergoline > 7OH-DPAT = pergolide = dopamine > dihydroergocristine > aripiprazole = bromocriptine > quinpirole > (+)-3-PPP > (-)-3-PPP.

None of the antagonists/inverse agonists tested were able to induce receptor internalisation following T6.34R mutation, despite a moderate effect of haloperidol in increasing D2L WT receptor endocytosis (**3.2.4**). As such, the ability of haloperidol (1-10nM) and sulpiride (30-300nM) to inhibit quinpirole-induced receptor internalisation was investigated (**Figure 4.12**). Schild analysis of these data derived pA_2s of 9.73 ± 0.06 and 8.09 ± 0.10 with Schild slopes of 1.17 ± 0.10 and 0.77 ± 0.07 for haloperidol and sulpiride respectively. The Schild slope for sulpiride (but not haloperidol) was significantly different to the theoretical value of one ($P<0.05$; One sample t-test). The pK_is for both haloperidol and sulpiride were significantly lower than the pK_Ds derived from the internalisation data (**Table 4.5**).

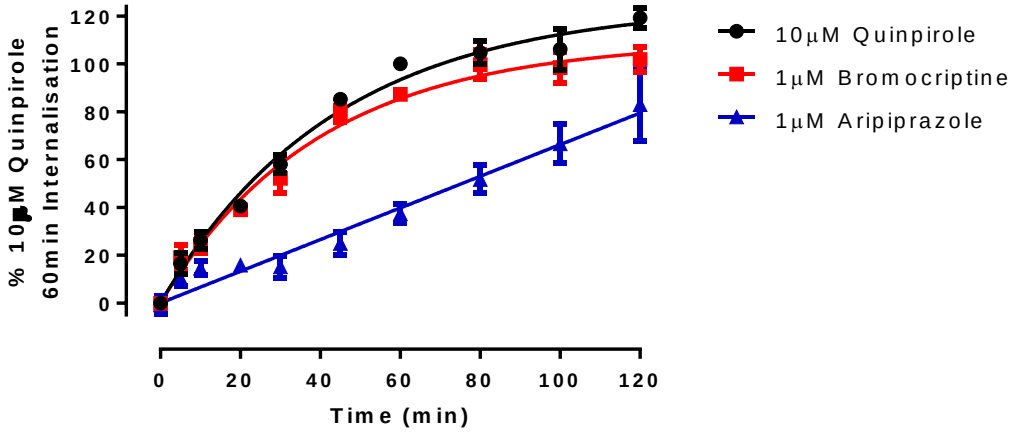


Figure 4.8: Time course of SNAP-tagged D2L T6.34R receptor internalisation in response to ligand treatment

CHOcs ssD2L T6.34R cells were labelled with SNAP-surface AF-488 for 30min before treatment with 10µM quinpirole, 1µM bromocriptine and 1µM aripiprazole for the indicated times. Data represent pooled data (mean ± SEM) of 5 independent experiments performed in duplicate, normalised to 60min 10µM quinpirole (100%) and vehicle (0%) controls.

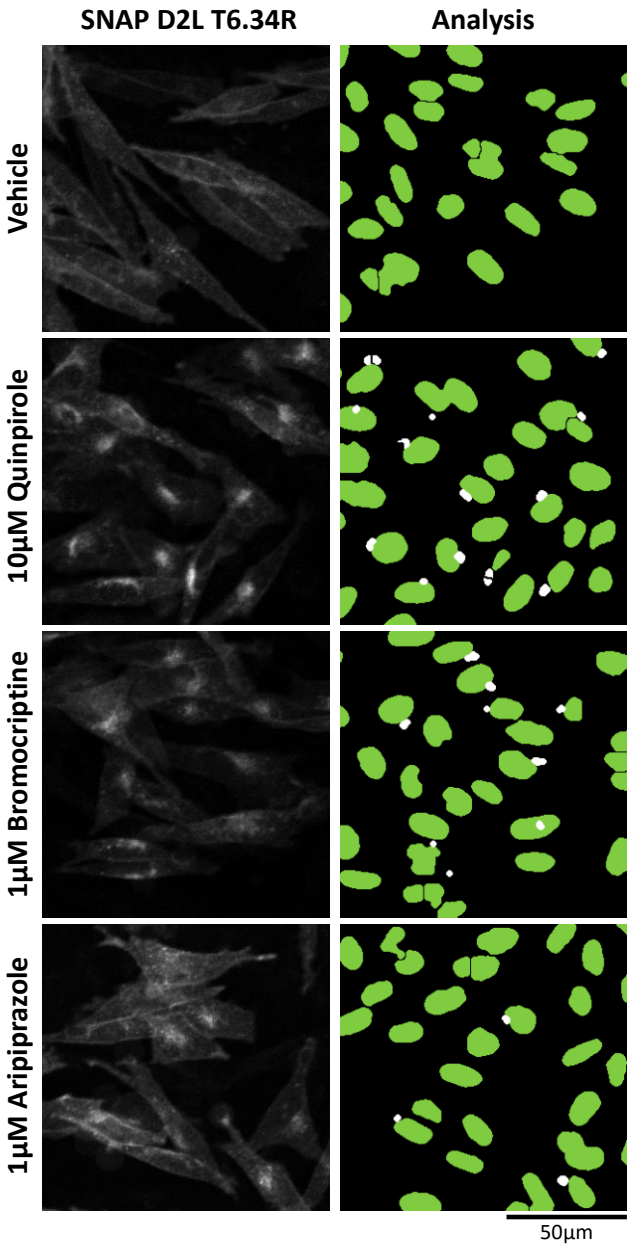


Figure 4.9: Internalisation of the SNAP-tagged D2L T6.34R receptor in response to ligand stimulation

Cells were SNAP-surface AF488 labelled for 30min then treated with increasing concentrations of ligands for 1h prior to fixation. Representative images show cells treated with vehicle and reference agonists, quinpirole, bromocriptine and aripiprazole. For clarity, the images above were cropped to 120µm x 120µm from the original 400µm x 400µm image used for analysis. The panels show the SNAP-tagged D2L T6.34R receptors identified by labelling (left) and associated granularity analysis (right), with nuclei in green (from H33342 image, not shown) and receptor containing granules of 6-10µm diameter in white. The internalisation of 16 D2 ligands was determined and quantified in **Figure 4.10**.

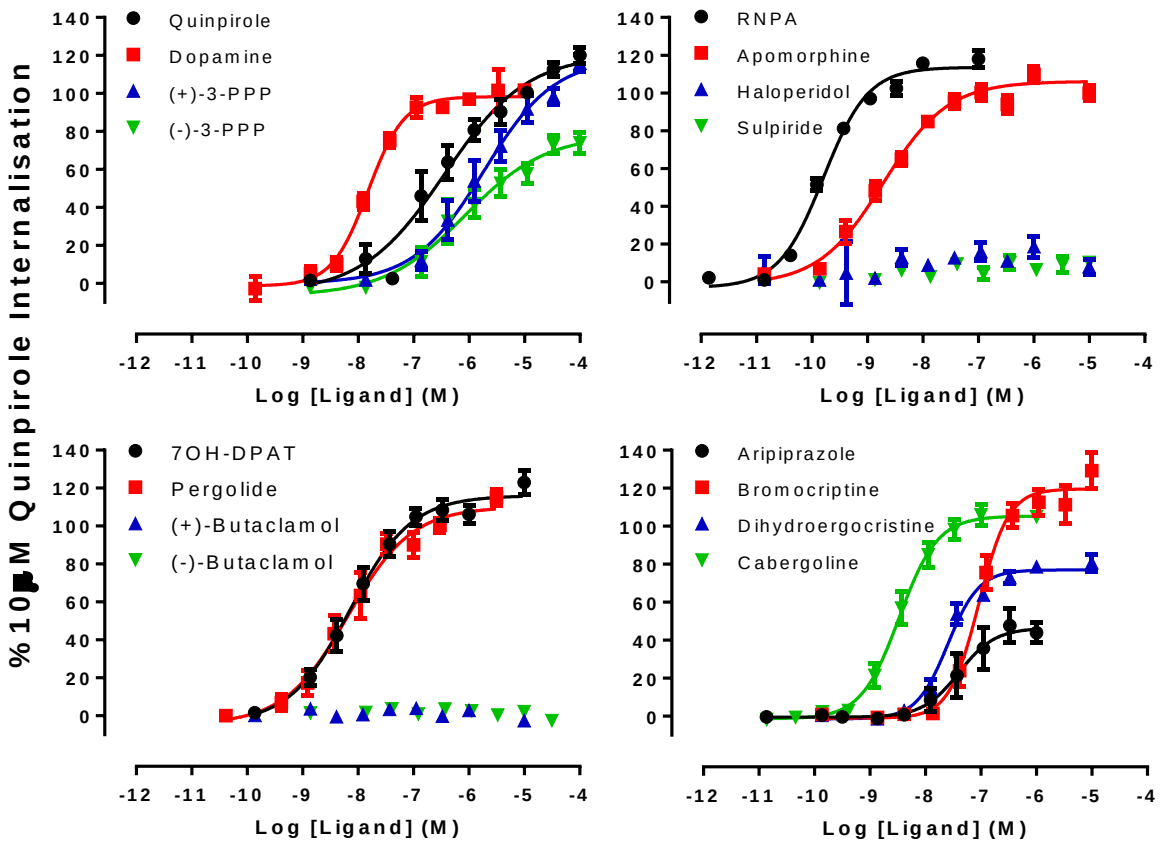


Figure 4.10: Quantification of D2L T6.34R receptor internalisation in response to treatment with a panel of dopamine D2 receptor ligands

Cells were SNAP labelled for 30min prior to 1h ligand treatment and fixation. Receptor internalisation was quantified by granularity analysis as previously described. Data represent pooled data (mean ± SEM) of 4 independent experiments performed in duplicate, normalised to 10μM quinpirole (100%) and vehicle (0%) responses with data summarised in **Table 4.4**.

Ligand	T6.34R		WT		Fold change in potency (EC_{50} ratio)
	pEC_{50}	R_{max}	pEC_{50}	R_{max}	
Quinpirole	6.84 ± 0.39	119.0 ± 6.0	6.51 ± 0.18	107.3 ± 5.0	+2.1
Dopamine	7.89 ± 0.10*	99.5 ± 1.7*	6.58 ± 0.08	129.9 ± 8.4	+20.4
(+)-3-PPP	6.27 ± 0.30*	122.5 ± 11.1*	5.14 ± 0.12	82.9 ± 7.7	+13.5
(-)-3-PPP	5.95 ± 0.36	79.7 ± 10.5	NE	NE	-
RNPA	9.79 ± 0.04*	111.5 ± 3.6	9.18 ± 0.04	99.7 ± 6.0	+4.1
Apomorphine	8.96 ± 0.26*	109.1 ± 4.6*	7.52 ± 0.15	58.3 ± 2.6	+27.5
Haloperidol	NE	NE	8.18 ± 0.32	19.7 ± 4.0	-
Sulpiride	NE	NE	NE	NE	-
7OH-DPAT	8.10 ± 0.26*	118.4 ± 6.4	6.96 ± 0.17	108.1 ± 3.7	+13.8
Pergolide	8.01 ± 0.30	120.6 ± 9.9*	7.83 ± 0.27	59.1 ± 4.6	+1.5
(+)-Butaclamol	NE	NE	NE	NE	-
(-)-Butaclamol	NE	NE	NE	NE	-
Aripiprazole	7.22 ± 0.29	48.7 ± 9.4	NE	NE	-
Bromocriptine	7.11 ± 0.11*	117.8 ± 8.6*	8.65 ± 0.07	43.5 ± 9.6	-34.7
Dihydroergocristine	7.59 ± 0.09	77.5 ± 4.7	NE	NE	-
Cabergoline	8.33 ± 0.12	107.8 ± 1.4*	8.36 ± 0.21	78.2 ± 5.3	-1.1

Table 4.4: Comparison of ligand responses in receptor internalisation assays in WT and T6.34R D2L receptors

Summary of ligand responses from **Figure 4.10**, compared to WT data (**Figure 3.12**). R_{max} is expressed as a percentage of 10μM quinpirole response. Data are pooled (mean ± SEM) of 4 independent experiments performed in duplicate or triplicate. NE = no effect, *P<0.05 cf. WT (Student's unpaired t-test). The EC_{50} ratio indicates the increased (+) or decreased (-) fold change in agonist potencies in T6.34R compared to WT.

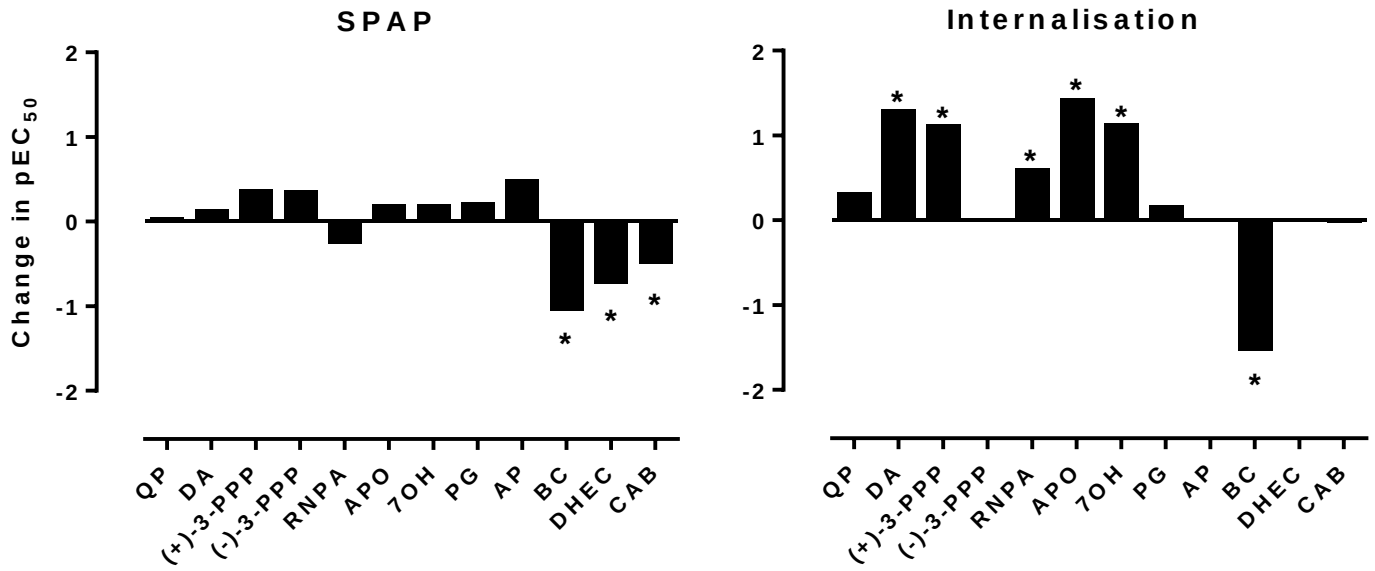


Figure 4.11: Summary of pEC_{50} changes following T6.34R mutation in CRE-SPAP reporter gene and internalisation assays

Change in pEC_{50}s (calculated from pEC_{50} T6.34R – pEC_{50} WT) in CRE-SPAP reporter gene and receptor internalisation assays between CHOcs ssD2L T6.34R and WT cells from **Table 4.3** and **Table 4.4**. *P<0.05 T6.34R cf. WT pEC_{50}. QP = quinpirole; DA = dopamine; APO = apomorphine; 7OH = 7OH-DPAT; PG = pergolide; AP = aripiprazole; BC = bromocriptine; DHEC = dihydroergocristine; CAB = cabergoline.

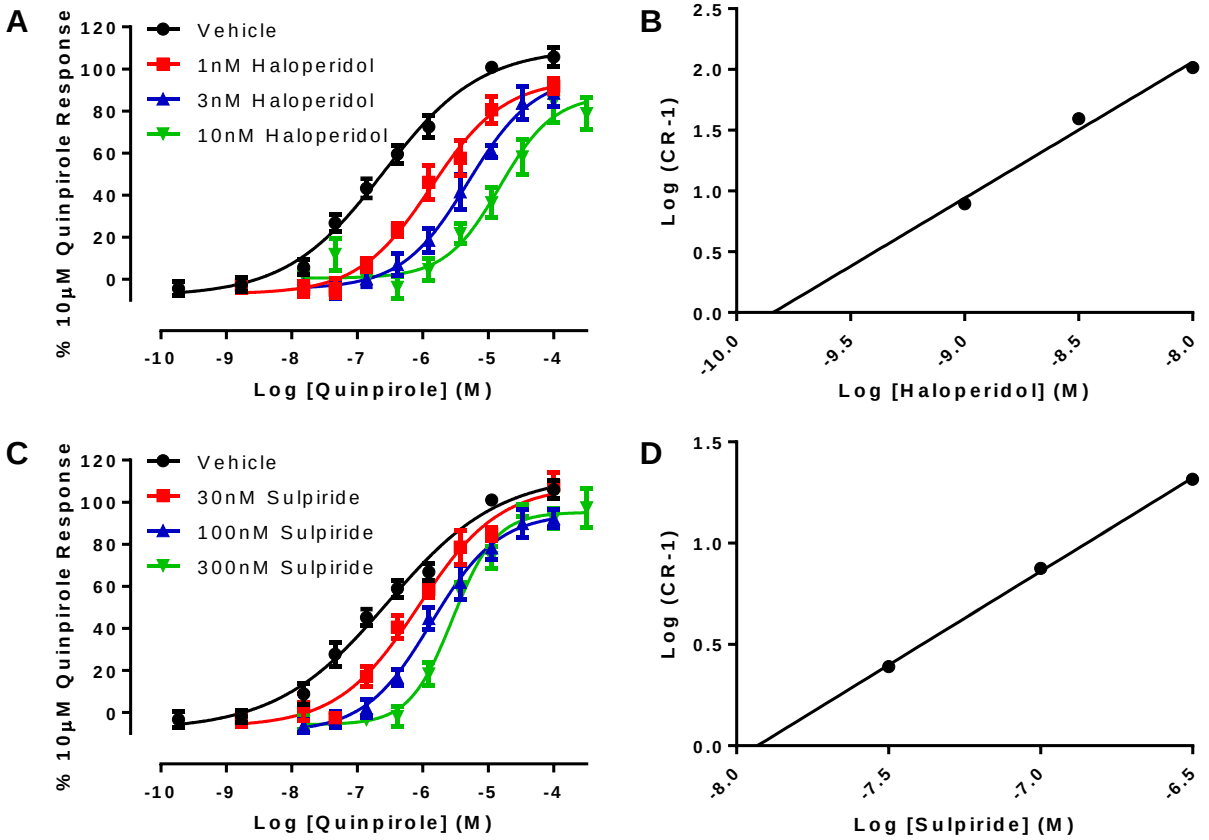


Figure 4.12: Determination of haloperidol and sulpiride affinities at the dopamine D2L T6.34R receptor

CHOcs ssD2L cells were SNAP-labelled, treated with 1-10nM haloperidol (**A**) or 30-300nM sulpiride for 30min (**C**), stimulated with increasing concentrations of quinpirole for 1h then fixed. Schild analysis of these graphs generated affinity values of 9.73 ± 0.06 for haloperidol and 8.09 ± 0.10 for sulpiride (example Schild plots **B, D**). Data represent pooled data (mean ± SEM) from 4 independent experiments performed in duplicate, normalised to 10µM quinpirole (100%) and vehicle (0%) responses in the absence of antagonist.

	Haloperidol		Sulpiride	
	WT	**T6.34R**	**WT**	**T6.34R**
pK_i binding	9.18 ± 0.05	8.93 ± 0.07*	7.03 ± 0.09	6.81 ± 0.19
pK_D internalisation	9.20 ± 0.20	9.73 ± 0.06*#	8.37 ± 0.04#	8.09 ± 0.10*#
pK_D SPAP	9.06 ± 0.18	ND	8.68 ± 0.19#	ND

Table 4.5: Summary of calculated affinities for haloperidol and sulpiride for both WT and T6.34R D2L receptors

Comparison of the calculated affinities for haloperidol and sulpiride from both binding and functional assays in WT and T6.34R D2L receptor expressing cells and membranes. Data are pooled (mean ± SEM) from 4 independent experiments performed in duplicate or triplicate. ND = not determined; *P<0.05 cf. WT (Student's unpaired t-test); #P<0.05 cf. pK_i binding (Student's unpaired t-test).

4.2.5 Effect of S5.42A mutation on CRE-SPAP reporter gene assays in WT and T6.34R backgrounds

To examine the apparent opposing effects of the T6.34R mutation on ligand functional responses between the ergo-derivatives and other agonists, point mutations of the TM5 binding site serines were performed in both D2L WT and T6.34R backgrounds. Effects on agonist CRE-SPAP reporter gene assay potencies following each mutation are summarised in **Figure 4.16**.

First, the effect of S5.42A mutation was examined. In the CRE-SPAP reporter gene assay, all agonists were able to inhibit forskolin-stimulated SPAP production (**Figure 4.13**). All ligands examined were full agonists relative to quinpirole responses except for (-)-3-PPP, which was a partial agonist with 52.1 ± 1.8% of 10µM quinpirole response. This mutation significantly increased the relative maximal response of aripiprazole, which was a full agonist in S5.42A cells compared to its partial agonist response in WT cells (**Figure 3.7**). Apomorphine results were highly variable between the 2 experiments conducted and were as follows; R_{max} 66.4% and pEC_{50} of 7.15 compared with R_{max} of 128.6% and pEC_{50} of 7.89. Compared to WT, S5.42A mutation increased the potencies of quinpirole (13.5-fold), cabergoline (4-fold) and pergolide (47.9-fold). In contrast, there were decreases in potency for (-)-3-PPP (22.9-fold), dopamine (162.2-fold), apomorphine (8.5-fold) and RNPA (11.5-fold) (**Table 4.6**). The rank order of potency was pergolide > cabergoline > quinpirole = bromocriptine = RNPA > dihydroergocristine > aripiprazole > 7OH-DPAT > apomorphine > (+)-3-PPP > dopamine > (-)-3-PPP.

To investigate the ligand specific differences between the WT and T6.34R receptors, the serine mutations were repeated in the T6.34R background. As shown **Figure 4.13**, surprisingly a number of agonists now potentiated, rather than inhibited, forskolin-stimulated SPAP production, consistent with inverse agonism. While the inverse agonism for (-)-3-PPP and (+)-3-PPP was only detected in 2/4 experiments, the inverse agonism with dopamine was consistently seen in all 3 independent experiments (R_{max} 127.4 ± 12.6% 3µM

forskolin response; pEC_{50} 5.79 ± 0.20). Furthermore, in one experiment, RNPA and apomorphine also acted as inverse agonists however, as they acted as agonists in the further two replicates, the agonism data has been shown. All other ligands were full agonists relative to quinpirole. When compared with the T6.34R D2L responses, there were decreases in potency for quinpirole (3-fold), 7OH-DPAT (38-fold), apomorphine (416.9-fold) and RNPA (218.8-fold). When compared to S5.42A D2L responses, there were significant decreases in maximal response for quinpirole, bromocriptine and 7OH-DPAT. Furthermore, almost every ligand had decreased potency relative to S5.42A responses with significant decreases for quinpirole (74.1-fold), bromocriptine (4.7-fold), 7OH-DPAT (15.1-fold), cabergoline (4.5-fold) and pergolide (11.7-fold) (**Table 4.7**). For agonists that continued to inhibit SPAP responses, the overall rank order of potency was pergolide = cabergoline > aripiprazole = dihydroergocristine > bromocriptine > RNPA > quinpirole > 7OH-DPAT > apomorphine.

There were differences in the effects of S5.42A mutation in WT and T6.34R backgrounds. Compared to WT, S5.42A increased quinpirole potency whereas it decreased potency in S5.42A T6.34R when compared to T6.34R alone. Furthermore, for compounds with decreased potency following S5.42A mutation, such as apomorphine and RNPA, the effects of S5.42A mutation were much greater in the T6.34R background compared to WT (e.g. apomorphine 8.5-fold decrease in S5.42A potency compared to WT whereas 416.9-fold decrease in potency with S5.42A T6.34R mutation compared to T6.34R alone).

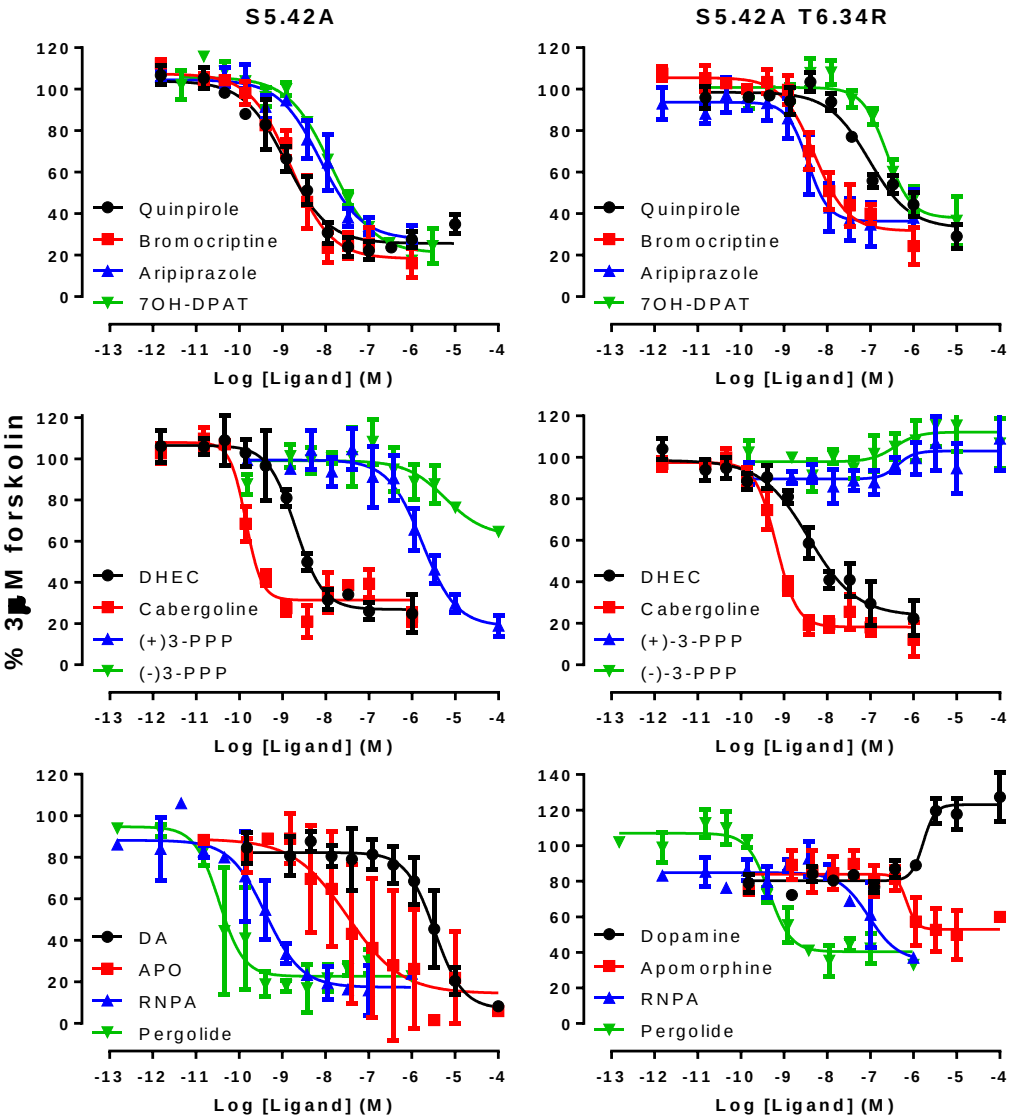


Figure 4.13: Ability of D2 receptor agonists to inhibit forskolin-stimulated SPAP production in CHOcs ssD2L S5.42A and CHOcs ssD2L S5.42A T6.34R cells

Cells were treated with increasing concentrations of dopamine D2 receptor agonists for 1h prior to 5h 3µM forskolin stimulation. Data represent pooled data (mean ± SEM, unless n=2 where mean ± range) of 2-4 independent experiments performed in duplicate, normalised to 3µM forskolin (100%) and vehicle (0%) controls. Data are summarised in **Table 4.6** and **Table 4.7**. DHEC = dihydroergocristine; DA = dopamine; APO = apomorphine.

Ligand	S5.42A			WT		Fold change in potency (EC_{50} ratio)
	R_{max}	pEC_{50}	n	R_{max}	pEC_{50}	
Quinpirole	117.6 ± 5.5*	8.93 ± 0.24*	3	99.3 ± 1.1	7.80 ± 0.23	+13.5
Bromocriptine	123.7 ± 6.9*	8.92 ± 0.06*	3	99.5 ± 4.1	9.31 ± 0.12	-2.5
Aripiprazole	106.5 ± 1.9*	8.26 ± 0.10	3	48.1 ± 0.5	8.02 ± 0.08	+1.7
7OH-DPAT	123.9 ± 4.5*	7.84 ± 0.13	3	100.7 ± 1.1	8.04 ± 0.16	-1.6
Dihydroergocristine	103.7 ± 24.1 (91.6, 115.7)	8.70 ± 0.02 (8.72, 8.69)	2	81.4 ± 3.7	8.97 ± 0.15	-1.9
Cabergoline	97.4 ± 12.1 (91.5, 104.0)	9.84 ± 0.12 (9.78, 9.90)	2	103.8 ± 3.9	9.24 ± 0.08	+4.0
(+)-3-PPP	115.8 ± 4.0 (111.8, 119.8)	5.77 ± 0.13 (5.64, 5.90)	2	100.3 ± 6.2	6.37 ± 0.29	-4.0
(-)-3-PPP	52.1 ± 1.8 (50.3, 53.9)	5.27 ± 0.11 (5.16, 5.38)	2	63.3 ± 10.7	6.63 ± 0.24	-22.9
Dopamine	113.5 ± 11.8 (101.7, 125.3)	5.49 ± 0.15 (5.34, 5.64)	2	102.9 ± 2.0	7.70 ± 0.04	-162.2
Apomorphine	97.5 ± 31.1 (66.4, 128.6)	7.52 ± 0.38 (7.15, 7.89)	2	100.3 ± 1.6	8.45 ± 0.04	-8.5
RNPA	102.8 ± 1.8 (101.0, 104.6)	8.90 ± 0.25 (9.15, 8.66)	2	103.6 ± 1.6	9.96 ± 0.02	-11.5
Pergolide	96.9 ± 7.2 (89.7, 104.0)	10.35 ± 0.36 (9.99, 10.71)	2	96.7 ± 3.1	8.67 ± 0.09	+47.9

Table 4.6: Comparison of ligand responses in the CRE-SPAP reporter gene assay in CHOcs ssD2L S5.42A and WT D2L cells

Summary of ligand parameters derived from concentration responses curves in **Figure 4.13** compared to ligand responses at the WT receptor (**Figure 3.7**). Data are pooled (mean ± SEM unless n=2 where mean ± range) of 2-4 independent experiments performed in duplicate or triplicate with R_{max} expressed as a percentage of 10μM quinpirole response. Where n=2, individual replicate values are given in brackets. The EC_{50} ratio indicates the increased (+) or decreased (-) fold change in agonist potencies in S5.42A compared to WT. *P<0.05 cf. WT; Student's unpaired t-test.

Ligand	S5.42A T6.34R			T6.34R			S5.42A		
	R_{max}	pEC_{50}	N	R_{max}	pEC_{50}	Fold change in potency (EC_{50} ratio)	R_{max}	pEC_{50}	Fold change in potency (EC_{50} ratio)
Quinpirole	96.5 ± 2.3$^{\#}$	7.06 ± 0.13*$^{\#}$	3	96.4 ± 6.1	7.54 ± 0.08	-3.0	117.6 ± 5.5	8.93 ± 0.24	-74.1
Bromocriptine	100.5 ± 1.0$^{\#}$	8.25 ± 0.16$^{\#}$	3	92.6 ± 6.8	8.27 ± 0.18	-	123.7 ± 6.9	8.92 ± 0.06	-4.7
Aripiprazole	90.6 ± 7.3	8.45 ± 0.10	3	96.1 ± 10.4	8.29 ± 0.29	+1.4	106.5 ± 1.9	8.26 ± 0.10	+1.5
7OH-DPAT	88.6 ± 8.3$^{\#}$	6.66 ± 0.11*$^{\#}$	3	92.3 ± 9.9	8.24 ± 0.10	-38.0	123.9 ± 4.5	7.84 ± 0.13	-15.1
Dihydroergocristine	97.6 ± 8.2	8.42 ± 0.07*$^{\#}$	4	112.8 ± 7.1	8.23 ± 0.04	+1.5	103.7 ± 12.1 (91.6, 115.7)	8.70 ± 0.02 (8.72, 8.69)	-1.9
Cabergoline	106.7 ± 4.1*	9.19 ± 0.12$^{\#}$	4	137.6 ± 6.2	8.74 ± 0.15	+2.8	97.4 ± 6.3 (91.5, 104.0)	9.84 ± 0.06 (9.78, 9.90)	-4.5
(+)3-PPP	133.2 ± 5.6 (%FSK) (127.6, 138.7)	5.27 ± 0.85 (4.42, 6.12)	2	105.1 ± 10.0	6.76 ± 0.16	-30.9	115.8 ± 4.0 (111.8, 119.8)	5.77 ± 0.13 (5.64, 5.90)	-3.2
	NE	NE	2			-			-
(-)3-PPP	132.4 ± 2.4 (%FSK) (130.0, 134.7)	6.25 ± 0.82 (5.43, 7.07)	2	109.4 ± 8.1	7.00 ± 0.09	-5.6	52.1 ± 1.8 (50.3, 53.9)	5.27 ± 0.11 (5.16, 5.38)	+9.5
	NE	NE	2			-			-
Dopamine	127.4 ± 12.6 (%FSK)*$^{\#}$	5.79 ± 0.20*	3	102.3 ± 11.9	7.85 ± 0.10	-114.8	113.5 ± 11.8 (101.7, 125.3)	5.49 ± 0.15 (5.34, 5.64)	+2.0
Apomorphine	88.6 ± 8.5 (80.1, 97.1)	6.04 ± 0.26 (6.30, 5.78)	2	116.3 ± 13.2	8.66 ± 0.08	-416.9	97.5 ± 31.1 (66.4, 128.6)	7.52 ± 0.38 (7.15, 7.89)	-30.2

RNPA	80.6 (80.6, NE)	7.35 (7.35, NE)	2	137.7 ± 24.9	9.69 ± 0.19	-218.8	102.8 ± 3.6 (101.0, 104.6)	8.90 ± 0.49 (9.15, 8.66)	-35.5
Pergolide	102.6 ± 12.3	9.28 ± 0.11$^{\#}$	3	87.4 ± 12.4	8.90 ± 0.26	+2.4	96.9 ± 14.3 (89.7, 104.0)	10.35 ± 0.72 (9.99, 10.71)	-11.7

Table 4.7: Summary of ligand responses in CRE-SPAP reporter gene assay in CHOcs ssD2L S5.42A T6.34R cells, compared with T6.34R and S5.42A responses

Summary of ligand parameters derived from the concentration response curves in **Figure 4.13,** compared to T6.34R and S5.42A responses. Data are pooled (mean ± SEM, unless n=2 where mean ± range) of 2-5 independent experiments performed in duplicate, with R_{max} expressed as a percentage of 10μM quinpirole response except for inverse agonist responses, which are expressed as a percentage of 3μM forskolin (FSK) response as indicated. For (+)-3-PPP and (-)-3-PPP data, where both no effect and inverse agonism was detected, both sets of results are presented. For apomorphine and RNPA, only the 2 experiments where agonism was detected are presented. Where n=2, replicate values are given in brackets. The EC_{50} ratio indicates the increased (+) or decreased (-) fold change in agonist potencies in S5.42A T6.34R compared to T6.34R or S5.42A. NE = no effect; *P<0.05 cf. T6.34R, $^{\#}$P<0.05 cf. S5.42A (Student's unpaired t-test).

4.2.6 Effect of S5.43A mutations in WT and T6.34R background on ligand CRE-SPAP reporter gene assay responses

The effect of S5.43A mutation on D2L responses in the CRE-SPAP reporter gene assay was then examined. All ligands were full agonists relative to quinpirole, except for aripiprazole and (-)-3-PPP, which were partial agonists with R_{max} of 46.4 ± 11.4% and 42.3 ± 8.0% respectively (**Figure 4.14**). While S5.43A mutation caused no significant changes in the relative maximal responses of any compounds, there was a 13.8-fold decrease in dopamine potency. There were also modest changes in potency for a number of ligands (**Table 4.8**). For the ergo-derived compounds, there were opposing effects on ligand potency; while bromocriptine and dihydroergocristine potencies decreased 3- and 2.8-fold respectively, cabergoline and pergolide potencies increased 3.8- and 3.4-fold (**Table 4.8**). The overall rank order of potency was cabergoline = RNPA > pergolide > bromocriptine > dihydroergocristine > apomorphine > aripiprazole > quinpirole > 7OH-DPAT > dopamine > (+)-3-PPP = (-)-3-PPP.

Next, the effect of S5.43A mutation on CHOcs ssD2L T6.34R CRE-SPAP responses was investigated. All agonists were full agonists relative to quinpirole (**Figure 4.14**). Generally, the double mutation had modest effects on agonist responses except quinpirole and cabergoline potencies, which were increased 4.7- and 4.3-fold relative to T6.34R mutation alone. When compared to S5.43A, the double mutation increased the relative maximal responses of both aripiprazole and (-)-3-PPP which were now full agonists. Furthermore, dopamine potency was increased 9.5-fold ($P<0.05$, Student's unpaired t-test; **Table 4.9**). The overall rank order of potency was RNPA > cabergoline = pergolide > apomorphine > bromocriptine = dihydroergocristine > aripiprazole > quinpirole > 7OH-DPAT > dopamine > (-)-3-PPP = (+)-3-PPP.

.

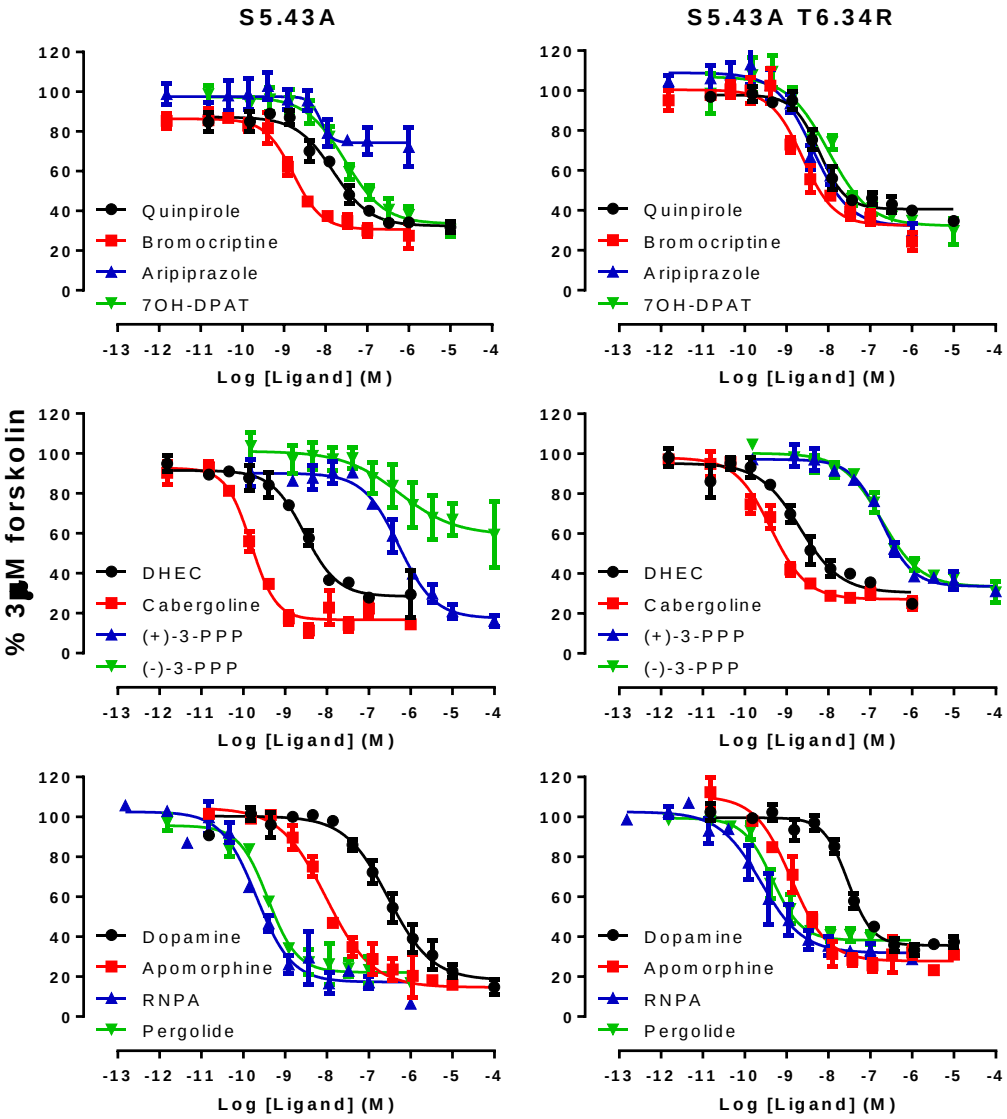


Figure 4.14: Ability of D2 receptor agonists to inhibit forskolin-stimulated SPAP production in CHOcs ssD2L S5.43A and CHOcs ssD2L S5.43A T6.34R cells

Cells were treated with increasing concentrations of dopamine D2 receptor agonists for 1h prior to 5h 3µM forskolin stimulation. Data represent pooled data (mean ± SEM, unless n=2 where mean ± range) of 2-5 independent experiments performed in duplicate, normalised to 3µM forskolin (100%) and vehicle (0%) controls. Data are summarised in **Table 4.8** and **Table 4.9**. DHEC = dihydroergocristine.

Ligand	S5.43A			WT		Fold change in potency (EC_{50} ratio)
	R_{max}	pEC_{50}	N	R_{max}	pEC_{50}	
Quinpirole	100.7 ± 1.4	7.77 ± 0.11	4	99.3 ± 1.1	7.80 ± 0.23	-1.1
Bromocriptine	102.6 ± 4.7	8.83 ± 0.13*	4	99.5 ± 4.1	9.31 ± 0.12	-3.0
Aripiprazole	46.4 ± 11.4	7.94 ± 0.06	4	48.1 ± 0.5	8.02 ± 0.08	-1.2
7OH-DPAT	96.1 ± 1.8	7.50 ± 0.09*	4	100.7 ± 1.1	8.04 ± 0.16	-3.5
Dihydroergocristine	77.6 ± 8.7 (86.2, 68.9)	8.52 ± 0.01 (8.53, 8.51)	2	81.4 ± 3.7	8.97 ± 0.15	-2.8
Cabergoline	89.7 ± 1.7 (88.0, 91.3)	9.82 ± 0.16 (9.98, 9.66)	2	103.8 ± 3.9	9.24 ± 0.08	+3.8
(+)-3-PPP	87.8 ± 3.1 (84.7, 90.9)	6.31 ± 0.22 (6.52, 6.09)	2	100.3 ± 6.2	6.37 ± 0.29	-1.1
(-)-3-PPP	42.3 ± 8.0	6.27 ± 0.27	4	63.3 ± 10.7	6.63 ± 0.24	-2.3
Dopamine	104.5 ± 4.3	6.56 ± 0.19*	5	102.9 ± 2.0	7.70 ± 0.04	-13.8
Apomorphine	95.5 ± 10.9 (84.6, 106.3)	8.12 ± 0.02 (8.10, 8.13)	2	100.3 ± 1.6	8.45 ± 0.04	-2.1
RNPA	99.3 ± 12.2 (87.1, 111.5)	9.72 ± 0.01 (9.73, 9.71)	2	103.6 ± 1.6	9.96 ± 0.02	-1.7
Pergolide	99.2 ± 6.5	9.20 ± 0.16*	5	96.7 ± 3.1	8.67 ± 0.09	+3.4

Table 4.8: Summary of CRE-SPAP responses in CHOcs ssD2L S5.43A cells, compared to ligand responses at WT receptor

Summary of the ligand parameters derived from the concentration response curves in **Figure 4.14**, compared with WT results (**Figure 3.7**). Data are pooled (mean ± SEM, unless n=2 then mean ± range) of 2-5 independent experiments performed in duplicate, with R_{max} expressed as a percentage 10μM quinpirole response. Where n=2, replicate values are given in brackets. The EC_{50} ratio indicates the increased (+) or decreased (-) fold change in agonist potencies in S5.43A compared to WT. *P<0.05 cf. WT response (Student's unpaired t-test)

Ligand	S5.43A T6.34R			T6.34R			S5.43A		
	R_{max}	pEC_{50}	N	R_{max}	pEC_{50}	Fold change in potency (EC_{50} ratio)	R_{max}	pEC_{50}	Fold change in potency (EC_{50} ratio)
Quinpirole	92.9 ± 0.5$^{\#}$	8.21 ± 0.10*$^{\#}$	4	96.4 ± 6.1	7.54 ± 0.08	+4.7	100.7 ± 1.4	7.77 ± 0.11	+2.8
Bromocriptine	103.8 ± 4.7	8.63 ± 0.11	4	92.6 ± 6.8	8.27 ± 0.18	+2.3	102.6 ± 4.7	8.83 ± 0.13	-1.6
Aripiprazole	95.8 ± 4.2$^{\#}$	8.36 ± 0.18	4	96.1 ± 10.4	8.29 ± 0.29	+1.2	46.4 ± 11.4	7.94 ± 0.06	+2.6
7OH-DPAT	101.1 ± 6.2	8.01 ± 0.18$^{\#}$	4	92.3 ± 9.9	8.24 ± 0.10	-1.7	96.1 ± 1.8	7.50 ± 0.09	+3.2
Dihydroergocristine	105.6 ± 7.8	8.62 ± 0.28	3	112.8 ± 7.1	8.23 ± 0.04	+2.5	77.6 ± 8.7 (86.2, 68.9)	8.52 ± 0.01 (8.53, 8.51)	+1.3
Cabergoline	107.0 ± 3.4*$^{\#}$	9.37 ± 0.20*	3	137.6 ± 6.2	8.74 ± 0.15	+4.3	89.7 ± 1.7 (88.0, 91.3)	9.82 ± 0.16 (9.98, 9.66)	-2.8
(+)-3-PPP	98.4 ± 0.7$^{\#}$	6.71 ± 0.03	3	105.1 ± 10.0	6.76 ± 0.16	-1.1	87.8 ± 3.1 (84.7, 90.9)	6.31 ± 0.22 (6.52, 6.09)	+2.5
(-)-3-PPP	96.3 ± 6.5$^{\#}$	6.75 ± 0.04*	6	109.4 ± 8.1	7.00 ± 0.09	-1.8	42.3 ± 8.0	6.27 ± 0.27	+3.0
Dopamine	85.7 ± 3.9$^{\#}$	7.54 ± 0.06*$^{\#}$	5	102.3 ± 11.9	7.85 ± 0.10	-2.0	104.5 ± 4.3	6.56 ± 0.19	+9.5
Apomorphine	94.8 ± 0.5	8.78 ± 0.18	3	116.3 ± 13.2	8.66 ± 0.08	+1.3	95.5 ± 10.9 (84.6, 106.3)	8.12 ± 0.02 (8.10, 8.13)	+4.6
RNPA	93.4 ± 3.0	9.50 ± 0.25	3	137.7 ± 24.9	9.69 ± 0.19	-1.5	99.3 ± 12.2 (87.1, 111.5)	9.72 ± 0.01 (9.73, 9.71)	-1.7
Pergolide	89.6 ± 2.6	9.31 ± 0.14	6	87.4 ± 12.4	8.90 ± 0.26	+2.6	99.2 ± 6.5	9.20 ± 0.16	+1.3

Table 4.9: Summary of ligand responses in the CRE-SPAP reporter gene assay in CHOcs ssD2L S5.43A T6.34R cells, compared to T6.34R and S5.43A responses

Summary of ligand parameters derived from the concentration response curves in **Figure 4.14**, compared to ligand responses in T6.34R and S5.43A D2L expressing cells. Data are pooled (mean ± SEM, unless n=2 where mean ± range) of 2-6 independent experiments performed in duplicate, with R_{max} expressed as a percentage of 10μM quinpirole response. Where n=2, replicate values are given in brackets. The EC_{50} ratio indicates the increased (+) or decreased (-) fold change in agonist potencies in S5.43A T6.34R compared to T6.34R or S5.43A. *P<0.05 cf. T6.34R, $^{\#}$P<0.05 cf. S5.43A (Student's unpaired t-test).

4.2.7 Effect of S5.46A mutations in WT background on ligand CRE-SPAP reporter gene assay responses

In the CRE-SPAP reporter gene assay, all ligands were full agonists except bromocriptine, aripiprazole, (-)-3-PPP and apomorphine which were partial agonists (**Figure 4.15**). In one experiment, there was no response to dopamine and in the other, it was a partial agonist (pEC_{50} 7.60, R_{max} 21.5%). The order of efficacy of the partial agonists was aripiprazole > (-)-3-PPP > bromocriptine > apomorphine. S5.46A mutation decreased the potency of quinpirole (5.8-fold), apomorphine (162.2-fold) and RNPA (25.1-fold) while aripiprazole and 7OH-DPAT potencies increased 4.4- and 4.7-fold respectively when compared to WT. For the ergo-derived compounds, while bromocriptine and dihydroergocristine potencies decreased 9.8- and 3.6-fold respectively, pergolide potency increased 4.6-fold (**Table 4.10**). Furthermore, the relative maximal responses of bromocriptine, dopamine and apomorphine were decreased whilst aripiprazole maximal response was increased relative to WT responses (**Table 4.10**). The overall rank order of potency was cabergoline > pergolide > 7OH-DPAT = aripiprazole > RNPA > dihydroergocristine = bromocriptine > dopamine > quinpirole > (+)-3-PPP = (-)-3-PPP > apomorphine.

The effect of S5.46A mutation on CHOcs ssD2L T6.34R responses was then examined. All ligands were full agonists relative to quinpirole, except for apomorphine (partial agonist; R_{max} 72.4 ± 0.1%) and dopamine, which had no effect in one experiment and was a weak partial agonist (pEC_{50} 5.05, R_{max} 21.6%) in the other (**Figure 4.15**). When compared to T6.34R responses, the double mutation only had modest effects on most agonists except for dopamine, apomorphine and RNPA responses where potencies decreased 631-, 616.6- and 67.6-fold respectively. Furthermore, there were decreases in relative maximal response for all three agonists. These effects were much greater in the T6.34R background than the WT background, described above. When compared to S5.46A responses, S5.46A T6.34R mutation increased the relative maximal responses of bromocriptine, dihydroergocristine,

aripiprazole and (-)-3-PPP. Furthermore, it decreased the potencies of cabergoline (5.2-fold) and RNPA (5-fold) (**Table 4.11**). The overall rank order of potency was cabergoline > pergolide > 7OH-DPAT = aripiprazole > dihydroergocristine > bromocriptine > RNPA > quinpirole > (+)-3-PPP = (-)-3-PPP > apomorphine.

The potency shifts for all mutations are summarised in **Figure 4.16.** Quinpirole responses were generally sensitive to all serine mutations, with only S5.43A not significantly changing potency compared to WT responses. Interestingly, S5.42A mutation had opposing effects on quinpirole potency in WT and T6.34R backgrounds. In contrast, aripiprazole responses were largely unaffected by serine mutations, with only S5.46A mutation significantly increasing potency compared to WT responses. The potencies of the catechol compounds, including the endogenous agonist dopamine, were generally decreased following all serine mutations in both backgrounds. However, the effects of S5.43A were modest compared with the 1-3 log fold decreases in potency observed following S5.42A and S5.46A mutations in both WT and T6.34R cells. The results for those compounds which contained a single hydroxyl group, 7OH-DPAT, (+)-3-PPP and (-)-3-PPP, were mixed, with specific mutations increasing or decreasing potencies for each ligand.

It was hypothesised that the ergo-derived compounds had a distinct mode of binding to the dopamine D2L receptor which resulted in the ligand specific effects on potency following T6.34R mutation. As observed in **Figure 4.16**, the effects of each serine mutation on the potencies of the ergo-derived compounds were greater in the WT background than T6.34R. Furthermore, in general there were opposing effects of serine mutations on bromocriptine and dihydroergocristine responses compared with pergolide and cabergoline responses.

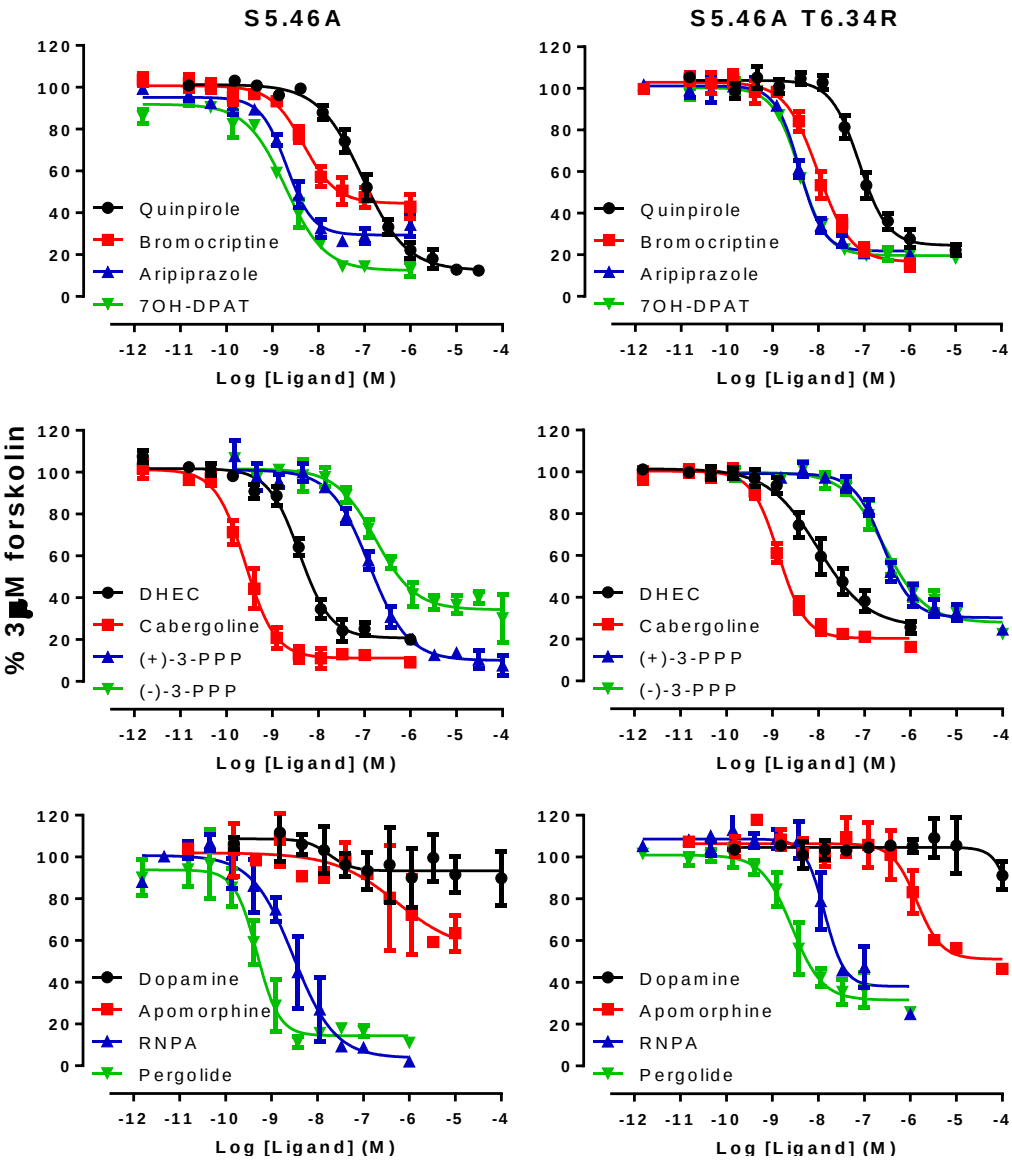


Figure 4.15: Ability of D2 receptor agonists to inhibit forskolin-stimulated SPAP production in CHOcs ssD2L S5.46A and CHOcs ssD2L S5.46A T6.34R cells

Cells were treated with increasing concentrations of dopamine D2 receptor agonists for 1h prior to 5h 3µM forskolin stimulation. Data represent pooled data (mean ± SEM, unless n=2 where mean ± range) of 2-5 independent experiments performed in duplicate, normalised to 3µM forskolin (100%) and vehicle (0%) controls. Data are summarised in **Table 4.10** and **Table 4.11.** DHEC = dihydroergocristine.

Ligand	S5.46A			WT		Fold change in potency (EC_{50} ratio)
	R_{max}	pEC_{50}	N	R_{max}	pEC_{50}	
Quinpirole	100.3 ± 3.5	7.04 ± 0.10*	4	99.3 ± 1.1	7.80 ± 0.23	-5.8
Bromocriptine	64.9 ± 7.9*	8.32 ± 0.05*	4	99.5 ± 4.1	9.31 ± 0.12	-9.8
Aripiprazole	84.3 ± 4.4*	8.66 ± 0.08*	4	48.1 ± 0.5	8.02 ± 0.08	+4.4
7OH-DPAT	104.1 ± 3.5	8.71 ± 0.14*	4	100.7 ± 1.1	8.04 ± 0.16	+4.7
Dihydroergocristine	87.9 ± 2.1	8.41 ± 0.07*	4	81.4 ± 3.7	8.97 ± 0.15	-3.6
Cabergoline	98.2 ± 3.6	9.59 ± 0.12	4	103.8 ± 3.9	9.24 ± 0.08	+2.2
(+)-3-PPP	100.0 ± 2.6	6.88 ± 0.07	4	100.3 ± 6.2	6.37 ± 0.29	+3.2
(-)-3-PPP	72.7 ± 5.3	6.75 ± 0.03	4	63.3 ± 10.7	6.63 ± 0.24	+1.3
Dopamine	21.5 (21.5, NE)	7.60 (7.60, NE)	2	102.9 ± 2.0	7.70 ± 0.04	-1.3
Apomorphine	41.9 ± 12.2 (29.7, 54.0)	6.24 ± 0.43 (5.81, 6.67)	2	100.3 ± 1.6	8.45 ± 0.04	-162.2
RNPA	98.7 ± 10.2 (88.5, 108.8)	8.56 ± 0.15 (8.41, 8.71)	2	103.6 ± 1.6	9.96 ± 0.02	-25.1
Pergolide	93.4 ± 6.6 (86.8, 100.0)	9.33 ± 0.14 (9.20, 9.47)	2	96.7 ± 3.1	8.67 ± 0.09	+4.6

Table 4.10: Summary of agonist CRE-SPAP responses in CHOcs ssD2L S5.46A cells, compared to WT responses

Summary of ligand parameters derived from the concentration response curves in **Figure 4.15,** compared to WT responses. Data are pooled (mean ± SEM, unless n=2 then mean ± range) of 2-4 independent experiments performed in duplicate or triplicate, with R_{max} expressed as a percentage 10μM quinpirole response. Where n=2, replicate values are given in brackets. The EC_{50} ratio indicates the increased (+) or decreased (-) fold change in agonist potencies in S5.46A compared to WT. *P<0.05 cf. WT response (Student's unpaired t-test); NE = no effect.

Ligand	S5.46A T6.34R			T6.34R			S5.46A		
	R_{max}	pEC_{50}	N	R_{max}	pEC_{50}	Fold change in potency (EC_{50} ratio)	R_{max}	pEC_{50}	Fold change in potency (EC_{50} ratio)
Quinpirole	97.7 ± 1.1	7.09 ± 0.10*	4	96.4 ± 6.1	7.54 ± 0.08	-2.8	100.3 ± 3.5	7.04 ± 0.10	+1.1
Bromocriptine	107.3 ± 4.7#	8.00 ± 0.13	4	92.6 ± 6.8	8.27 ± 0.18	-1.9	64.9 ± 7.9	8.32 ± 0.05	-2.1
Aripiprazole	101.4 ± 2.5#	8.40 ± 0.07#	4	96.1 ± 10.4	8.29 ± 0.29	+1.3	84.3 ± 4.4	8.66 ± 0.08	-1.8
7OH-DPAT	103.8 ± 3.1	8.40 ± 0.05	4	92.3 ± 9.9	8.24 ± 0.10	+1.4	104.1 ± 3.5	8.71 ± 0.14	-2.0
Dihydroergocristine	100.9 ± 3.5#	8.29 ± 0.05	5	112.8 ± 7.1	8.23 ± 0.04	+1.1	87.9 ± 2.1	8.41 ± 0.07	-1.3
Cabergoline	110.7 ± 4.1*	8.87 ± 0.07#	5	137.6 ± 6.2	8.74 ± 0.15	+1.3	98.2 ± 3.6	9.59 ± 0.12	-5.2
(+)-3-PPP	96.6 ± 3.6	6.66 ± 0.02#	5	105.1 ± 10.0	6.76 ± 0.16	-1.3	100.0 ± 2.6	6.88 ± 0.07	-1.7
(-)-3-PPP	97.9 ± 5.1#	6.63 ± 0.12*	5	109.4 ± 8.1	7.00 ± 0.09	-2.4	72.7 ± 5.3	6.75 ± 0.03	-1.3
Dopamine	21.6 (2.16, NE)	5.05 (5.05, NE)	2	102.3 ± 11.9	7.85 ± 0.10	-631	21.5 (21.5, NE)	7.60 (7.60, NE)	-354
Apomorphine	72.4 ± 0.1 (72.4, 72.5)	5.87 ± 0.06 (5.82, 5.93)	2	116.3 ± 13.2	8.66 ± 0.08	-616.6	41.9 ± 12.2 (29.7, 54.0)	6.24 ± 0.43 (5.81, 6.67)	-2.3
RNPA	85.1 ± 12.1 (73.0, 97.1)	7.86 ± 0.05 (7.81, 7.91)	2	137.7 ± 24.9	9.69 ± 0.19	-67.6	98.7 ± 10.2 (88.5, 108.8)	8.56 ± 0.15 (8.41, 8.71)	-5.0
Pergolide	101.4 ± 9.1 (110.4, 92.3)	8.59 ± 0.17 (8.42, 8.76)	2	87.4 ± 12.4	8.90 ± 0.26	-2.0	93.4 ± 6.6 (86.8, 100.0)	9.33 ± 0.14 (9.20, 9.47)	-5.5

Table 4.11: Summary of CRE-SPAP reporter gene assay responses in CHOcs ssD2L S5.46A T6.34R cells, compared to T6.34R and S5.46A responses

Summary of ligand parameters derived from the concentration response curves in **Figure 4.15**, compared to T6.34R and S5.46A responses. Data are pooled (mean ± SEM, unless n=2 where mean ± range) of 2-5 independent experiments performed in duplicate, with R_{max} expressed as a percentage of 10μM quinpirole response. Where n=2, replicate values are given in brackets. The EC_{50} ratio indicates the increased (+) or decreased (-) fold change in agonist potencies in S5.46A T6.34R compared to T6.34R and S5.46A. NE = no effect; *P<0.05 cf. T6.34R, $^{\#}$P<0.05 cf. S5.46A (Student's unpaired t-test).

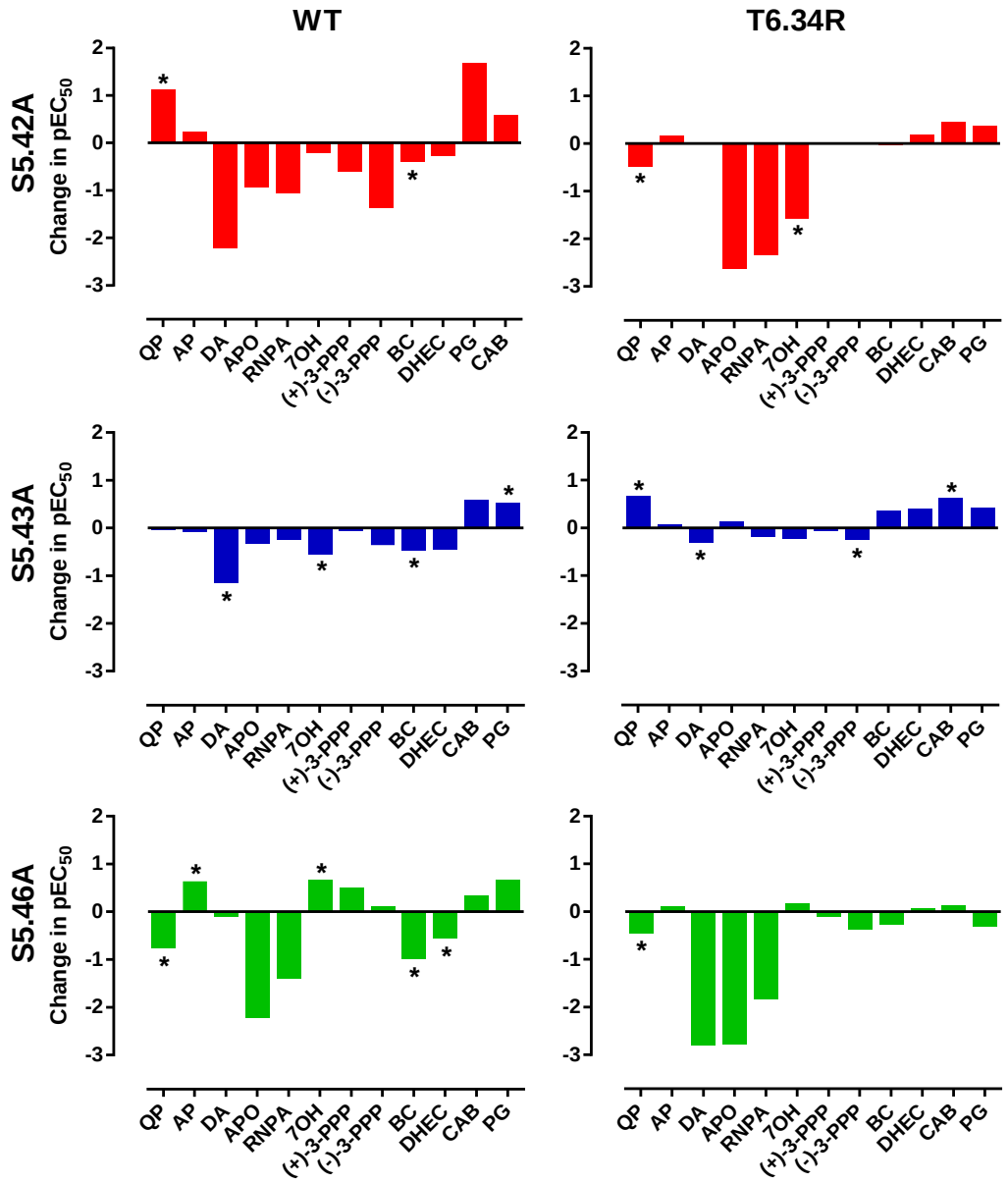


Figure 4.16: Summary of pEC_{50} changes in the CRE-SPAP reporter gene assay for S5.42A, S5.43A and S5.46A mutations

Summary of the change in pEC_{50} (calculated as pEC_{50} mutant – pEC_{50} WT/T6.34R) from CRE-SPAP reporter gene assay data. The data for (-)-3-PPP, (+)-3-PPP and dopamine have been excluded from S5.42 T6.34R graph due to inverse agonist effects. *P<0.05 cf WT/T6.34R, Student's unpaired t-test. QP = quinpirole; AP = aripiprazole; DA = dopamine; APO = apomorphine; 7OH = 7OH-DPAT; BC = bromocriptine; DHEC = dihydroergocristine; CAB = cabergoline; PG = pergolide.

4.2.8 Effect of serine mutations on receptor internalisation responses in all cell lines

In order to verify that the mutant receptors were targeted to the plasma membrane, cells were labelled with a membrane impermeant SNAP fluorophore and imaged as previously described (**2.7.2**). All receptors were expressed at the plasma membrane, although there appeared to some low levels of constitutive internalisation for both the S5.42A and S5.42A T6.34R cell lines. Ligand treatment for 1h promoted receptor internalisation in all cell lines (**Figure 4.17**, **Figure 4.18, Figure 4.19**). A subset of reference ligands – quinpirole, bromocriptine, aripiprazole and 7OH-DPAT were screened for their ability to promote receptor internalisation in all cell lines. The results are summarised in **Table 4.12** and **Figure 4.20**.

In CHOcs ssD2L S5.42A cells, all compounds except for 7OH-DPAT could induce receptor internalisation but only quinpirole was a full agonist (**Figure 4.19**, **Table 4.12**). In comparison to the CRE-SPAP reporter gene assay results (where quinpirole potency was increased 13.5-fold compared to WT), the potency increase with quinpirole was modest (2.5-fold) and not significant. Furthermore, there was a significant potency decrease for bromocriptine (17-fold) when compared to WT responses, which was greater than 2.5-fold decrease observed in the CRE-SPAP reporter gene assay. There was also a modest internalisation response to aripiprazole (pEC_{50} 7.21 ± 0.31; R_{max} 21.3 ± 10.0; n=3) which was not detectable in WT cells. In contrast, the response to 7OH-DPAT was abolished in this cell line despite the mutation having little effect on CRE-SPAP reporter gene assay responses (**Table 4.6**).

Conversely, S5.43A mutation had very little effect on agonist responses. Only quinpirole was a full agonist, with bromocriptine and 7OH-DPAT partial agonists and aripiprazole unable to induce receptor internalisation (**Figure 4.19**, **Table 4.12**). Only 7OH-DPAT responses were a significantly different to WT cells, with a 49.5% reduction in relative maximal response. This is similar

to the CRE-SPAP reporter gene assay where S5.43A mutation had only modest effects on ligand responses (**Table 4.8**).

In CHOcs ssD2L S5.46A cells, all compounds induced receptor internalisation with quinpirole and 7OH-DPAT full agonists and bromocriptine and aripiprazole partial agonists (**Figure 4.19**, **Table 4.12**). There was a significant decrease in quinpirole potency (33-fold) compared to WT, which was greater than the 5.8-fold potency decrease observed in the CRE-SPAP reporter gene assay. Furthermore, bromocriptine potency decreased 8.9-fold with respect to WT responses, which was comparable to the 9.8-fold potency decrease observed in the CRE-SPAP reporter gene assay. (**Table 4.10**). In contrast, while 7OH-DPAT potency significantly decreased in the CRE-SPAP reporter gene assay, there no significant change in receptor internalisation responses following S5.46A mutation compared to WT.

In the T6.34R background, the serine mutations appeared to affect ligand responses in a different manner. In CHOcs ssD2L S5.42A T6.34R cells, all ligands could induce receptor internalisation however only quinpirole was a full agonist (**Figure 4.19**, **Table 4.12**). This resulted in significantly reduced relative maximal responses for both bromocriptine (48.1% decrease) and 7OH-DPAT (51.9% decrease) when compared to the WT T6.34R receptor. Moreover, there were significant decreases in potency for both quinpirole (11.8-fold) and 7OH-DPAT (53.8-fold) compared to WT T6.34R responses, which were greater than the potency decreases in the CRE-SPAP reporter gene assay for these ligands (**Table 4.7**). When compared to S5.42A responses, the double mutation significantly decreased quinpirole potency 13.8-fold. Furthermore, it increased the relative maximal response of bromocriptine and restored the internalisation response of 7OH-DPAT.

In CHOcs ssD2L S5.43A T6.34R cells, all ligands except for aripiprazole were full agonists relative to quinpirole (**Figure 4.19**, **Table 4.12**). S5.43A mutation decreased the maximal response of bromocriptine but increased its potency 5.8-fold when compared to T6.34R responses. 7OH-DPAT potency decreased

87-fold. In contrast to the CRE-SPAP reporter gene assay results (**Table 4.9**), where quinpirole potency increased 4.7-fold compared to T6.34R responses, its potency decreased 3.8-fold. When compared to S5.43A, the double mutation increased the relative maximal responses of aripiprazole and 7OH-DPAT.

Effects on ligand responses were greatest following S5.46A mutation in the T6.34R background (**Figure 4.19**, **Table 4.12**). While both quinpirole and 7OH-DPAT were full agonists, potencies were decreased 41.7- and 22.9-fold compared to T6.34R. Furthermore, bromocriptine responses were abolished following this mutation which contrasts to the CRE-SPAP reporter gene assay results where S5.46A had no significant effect on T6.34R responses (**Table 4.11**). When compared to S5.46A responses, the double mutation had no effect except for the loss of bromocriptine responses as previously described.

When these changes in functional responses were compared between the CRE-SPAP reporter gene and receptor internalisation assays, there was generally good agreement in the results (**Figure 4.20**). In general, potency changes were greater in the receptor internalisation assay than the CRE-SPAP reporter gene, consistent with the reduced receptor reserve in the receptor internalisation assay. However there were a couple of exceptions, as described in the text above. Notably, for S5.43A T6.34R, quinpirole potencies were increased in the CRE-SPAP reporter gene assay but decreased in the receptor internalisation assay.

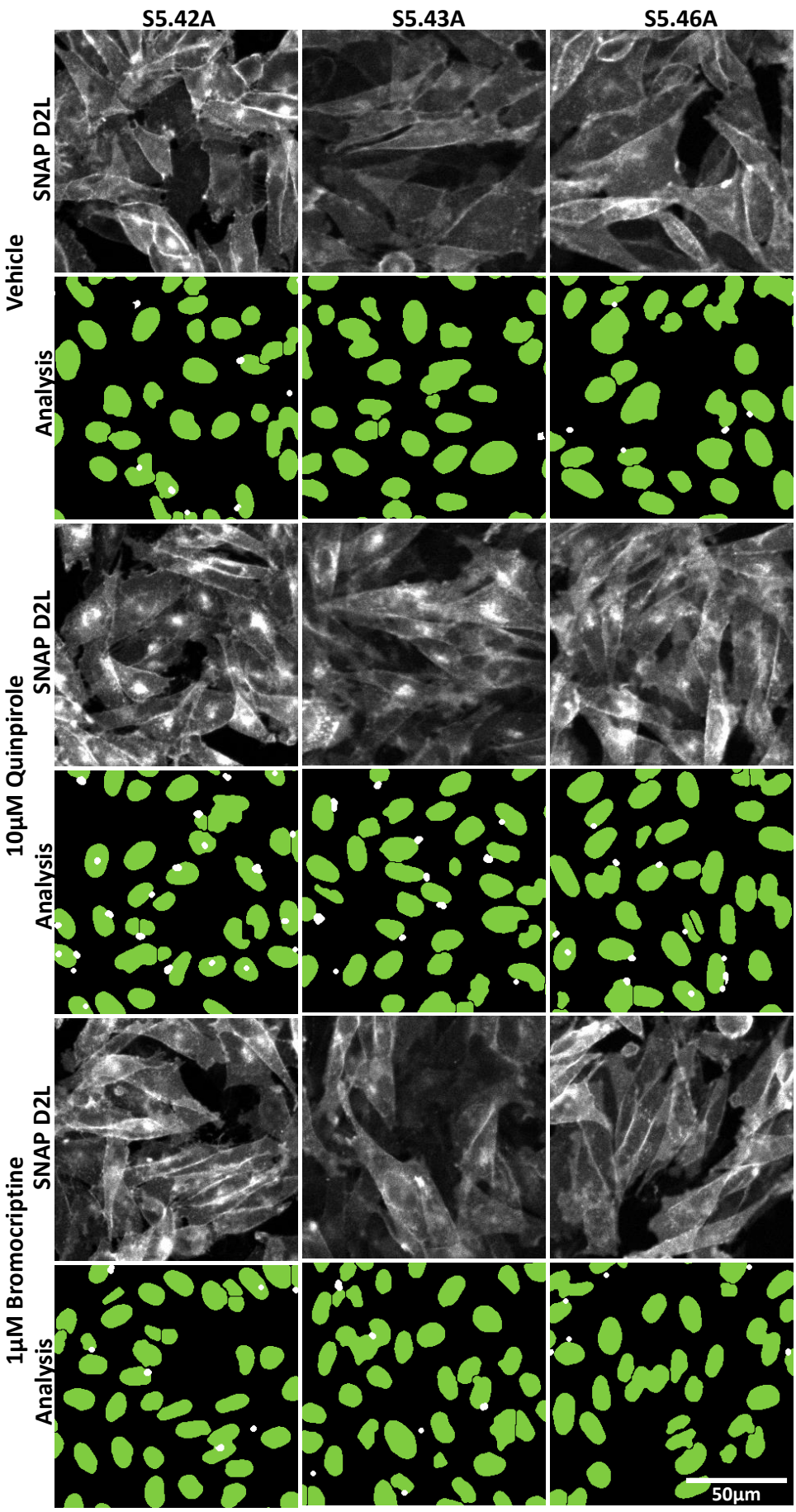

S5.42A
S5.43A
S5.46A
Vehicle
SNAP D2L
Analysis
10µM Quinpirole
SNAP D2L
Analysis
1µM Bromocriptine
SNAP D2L
Analysis
50µm

Figure 4.17: Internalisation of the SNAP-tagged D2L S5.42A, S5.43A and S5.46A receptor in response to ligand treatment

Cells were SNAP-labelled for 30min then treated with increasing concentrations of ligands for 1h prior to fixation. Representative images show cells treated with vehicle, 10µM quinpirole and 1µM bromocriptine. For clarity, the images above were cropped to 120µm x 120µm from the original 400µm x 400µm image used for analysis. The panels show the SNAP-tagged receptor with the associated granularity analysis below, with nuclei in green and receptor containing granules of 6-10µm diameter in white. The internalisation of 4 representative dopamine ligands was determined and quantified in **Figure 4.19**.

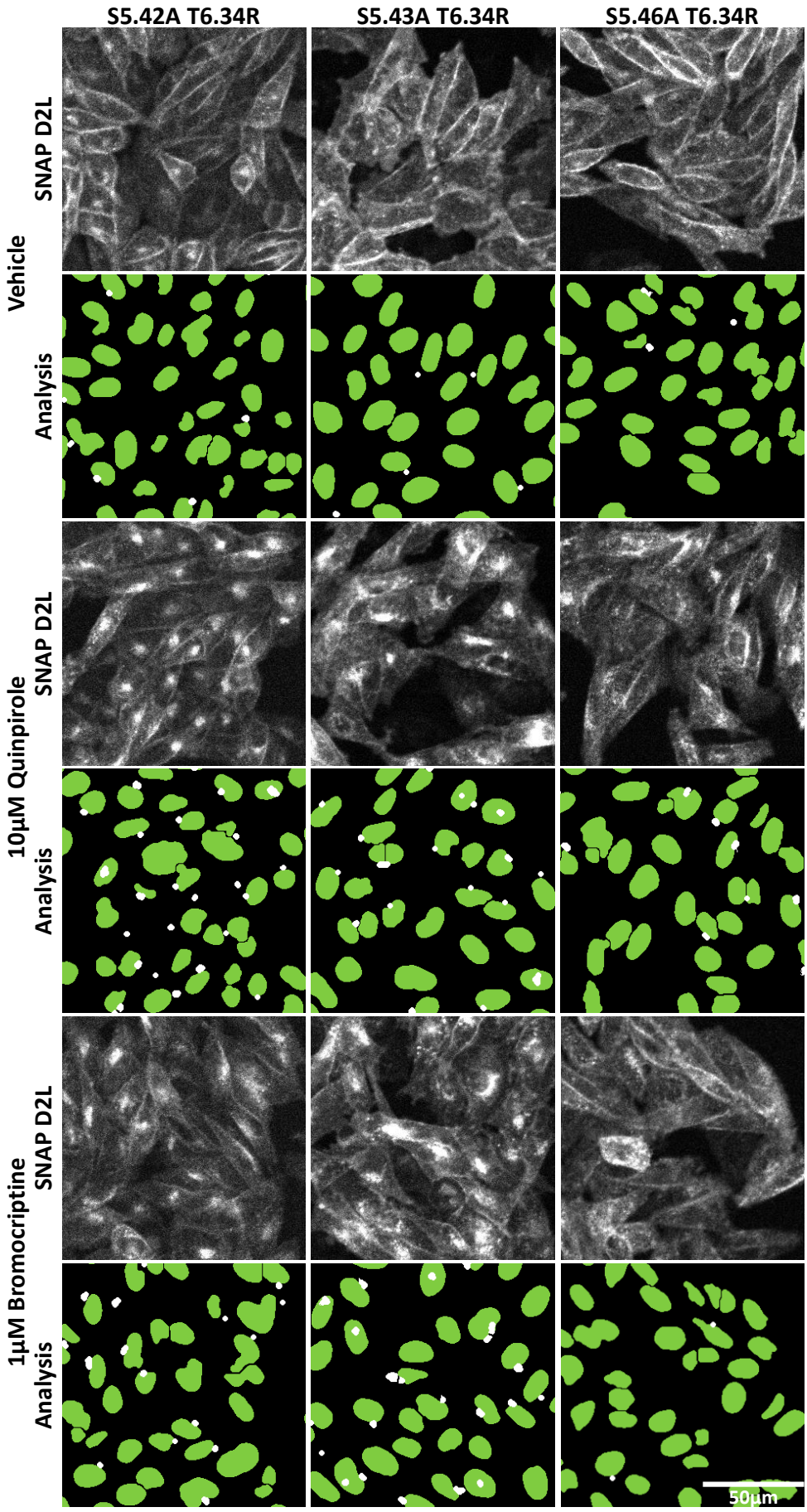

S5.42A T6.34R
S5.43A T6.34R
S5.46A T6.34R
Vehicle
SNAP D2L
Analysis
10µM Quinpirole
SNAP D2L
Analysis
1µM Bromocriptine
SNAP D2L
Analysis
50µm

Figure 4.18: Internalisation of the SNAP-tagged D2L T6.34R S5.42A, S5.43A and S5.46A in response to ligand stimulation

Cells were SNAP-labelled for 30min then treated with increasing concentrations of ligands for 1h prior to fixation. Representative images show cells treated with vehicle, 10µM quinpirole and 1µM bromocriptine. For clarity, the images above were cropped to 120µm x 120µm from the original 400µm x 400µm image used for analysis. The panels show the SNAP-tagged receptor with the associated granularity analysis below, with nuclei in green and receptor containing granules of 6-10µm diameter in white. The internalisation of 4 representative dopamine ligands was determined and quantified in **Figure 4.19**.

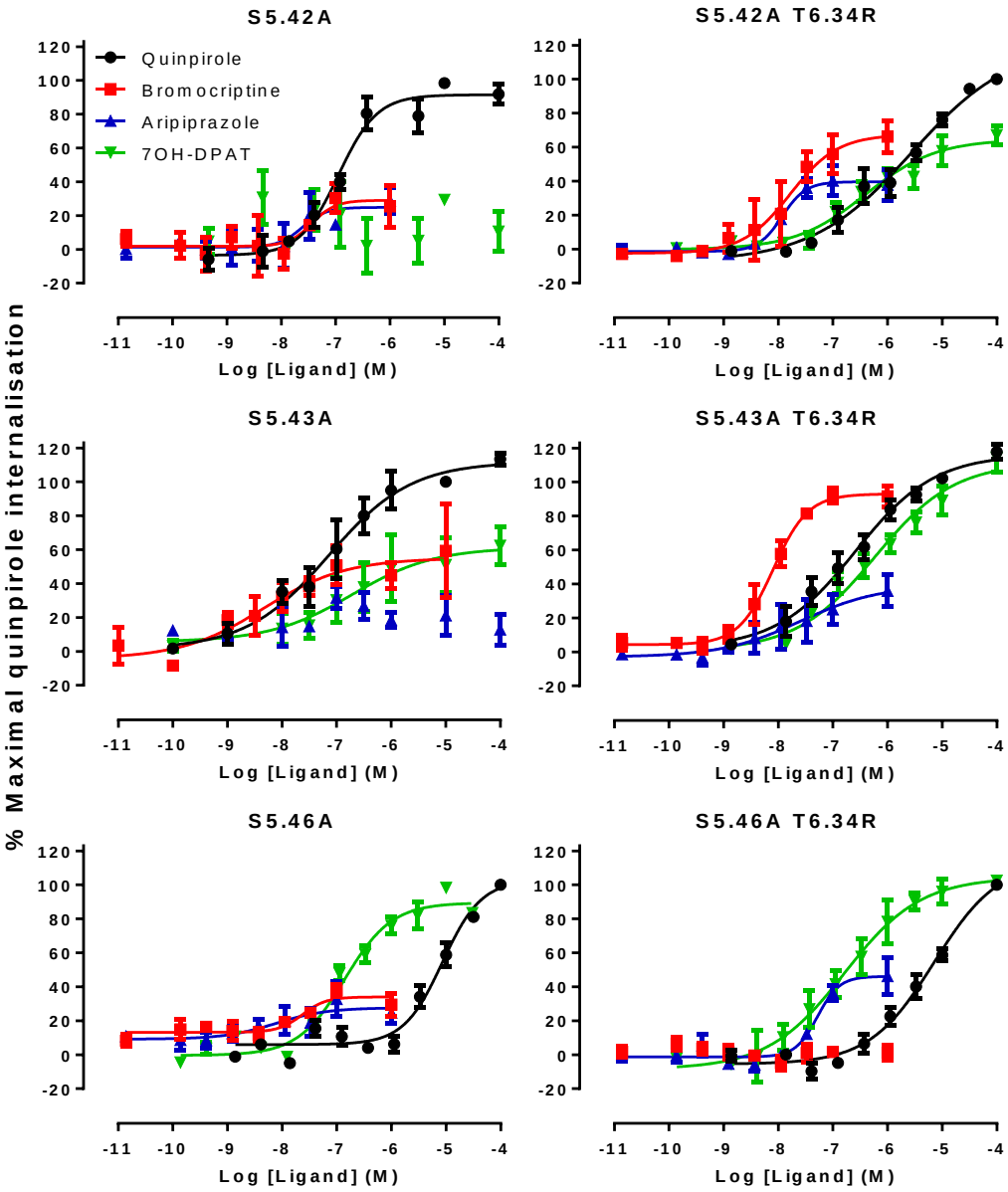


Figure 4.19: Quantification of agonist promoted internalisation of the serine mutant receptors

Cells were SNAP-labelled for 30min before treatment with increasing concentrations of ligand of 1h and fixation. Internalisation was quantified by an automated granularity algorithm as previously described (see example images in **Figure 4.17, Figure 4.18**). Data points represent pooled data (mean ± SEM, unless n=2 where mean ± range) of 2-6 independent experiments performed in duplicate or triplicate, normalised to vehicle (0%) and 10µM quinpirole (100%) controls, except S5.42A T6.34R, S5.46A and S5.46A T6.34R experiments where 100% represents 100µM quinpirole response.

Ligand	Cell line	Wild Type			T6.34R		
		R_{max}	pEC_{50}	N	R_{max}	pEC_{50}	N
Quinpirole	**WT**	107.3 ± 5.0	6.51 ± 0.18	4	119.6 ± 6.0	6.84 ± 0.39	4
	S5.42A	94.3 ± 2.4	6.91 ± 0.17	3	106.6 ± 1.2	5.77 ± 0.21*#	3
	S5.43A	106.2 ± 3.7	7.09 ± 0.33	3	114.4 ± 4.6	6.40 ± 0.29	4
	S5.46A	109.1 ± 4.9	4.99 ± 0.11*	4	110.0 ± 6.0	5.22 ± 0.12*	4
Bromocriptine	**WT**	43.5 ± 9.6	8.65 ± 0.07	4	117.8 ± 8.6	7.11 ± 0.11	4
	S5.42A	40.1 ± 3.5 (43.6, 36.6)	7.41 ± 0.10 (7.31, 7.51)	2	69.7 ± 1.5*#	7.76 ± 0.51	3
	S5.43A	55.2 ± 16.9	8.31 ± 0.41	3	88.8 ± 7.0*	7.87 ± 0.27*	4
	S5.46A	36.4 ± 5.0	7.70 ± 0.02*	3	NE	NE	4
Aripiprazole	**WT**	NE	NE	4	48.7 ± 9.4	7.22 ± 0.29	4
	S5.42A	21.3 ±10.0	7.21 ± 0.31	3	41.5 ± 8.4	8.01 ± 0.13	3
	S5.43A	NE	NE	3	46.1 ± 10.2	7.39 ± 0.43	4
	S5.46A	28.9 ± 10.8	8.20 ± 0.50	3	53.5 ± 10.5	7.17 ± 0.15	4
7OH-DPAT	**WT**	108.1 ± 3.7	6.96 ± 0.17	4	118.4 ± 6.4	8.10 ± 0.26	4
	S5.42A	NE	NE	2	66.5 ± 7.4*	6.37 ± 0.14*	4
	S5.43A	61.8 ± 9.5*	6.37 ± 0.79	3	111.3 ± 8.2#	6.16 ± 0.10*	6
	S5.46A	92.6 ± 7.3	6.78 ± 0.16	3	104.2 ± 8.0	6.74 ± 0.20*	4

Table 4.12: Summary of maximal responses and pEC_{50}s from internalisation assays in all cell lines

Data were derived from ligand concentration response curves in **Figure 4.19**. Data are pooled (mean ± SEM, unless n=2 where mean ± range) of 2-6 independent experiments performed in duplicate or triplicate, with R_{max} expressed as a percentage of 10µM quinpirole response except for S5.42A T6.34R, S5.46A and S5.46A T6.34R cell lines where R_{max} is expressed as a percentage of 100µM quinpirole response. NE = no effect; *P<0.05 compared to corresponding WT/T6.34R R_{max} and pEC_{50}; #P<0.05 compared to Wild Type responses (Student's unpaired t-test).

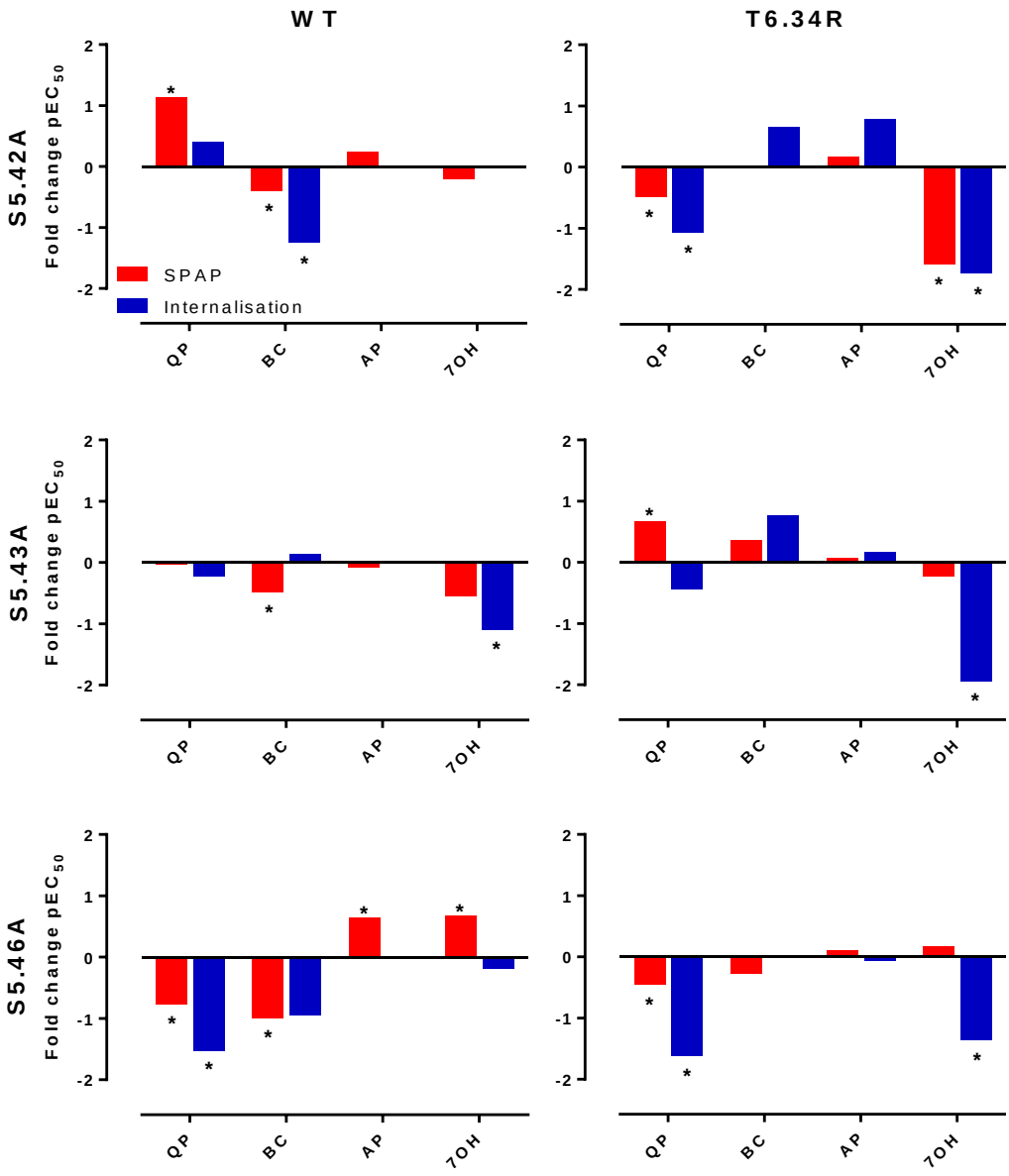


Figure 4.20: Comparison of potency changes following serine mutations in CRE-SPAP reporter gene and receptor internalisation assays

Summary of the fold change in pEC_{50} (calculated as pEC_{50} mutant – pEC_{50} WT/ T6.34R) from CRE-SPAP reporter gene (red) and receptor internalisation (blue) assay data. *P<0.05 cf WT/T6.34R, Student's unpaired t-test. QP = quinpirole; BC = bromocriptine; AP = aripiprazole; 7OH = 7OH-DPAT.

4.3 Discussion

As previous data with the CHOcs ssD2L cell line showed little evidence for the necessary constitutive activity required for application of the Slack and Hall operational model, site-directed mutagenesis was conducted in an attempt to create a constitutively active receptor. Three mutations were examined, an ionic lock mutation (E6.30A) and two mutants of the BBXXB motif, T6.34K and T6.34R. Initial studies revealed that both the E6.30A and T6.34K mutants were poorly expressed, displayed significant constitutive internalisation and limited agonist responses. However, following T6.34R mutation, the receptor was cell surface expressed and localised to the plasma membrane, and had robust agonist responses in functional assays. Furthermore, literature reports demonstrated that T6.34R mutation in the D2S receptor generated a receptor displaying evidence of constitutive activity including increased ability to detect inverse agonism and increased agonist affinity (Wilson *et al.*, 2001). Thus, this mutation was further profiled, with evidence for increased agonist responses and potencies in functional assays. However, this mutation appeared to have opposing effects on the functional responses of the ergo-derived compounds. As such, site directed mutagenesis of receptor binding site TM5 serine residues was conducted to further explore the mode of ligand binding in both WT and T6.34R receptor backgrounds.

4.3.1 Profiling the behaviour of the T6.34R mutation: ligand binding

In order to profile the effects of T6.34R mutation on ligand responses at the dopamine D2L receptor, radioligand binding, CRE-SPAP reporter gene and receptor internalisation assays were conducted. If T6.34R mutation generates a CAM receptor, it is expected that receptor more readily adopts the active R* state, as described by the two-state model (**1.7.3**). This should lead to increased agonist affinities, or the proportion of high affinity binding (representative of the G protein bound state (Strange, 2008)), or both. In functional assays, CAM receptors should increase agonist potencies and maximal responses. The ability to detect this is however dependent on the

receptor reserve of the assay and the intrinsic efficacy of the ligand. Finally, CAM receptors are expected to display increased levels of receptor constitutive activity resulting in an increased ability to detect inverse agonism (Seifert *et al.*, 2002).

Unlike the previous study (Wilson *et al.*, 2001), most agonists had generally no change in affinity but increased the number of high affinity binding sites, consistent with the behaviour of an activating mutation. In contrast, there was a loss of high affinity binding for both RNPA and (+)-3-PPP following the T6.34R mutation which suggests these compounds may have reduced ability to couple to G protein at this receptor. However, both of these compounds maintained responses in both the receptor internalisation and CRE-SPAP reporter gene assays suggesting G protein coupling is not affected. Alternatively, it might be that these compounds are stabilising a conformation similar to the active state of the receptor (as has been suggested for bromocriptine at the WT receptor (Gardner *et al.*, 1997; Roberts *et al.*, 2004)). This also may indicate specific differences in the mode of binding of the enantiomers of 3-PPP (discussed further in **4.3.6**) as (-)-3-PPP maintains two-site binding following T6.34R mutation.

Despite significant decreases in potency in functional responses for the ergo-derived compounds, only bromocriptine had a significant reduction in affinity at the T6.34R receptor (3.1-fold; **Table 4.1**). However, both cabergoline and dihydroergocristine failed to increase in affinity despite increased high affinity binding for most other agonists, most of which display two-site binding. This may provide an explanation for the significant reductions in potencies for the ergo-derived compounds despite increases in maximal response.

4.3.2 The pharmacology of the T6.34R mutant receptor is broadly consistent with constitutive activation

When a panel of ligands were examined for their ability to inhibit forskolin-stimulated SPAP production, all agonists were now full agonists relative to a maximal quinpirole response (**Figure 4.7**). Potencies for a number of ligands

also increased with the mutation, despite the reduced receptor expression of D2L T6.34R compared to WT. Furthermore, when receptor internalisation was investigated, there was a significant increase in the ability of ligands to internalise the receptor (**Figure 4.9**). The markedly reduced receptor reserve in this assay revealed much more pronounced potency and maximal response changes compared with the CRE-SPAP reporter gene assay. This is because, in this more poorly coupled assay, the system is not limiting agonist responses (Stott *et al.*, 2016) thus providing a better platform for the mutation to reveal its effects. Following T6.34R mutation, even very low efficacy agonists such as aripiprazole and (-)-3-PPP can induce receptor internalisation, which is not detectable in WT. This behaviour is consistent with a CAM receptor that is more readily adopting the active state.

However in the CRE-SPAP reporter gene assay, the ergo-derived compounds, bromocriptine, dihydroergocristine and cabergoline, demonstrated decreased potency compared to WT. Furthermore, in the receptor internalisation assay, bromocriptine potencies significantly decreased (34.7-fold) despite an increased maximal response. In contrast to the other agonists, this behaviour is not consistent with the proposed CAM receptor. These selective effects on potency, especially for bromocriptine, suggest this mutation is having effects other than to promote a common single receptor active state. It is possible that T6.34R is stabilising an alternative active conformation to WT receptor whereby the binding of ergo-derived compounds is not favoured. In the previous report of this mutation in the D2S receptor, bromocriptine, unlike the other agonists examined (dopamine, NPA, *m*-tyramine and β-phenylethylamine), did not show increased affinity or potency in cAMP accumulation assays (Wilson *et al.*, 2001). It has been previously suggested that bromocriptine stabilises the receptor in a conformation close to the active state due its consistently observed single site binding profile (Gardner *et al.*, 1997; Roberts *et al.*, 2004). However, it appears more likely that bromocriptine, and potentially the other ergo-derived compounds, stabilise a different active conformation from other agonists. These compounds may

have different interactions with the receptor (discussed further in **4.3.9**), stabilising distinct receptor conformations, which results in the ligand-specific effects of T6.34R mutation.

One compound which appeared to lose efficacy following this mutation was haloperidol, which could no longer induce receptor internalisation. While this may be due to the reduced receptor expression level making it more difficult to detect haloperidol-induced receptor internalisation, it may also be due to the structure of haloperidol not favouring the T6.34R receptor conformation. While there were no differences between functional and radioligand binding derived affinities in the WT receptor for haloperidol, the functional pK_D measured from internalisation assays was 6.3-fold increased relative to the pK_i in the T6.34R receptor. Furthermore, there were opposing effects of T6.34R mutation on [^{3}H]-spiperone binding (decreased relative to WT) and receptor internalisation (increased) (**Table 4.5**). As discussed in **3.3.6**, the main difference between these assays is the buffer chosen and the requirement for sodium when measuring whole cell responses. These changes may reflect an altered sensitivity of haloperidol to sodium following T6.34R mutation. Wilson *et al* (2001) reported enhanced sensitivity of dopamine binding to sodium following T6.34R mutation in the D2S receptor (Wilson *et al.*, 2001). As discussed further in **5.3.2**, the removal of buffer sodium generates a receptor which more readily adopts the active state (Lin *et al.*, 2006). Molecular dynamic simulations suggest that sodium moves through the TM bundle, interacting initially with the orthosteric binding site before reaching its own binding site deep in the bundle, mediated by D2.50. This binding triggers the rotation of the so-called 'toggle switch' W6.48 to lock the receptor in its inactive state (Selent *et al.*, 2010). It is possible that the T6.34R receptor conformation may alter the binding of sodium to the receptor, leading differential sensitivities of ligands to sodium binding.

4.3.3 No evidence for inverse agonism in D2L T6.34R: differences in constitutive activity between dopamine D2 receptor isoforms

Thus far, there is little evidence for receptor constitutive activity of the dopamine D2L T6.34R receptor; there was no potentiation of forskolin-stimulated SPAP production with any of the reported inverse agonists and no constitutive receptor internalisation. This is in contrast to the earlier report with the dopamine D2S T6.34R receptor in which the detection of inverse agonists in cAMP accumulation assays was observed (Wilson *et al.*, 2001). This highlights potential differences in the level of basal signalling between the splice variants, which was further highlighted in future experiments that demonstrated that the D2S receptor, but not the D2L, was constitutively active in [^{35}S]-GTPγS binding experiments (**5.2.2**). As such, it is also possible that there are receptor specific effects of the corresponding T6.34R mutations. As described in **4.1.1**, the location of the mutation probably facilitates G protein coupling by causing conformational changes within GPCR and specifically the cytoplasmic half of TM6, the outward movement of which is thought to be key to G protein binding (Kling *et al.*, 2013; Kling *et al.*, 2014; Rasmussen *et al.*, 2011a). The location of the deletion in D2S (ICL3, highlighted in **Figure 4.2**) is also thought to be involved in G protein binding to the D2 receptor (Kling *et al.*, 2014). It is possible that TM6 conformational changes induced by the T6.34R mutation have distinct effects on the splice variants because the increased length of ICL3 in the D2L receptor causes distinct differences in the available receptor conformations, altering the ability of the G protein to bind.

Furthermore, it is possible that long-term adaptations in stably expressing cell lines could be preventing the detection of receptor constitutive activity. CAM receptors are often poorly expressed at the cell surface due to the conformational instability induced by mutations and down regulation of the receptors due to increased basal signalling (Alewijnse *et al.*, 2000; Li *et al.*, 2001). This was observed with the T6.34K and E6.30A D2L mutants previously

investigated (data not shown). While the T6.34R receptor was expressed at significantly lower levels than the WT receptor, imaging demonstrates it is localised to the cell surface. Future experiments would confirm the lack of constitutive activity at this receptor using [^{35}S]-GTPγS binding assays (**5.2.2**) which suggests the low expressing cell line makes it more difficult to detect constitutive activity due to the lower number of receptors in the R* state. However, it would be interesting to examine whether long term treatment with inverse agonists would increase the cell surface expression of the D2L T6.34R receptor as has been described for mutated histamine H_2 and μ-opioid receptors (Alewijnse *et al.*, 2000; Huang *et al.*, 2001; Li *et al.*, 2001).

4.3.4 Investigation of the ligand-specific effects of T6.34R mutations: contribution of TM5 serine residues to agonist responses

As discussed previously, the behaviour of the ergo-derived compounds, particularly bromocriptine, following T6.34R mutation is difficult to reconcile with a simple two-state model. These ligand-specific effects on functional potencies suggests there are fundamental differences in the binding of these compounds to the D2L receptor and the receptor conformations adopted. It is proposed that bromocriptine (and possibly the other ergo-derived compounds) adopt a distinct active state with a lower ability to couple to signalling pathways, as observed by its partial agonism in low receptor reserve assays at the WT receptor and its single-site binding profile (**3.2**) (Gardner *et al.*, 1998; Gardner *et al.*, 1997). This conformation appears distinct from other partial agonists, such as aripiprazole and (-)-3-PPP, which have low efficacy due a decreased ability to shift the receptor equilibrium to the R* state. T6.34R mutation increases the ability of the D2L receptor to adopt the active state, which corresponds well with the increased relative maximal responses and potencies observed for most agonists. However, this mutation restricts the ability of the receptor to adopt the active state conformation adopted by bromocriptine, altering the binding mode of the compound perhaps to that of traditional agonists such as dopamine. This

results in increased maximal responses, consistent with the CAM receptor, but reduces potencies and affinities. If true, this would imply that the ergo-derived compounds have a different dependence on D2L binding site residues compared with other agonists, which will be altered in the T6.34R receptor. We aimed to explore this hypothesis by investigating ligand interactions with three key TM5 binding site serine residues, S5.42, S5.43 and S5.46.

As has been previously described (**4.1.3**), these residues are thought to be vital to ligand binding at dopamine D2 receptor and may influence the subsequent receptor activation (Fowler *et al.*, 2012; Kling *et al.*, 2014). Furthermore, ligands have previously been shown to have differential dependence on these residues for binding and functional responses (Coley *et al.*, 2000; Fowler *et al.*, 2012; Wiens *et al.*, 1998). These serine residues were mutated to alanine in both WT and T6.34R receptors to investigate whether there were differences in ligand responses between the receptors following removal of potential hydrogen bond interactions. Ligands were initially screened for their activity in the CRE-SPAP reporter gene assay, which highlighted some distinct differences between ligand classes on the dependency of serine residues for functional responses. Subsequently, a subset of ligands were investigated in receptor internalisation assays. This low receptor reserve assay is particularly useful in highlighting ligand specific differences in responses following serine mutations.

Along with examining the functionality of the mutated receptors, it was important to know that the receptors were reaching the cell surface. None of the published data on these mutants thus far confirms the receptor cell surface expression despite evidence that mutations can impair GPCR export to the cell surface due to improper folding or by preventing necessary post-translational modifications (Dong *et al.*, 2007). The use of a cell impermeant SNAP-fluorophore allows selective labelling of cell surface receptors, confirming that these mutant receptors were indeed well expressed at the cell surface (**Figure 4.17** and **Figure 4.18**).

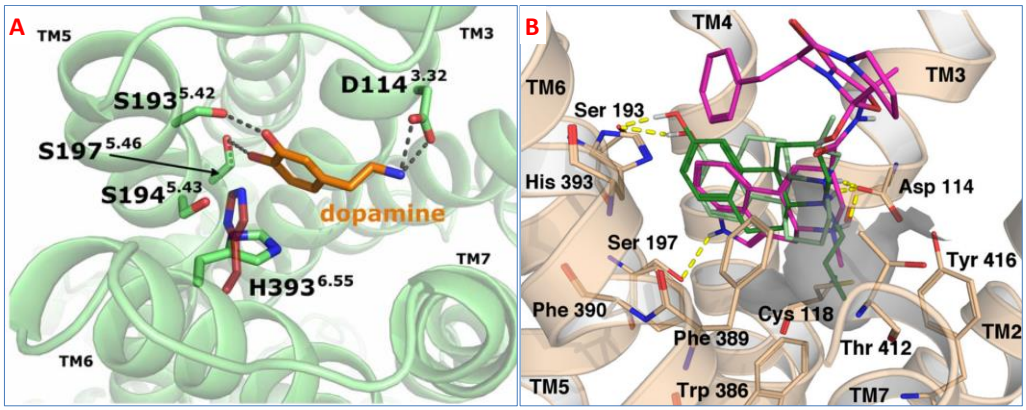


Figure 4.21: Modelling of the dopamine D2 receptor binding site with selected agonists

Examples of modelling studies with dopamine (A) and ergotamine (B, magenta) docked into the D2 receptor binding site from the literature. As described in **4.1.2** and **4.1.3**, dopamine binding is mediated by hydrogen bond interactions with TM5 serine residues S5.42 and S5.46 and with the highly conserved aspartic acid 3.32 (A). Figure B models the binding of ergotamine (magenta), structurally related to bromocriptine and dihydroergocristine, to the D2 receptor binding site. In contrast to dopamine, ergotamine is shown to bind deeper in the binding pocket, engaging preferentially with S5.46 (Ser 197).

Figure derived from (Kling *et al.*, 2013) (A) and (Krogsgaard-Larsen *et al.*, 2014) (B)

4.3.5 Catechol receptor agonists are particularly dependent on S5.42 and S5.46 for CRE-SPAP reporter gene assay responses

The catechol containing agonists, dopamine, apomorphine and RNPA, contain two hydroxyl groups for potential hydrogen bond interactions with the receptor (**Figure 4.3, Figure 4.21**). Modelling studies have suggested that dopamine binding to the dopamine D2 receptor is stabilised by a hydrogen bond network between the ligand and the receptor TM5 serine and H6.55 residues. Dopamine forms hydrogen bonds with S5.42 and S5.46 and may promote a receptor conformation that stabilises hydrogen bonding between S5.43 and H6.55 (Kalani *et al.*, 2004; Kling *et al.*, 2014). In agreement with previous studies (Fowler *et al.*, 2012; Wiens *et al.*, 1998), dopamine functional responses examined were sensitive to all serine point mutations. The most pronounced effects were following S5.42A and S5.46A where CRE-SPAP responses demonstrated a 162-fold drop in potency and were abolished in 1 of 2 experiments respectively (**Figure 4.13**). A similar trend of significant decreases in potencies and maximal responses was observed for apomorphine and RNPA. In comparison to other compounds, the catechols were particularly sensitive to these mutations (**Figure 4.16**). This supports the hypothesis that catechol agonists are dependent on direct hydrogen bond interactions with both S5.42 and S5.46 for stabilisation and activation of the ligand-receptor complex.

Contradictory reports have described a loss of dopamine-induced inhibition of cAMP production following either S5.43A (Wiens *et al.*, 1998) or S5.42A and S5.46A (Fowler *et al.*, 2012) mutations however the former report utilised the rat D2S receptor while the latter used the human D2L receptor, like here. The data presented here support the latter study by Fowler *et al* (2012) whereby dopamine functional responses, at least for cAMP inhibition at the human D2L receptor, are dependent on S5.42 and S5.46. It does highlight however that there might be distinct differences in ligand binding between rat and human dopamine D2 receptors, and/or between short and long isoforms of the

receptor. The rat and human D2L receptors share around 95% homology, with the rat receptor one amino acid shorter due to the absence of an isoleucine in ECL3 (Neve *et al.*, 1997). This suggests there are probably conformational differences between the rat and human dopamine receptors, which may result in different sensitivities to serine point mutations.

4.3.6 Opposing effects of serine mutations on single hydroxyl containing compounds in the CRE-SPAP reporter gene assay

In contrast to the catechols, 7OH-DPAT, (-)-3-PPP and (+)-3-PPP contain only a single hydroxyl group available for hydrogen bonding (**Figure 4.3**) which may be the cause of the more subtle effects of the serine mutations on these ligands. The enantiomers (-)-3-PPP and (+)-3-PPP were largely unaffected by serine mutations except for (-)-3-PPP, whose potency decreased 22.9-fold following S5.42A mutation (**Table 4.6**). There was also a reversal in the order of potency between the two enantiomers at the S5.42A mutation which was the only cell line where (+)-3-PPP had a higher potency than (-)-3-PPP. Together, this suggests that (-)-3-PPP binding is governed by S5.42 whereas (+)-3-PPP is less sensitive to serine hydrogen bond interactions. Differences in receptor binding has previously been demonstrated using the 2-dipropylaminotetralin series at the dopamine D2 receptor (Coley *et al.*, 2000; Payne *et al.*, 2002) supporting ligand-specific interactions with the binding site even for closely related stereoisomers.

The effects of serine mutations on 7OH-DPAT binding lend support to published results. While S5.43A mutation decreased potency 3.5-fold, S5.46A mutation increased 7OH-DPAT potency 4.7-fold compared to WT. The 7OH-DPAT used in this study is the racemate form; *R*-7OH-DPAT is the active enantiomer with increased functional responses and higher affinity than *S*-7OH-DPAT (Payne *et al.*, 2002). Mutagenesis and early modelling studies have indicated that *R*-7OH-DPAT binds S5.42 whereas the inactive *S*- enantiomer binds S5.46 (Coley *et al.*, 2000; Malmberg *et al.*, 1994). While there was little

effect of S5.42A mutation on 7OH-DPAT responses, the increase in potency observed with S5.46A mutation may indicate a reduced ability of the inactive enantiomer to bind, thus promoting binding of the active enantiomer.

4.3.7 Aripiprazole responses are enhanced by S5.42A or S5.46A mutations

Aripiprazole responses were modestly enhanced by S5.42A or S5.46A mutations, which may indicate an enhanced ability of this compound to bind and activate the receptor. Molecular dynamics simulations have suggested that aripiprazole does not engage in hydrogen bonding with any TM5 serines (Kling *et al.*, 2014) which is in agreement with mutagenesis studies with structurally similar antagonists, such as haloperidol, which are not effected by serine mutations (Coley *et al.*, 2000). This suggests that aripiprazole receptor activation might be enhanced by the loss of a binding site serine residue, perhaps by removing steric hindrances to receptor activation.

4.3.8 Quinpirole responses in the CRE-SPAP reporter gene assay are mostly dependent on S5.42 and S5.46

Structurally, quinpirole is similar to the ergo-derived compounds but has a tricyclic rather than tetracyclic pharmacophore (**Figure 4.3**). Previous mutagenesis studies have shown that at both the rat D2S and human D2L receptors, quinpirole affinity is reduced by all three serine mutations although in both cases, S5.43A mutation tended to have the greatest effects on both binding affinity and functional responses (Fowler *et al.*, 2012; Wiens *et al.*, 1998). This contrasts to the results here whereby there was no change in potency following S5.43A mutation. When the binding of quinpirole was modelled computationally, it was suggested that the aromatic (5 membered ring) nitrogen of quinpirole is too distant from the receptor serines to facilitate hydrogen bonding. Instead, the compound has hydrogen bond interactions with H6.55 and receptor activation is achieved through rotation of TM5 to relieve steric clashes between the ligand and receptor side chains (Fowler *et al.*, 2012). This is supported by data from the related dopamine D3

receptor, where serine mutations had no effect on quinpirole binding (Sartania *et al.*, 1999). However, the homology modelling was based on the inactive state crystal structures of the β2AR, dopamine D3 receptor and rhodopsin. As previously described (**1.4.2, 4.1.3**), receptor activation is associated with inward movement of TM5 which can promote hydrogen bond interactions between the ligand and receptor binding site serines (Dror *et al.*, 2011). Furthermore, agonist engagement of binding site serines is thought aid the contraction of the binding site and inward movement of TM5 (Sato *et al.*, 2015; Warne *et al.*, 2011). As such, inactive state receptor models may not generate a structure that best represents the agonist binding to an active receptor.

In contrast, the results obtained here suggest that quinpirole binding is influenced by receptor serine residues. Unlike S5.43A mutation, there were opposing effects on potency for S5.42A and S5.46A mutations; while S5.42A significantly increased potency, S5.46A significantly decreased potency. This suggests that S5.42A mutation has increased the ability of quinpirole to activate the receptor, perhaps by changing the receptor conformation such that hydrogen bonding interactions with the receptor (e.g. to S5.46) are facilitated by S5.42A mutation.

4.3.9 Effect of serine mutations on ergo-derived compounds in the CRE-SPAP reporter gene assay

Generally, there were opposing effects of the TM5 serine mutations on the ergo-derived compounds and as such, they could be further split into two groups – the larger peptide ergot alkaloids bromocriptine and dihydroergocristine and the smaller synthetic ergolines pergolide and cabergoline. Bromocriptine and dihydroergocristine, as described in **4.3.2**, showed significantly decreased potencies following T6.34R mutation, which was hypothesised to be due to a different mode of binding of these compounds. When the serine residues were mutated in the WT background, there were decreases in potency for bromocriptine with all mutations and

dihydroergocristine for S5.46A, which also decreased bromocriptine relative maximal response. Together, this indicates the importance of S5.46 for the binding of these two compounds, which corresponds well with recent molecular modelling studies. It has been suggested that ergotamine (structurally similar to both compounds) binds deeper in the dopamine D2 receptor binding pocket, forming hydrogen bonds preferentially with S5.46 (**Figure 4.21**) (Krogsgaard-Larsen *et al.*, 2014). Furthermore, earlier modelling studies had suggested that bromocriptine binds both S5.42 and S5.46 (Kalani *et al.*, 2004) which may be supported by the modest changes in potency with S5.42A.

In contrast, responses of the synthetic ergolines cabergoline and pergolide were largely enhanced by the serine mutations, with increases in potency for both compounds in all three cell lines. This suggests that these compounds bind in a different manner to the larger peptide alkaloid ergots and that interactions with TM5 serines are less important to their binding, like for aripiprazole (**4.3.7**). It is also possible however, as hypothesised for quinpirole, that the conformational changes induced by the serine mutations promote hydrogen bond interactions between the receptor and cabergoline and pergolide, thereby enhancing their binding.

4.3.10 Are the effects of serine mutations the same in T6.34R background?

One of the issues surrounding CAM receptors is whether the mutant receptor stabilises the same agonist activated state as the WT receptor. Using a substituted cysteine accessibility method in both WT and CAM β2ARs, it was shown that the CAM receptor had accessible cysteines in the binding site which were absent in the WT receptor. The authors traced this to a TM6 cysteine, suggesting rotation or tilting of this TM region in the CAM compared to WT receptors; however it unknown whether this receptor represents an alternative active conformation, or just a conformation which more readily adopts the active state (Javitch *et al.*, 1997).

If the CAM receptor stabilises the same agonist active receptor state then it would be expected that the dependence of specific serine mutations would be the same between the WT and T6.34R receptors. While this holds true for a number of compounds, a few notable exceptions suggest there may be distinct conformational differences between the WT and T6.34R receptors. Quinpirole potency was increased following S5.42A mutation however in the T6.34R background, S5.42A decreased quinpirole potency. These opposing effects of S5.42A mutation suggests distinct differences in the mode of quinpirole binding between the WT and T6.34R receptors. Furthermore, the effects of serine mutations on bromocriptine and dihydroergocristine were largely eliminated in the T6.34R background, with no significant changes in potency in the CRE-SPAP reporter gene assay. This suggests these two compounds are engaging differently with the T6.34R receptor binding site and that hydrogen bond interactions with TM5 serine residues may be less important in binding to this receptor.

The most surprising result of the serine mutations in the T6.34R background was the apparent inverse agonism of dopamine, (-)-3-PPP and (+)-3-PPP (**Figure 4.13**). While the inverse agonism of (-)-3-PPP and (+)-3-PPP was not consistently observed, this might be due to their lower efficacy than the endogenous ligand dopamine (**3.2**, (Gardner *et al.*, 1997; Jordan *et al.*, 2007)) which may lead to a decreased ability to detect their responses. The ability of these compounds to potentiate forskolin-stimulated SPAP production suggests they are promoting an inactive receptor conformation to reduce basal receptor signalling and alludes to distinct differences in their binding to WT and T6.34R receptors. However, the apparent constitutive activity of this mutant needs further experiments with inverse agonists such as (+)-butaclamol or haloperidol to determine whether this effect persists with more traditional inverse agonists.

It is also noted that for dopamine, RNPA and apomorphine, all of which require buffer ascorbic acid to prevent ligand oxidation, there was a basal inhibition of forskolin-stimulated SPAP production. This effect was specific to

the S5.42A mutations, as it was only observed in S5.42A T6.34R and to a lesser degree, with the single S5.42A mutation. This suggests that the ascorbic acid may itself be having an effect on forskolin-stimulated SPAP production but additional experiments would be required to further investigate the precise mechanism. While it is assumed that the presence of ascorbic acid prevents ligand oxidation, there has been a suggestion that ascorbic acid can bind extracellularly to aminergic receptors, potentiating agonist responses by either an allosteric mechanism or by blocking ligand dissociation from the receptor (Root-Bernstein *et al.*, 2014). Binding studies at both D1 and D2 receptors have shown that ascorbic acid can inhibit radioligand binding (Tolbert *et al.*, 1992) which, alongside other studies on β-adrenergic receptors, suggest that ascorbic acid may have a binding site on aminergic receptors in close proximity to the ligand binding site (Root-Bernstein *et al.*, 2014). It is therefore possible that the receptor conformation following S5.42A mutation may promote or alter ascorbic acid binding to the receptor thus transforming this usually inert compound into an agonist. However, more experiments would be required to investigate this and to probe a potential ascorbic acid binding site.

4.3.11 Assessment of receptor internalisation: is there evidence for pathway-selective effects of serine mutations?

It has been previously proposed that specific serine interactions may govern downstream dopamine D2 receptor signalling (Fowler *et al.*, 2012; Wiens *et al.*, 1998). In an investigation of [^{3}H]-arachidonic acid release, MAPK phosphorylation and cAMP accumulation following S5.42A, S5.43A and S5.46A mutations of the dopamine D2L receptor, it was proposed that agonists can stabilise 2 distinct receptor conformations through hydrogen bond interactions with the TM5 serines. S5.43 was required to stabilise the receptor conformation which promotes [^{3}H]-arachidonic acid release while cAMP and MAPK responses were largely unaffected. However, S5.46 was required for stabilisation of both receptor states and thus mutation of S5.46 led to a loss of activity at all 3 pathways. The effects of S5.42A mutation were

ligand specific depending on the presence of hydrogen bond interactions between ligand and receptor. The exception was quinpirole, whose binding was not thought to be governed by hydrogen bond interactions and was largely insensitive to all serine mutations (Fowler *et al.*, 2012). In contrast, an earlier study with the rat D2S receptor proposed that dopamine and DHX induced inhibition of cAMP was dependent on S5.43 (Wiens *et al.*, 1998) although this may reflect conformational differences between rat D2S and human D2L receptors.

When a subset of ligands were examined in the receptor internalisation assay, the results largely supported the data from the CRE-SPAP reporter gene assay. The greatest effects on quinpirole and bromocriptine responses were observed with S5.42A and S5.46A mutations while 7OH-DPAT responses were more affected by S5.42A and S5.43A mutations (**Figure 4.19**, **Figure 4.20**). Furthermore, aripiprazole maximal responses were increased following S5.42A and S5.46A mutations. As expected by the reduced receptor reserve in the internalisation assay, the effects of the mutations were more pronounced in this assay; there were greater potency changes than the CRE-SPAP reporter gene assay (**Figure 4.20**) and more effects on agonist maximal responses. Furthermore, the receptor internalisation data supports the apparent constitutive activity of the S5.42A T6.34R receptor as there was reproducible constitutive internalisation in this cell line (**Figure 4.18**).

However, there were a few exceptions. Interestingly, receptor internalisation responses to bromocriptine were abolished in S5.46A T6.34R cell line, confirming that S5.46 might remain a key interaction for bromocriptine in the T6.34R receptor. This contrasts to the CRE-SPAP reporter gene assay results whereby there was no significant change in bromocriptine responses compared to WT. Likewise, S5.42A mutation had only modest effects on 7OH-DPAT responses in the CRE-SPAP reporter gene assay while abolishing receptor internalisation responses. While this may be due to the reduced receptor reserve in the internalisation assay, it may also highlight specific requirements of ligand-serine interactions in governing cellular responses.

This supported by the opposing effects of S5.43A mutation on quinpirole potencies in receptor internalisation and CRE-SPAP reporter gene assays for the T6.34R receptor (**Figure 4.20**). While this has previously been examined with respect to downstream signalling endpoints as described above (Fowler *et al.*, 2012; Wiens *et al.*, 1998), receptor internalisation has not been examined. Further experiments to increase the agonist data set may provide more information on this.

4.3.12 Study limitations and next steps

Thus far, the functionality of the mutant receptors has been explored in CRE-SPAP reporter gene and receptor internalisation assays. This has provided measures of relative agonist efficacy through investigation of agonist maximal responses and potency measurements. However it would be very useful to conduct [^{3}H]-spiperone saturation and competition binding experiments to generate receptor expression levels and agonist affinities respectively. It is acknowledged that in the absence of receptor expression levels, agonist potency changes must be treated with care. As described in **1.8.1**, potency is a highly system dependent parameter which can be significantly affected by receptor expression levels and the point in the signalling cascade under measure (Stott *et al.*, 2016). It is possible that increases or decreases in potency may be due to increased or decreased receptor expression levels compared with WT receptors respectively. However, as observed in **4.2.8**, all mutant receptors were cell surface expressed and appear largely to be expressed at similar levels from the brightness of the SNAP-labelling. Furthermore, it would be useful to expand the ligand data set, both to include reported inverse agonists and to expand the agonists investigated in the receptor internalisation assays. Inclusion of inverse agonists would further explore the apparent constitutive activity of the S5.42A T6.34R double mutant.

4.4 Conclusions

In this chapter, we have explored a constitutively activating mutation of the dopamine D2L receptor. While there was little evidence of enhanced basal signalling corresponding to constitutive activity following T6.34R mutation, increases in agonist efficacy and potency in signalling assays supported the hypothesis that this mutation enhances the transition to an active receptor conformation. However, ligand specific effects of this mutation were observed, particularly for the ergo-derived compounds, which displayed decreased potencies despite increases in relative maximal response. It was hypothesised that ergo-derived compounds, such as bromocriptine, select different active conformations from other agonists, and that the T6.34R mutation promotes a subset of active conformations that have differential effects on the modes of binding for these compounds. This was further explored by mutagenesis of 3 key binding site TM5 serine residues in both WT and T6.34R backgrounds. In agreement with the literature, there were ligand specific effects of serine mutations, which suggests that ligands engage differentially with binding site serine residues – in particular the relative importance of S5.46 for bromocriptine agonist effects, compared to both S5.42 and S5.46 for catechol based ligands. We also obtained evidence of more general differences in ligand binding between WT and T6.34R receptors, suggesting that the T6.34R receptor conformation may be distinct from the active states of the WT receptor.

Chapter Five: Exploration of novel operational model approaches to assess dopamine D2 agonist efficacy through [^{35}S]-GTPγS binding assays

5.1 Introduction

In this chapter, we will consider the application of novel operational model approaches to analyse ligand functional data. These approaches are particularly amenable to the analysis of receptor-G protein coupling using [^{35}S]-GTPγS binding assays.

5.1.1 Measuring G protein activation with GTPγS binding assays

One of the key initial stages for signal transduction in GPCRs is the activation and subsequent dissociation of heterotrimeric G proteins, which can be measured through GTPγS binding assays (Harrison *et al.*, 2003; Strange, 2010). GTPγS binding assays rely on poorly hydrolysable forms of GTP, usually [^{35}S]-GTPγS or more recently, GTPγS labelled with Europium (Eu-GTPγS) for time-resolved fluorescence studies (Strange, 2010). As described in **1.4.4**, under normal cellular conditions, receptor activation promotes GDP release by initiating conformational changes within the G protein, which weakens GDP-G protein interactions. This allows GDP to escape upon the spontaneous separation of the Ras and helical domains (Dror *et al.*, 2015; Westfield *et al.*, 2011). The G protein is then free to bind GTP. Gα-GTP can dissociate from the receptor to modulate intracellular signalling pathways (Westfield *et al.*, 2011). GTPγS compounds can bind in place of GTP but the GTPase of the Gα subunit poorly hydrolyses the γ-thiophosphate bond present in GTPγS. As such, GTPγS-bound Gα subunits accumulate in membrane preparations, which allows the separation of bound from free GTPγS by filtration (Harrison *et al.*, 2003; Strange, 2010). For [^{35}S]-GTPγS, bound [^{35}S]-GTPγS can be detected and quantified by scintillation counting of samples to detect the retained radioactivity (Harrison *et al.*, 2003). Alternatively, Eu-GTPγS assays are performed in a similar manner to [^{35}S]-GTPγS, with bound Eu-GTPγS measured using a fluorescent plate reader (Labrecque *et al.*, 2009). While it has been shown to be amenable to the same assay conditions with similar experimental considerations as [^{35}S]-GTPγS-binding (such as Mg^{2+} and Na^{+} buffer concentrations (Labrecque *et al.*, 2009), discussed below), Eu-GTPγS

has a lower affinity for Gα than its radiolabelled counterpart (Koval *et al.*, 2010). This can lead to reduced ligand potencies when the two labels are compared under identical assay conditions (Engström *et al.*, 2004).

Generally, GTPγS binding assays are most widely used for $G\alpha_{i/o}$-coupled GPCRS. Mammalian cells tend to express these G proteins at much higher levels, with a greater basal guanine nucleotide exchange, than other families such as $G\alpha_s$ or $G\alpha_q$. As such, GTPγS binding assays with other G proteins tend to be significantly limited by a low signal:noise ratio (Milligan, 2003). G protein fusions whereby the GPCR is expressed as a fusion protein with the corresponding Gα subunit, in combination with co-immunoprecipitation to isolate the G proteins of interest, have offered improvements in this respect. This has allowed the detection of agonist-stimulated [^{35}S]-GTPγS binding in both $G\alpha_s$-coupled receptors such as the β_1-adrenoceptor and $G\alpha_{q/11}$-coupled receptors such as the α_{1B}-adrenoceptor (Carrillo *et al.*, 2002; McLean *et al.*, 2002). These G protein fusions also offer the opportunity to examine ligand induced receptor binding to individual G proteins (Gazi *et al.*, 2003; Lane *et al.*, 2007). This naturally requires the generation and transfection of fusion proteins whereas the high endogenous expression of $G\alpha_{i/o}$ G proteins allows the quantification of ligand induced GTPγS binding in native tissues (Odagaki *et al.*, 2006; Selley *et al.*, 1998; Selley *et al.*, 1997).

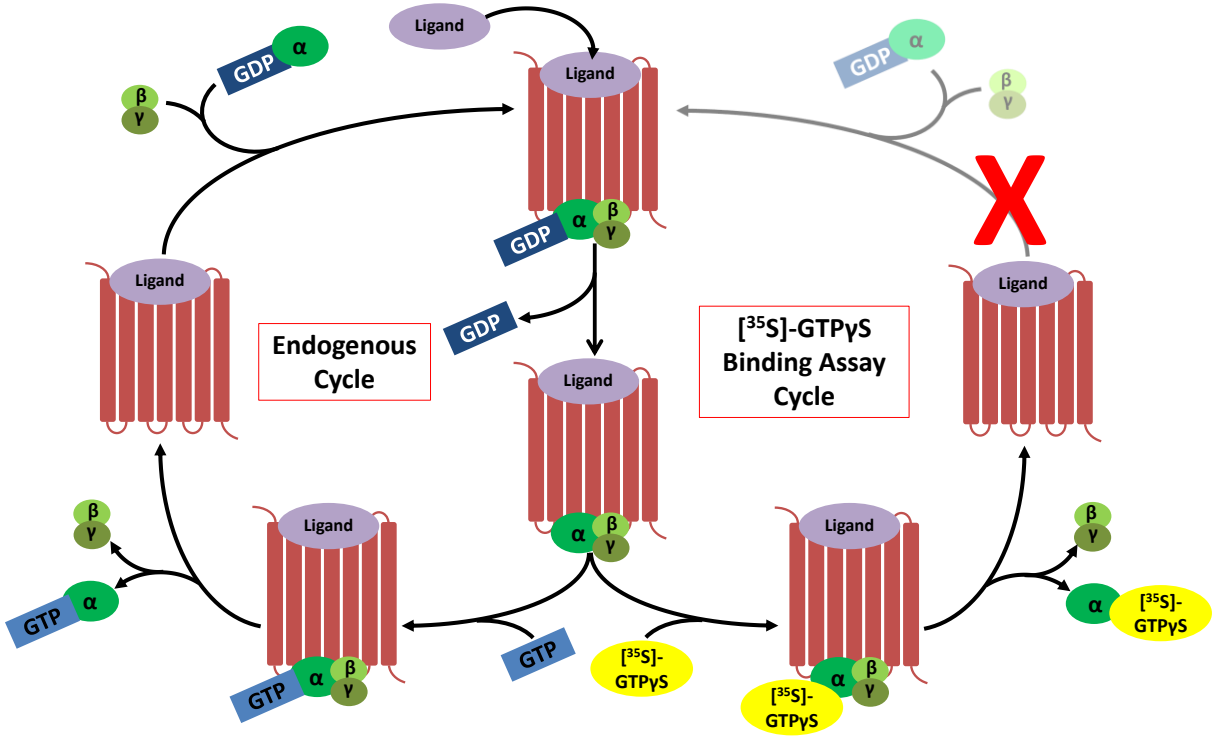


Figure 5.1: [^{35}S]-GTPγS binding assay

Ligand binding and receptor activation leads to GDP-GTP exchange and the subsequent dissociation of G protein subunits to regulate downstream signalling. Following this, the receptor-G protein complex is free to reform (endogenous cycle). However, in the presence of [^{35}S]-GTPγS, [^{35}S]-GTPγS can bind instead of GTP and because it is poorly hydrolysed, it remains bound to the G protein. Since the Gα subunit remains bound to the membrane, filtration and subsequent scintillation counting of samples can detect the retained radioactivity to measure [^{35}S]-GTPγS binding.

5.1.2 [^{35}S]-GTPγS binding assays: experimental considerations

Early studies employing [^{35}S]-GTPγS binding assays revealed the absolute requirement of Mg^{2+} ions in the buffer, the importance of GDP concentration and the effect of Na^{+} ions on the assay results (Hilf *et al.*, 1989). Mg^{2+} ions have a biphasic effect on [^{35}S]-GTPγS binding responses with optimal conditions usually around 5-10mM $MgCl_2$ (Harrison *et al.*, 2003; Hilf *et al.*, 1989; Szekeres *et al.*, 1997). While increasing concentrations of Mg^{2+} increase both basal and agonist stimulated [^{35}S]-GTPγS binding up to around 10mM $MgCl_2$, effects are much greater in the presence of agonist (Hilf *et al.*, 1989; Szekeres *et al.*, 1997). It has been shown for the M_2 muscarinic receptor, when expressed as an M_2-$G\alpha_{i1}$ fusion protein, that increasing the assay concentration of Mg^{2+} decreases the apparent affinity of GDP for the fusion protein, but only in the presence of agonist. As no effect was seen in the presence of antagonist, the authors suggest that Mg^{2+} is involved in the formation of the agonist-receptor-G protein complex either through competition of Mg^{2+} with GDP for G protein binding or that Mg^{2+} is necessary to facilitate $G\alpha_{i1}$ binding to the agonist-bound receptor (Zhang *et al.*, 2004). The crystal structure of $G\alpha_s$-GTPγS shows a Mg^{2+} ion present in the nucleotide binding pocket; the side chains which contact both GTPγS and coordinate Mg^{2+} are conserved between $G\alpha_S$ and $G\alpha_i$ suggesting the latter is more likely (Sunahara *et al.*, 1997).

Another important consideration in [^{35}S]-GTPγS binding assays is GDP concentration. As previously described, GDP competes with [^{35}S]-GTPγS for G protein binding and as such, significantly affects the assay window. At low GDP concentrations, basal [^{35}S]-GTPγS binding is high (Hilf *et al.*, 1989; McLoughlin *et al.*, 2000; Szekeres *et al.*, 1997). GDP stabilises the closed conformation of the G protein whereby the Ras and helical domains enclose GDP. Receptor activation induces conformational changes that promote GDP release by weakening GDP-G protein interactions and allowing it to escape upon spontaneous separation of the Ras and helical domains (Dror *et al.*,

2015). In this open conformation, either GDP or [^{35}S]-GTPγS can bind, however at lower GDP concentrations, there is an increased likelihood that [^{35}S]-GTPγS will bind instead. Upon [^{35}S]-GTPγS binding, it is assumed that the Ras and helical domains return to their original positions; the crystal structure of $G\alpha_s$ bound to GTPγS shows these domains enclosing the nucleotide similar to the GDP bound G protein in molecular dynamic simulations (Dror *et al.*, 2015; Sunahara *et al.*, 1997). This closed conformation is thought to be essential for the hydrolysis of GTP to GDP (Shnerb *et al.*, 2007). However, as previously described, GTPγS is poorly hydrolysed and as such, accumulates. Therefore at low GDP concentrations, there is high basal [^{35}S]-GTPγS binding. Increasing the concentration of GDP can increase the assay window by suppressing basal [^{35}S]-GTPγS binding such that agonist-stimulated responses are detectable, with decreased potency (McLoughlin *et al.*, 2000). However, when measuring inverse agonist activity, a level of basal activity is required. As such, increasing GDP concentrations reduces receptor constitutive activity and consequently reduces the detection of inverse agonist activity (McLoughlin *et al.*, 2000; Roberts *et al.*, 2005). At high GDP concentrations, the ability to detect inverse agonism is lost (Roberts *et al.*, 2005).

Similarly, the presence of buffer Na^+ can have distinct effects on both agonist and inverse agonist responses. Na^+ is a known allosteric modulator of a number of class A GPCRs including adenosine, adrenergic, dopamine and opioid receptors and is thought to be key to receptor activation. Mutagenesis studies across the GPCR superfamily pinpoint the highly conserved D2.50 as the residue vital to Na^+ binding (Costa *et al.*, 1990; Fenalti *et al.*, 2014; Katritch *et al.*, 2014; Massink *et al.*, 2015; Neve *et al.*, 1991). This has been further supported by a high resolution crystal structure of the adenosine A_{2A} receptor whereby the Na^+ binding site could be identified; Na^+ binding was shown to be modulated by D2.50, S3.39 and three water molecules involved in hydrogen bonding to several highly conserved residues (Liu *et al.*, 2012). Following receptor activation, the inward movement of TM7 collapses this pocket precluding Na^+ binding. The Na^+ binding site was also mapped in a

subsequent study detailing the crystallisation of the δ-opioid receptor, in which a larger hydrogen bonding network with additional water molecules and direct side chain contacts with Na^+ was observed (Fenalti *et al.*, 2014). In [^{35}S]-GTPγS binding assays, the presence of buffer Na^+ has been shown to decrease agonist potency and decrease relative efficacy of partial agonists but it also reduces basal binding, increasing the assay window for agonist responses (Hilf *et al.*, 1989; Selley *et al.*, 2000; Szekeres *et al.*, 1997). Furthermore, buffer Na^+ is a requirement to detect agonist responses in some receptor systems, such as the μ-opioid receptor expressed in CHO cells (Selley *et al.*, 2000). On the other hand, removing buffer Na^+, usually through replacement with NMDG, can reveal efficacy of weak partial agonists whose responses are undetectable in Na^+ containing buffer (Lin *et al.*, 2006). This substitution also allows the detection of inverse agonists by increasing receptor constitutive activity (Roberts *et al.*, 2004; Roberts *et al.*, 2005).

While [^{35}S]-GTPγS binding is thought to be pseudo-irreversible, it will dissociate from the receptor with a high concentration of competing unlabelled GTPγS in a number of systems (Alt *et al.*, 2002; Quirk *et al.*, 2007; Wenzel-Seifert *et al.*, 2000). Dissociation experiments with the dopamine D2 receptor have shown that the presence of high agonist concentrations can accelerate the dissociation of [^{35}S]-GTPγS. However, despite an excess of unlabelled GTPγS, agonists could not dissociate all of the bound [^{35}S]-GTPγS. This led the authors to propose that bound [^{35}S]-GTPγS exists in two species: bound to the agonist-receptor-G protein complex and bound to a dissociated Gα protein (Quirk *et al.*, 2007).

5.1.3 The use of [^{35}S]-GTPγS binding assays for operational modelling

The range of experimental manipulations discussed above allows the generation of a data set applicable to operational modelling without the need for irreversible antagonists, which are not available for every receptor. Moreover, there can be issues with irreversibility and specificity of irreversible

antagonists (discussed further in **3.3.7**); for example, phenoxybenzamine is a reported irreversible antagonist of a number of monoamine receptors including the dopamine D2 receptor and α_{2A}-adrenoceptor (Frang *et al.*, 2001; Hamblin *et al.*, 1982). This can make targeting only the receptor under investigation difficult. Instead of reducing the receptor concentration (R_T) through alkylation, the versatility of the [^{35}S]-GTPγS binding assay allows the manipulation of the system coupling efficiency (K_E) through varying assay GDP or Na^+ concentration, both of which can significantly alter both ligand induced [^{35}S]-GTPγS binding and receptor constitutive activity (**5.1.2**). This allows the generation of a ligand concentration response curve series with changing R_{max} and EC_{50} to which an operational model can be applied. By altering K_E rather than R_T, the data can be derived from the same membrane preparation, removing a potential source of variation between data sets. Furthermore, one of the key assumptions of the operational model is that a dynamic equilibrium between the ligand and receptor has been achieved (Black *et al.*, 1983; Black *et al.*, 1985; Stott *et al.*, 2016). While this is often difficult to achieve for a number of cellular assays (discussed further in **5.3.3**), the ligand pre-incubation step in [^{35}S]-GTPγS binding assays allows equilibrium to be reached prior to the addition of radioligand.

5.1.4 The Slack and Hall Operational Model

As described in **1.8**, quantification of ligand efficacy has historically proved difficult because system and ligand-dependent components are challenging to separate and define. While the Black and Leff operational model (Black *et al.*, 1983; Black *et al.*, 1985) (**1.8.3**) offers improved measures of relative ligand efficacy compared to traditional maximal response comparisons, its efficacy parameter τ is still fundamentally a system dependent parameter. Furthermore, as the model was derived before the recognition of GPCR constitutive activity (Costa *et al.*, 1989), it does not account for any basal receptor signalling in the absence of agonist. However, this agonist independent signalling offers an opportunity to further tease out ligand parameters, and this has been explored in the Slack and Hall modification of

the operational model (Slack *et al.*, 2012) (**2.8.8**). Constitutive activity allows the coupling efficiency of the system to be estimated in the absence of ligand and as such, allows the removal of the system dependent component of τ to allow estimation of intrinsic ligand efficacy (ε). This introduces the parameter χ (system coupling efficiency) which is now equal to the ratio of R_T and K_E. In principle, this model offers a measure of system independent ligand efficacy for the first time and can be used for both agonists and inverse agonists, whereby agonists have ε values greater than 1, and inverse agonists have ε values less than 1.

This model has so far been applied to compare affinities and intrinsic efficacies of CCL17 and CCL22 at the chemokine receptor CCR4 using both [^{35}S]-GTPγS binding assays and measurements of T cell F-actin content. In these assays, χ was modulated with either increasing GDP concentrations ([^{35}S]-GTPγS binding) or receptor expression levels (F-actin) (Slack *et al.*, 2012). More recently, it was applied to yeast biogrowth assay data from yeast expressing the human free fatty acid receptor 2 (FFA2) (Brown *et al.*, 2015). This reporter gene assay was designed such that GPCR activation is directly correlated with yeast growth, and this can be independently adjusted by altering the concentration of an inhibitor of histidine biosynthesis, 3-aminotriazole (3AT). It was found that the yeast displayed agonist-independent growth i.e. constitutive activity, which could be varied by modulating the concentration of 3AT thus generating a data set amenable to modelling. Agonist and inverse agonist data sets were globally analysed to derive affinities and intrinsic efficacies for a number of synthesised FFA2 ligands (Brown *et al.*, 2015).

The key challenge for this model to be successfully applied to functional data is to define receptor-dependent constitutive activity. There are a number of approaches by which to do this; in the original study, in order to account for receptor independent G protein coupling, the model was modified to include a second receptor species to account for non-receptor mediated [^{35}S]-GTPγS binding. The [^{35}S]-GTPγS agonist binding data was simultaneously analysed

with a GDP concentration response curve from non-transfected cells to account for the contribution of endogenously expressed receptors to the signal (Slack *et al.*, 2012). Another approach is to utilise inverse agonists (if available); inverse agonists should inhibit the receptor dependent constitutive activity to provide the model with the true basal for the system (Brown *et al.*, 2015). This does however assume that the inverse agonist is specific for the receptor under measure and is fully inhibiting constitutive activity.

5.1.5 The GDP-dependence Operational Model

The Slack and Hall operational model requires receptor constitutive activity, which can often be difficult to detect in several types of signalling assays, and to discriminate from other forms of basal receptor activation. In previous chapters, we obtained limited evidence for D2L receptor constitutive activity in both CRE-SPAP reporter gene and receptor internalisation assays, despite high receptor expression levels and the evidence in the literature for D2 receptor ligand inverse agonism (Hall *et al.*, 1997; Roberts *et al.*, 2004; Roberts *et al.*, 2005). As such, we aimed to explore the possibility of reducing the system dependence of the τ parameter in a non-constitutively active system through the analysis of [^{35}S]-GTPγS binding assays.

As previously described, generating agonist concentration response curves in the presence of multiple concentrations of GDP can generate a curve series amenable to operational modelling. To fit these data, we proposed a new model, which incorporates a term to account for the effect of GDP on the system, by including both the assay concentration of GDP and the apparent affinity of GDP for the agonist-receptor complex (K_{GDP}) as determined by a concurrently performed GDP concentration response curve (**2.8.9**). Ligand efficacy is denoted as τ_0, the τ value for the ligand in the absence of GDP. One of the disadvantages of the Black and Leff operational model is that it provides a different agonist τ value for every condition, generating large data tables. It would be predicted for each ligand under examination that the differences between τ values at each condition would be consistent. This

model accounts for these differences by using the data from the GDP concentration response curve to determine the system contribution of GDP to ligand responses and so calculate a global τ value for each ligand. While this model should reduce the system dependence of derived efficacy term, it cannot completely exclude the effect of receptor-G protein coupling. However, it is hoped that by estimating τ_0, ligand efficacy is determined for the G protein coupled, active state of the receptor. Rasmussen *et al* (2011) have suggested that the active state of the receptor is that which couples to and stabilises a nucleotide free G protein (Rasmussen *et al.*, 2011a). Furthermore, single particle electron microscopy studies have demonstrated that addition of guanine nucleotide uncouples the receptor from the G protein (Westfield *et al.*, 2011). Radioligand binding studies often show the presence of both high and low affinity states for agonist binding to GPCRs which can be reduced to a single, low affinity site upon addition of guanine nucleotide (Gardner *et al.*, 1998; Gardner *et al.*, 1997; Payne *et al.*, 2002). The high affinity state is thought to represent the GPCR coupled to G protein and the low affinity state, the uncoupled form of the receptor. It has been argued that for binding studies, high concentrations of added guanine nucleotide uncouple the receptor and as such, provide affinity estimates which are not contaminated by efficacy (Strange, 2008). Therefore, it could be argued that in the absence of guanine nucleotides, the receptor is likely to be coupled to G protein and that efficacy in this case, represents the ability of the ligand to induce the conformational changes necessary for adoption of the receptor active state.

5.1.6 Chapter Aims

The aim of this chapter is to explore the use of the novel GDP dependence and Slack and Hall operational models in the analysis of functional [^{35}S]-GTPγS responses at the dopamine D2 receptor, in comparison to the standard Black and Leff analysis. We will consider the conditions required for the successful application of each model, and the extent to which they succeed in providing parameters that reflect true agonist intrinsic efficacy.

5.2 Results

5.2.1 Optimisation of [^{35}S]-GTPγS Binding

The time course of [^{35}S]-GTPγS binding was examined in SNAP-tagged D2L, D2L T6.34R and D2S expressing cell membranes, using the CHO-K1 cell lines previously described in **3.2.1**, **4.2.1** (**Figure 5.2**). Membranes were incubated with vehicle or ligand for 1h prior to addition of [^{35}S]-GTPγS for increasing time points and filtration. The half time for binding for all vehicle treated membranes was 18-20.4min, with addition of 10μM quinpirole, 1μM bromocriptine or 10μM 7OH-DPAT not significantly altering the time course for any cell line (**Table 5.1**, $P<0.05$; One way ANOVA followed by Tukey's multiple comparisons test). In order to prevent saturation of the signal, a time point for assay termination by filtration was chosen, within the range over which the increase in [^{35}S]-GTPγS was linear. A 20min time point was chosen to maximise the signal window (**Figure 5.2, D**). The D2S receptor expressing cell line also displayed greater ligand induced [^{35}S]-GTPγS binding, with 10μM quinpirole increasing [^{35}S]-GTPγS binding by 206.9 ± 34.1% (compared to vehicle, 20 min), versus 152.1 ± 8.2% in the D2L and 122.7 ± 7.5% in the D2L T6.34R cell lines (n=3-4). The effect of altering ligand preincubation time was also briefly examined in CHO D2L membranes. Increasing the pre-incubation time to 2h had very little effect on ligand responses (**Figure 5.3**). As such, the 1h pre-incubation was maintained for further experiments.

Using the optimised assay times, the effect of altering buffer concentrations of NaCl and GDP on detecting agonist and inverse agonist responses was also investigated in preliminary studies using CHO D2L membranes (**Figure 5.4**). However for all concentrations of NaCl, there was no effect of either (+)-butaclamol or (-)-butaclamol inverse agonist treatment on D2L [^{35}S]-GTPγS binding. The maximum response to agonist (10μM quinpirole), relative to basal, was enhanced by increasing the concentration of NaCl. In general, increasing the concentration of GDP increased the assay window, with peak agonist responses obtained at 100μM GDP (50mM NaCl), 30μM GDP (100mM NaCl) and 10μM GDP (150mM NaCl).

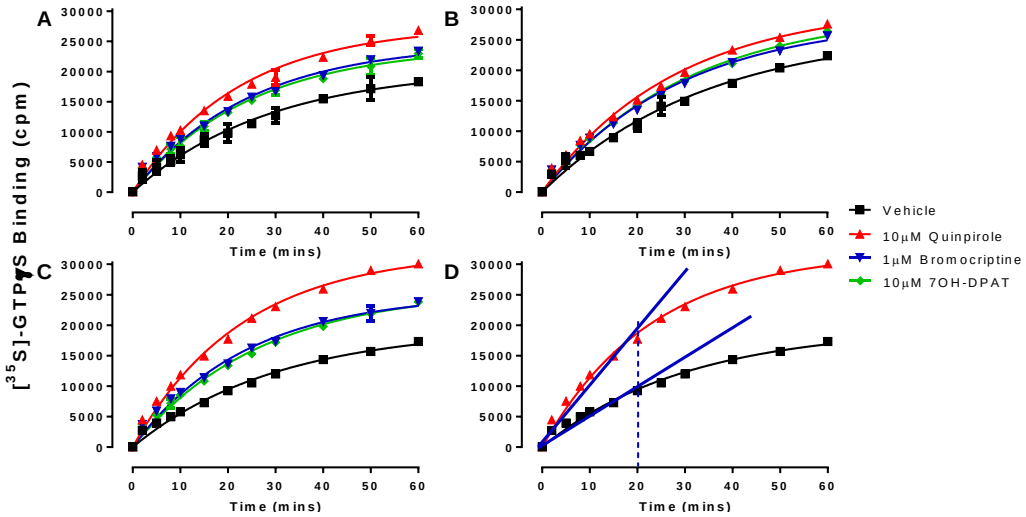


Figure 5.2: Time course of [^{35}S]-GTPγS binding in D2L, D2L T6.34R and D2S membranes

CHO D2L (**A**), D2L T6.34R (**B**) and D2S (**C, D**) membranes were incubated with 200pM [^{35}S]-GTPγS for increasing times following 1h incubation with either vehicle, 10μM quinpirole, 1μM bromocriptine or 10μM 7OH-DPAT before filtration. Time point for filtration was chosen (**D**) for being on the initial, linear part of the graph which has the greatest signal window. Data are from a single experiment (mean ± range) representative of 3-4 independent experiments performed in duplicate. Data were fit to a one-site association from which half times were determined and summarised in **Table 5.1** below.

Cell line	Vehicle	Quinpirole	Bromocriptine	7OH-DPAT
D2L	20.4 ± 4.3	17.2 ± 2.7	18.4 ± 3.0	19.1 ± 2.9
D2L T6.34R	18.2 ± 3.1	17.1 ± 1.2	18.8 ± 1.8	19.3 ± 1.7
D2S	18.0 ± 2.7	14.5 ± 0.9	16.2 ± 1.4	16.9 ± 1.2

Table 5.1: [^{35}S]-GTPγS binding half times in D2L, D2L T6.34R and D2S expressing membranes

Summary of the half times (in min) determined for each treatment in each cell line from the time courses shown in **Figure 5.2**. Data are pooled (mean ± SEM) of 3-4 independent experiments performed in duplicate.

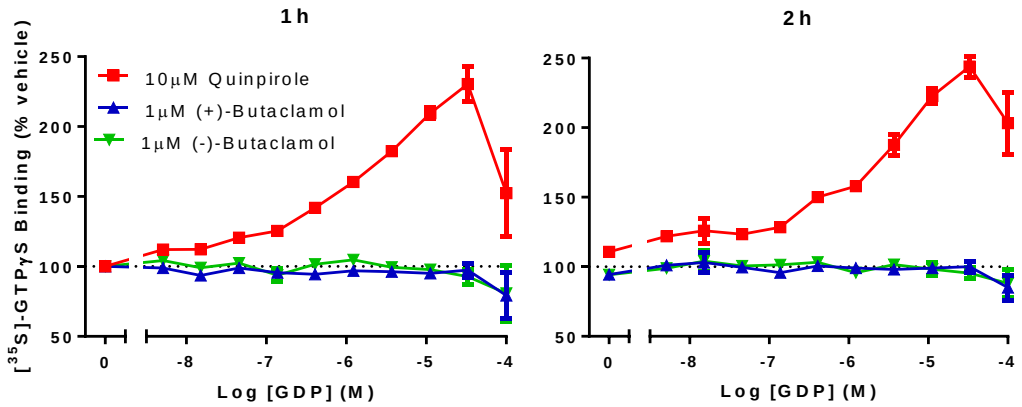


Figure 5.3: The effect of increasing ligand pre-incubation on [^{35}S]-GTPγS binding responses

CHO D2L membranes were pre-incubated with 10µM quinpirole, 1µM (+)-butaclamol or 1µM (-)-butaclamol for either 1h or 2h prior to addition of 200pM [^{35}S]-GTPγS for 20min and filtration. Data are from a single experiment (mean ± range) representative of 2 independent experiments performed in duplicate.

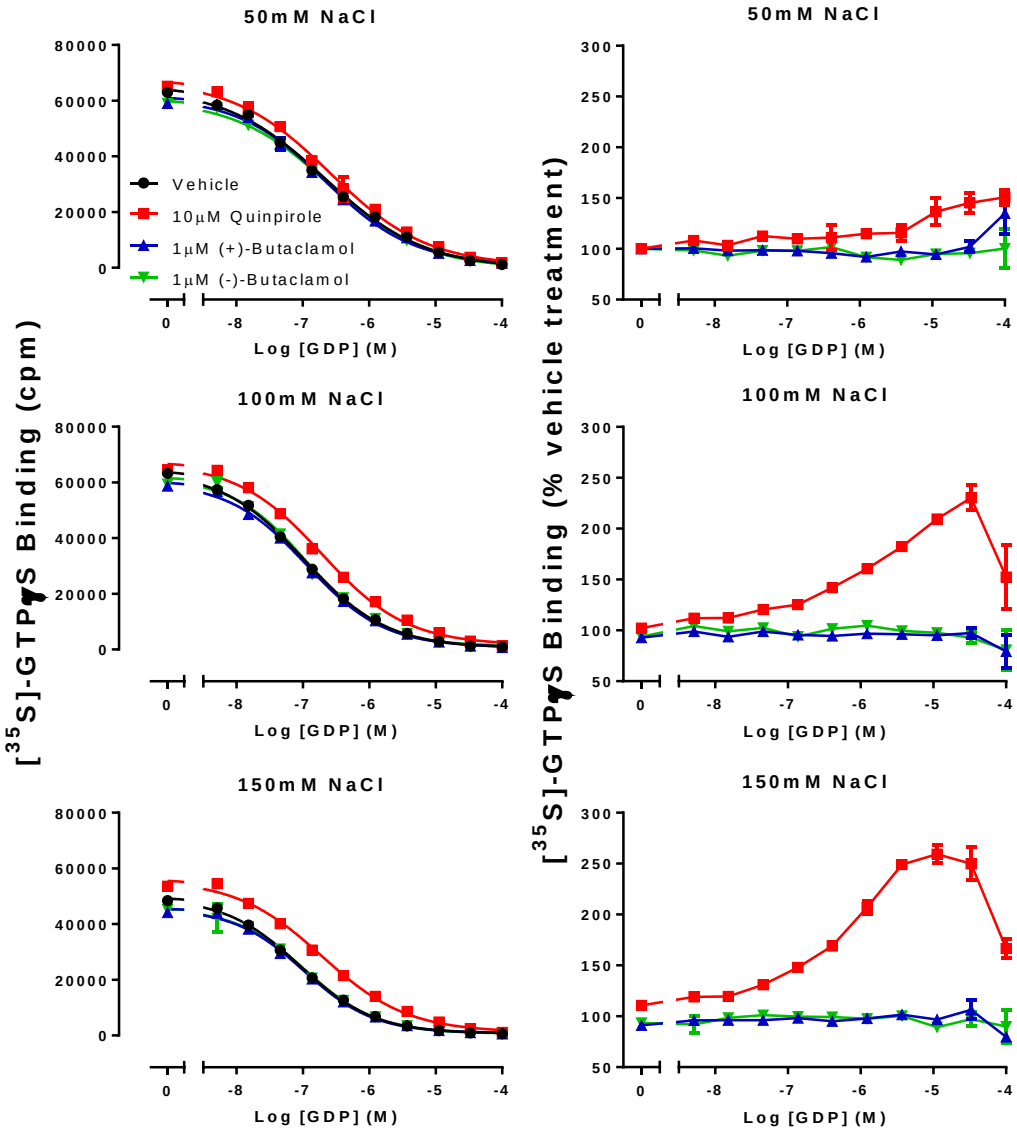


Figure 5.4: Effect of NaCl concentration on [^{35}S]-GTPγS binding in D2L membranes

Vehicle, 10µM quinpirole, 1µM (+)-butaclamol and 1µM (-)-butaclamol were incubated with increasing concentrations of GDP for 1h prior addition of 200pM [^{35}S]-GTPγS for 20min and filtration. The left hand panel shows the raw cpm data and the right hand panel, the normalised percentage change from vehicle treated membranes. Data are from a single experiment (mean ± range) representative of 3 independent experiments performed in duplicate.

5.2.2 Detecting constitutive activity at the D2 receptor

To allow fitting of the Slack and Hall operational model, a constitutively active system was required. This was not readily evident in preliminary data using the D2L line, even when varying the NaCl and GDP concentrations. For this reason, the most appropriate receptor for study was further investigated by attempting to detect the presence of constitutive activity in D2L, D2L T6.34R and D2S cell lines using a variety of reported inverse agonists – haloperidol, sulpiride, risperidone and (+)-butaclamol. Furthermore, the standard 100mM NaCl condition was compared with a buffer in which the NaCl was replaced by 100mM NMDG, both in the absence of GDP (**Figure 5.5**). In the NaCl buffer, there was no response to any ligands in any cell line over the concentration range examined. With NMDG buffer substitution, a modest inhibition by inverse agonists was detectable in D2L expressing membranes although responses were not consistently seen (2 of 4 experiments). There was no effect in D2L T6.34R membranes. However, there was a robust inhibition of basal [^{35}S]-GTPγS binding in D2S membranes in the NMDG buffer, with a rank order of potency of haloperidol = risperidone = (+)-butaclamol > sulpiride. All ligands induced the same maximum inhibition of basal activity (**Table 5.2**). From these data, it was concluded that receptor-dependent constitutive activity was most readily observed in D2S membranes in the absence of buffer Na^+. Therefore, D2S membranes were the focus for all subsequent experiments.

The effect of both agonist (10μM quinpirole) and inverse agonist (1μM (+)-butaclamol) treatment on basal [^{35}S]-GTPγS binding was examined in D2S membranes in both NaCl and NMDG containing buffers (**Figure 5.6**). There was a concentration dependent decrease in [^{35}S]-GTPγS binding with increasing GDP concentration, under both basal and ligand stimulated conditions. High GDP concentrations increased the signal to noise ratio for quinpirole-stimulated responses (**Figure 5.6, B**), though these became smaller when monitored as raw count changes over basal (**Figure 5.6, C**). There was no effect of (+)-butaclamol in the NaCl buffer, but this inverse agonist reduced

basal [^{35}S]-GTPγS binding at low GDP concentrations in NMDG buffer, providing further evidence of receptor constitutive activity. However, NMDG substitution decreased the signal window following agonist treatment. While (+)-butaclamol treatment had no effect on GDP pIC_{50}s, there were small but significant decreases in potency with 10μM quinpirole in both NaCl and NMDG buffers (1.8- and 3.3-fold respectively) (**Table 5.3**).

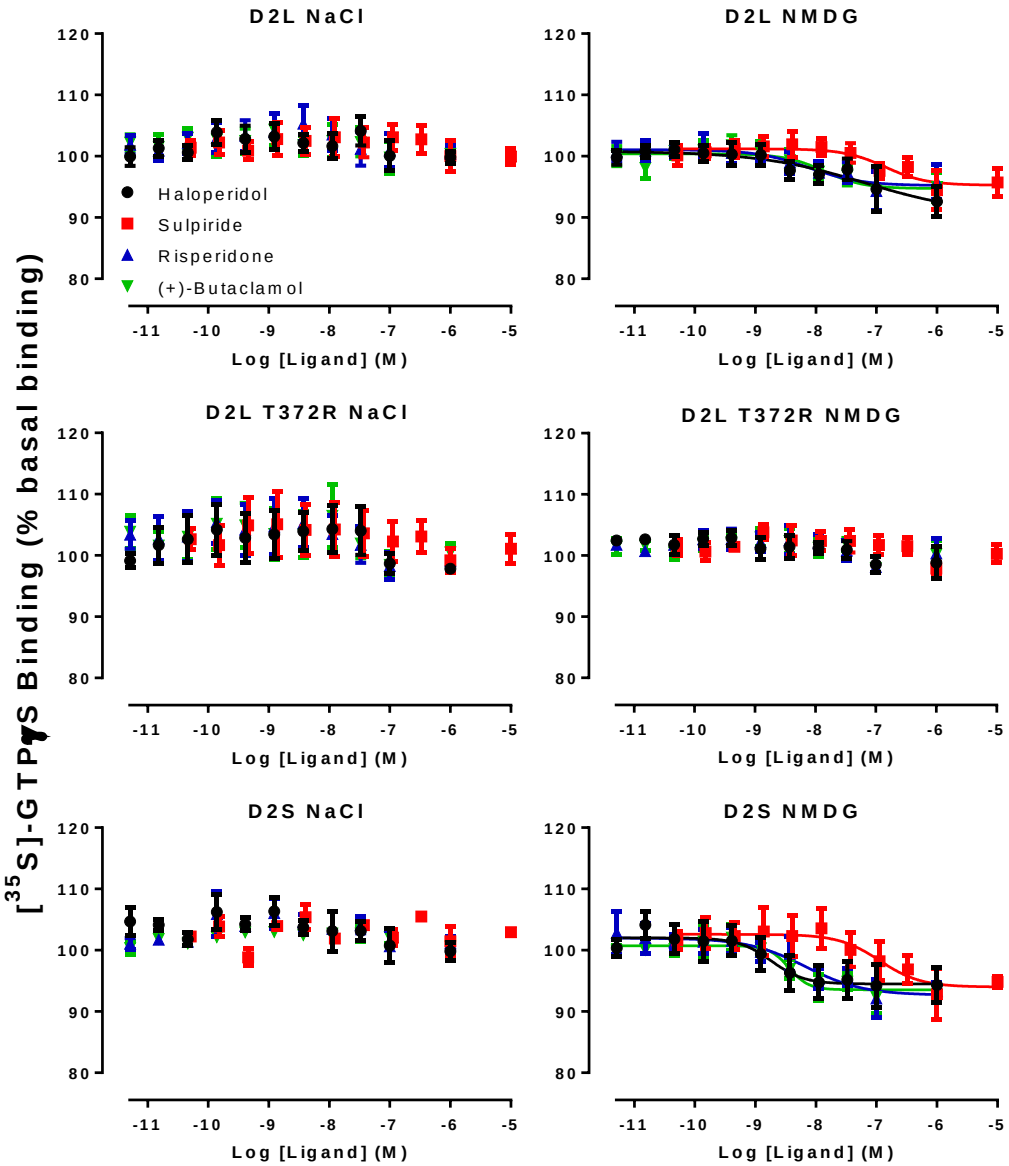


Figure 5.5: Inverse agonism in D2L, D2S and D2L T6.34R cell lines in both NaCl and NMDG buffers

D2L, D2L T6.34R and D2S expressing membranes were incubated with inverse agonists for 1h prior to [^{35}S]-GTPγS addition and subsequent filtration in both 100mM NaCl (left) and 100mM NMDG (right) containing buffers in the absence of GDP. Data points are pooled data (mean ± SEM) from 4 independent experiments performed in duplicate with D2S data summarised in **Table 5.2**.

Ligand	pEC_{50}	R_{max}
(+)-Butaclamol	8.71 ± 0.25	6.8 ± 1.7
Haloperidol	9.02 ± 0.28	7.7 ± 2.9
Sulpiride	8.12 ± 0.82	6.4 ± 1.2
Risperidone	8.63 ± 0.57	6.8 ± 1.7

Table 5.2: Summary of inverse agonist responses in D2S membranes in NMDG buffer

Summary of the D2S inverse agonist data from **Figure 5.5** in NMDG buffer. Data are pooled (mean ± SEM) from 4 independent experiments performed in duplicate with R_{max} expressed as a percentage reduction in basal [^{35}S]-GTPγS binding.

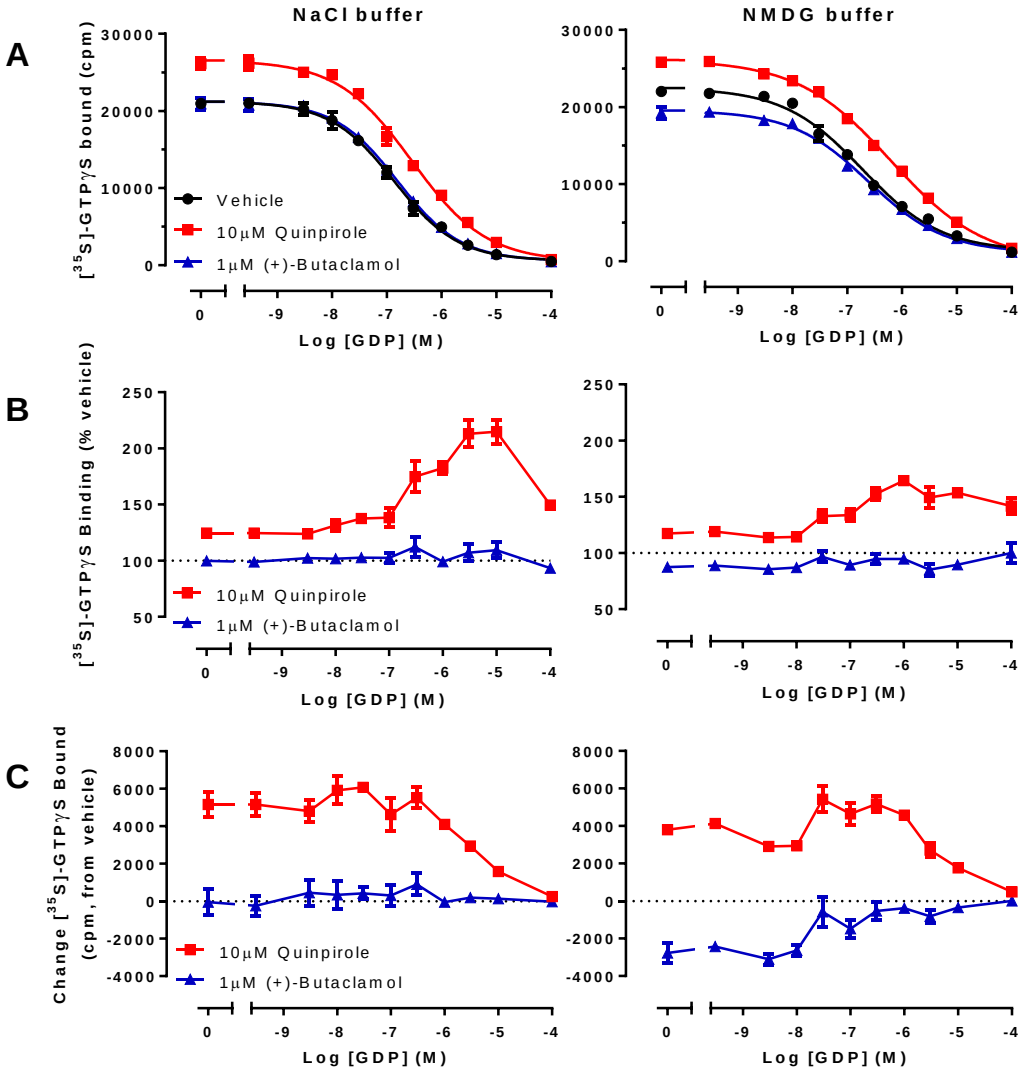


Figure 5.6: Effect of increasing GDP concentration on basal [^{35}S]-GTPγS binding and ligand responses in NaCl or NMDG buffers

GDP concentration response curves were conducted in the presence of vehicle, 10μM quinpirole or 1μM (+)-butaclamol in 100mM NaCl (**A**, left) and 100mM NMDG containing buffers (**A**, right) with pIC_{50}s summarised in **Table 5.3**. To show effects on signal window, ligand data were expressed as a percentage of vehicle binding at each concentration (**B**). Ligand response data are also shown as cpm changes from vehicle data (**C**). Data are from a single experiment (mean ± range) representative of 7-8 independent experiments performed in duplicate in D2S membranes.

Treatment	NaCl buffer	NMDG buffer
Vehicle	6.91 ± 0.06	6.71 ± 0.04
10µM Quinpirole	6.66 ± 0.07*	6.19 ± 0.08*
1µM (+)-Butaclamol	6.88 ± 0.07	6.64 ± 0.05

Table 5.3: Summary of pIC_{50} values from GDP concentration response curves in NaCl and NMDG buffers

Summary of pIC_{50} values from **Figure 5.6A**. Data are pooled (mean ± SEM) from 7-8 independent experiments performed in duplicate. *P<0.05 c.f. vehicle; One-way ANOVA followed by Dunnett's post hoc analysis.

5.2.3 Black and Leff operational model fitting of [^{35}S]-GTPγS binding data

Following assay optimisation, 12 ligands were examined for their ability to induce [^{35}S]-GTPγS binding at 10μM, 1μM, 300nM and 30nM GDP in NaCl-containing buffer, using D2S membranes (**Figure 5.7, Figure 5.8, Figure 5.9**). These data were then globally fit in sets of 4-5 ligands to the Black and Leff operational model as described, including quinpirole data as a control reference each time (**2.8.7**). Derived parameters are summarised in **Table 5.4**.

Operational model fitting gave an order of affinity as determined by pK_A values of lisuride > cabergoline = dihydroergocristine > bromocriptine = pergolide > apomorphine = 7OH-DPAT = (-)-3-PPP > quinpirole = dopamine = (+)-3-PPP. The order of efficacy as determined by τ values was dopamine = quinpirole = apomorphine > (+)-3-PPP = cabergoline = pergolide > bromocriptine > 7OH-DPAT = lisuride > (-)-3-PPP > dihydroergocristine. Only 7OH-DPAT, lisuride, (-)-3-PPP and dihydroergocristine had significantly lower τ values than the reference compound quinpirole at every concentration of GDP. Bromocriptine had significantly lower τ value than quinpirole at every GDP concentration except 10μM GDP ($P<0.05$; One-way ANOVA followed by Dunnett's post hoc analysis). Aripiprazole had no effect at any concentration of GDP and (-)-3-PPP and dihydroergocristine had no effect at 10μM GDP; as such these data sets were excluded from the analysis.

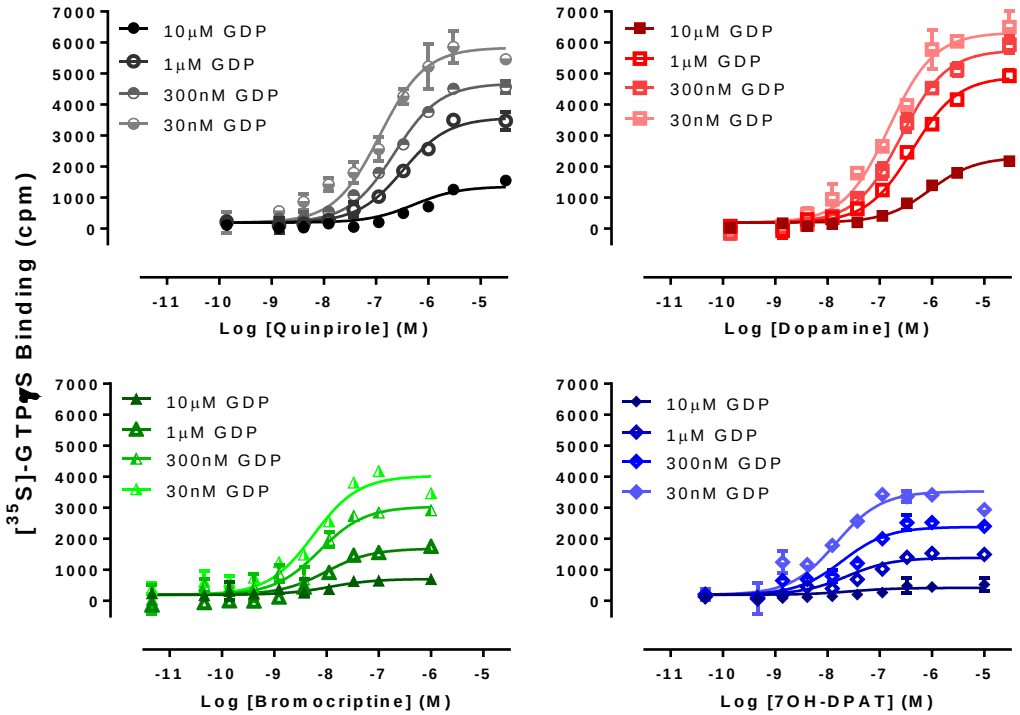


Figure 5.7: Fitting the Black and Leff operational model to D2S agonist responses in the [^{35}S]-GTPγS binding assay (1)

Increasing concentrations of D2 ligands were incubated with D2S membranes and 10µM, 1µM, 300nM or 30nM GDP for 1h in NaCl buffer prior to 20min treatment with [^{35}S]-GTPγS and filtration. Data were baseline corrected using total binding in the absence of ligand then globally fit to the operational model as described with data summarised in **Table 5.4**. Data are from a single experiment (mean ± range) representative of 5 independent experiments performed in duplicate.

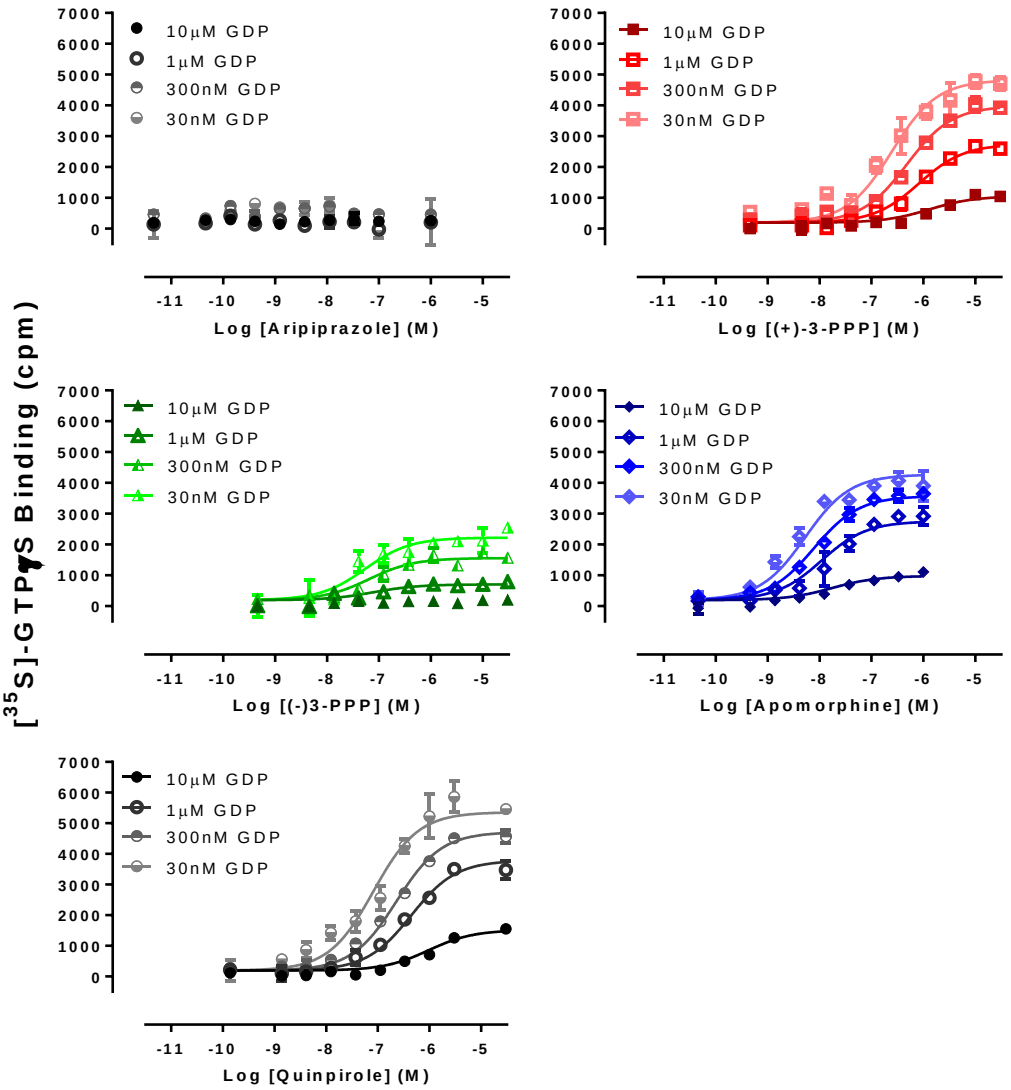


Figure 5.8: Fitting the Black and Leff operational model to D2 agonist responses in the [^{35}S]-GTPγS binding assay (2)

Increasing concentrations of D2 ligands were incubated with D2S membranes and 10µM, 1µM, 300nM or 30nM GDP for 1h prior in NaCl buffer to 20min incubation with [^{35}S]-GTPγS and filtration. Data were then globally fit to the operational model as described, including reference quinpirole data set and excluding the entire aripiprazole and 10µM (-)-3-PPP data sets due to no effect. Data fits are summarised in **Table 5.4**. Data are from a single experiment (mean ± range) representative of 6 independent experiments performed in duplicate.

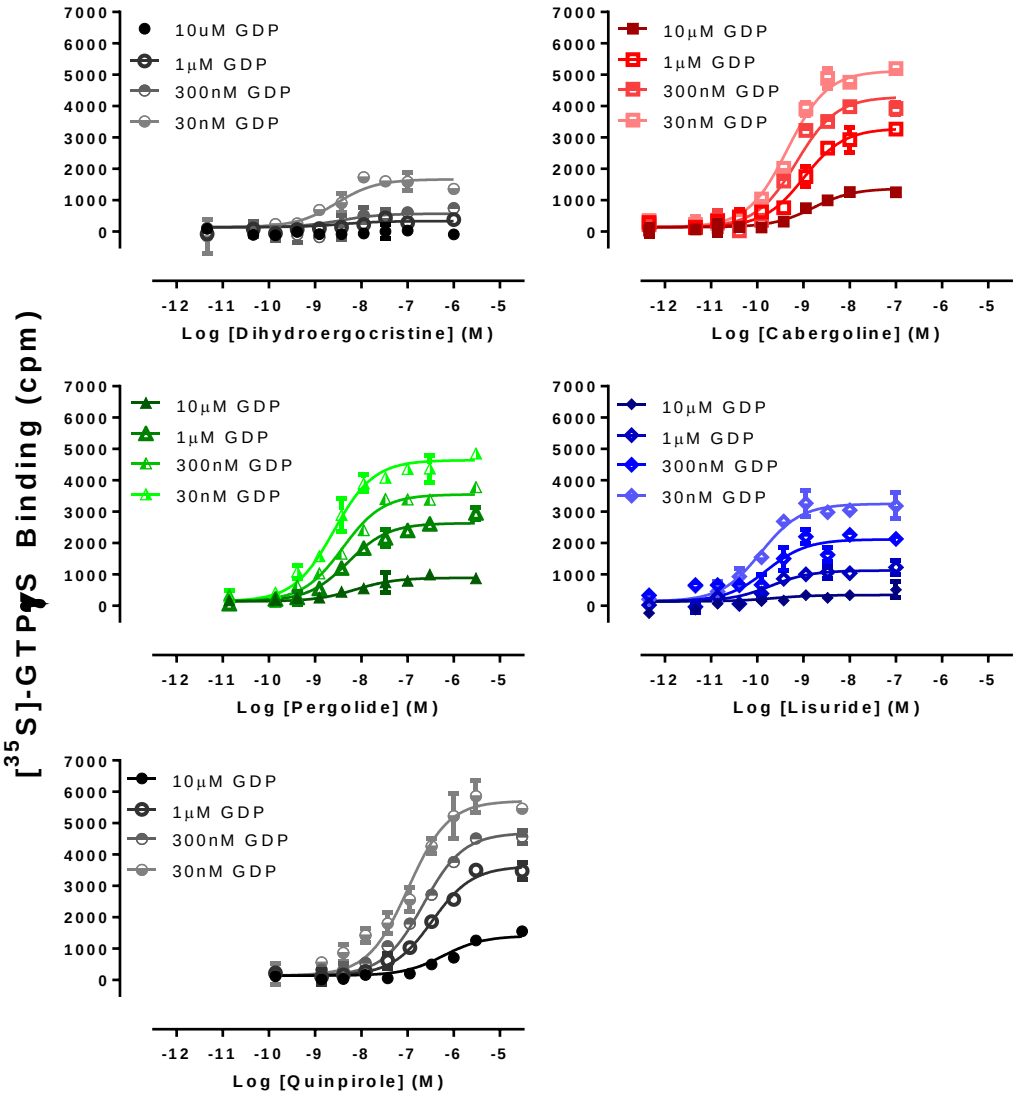


Figure 5.9: Fitting the Black and Leff operational model to D2 agonist responses in the [^{35}S]-GTPγS binding assay (3)

Increasing concentrations of D2 ligands were incubated with D2S membranes and 10µM, 1µM, 300nM or 30nM GDP for 1h in NaCl buffer prior to 20min incubation with [^{35}S]-GTPγS and filtration. Data were then globally fit to the operational model as described including reference quinpirole data set and excluding the 10µM dihydroergocristine data sets due to no effect. Data fits are summarised in **Table 5.4**. Data are from a single experiment (mean ± range) representative of 6 independent experiments performed in duplicate.

Ligand	pK_A	Logτ 10μM	Logτ 1μM	Logτ 300nM	Logτ 30nM
Quinpirole (1)	6.07 ± 0.12	-0.66 ± 0.13	0.16 ± 0.17	0.47 ± 0.17	0.99 ± 0.26
Dopamine	5.83 ± 0.05	-0.32 ± 0.07	0.43 ± 0.11	0.78 ± 0.08	1.07 ± 0.11
Bromocriptine	8.09 ± 0.07	-1.13 ± 0.14*	-0.47 ± 0.09*	-0.15 ± 0.08*	0.22 ± 0.04
7OH-DPAT	7.45 ± 0.04	-1.25 ± 0.09*	-0.75 ± 0.13*	-0.35 ± 0.11*	0.02 ± 0.08*
Quinpirole (2)	*5.92 ± 0.12*	*-0.52 ± 0.11*	*0.31 ± 0.15*	*0.69 ± 0.17*	*1.27 ± 0.22*
Aripiprazole	ND	ND	ND	ND	ND
(+)-3-PPP	5.71 ± 0.14	-0.78 ± 0.06	-0.01 ± 0.05	0.39 ± 0.09	0.79 ± 0.12
(-)-3-PPP	7.46 ± 0.17	ND	-0.93 ± 0.08*	-0.83 ± 0.20*	-0.27 ± 0.03*
Apomorphine	7.53 ± 0.07	-0.69 ± 0.07	0.06 ± 0.13	0.39 ± 0.09	1.11 ± 0.40
Quinpirole (3)	*6.05 ± 0.11*	*-0.59 ± 0.09*	*0.19 ± 0.11*	*0.53 ± 0.12*	*1.07 ± 0.18*
Dihydroergocristine	8.58 ± 0.17	ND	-1.20 ± 0.12*	-0.92 ± 0.08*	-0.49 ± 0.04*
Cabergoline	8.60 ± 0.11	-0.60 ± 0.07	0.11 ± 0.11	0.44 ± 0.10	0.71 ± 0.16
Pergolide	7.87 ± 0.15	-0.83 ± 0.10	-0.09 ± 0.09	0.24 ± 0.08	0.70 ± 0.16
Lisuride	9.52 ± 0.13	-1.42 ± 0.07*	-0.73 ± 0.06*	-0.39 ± 0.07*	0.02 ± 0.07*

Table 5.4: Estimations of D2S agonist affinity and τ values as determined by the Black and Leff operational model

Summary of Black and Leff operational model fits (example data sets shown in **Figure 5.7, Figure 5.8** and **Figure 5.9**). Quinpirole data are given for each set of fits performed with each set of 4-5 ligands. The aripiprazole, 10μM (-)-3-PPP and 10μM dihydroergocristine data sets were not determined (ND) in the analysis due to lack of response. Data are pooled (mean ± SEM) of 5-6 independent experiments performed in duplicate. *P<0.05 c.f. respective quinpirole τ value (One-way ANOVA followed by Dunnett's post-hoc test).

5.2.4 Fitting the GDP dependence operational model to [^{35}S]-GTPγS binding data

To explore the applicability of the novel GDP dependence operational model, the data sets from **5.2.3** were re-analysed (**Figure 5.10, Figure 5.11, Figure 5.12**) with data summarised in **Table 5.5**. This analysis incorporated the GDP concentration response curves that were collected in parallel to the agonist response curves in each experiment (examples in **Figure 5.6**). As GraphPad Prism cannot fit two data sets simultaneously where the independent variable (*X*) is a different parameter (in this case, agonist and GDP concentrations), the GDP dependence model fits were constrained using the parameters from the concurrently performed vehicle GDP concentration response curve; the GDP IC_{50} was used to approximate K_{GDP} and the Hill slope to constrain s. These were determined as 6.91 ± 0.06 (K_{GDP}) and 0.73 ± 0.02 (s) (from n=7). The data were then globally fit to the GDP dependence operational model as described (**2.8.9**).

This model generated the same rank order of affinity and efficacy for the compounds as the Black and Leff operational model but instead determined a single τ (τ_0) rather than one for each GDP treatment (**Table 5.6**). While pK_A estimations on the whole were comparable between the two analyses (**Figure 5.13**), there were small but significant increases in affinity for apomorphine (2.1-fold) and quinpirole for data sets 2 and 3 (2.0 and 2.7-fold respectively) compared with the Black and Leff operational model fits ($P<0.05$; Student's unpaired t-test). When τ_0 values were compared to the value of τ at 30nM GDP from the Black and Leff operational model, only apomorphine demonstrated a significant difference ($P<0.05$; Student's unpaired t-test; **Table 5.6**, **Figure 5.13**).

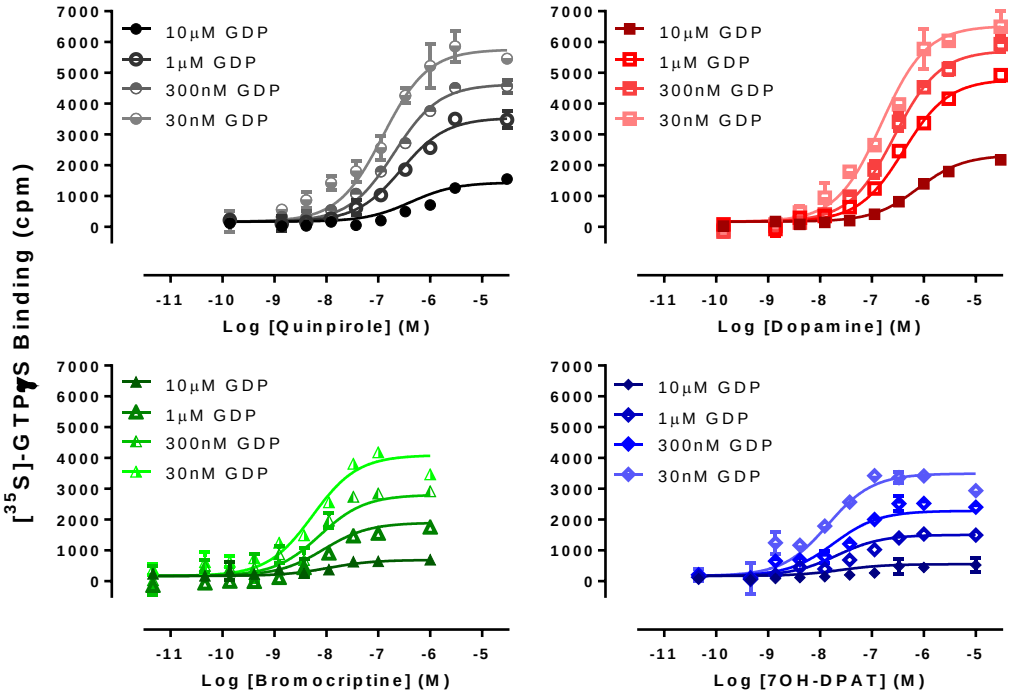


Figure 5.10: Fitting the GDP dependence operational model to [^{35}S]-GTPγS binding data sets (1)

The same data set from **Figure 5.7** were re-analysed using the GDP dependence operational model. Data were globally fit as described with data summarised in **Table 5.5**. Data are from a single experiment (mean ± range) representative of 5 independent experiments performed in duplicate.

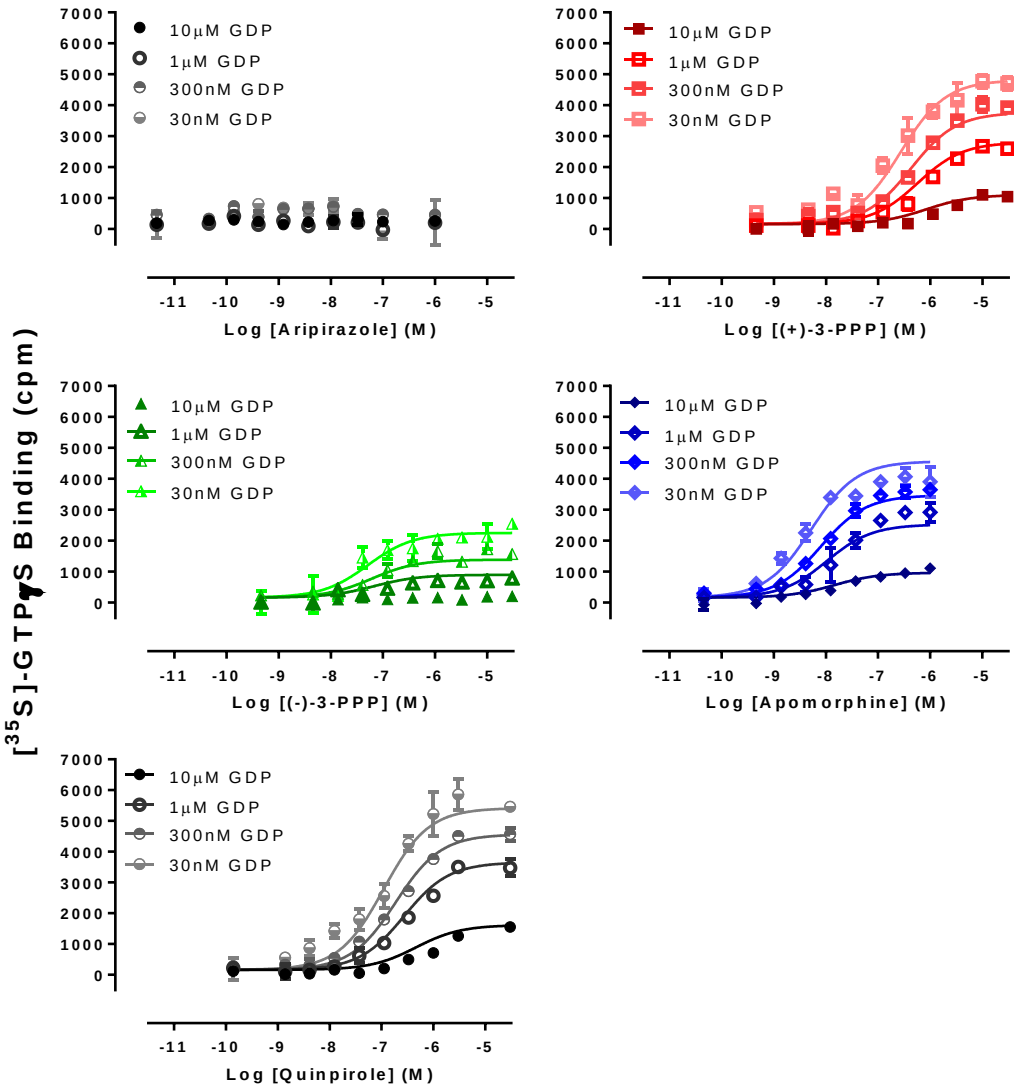


Figure 5.11: Fitting the GDP dependence operational model to [^{35}S]-GTPγS binding data sets (2)

The same data set from **Figure 5.8** were re-analysed using the GDP dependence operational model. Data were globally fit including reference quinpirole data set as described and excluding the aripiprazole and 10μM (-)-3-PPP data sets due to no effect. Data fits are summarised in **Table 5.5**. Data are from a single experiment (mean ± range) representative of 6 independent experiments performed in duplicate.

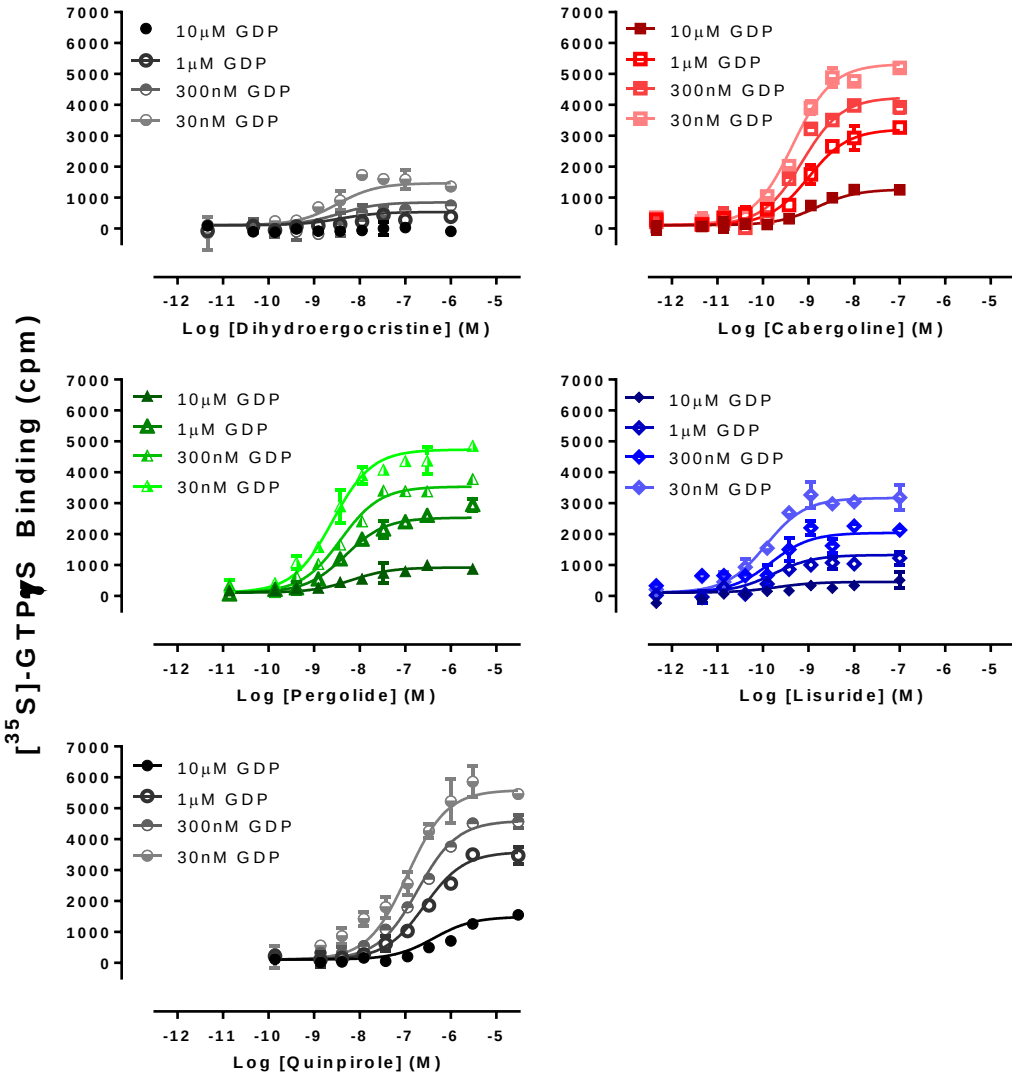


Figure 5.12: Fitting the GDP dependence operational model to [^{35}S]-GTPγS binding data sets (3)

The same data set from **Figure 5.9** were re-analysed using the GDP dependence operational model. Data were globally fit as described including reference quinpirole data set and excluding the 10µM dihydroergocristine data set due to no effect. Data fits are summarised in **Table 5.5**. Data are from a single experiment (mean ± range) representative of 6 independent experiments performed in duplicate.

Ligand	pK_A	$Log\tau_0$
Quinpirole (1)	6.29 ± 0.09	0.80 ± 0.22
Dopamine	5.96 ± 0.02	1.07 ± 0.19
Bromocriptine	8.12 ± 0.10	0.30 ± 0.13*
7OH-DPAT	7.46 ± 0.05	0.09 ± 0.15*
Quinpirole (2)	*6.35 ± 0.07*	*0.71 ± 0.07*
Aripiprazole	ND	ND
(+)-3-PPP	5.96 ± 0.10	0.54 ± 0.06
(-)-3-PPP	7.50 ± 0.18	-0.30 ± 0.04*
Apomorphine	7.86 ± 0.13	0.56 ± 0.06
Quinpirole (3)	*6.36 ± 0.04*	*0.73 ± 0.08*
Dihydroergocristine	8.56 ± 0.15	-0.45 ± 0.03*
Cabergoline	8.69 ± 0.11	0.68 ± 0.10
Pergolide	8.04 ± 0.11	0.53 ± 0.09
Lisuride	9.60 ± 0.15	0.02 ± 0.06*

Table 5.5: Summary of GDP dependence operational model data fits

Summary of the GDP dependence operational model fits derived from the D2S data in **Figure 5.10, Figure 5.11** and **Figure 5.12**. Quinpirole data are given for each set of fits performed with each set of 4-5 ligands. Data shown are pooled (mean ± SEM) of 5-6 independent experiments performed in duplicate. ND = not determined; *P<0.05 c.f. quinpirole τ (One-way ANOVA followed by Dunnett's post hoc test).

Ligand	Black and Leff Operational Model					GDP Dependence Operational Model	
	pK_A	Logτ 10μM	Logτ 1μM	Logτ 300nM	Logτ 30nM	pK_A	$Log\tau_0$
Quinpirole (1)	6.07 ± 0.12	-0.66 ± 0.13	0.16 ± 0.17	0.47 ± 0.17	0.99 ± 0.26	6.29 ± 0.09	0.80 ± 0.22
Dopamine	5.83 ± 0.05	-0.32 ± 0.07	0.43 ± 0.11	0.78 ± 0.08	1.07 ± 0.11	5.96 ± 0.02	1.07 ± 0.19
Bromocriptine	8.09 ± 0.07	-1.13 ± 0.14	-0.47 ± 0.09	-0.15 ± 0.08	0.22 ± 0.04	8.12 ± 0.10	0.30 ± 0.13
7OH-DPAT	7.45 ± 0.04	-1.25 ± 0.09	-0.75 ± 0.13	-0.35 ± 0.11	0.02 ± 0.08	7.46 ± 0.05	0.09 ± 0.15
Quinpirole (2)	*5.92 ± 0.12*	*-0.52 ± 0.11*	*0.31 ± 0.15*	*0.69 ± 0.17*	*1.27 ± 0.22*	*6.35 ± 0.07**	*0.71 ± 0.07*
Aripiprazole	ND	ND	ND	ND	ND	ND	ND
(+)-3-PPP	5.71 ± 0.14	-0.78 ± 0.06	-0.01 ± 0.05	0.39 ± 0.09	0.79 ± 0.12	5.96 ± 0.10	0.54 ± 0.06
(-)-3-PPP	7.46 ± 0.17	ND	-0.93 ± 0.08	-0.83 ± 0.20	-0.27 ± 0.03	7.50 ± 0.18	-0.30 ± 0.04
Apomorphine	7.53 ± 0.07	-0.69 ± 0.07	0.06 ± 0.13	0.39 ± 0.09	1.11 ± 0.40	7.86 ± 0.13*	0.56 ± 0.06
Quinpirole (3)	*6.05 ± 0.11*	*-0.59 ± 0.09*	*0.19 ± 0.11*	*0.53 ± 0.12*	*1.07 ± 0.18*	*6.36 ± 0.04**	*0.73 ± 0.08*
Dihydroergocristine	8.58 ± 0.17	ND	-1.20 ± 0.12	-0.92 ± 0.08	-0.49 ± 0.04	8.56 ± 0.15	-0.45 ± 0.03
Cabergoline	8.60 ± 0.11	-0.60 ± 0.07	0.11 ± 0.11	0.44 ± 0.10	0.71 ± 0.16	8.69 ± 0.11	0.68 ± 0.10
Pergolide	7.87 ± 0.15	-0.83 ± 0.10	-0.09 ± 0.09	0.24 ± 0.08	0.70 ± 0.16	8.04 ± 0.11	0.53 ± 0.09
Lisuride	9.52 ± 0.13	-1.42 ± 0.07	-0.73 ± 0.06	-0.39 ± 0.07	0.02 ± 0.07	9.60 ± 0.15	0.02 ± 0.06

Table 5.6: Comparison of Black and Leff and GDP dependence operational model fits to D2S [^{35}S]-GTPγS binding data

Comparison of model fits from **Table 5.4** and **Table 5.5**. Data shown are pooled (mean ± SEM) of 5-6 independent experiments performed in duplicate. ND = not determined; *P<0.05 c.f. Black and Leff operational model pK_A (Student's unpaired t-test).

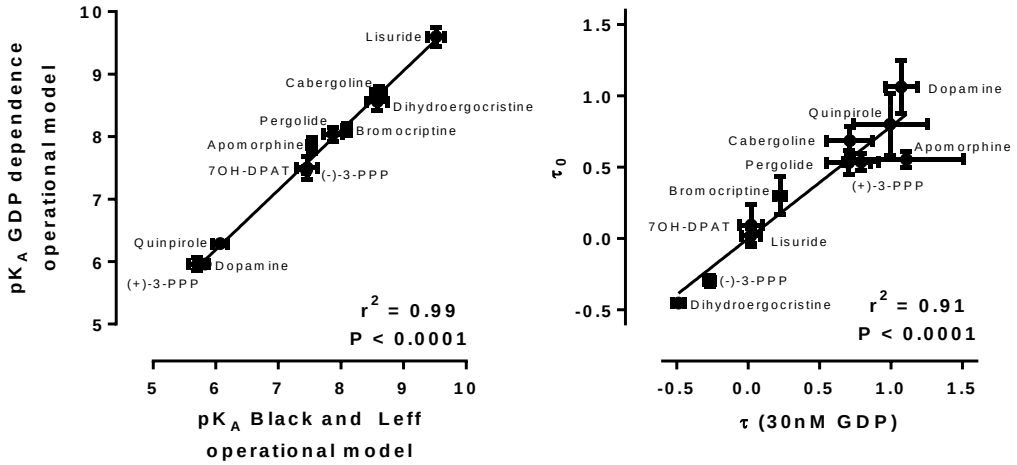


Figure 5.13: Correlation between Black and Leff and GDP dependence operational model fits

Relationship between the derived affinities and τ values from the application of the Black and Leff and GDP dependence operational models to the [^{35}S]-GTPγS binding data derived in NaCl containing buffer. Data are reproduced from **Table 5.6**. Data points are mean ± SEM of 5 independent experiments performed in duplicate.

5.2.5 Slack and Hall operational model fitting of D2S [^{35}S]-GTPγS binding data

The presence of D2S receptor constitutive activity in the NMDG buffer allowed the application of the Slack and Hall operational model. Families of agonist curves in the presence of 10μM, 1μM, 300nM and 30nM GDP, baseline corrected using (+)-butaclamol data at each GDP concentration to remove receptor constitutive activity, were globally fit to the Slack and Hall operational model (**Figure 5.14, Figure 5.15, Figure 5.16**) as described (**2.8.8**). Data are summarised in **Table 5.7** and **Table 5.8**.

Unlike the NaCl buffer data, all compounds at all GDP concentrations were able to induce [^{35}S]-GTPγS binding responses. Fitting of the Slack and Hall operational model gave an order of affinity of lisuride > cabergoline = aripiprazole = pergolide = apomorphine > dihydroergocristine > bromocriptine > 7OH-DPAT > dopamine = quinpirole > (-)-3-PPP = (+)-3-PPP. This order was similar to the Black and Leff operational model fits, with the exception of dihydroergocristine (3.1-fold lower affinity), and pergolide and apomorphine (increased affinity 4.8 and 7.4-fold, changing their rank order). Unlike the NaCl model fits which demonstrated a large distribution of τ or τ_0 values, the ligand intrinsic efficacy (ε) values were similar for most agonists. Only aripiprazole and dihydroergocristine demonstrated a significantly lower ε value than the reference agonist quinpirole ($P<0.05$; One-way ANOVA followed by Dunnett's post hoc analysis) (**Table 5.7**).

Each set of agonist group data fits generated a family of system coupling efficiency (χ) values for each concentration of GDP with χ values increasing with decreasing GDP concentration (**Table 5.8**). Between the different fits, there were no significant differences between the χ values except for the χ for 30nM GDP between agonist data sets 2 and 3 ($P<0.05$; One-way ANOVA followed by Tukey's post hoc analysis).

As a number of agonist data sets appeared poorly fit to the model when globally fit to individual experiments, the data were normalised and pooled to

examine whether the individual deviations in the fit would be maintained. As shown by the 4 representative data sets in **Figure 5.17**, pooling the data largely removed the deviations in the data points from the fits.

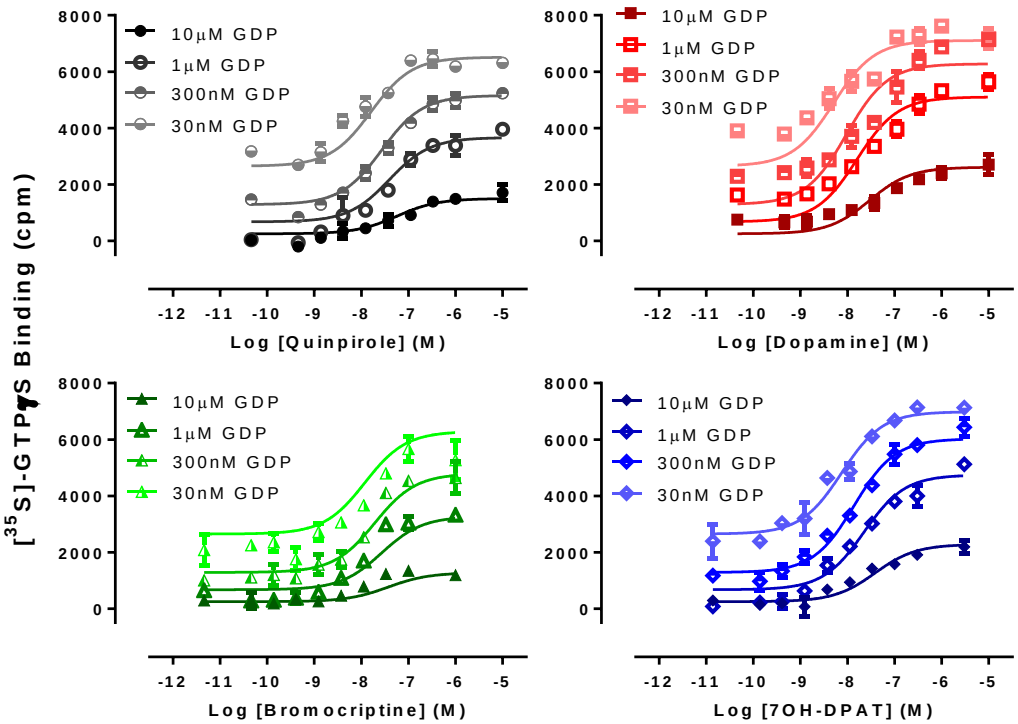


Figure 5.14: Fitting the Slack and Hall operational model to [^{35}S]-GTPγS binding data (1)

Increasing concentrations of D2 receptor ligands were incubated with D2S membranes and 10μM, 1μM, 300nM or 30nM GDP in NMDG buffer for 1h prior to 20min incubation with [^{35}S]-GTPγS and filtration. Data were globally fit to the Slack and Hall operational model as described with data summarised in **Table 5.7** and **Table 5.8**. Data are from a single experiment (mean ± range) representative of 5 independent experiments performed in duplicate.

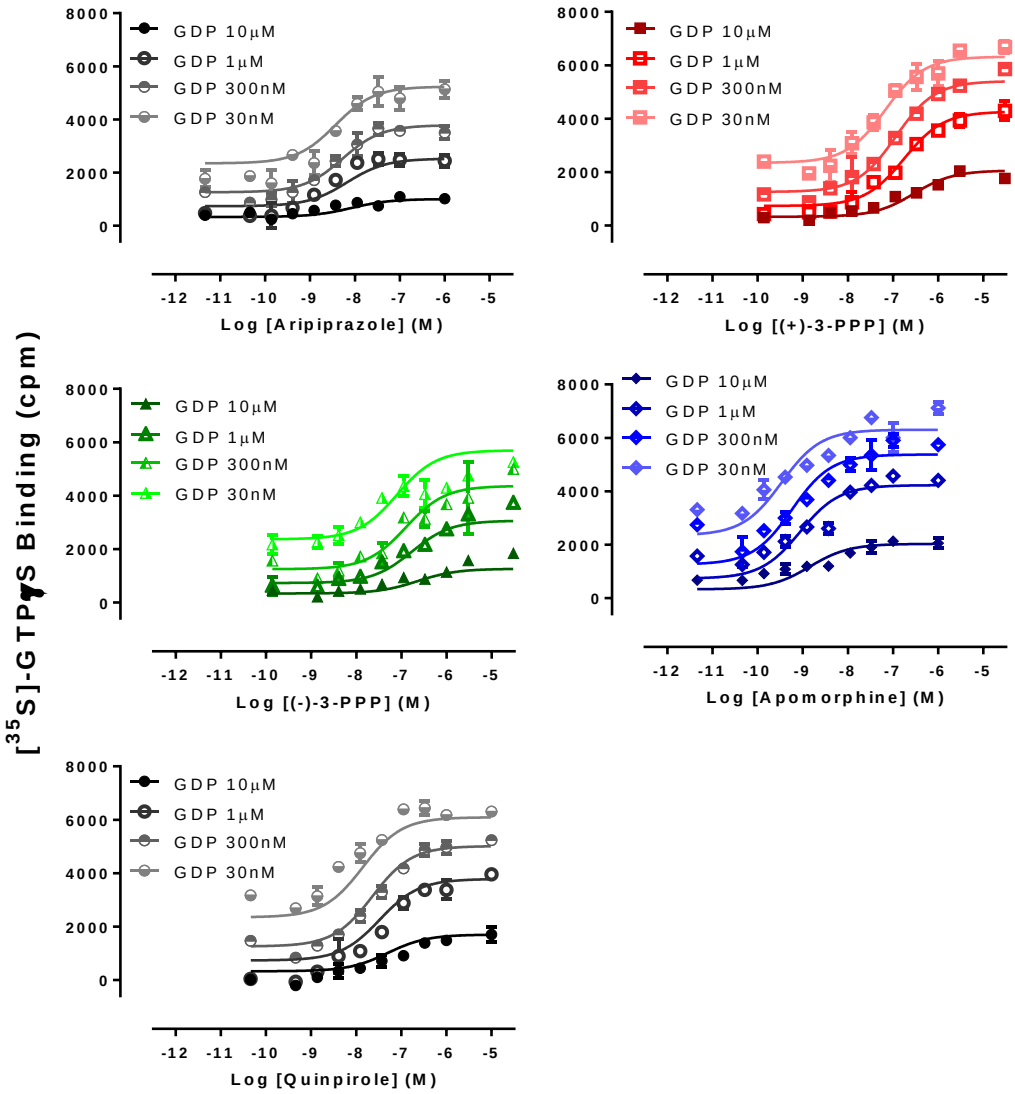


Figure 5.15: Fitting the Slack and Hall operational model to [^{35}S]-GTPγS binding data (2)

Increasing concentrations of D2 receptor ligands were incubated with D2S membranes and 10µM, 1µM, 300nM or 30nM GDP in NMDG buffer for 1h prior to 20min incubation with [^{35}S]-GTPγS and filtration. Data were globally fit to the Slack and Hall operational model, including the reference quinpirole data set, as described with data summarised in **Table 5.7** and **Table 5.8**. Data are from a single experiment (mean ± range) representative of 5 independent experiments performed in duplicate.

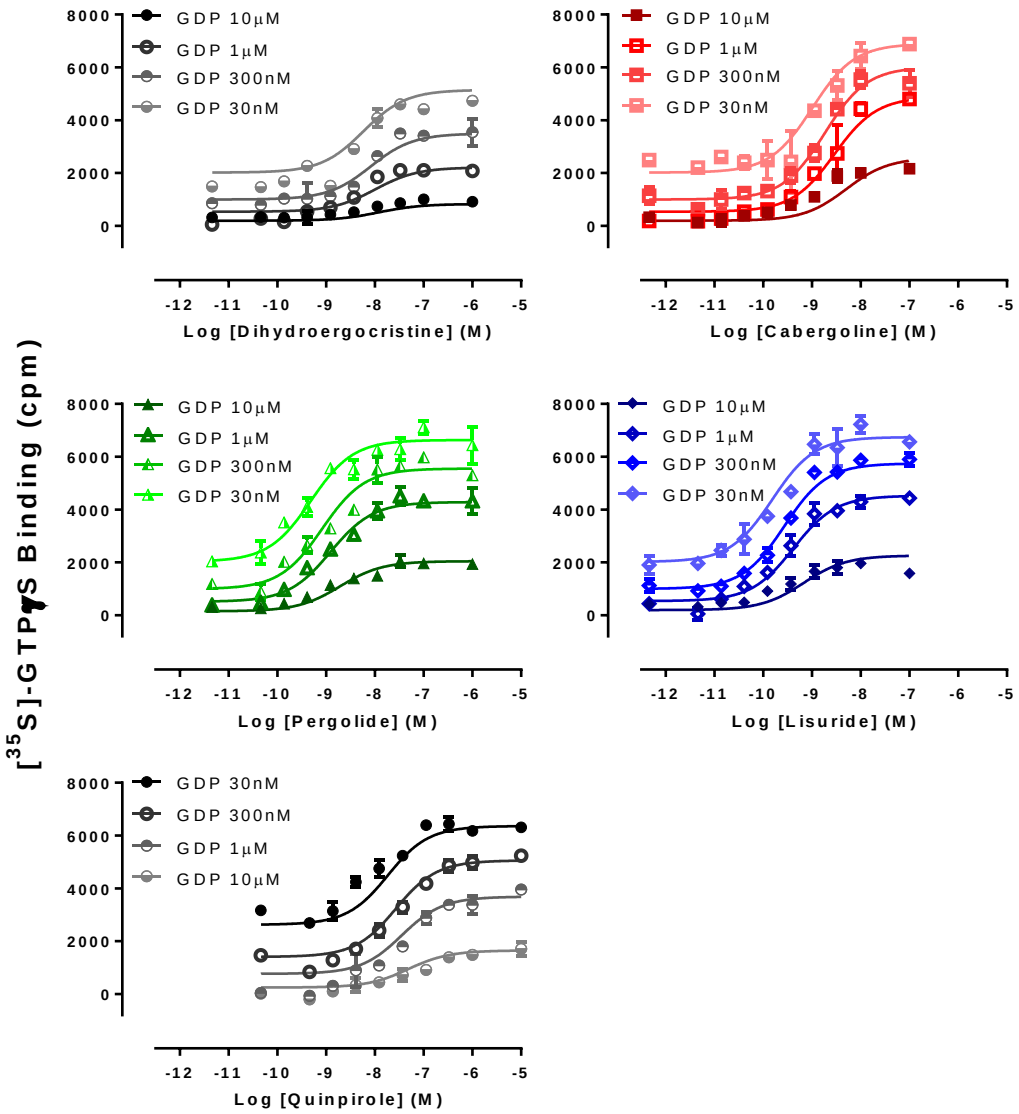


Figure 5.16: Fitting the Slack and Hall operational model to [^{35}S]-GTPγS binding data (3)

Increasing concentrations of D2 receptor ligands were incubated with D2S membranes and 10µM, 1µM, 300nM or 30nM GDP in NMDG buffer for 1h prior to 20min incubation with [^{35}S]-GTPγS and filtration. Data were globally fit to the Slack and Hall operational model, including the reference quinpirole data set, as described with data summarised in **Table 5.7** and **Table 5.8**. Data are from a single experiment (mean ± range) representative of 5 independent experiments performed in duplicate.

Ligand	pK_A	Logε
Quinpirole (1)	6.87 ± 0.14	1.36 ± 0.21
Dopamine	7.05 ± 0.16	1.52 ± 0.16
Bromocriptine	7.57 ± 0.12	1.28 ± 0.20
7OH-DPAT	7.21 ± 0.10	1.44 ± 0.20
Quinpirole (2)	*6.97 ± 0.18*	*1.22 ± 0.08*
Aripiprazole	8.64 ± 0.52	0.74 ± 0.03*
(+)-3-PPP	6.29 ± 0.10	1.24 ± 0.10
(-)-3-PPP	6.34 ± 0.21	1.06 ± 0.12
Apomorphine	8.40 ± 0.09	1.29 ± 0.07
Quinpirole (3)	*7.06 ± 0.18*	*1.24 ± 0.04*
Dihydroergocristine	8.09 ± 0.33	0.70 ± 0.04*
Cabergoline	8.68 ± 0.19	1.40 ± 0.05
Pergolide	8.55 ± 0.12	1.23 ± 0.04
Lisuride	9.31 ± 0.08	1.20 ± 0.05

Table 5.7: D2S agonist affinities and intrinsic efficacies as determined by the Slack and Hall operational model

Summary of derived parameters from fitting the Slack and Hall operational model to data shown in **Figure 5.14**, **Figure 5.15** and **Figure 5.16**. Quinpirole data are given for each set of fits performed with each set of 4-5 ligands. Data are pooled (mean ± SEM) from 5 independent experiments performed in duplicate; *P<0.05 (c.f. quinpirole; One-way ANOVA followed by Dunnett's post hoc analysis).

χ Values	Logχ (1)	Logχ (2)	Logχ (3)
χ1 (10μM GDP)	-1.73 ± 0.07	-1.74 ± 0.06	-1.76 ± 0.04
χ2 (1μM GDP)	-0.97 ± 0.12	-1.12 ± 0.05	-1.16 ± 0.04
χ3 (300nM GDP)	-0.56 ± 0.13	-0.75 ± 0.06	-0.82 ± 0.04
χ4 (30nM GDP)	-0.21 ± 0.12	-0.42 ± 0.04	-0.52 ± 0.02*

Table 5.8: Logχ values derived from fitting of the Slack and Hall operational model to D2S receptor [^{35}S]-GTPγS binding data

Summary of derived χ values, the measure of basal system coupling efficiency, from fitting the Slack and Hall operational model to each set of 4-5 data sets. Data are pooled (mean ± SEM) of 5 independent experiments performed in duplicate. *P<0.05 cf. set 1 (One-way ANOVA followed by Tukey's post hoc analysis).

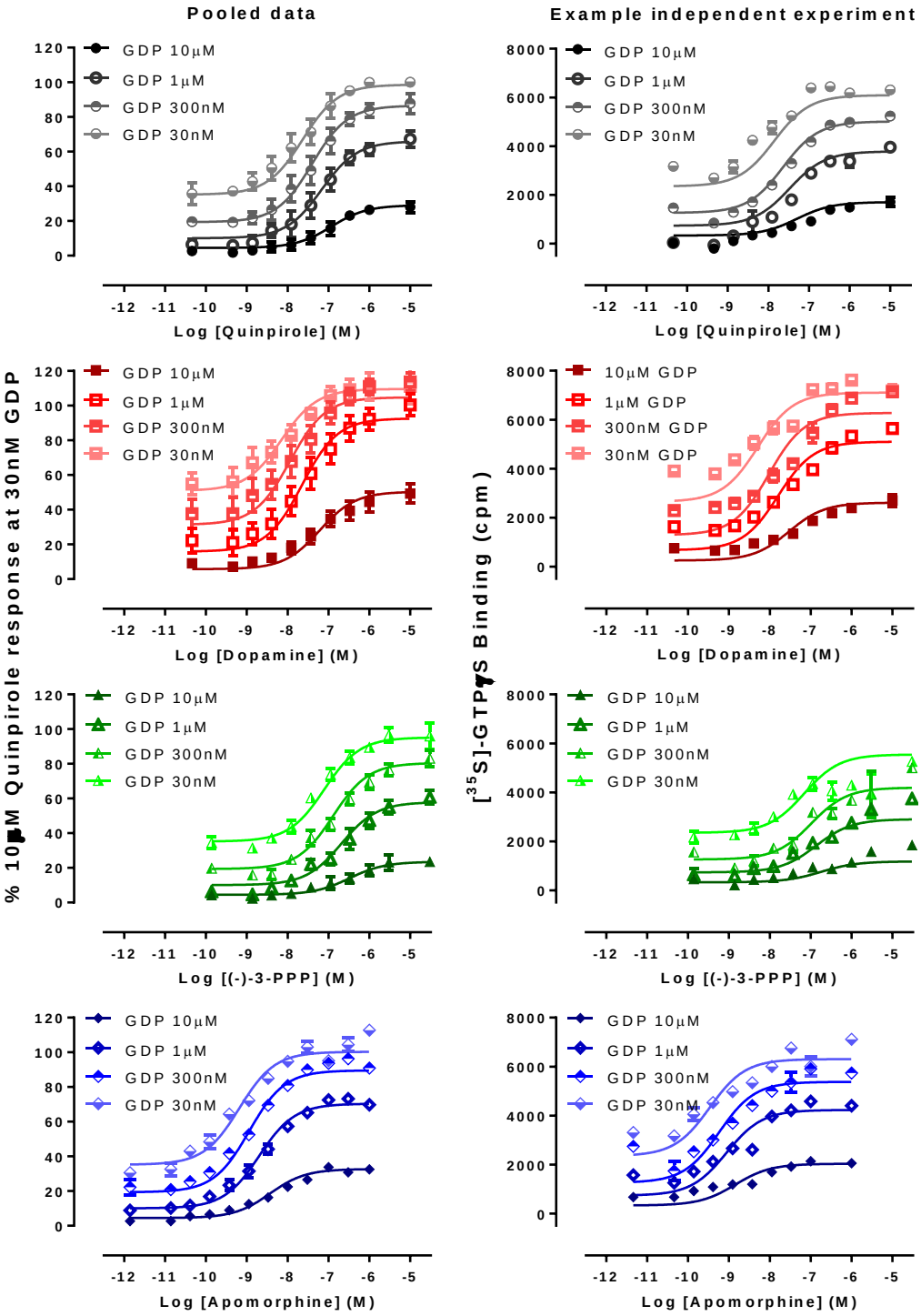


Figure 5.17: Comparison of Slack and Hall operational model fits between pooled data and an individual representative experiment

Comparison of pooled and individual data set operational model fits. Data on the left are pooled (mean ± SEM) of 5 independent experiments performed in duplicate, expressed as a percentage of 10µM quinpirole response at 30nM GDP. Data on the right are reproduced from **Figure 5.14** and **Figure 5.15.**

5.2.6 Reanalysis of NMDG data to determine whether limitations to efficacy discrimination are due to altered buffer composition

The main difference in the data sets derived from the NaCl and NMDG containing buffers is the reduced number of compounds that have significantly lower efficacy than the reference compound following buffer substitution. In order to examine whether this was down to buffer differences or a lack of power in the Slack and Hall operational model to distinguish between compounds, the data were reanalysed using the Black and Leff and GDP dependence operational models (GDP dependence fits shown in **Figure 5.18, Figure 5.19, Figure 5.20**). Instead of using (+)-butaclamol data to correct for the contribution of constitutive activity to responses, data were corrected to total binding in the absence of ligand so that only ligand stimulated [^{35}S]-GTPγS binding was accounted for. As shown in **Table 5.9**, like the Slack and Hall operational model fits, there were only significant differences in τ values for aripiprazole and dihydroergocristine when compared with the reference agonist quinpirole for 10μM GDP Black and Leff model and τ_0 GDP dependence operational model.

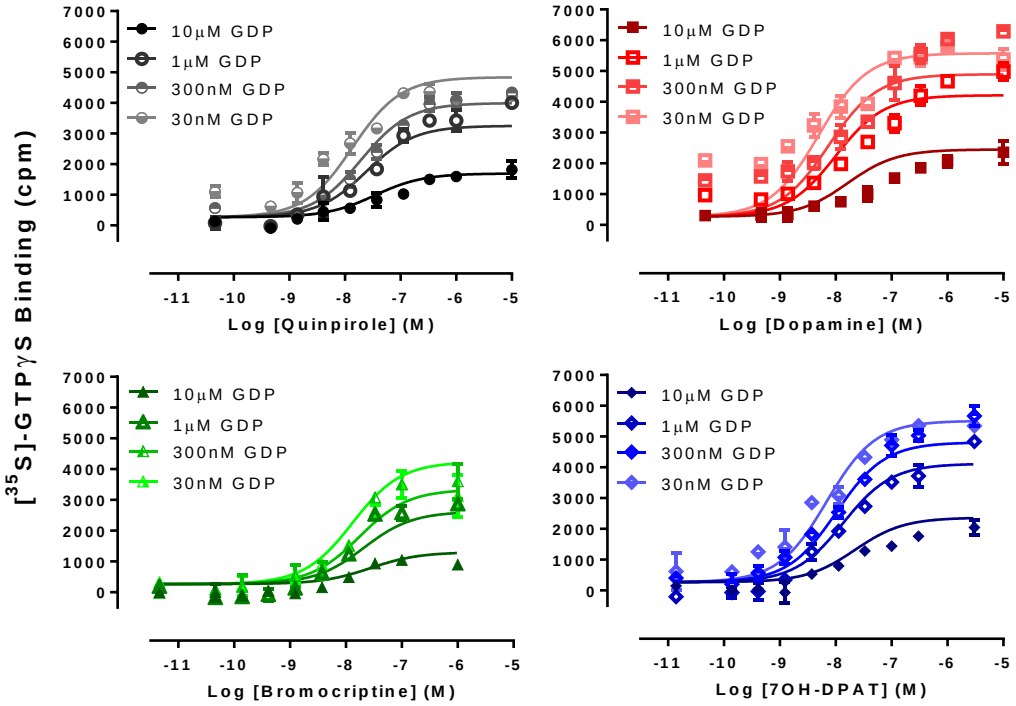


Figure 5.18: Fitting the GDP dependence operational model to [^{35}S]-GTPγS binding data sets in NMDG containing buffer (1)

Increasing concentrations of D2 receptor ligands were incubated with D2S membranes and 10μM, 1μM, 300nM or 30nM GDP in NMDG buffer for 1h prior to 20min incubation with [^{35}S]-GTPγS and filtration. Data were globally fit to the GDP dependence operational model as described with data summarised in **Table 5.9**. Data are from a single experiment (mean ± range) representative of 5 independent experiments performed in duplicate.

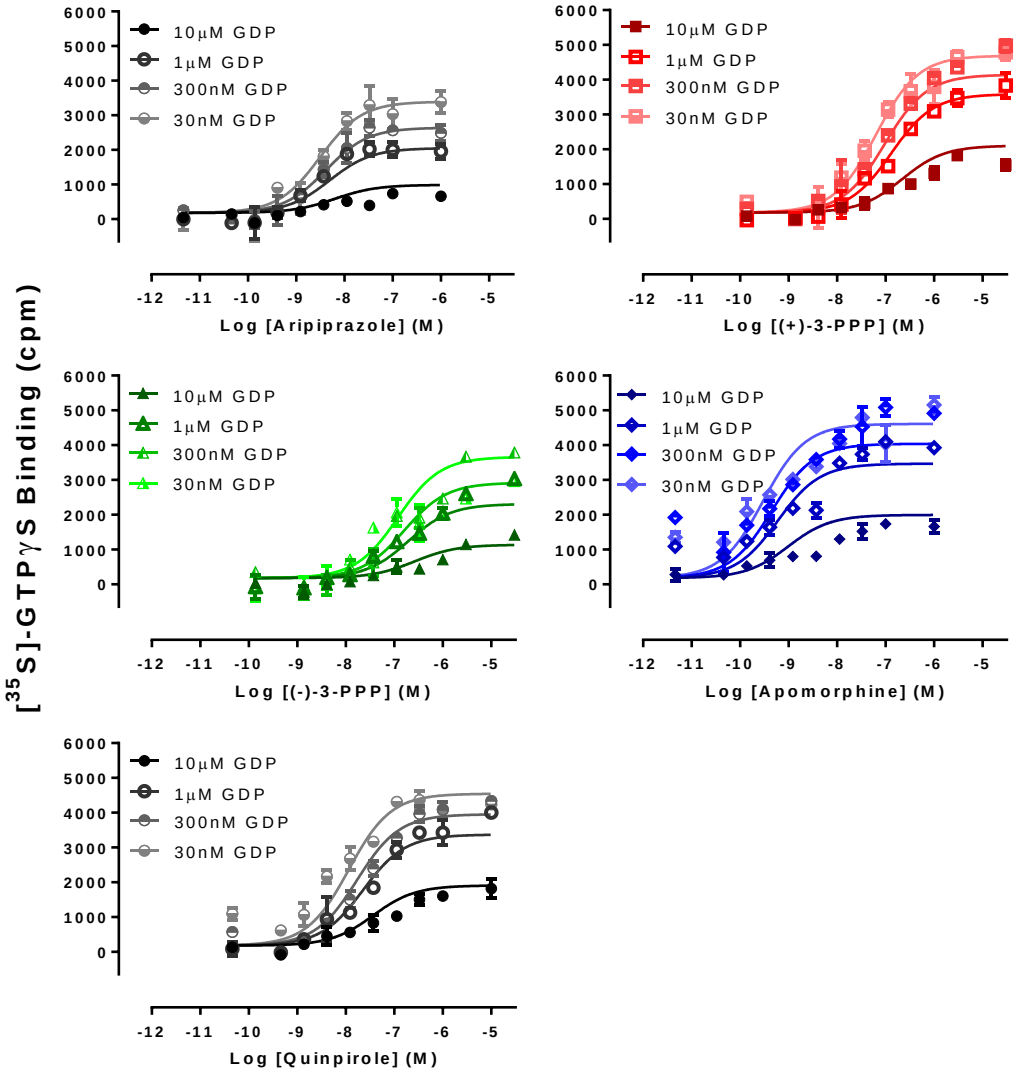


Figure 5.19: Fitting the GDP dependence operational model to [^{35}S]-GTPγS binding data sets in NMDG containing buffer (2)

Increasing concentrations of D2 receptor ligands were incubated with D2S membranes and 10μM, 1μM, 300nM or 30nM GDP in NMDG buffer for 1h prior to 20min incubation with [^{35}S]-GTPγS and filtration. Data were globally fit to the GDP dependence operational model as described with data summarised in **Table 5.9**. Data are from a single experiment (mean ± range) representative of 5 independent experiments performed in duplicate.

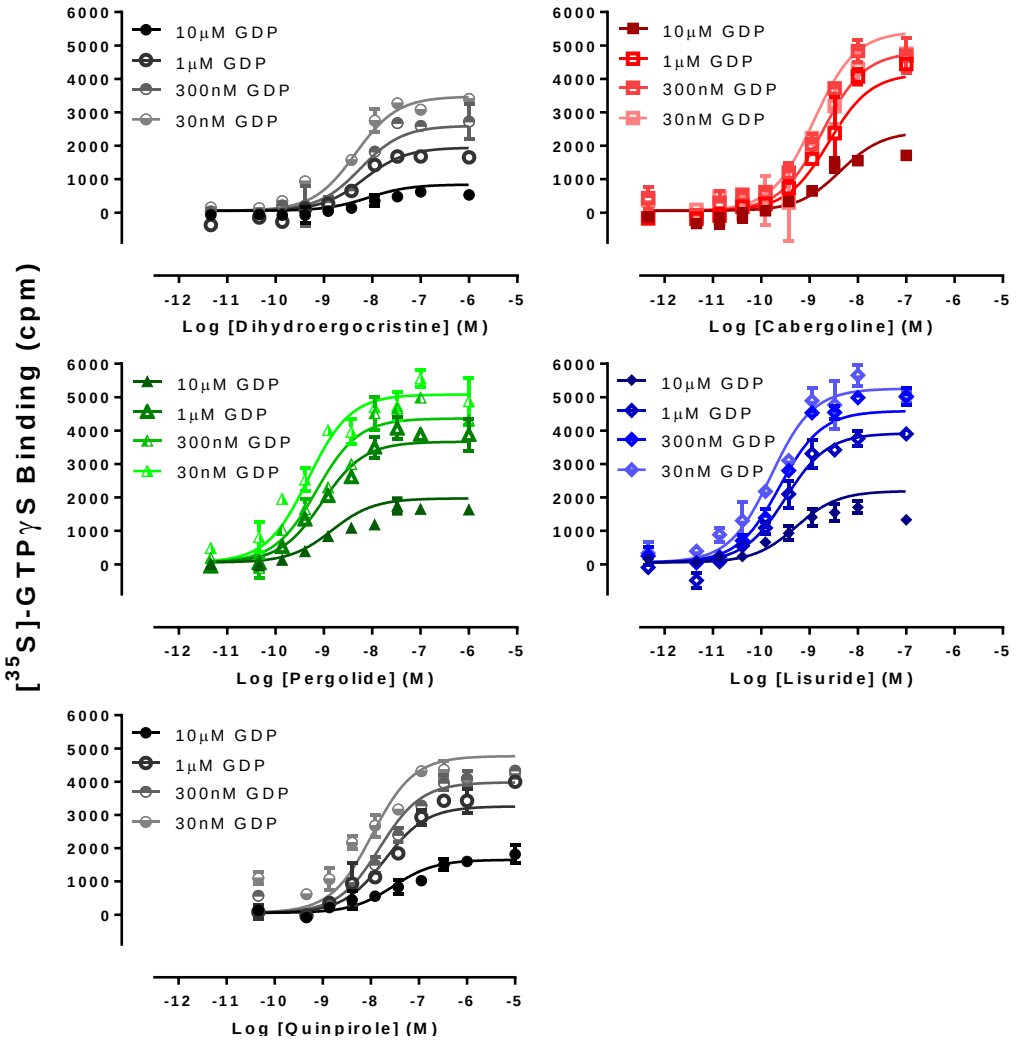


Figure 5.20: Fitting the GDP dependence operational model to [35S]-GTPγS binding data sets in NMDG containing buffer (3)

Increasing concentrations of D2 receptor ligands were incubated with D2S membranes and 10μM, 1μM, 300nM or 30nM GDP in NMDG buffer for 1h prior to 20min incubation with [^{35}S]-GTPγS and filtration. Data were globally fit to the GDP dependence operational model as described with data summarised in **Table 5.9**. Data are from a single experiment (mean ± range) representative of 5 independent experiments performed in duplicate.

Ligand	Black and Leff Operational Model					GDP Dependence Operational Model	
	pK_A	Logτ 10μM	Logτ 1μM	Logτ 300nM	Logτ 30nM	pK_A	$Log\tau_0$
Quinpirole (1)	7.17 ± 0.28	-0.45 ± 0.16	0.26 ± 0.27	0.38 ± 0.28	0.22 ± 0.22	7.04 ± 0.21	0.86 ± 0.21
Dopamine	7.21 ± 0.38	-0.31 ± 0.19	0.49 ± 0.28	0.71 ± 0.35	0.57 ± 0.41	7.22 ± 0.25	1.04 ± 0.20
Bromocriptine	7.68 ± 0.24	-0.55 ± 0.20	0.18 ± 0.33	0.33 ± 0.30	0.23 ± 0.26	7.59 ± 0.16	0.77 ± 0.25
7OH-DPAT	7.45 ± 0.28	-0.33 ± 0.19	0.41 ± 0.28	0.57 ± 0.32	0.43 ± 0.32	7.34 ± 0.17	1.03 ± 0.25
Quinpirole (2)	*6.72 ± 0.22*	*-0.41 ± 0.10*	*0.38 ± 0.15*	*0.63 ± 0.18*	*0.86 ± 0.22*	*6.98 ± 0.16*	*0.67 ± 0.16*
(+)3-PPP	6.09 ± 0.14	-0.37 ± 0.09	0.40 ± 0.12	0.77 ± 0.13	1.06 ± 0.24	6.77 ± 0.19	0.21 ± 0.09
(-)3-PPP	6.15 ± 0.10	-0.53 ± 0.04	0.31 ± 0.14	0.67 ± 0.22	0.82 ± 0.34	6.40 ± 0.14	0.74 ± 0.16
Apomorphine	8.03 ± 0.20	-0.32 ± 0.12	0.51 ± 0.17	0.90 ± 0.23	1.12 ± 0.29	8.48 ± 0.10	0.71 ± 0.12
Aripiprazole	8.34 ± 0.19	-1.20 ± 0.26*	-0.30 ± 0.15	0.02 ± 0.09	0.29 ± 0.03	8.58 ± 0.27	0.07 ± 0.10*
Quinpirole (3)	*6.94 ± 0.22*	*-0.47 ± 0.06*	*0.22 ± 0.08*	*0.42 ± 0.08*	*0.57 ± 0.10*	*7.00 ± 0.20*	*0.69 ± 0.14*
Dihydroergocristine	8.13 ± 0.21	-1.36 ± 0.32*	-0.50 ± 0.08	-0.16 ± 0.10	0.04 ± 0.09	8.20 ± 0.21	0.05 ± 0.09*
Cabergoline	8.55 ± 0.14	-0.27 ± 0.03	0.48 ± 0.07	0.80 ± 0.13	0.82 ± 0.20	8.70 ± 0.21	0.89 ± 0.13
Pergolide	8.53 ± 0.16	-0.44 ± 0.03	0.43 ± 0.24	0.48 ± 0.08	0.61 ± 0.09	8.59 ± 0.22	0.76 ± 0.14
Lisuride	9.15 ± 0.10	-0.50 ± 0.05	0.45 ± 0.30	0.47 ± 0.10	0.58 ± 0.12	9.27 ± 0.09	0.70 ± 0.11

Table 5.9: Summary of Black and Leff and GDP dependence operational model fits to NMDG buffer data

Summary of both operational model fits to the NMDG buffer [^{35}S]-GTPγS binding data, corrected to account for only ligand dependent effects. Data are pooled (mean ± SEM) of 5 independent experiments performed in duplicate. *P<0.05; cf. corresponding quinpirole τ/τ_0.

5.2.7 Determination of agonist affinities using [^{3}H]-spiperone radioligand binding

In order to further examine the validity of the pK_As derived from operational modelling, radioligand binding experiments were conducted on D2S membranes in binding buffer containing either 100mM NaCl or 100mM NMDG in order to closely match experimental conditions to the [^{35}S]-GTPγS binding experiments. Initially, saturation experiments were conducted on D2S membranes in both NaCl and NMDG buffers (**Figure 5.21**). B_{max} values were calculated as 4.73 ± 0.56 pmol mg^{-1} and 4.16 ± 0.96 pmol mg^{-1} with [^{3}H]-spiperone pK_Ds calculated as 9.79 ± 0.08 and 9.94 ± 0.13 for NaCl and NMDG buffers respectively (n=4). The differences in B_{max} and pK_D between the buffers were not significant (P>0.05; Student's unpaired t-test).

Competition binding experiments were then performed with the same panel of ligands used for modelling in both buffers (**Figure 5.22, Table 5.10**). Ligands were fitted to either one- or two-site binding models as appropriate, determined by an extra sum of squares F-test in GraphPad Prism. In the NaCl buffer, most ligands were best fit with a two-site binding model, except for the ergo-derivatives, aripiprazole and 7OH-DPAT. Substitution of NaCl for NMDG in the binding buffer appeared to increase the detection of high affinity binding sites for a number of compounds; for example a second binding site was detected for 7OH-DPAT (P<0.05; extra sum of squares F-test) and the percentage of high affinity binding was increased for most ligands displaying two site binding. However, when statistical comparisons were made for each individual ligand, no changes were significant (P>0.05; Student's unpaired t-test).

Affinities derived through operational modelling (pK_A) were compared to those derived from competition binding experiments (pK_i) in both NaCl and NMDG buffers (**Table 5.11, Table 5.12, Figure 5.23**). For NaCl buffer experiments, those ligands which displayed a single site in the [^{3}H]-spiperone competition binding experiments showed no significant differences to the

functionally derived pK_As for either operational model except for 7OH-DPAT and (-)-3-PPP ($P<0.05$, Student's unpaired t-test). 7OH-DPAT pK_As were 4.6-fold higher than the derived pK_i and (-)-3-PPP pK_As 28.8-31.6-fold higher. For those compounds that displayed two site binding, while there were significant differences in the derived pK_is and pK_As, the pK_A values tended to lie between the pK_i low and pK_i high values. However, there was a good correlation between pK_i low and pK_A for both operational models in the NaCl buffer (**Figure 5.23**). Similar results were obtained in the NMDG buffer, with no significant differences between pK_A and pK_i for single site binders and pK_As for two-site binders lying between pK_i low and pK_i high. The exceptions were pergolide and (-)-3-PPP whose pK_A was not significantly different from pK_i high ($P>0.05$; Student's unpaired t-test).

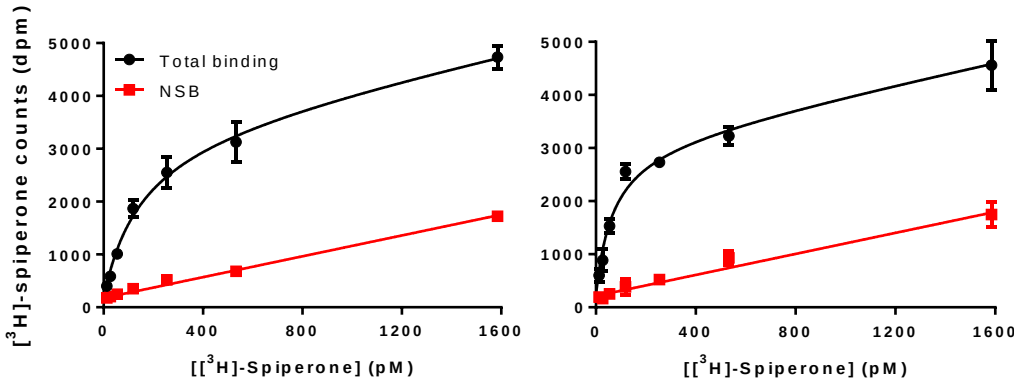


Figure 5.21: Saturation binding of D2S membranes in NaCl and NMDG binding buffers

Membranes were incubated with increasing concentrations of [^{3}H]-spiperone for 3h prior to filtration in both NaCl (left) and NMDG (right) binding assay buffers. Non-specific binding (NSB) was determined in the presence of 3µM (+)-butaclamol. Data are from a single experiment (mean ± range) representative of 5 independent experiments performed in duplicate.

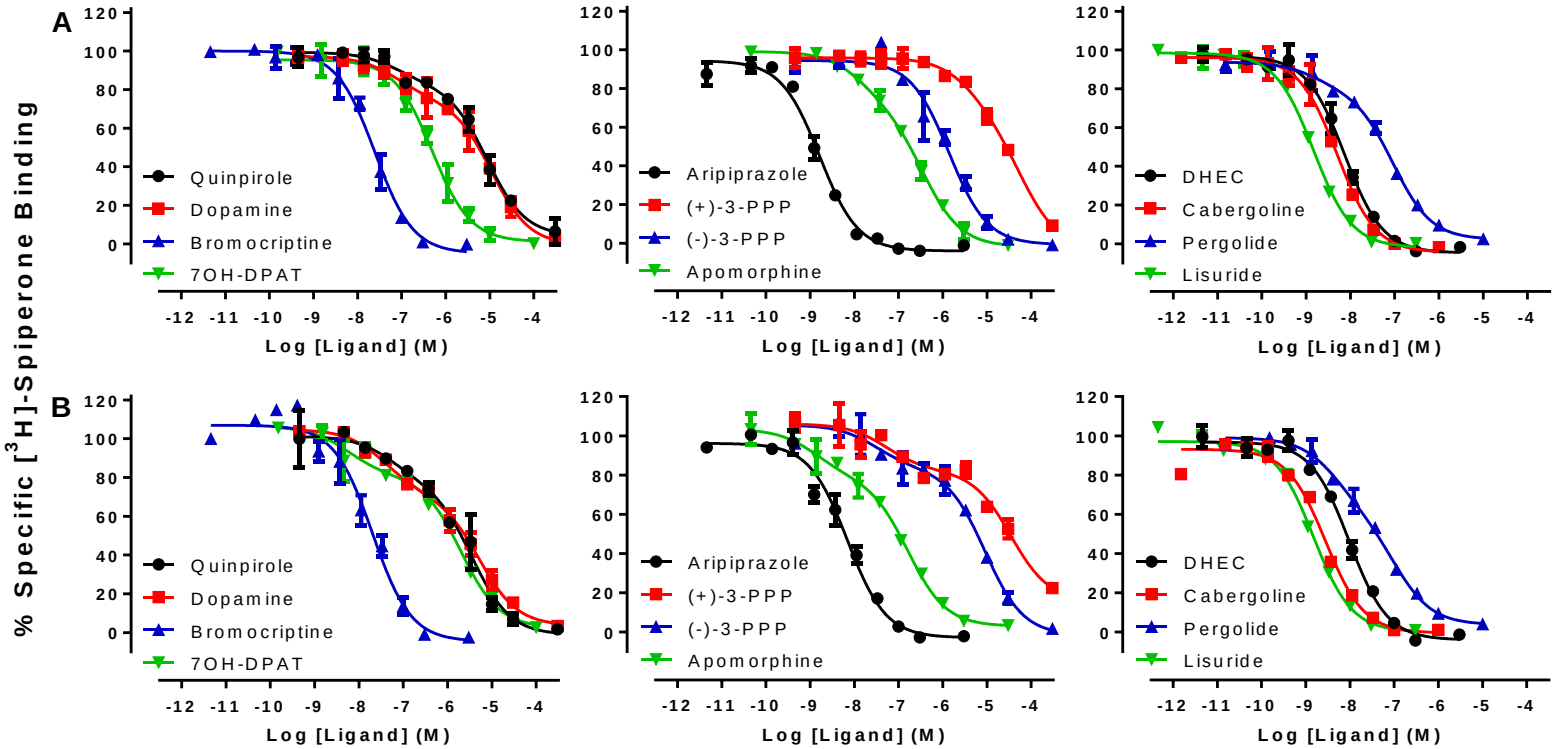


Figure 5.22: Determination of ligand affinities at the dopamine D2S receptor

Increasing concentrations of competing ligands were incubated with 80-150pM [^{3}H]-spiperone for 3h prior to filtration in both NaCl (**A**) and NMDG binding buffers (**B**). Ligand affinities were calculated using the Cheng-Prusoff correction with data are summarised in **Table 5.10**. Data points show a representative experiment (mean ± range) of 4 independent experiments performed in duplicate.

Ligand	NaCl			NMDG		
	pK_i Low	pK_i High	% High	pK_i Low	pK_i High	% High
Quinpirole	5.55 ± 0.11	7.30 ± 0.27	20.9 ± 2.9	5.70 ± 0.09	7.71 ± 0.17	30.6 ± 3.0
Dopamine	5.50 ± 0.09	7.46 ± 0.19	29.8 ± 4.2	5.45 ± 0.06	7.88 ± 0.19	38.4 ± 3.1
Bromocriptine	8.03 ± 0.15	-	-	7.90 ± 0.06	-	-
7OH-DPAT	6.79 ± 0.14	-	-	5.94 ± 0.04	8.37 ± 0.23	32.8 ± 2.9
Aripiprazole	8.68 ± 0.15	-	-	8.63 ± 0.17	-	-
(+)-3-PPP	4.71 ± 0.16	6.72 ± 0.47	18.6 ± 3.4	4.96 ± 0.09	7.29 ± 0.15	27.5 ± 1.1
(-)-3-PPP	6.00 ± 0.14	-	-	5.46 ± 0.05	7.24 ± 0.30	28.6 ± 1.9
Apomorphine	6.84 ± 0.15	8.79 ± 0.20	26.1 ± 3.6	6.94 ± 0.09	8.97 ± 0.19	25.6 ± 2.9
Dihydroergocristine	8.30 ± 0.03	-	-	8.34 ± 0.06	-	-
Cabergoline	8.67 ± 0.22	-	-	8.75 ± 0.06	-	-
Pergolide	7.46 ± 0.21	9.28 ± 0.17	18.8 ± 2.9	7.21 ± 0.20	8.64 ± 0.23	47.6 ± 9.4
Lisuride	9.31 ± 0.12	-	-	9.12 ± 0.04	-	-

Table 5.10: Summary of ligand affinities at the D2S receptor in both NaCl and NMDG binding buffers

Summary of competition binding data shown in **Figure 5.22**. IC_{50}s were converted to pK_is using the Cheng-Prusoff correction and the [^{3}H]-spiperone pK_D calculated from saturation binding experiments. Data represent pooled data (mean ±SEM) of 4 independent experiments performed in duplicate.

Ligand	Modelling pK_A		NaCl Radioligand Binding		
	Receptor Depletion	GDP Dependence	pK_i Low	pK_i High	% High
Quinpirole (1)	6.07 ± 0.12*	6.29 ± 0.09*			
Quinpirole (2)	5.92± 0.12	6.35 ± 0.07*	5.55 ± 0.11	7.30 ± 0.27	20.9 ± 2.9
Quinpirole (3)	6.05 ± 0.11*	6.36 ± 0.04*			
Dopamine	5.83 ± 0.05*	5.96 ± 0.02*	5.50 ± 0.09	7.46 ± 0.19	29.8 ± 4.2
Bromocriptine	8.09 ± 0.07	8.12 ± 0.10	8.03 ± 0.15	-	-
7OH-DPAT	7.45 ± 0.04*	7.46 ± 0.05*	6.79 ± 0.14	-	-
Aripiprazole	ND	ND	8.68 ± 0.15	-	-
(+)-3-PPP	5.71 ± 0.14*	5.96 ± 0.10*	4.77 ± 0.21	6.76 ± 0.66	20.1 ± 4.3
(-)-3-PPP	7.46 ± 0.17*	7.50 ± 0.18*	6.00 ± 0.14	-	-
Apomorphine	7.53 ± 0.07*	7.86 ± 0.13*	6.84 ± 0.15	8.79 ± 0.20	26.1 ± 3.6
Dihydroergocristine	8.58 ± 0.17	8.56 ± 0.15	8.30 ± 0.03	-	-
Cabergoline	8.60 ± 0.11	8.69 ± 0.11	8.67 ± 0.22	-	-
Pergolide	7.87 ± 0.15	8.04 ± 0.11	7.46 ± 0.21	9.28 ± 0.17	18.8 ± 2.9
Lisuride	9.52 ± 0.13	9.60 ± 0.15	9.31 ± 0.12	-	-

Table 5.11: Comparison of modelling pK_A values with competition binding derived pK_i values from NaCl buffer experiments

Summary of derived affinities of agonists from both operational modelling and competition binding experiments. Data are pooled (mean ± SEM) of 4-6 independent experiments performed in duplicate. ND = not determined;* $P<0.05$ c.f. pK_i low (Student's unpaired t-test)

Ligand	Modelling pK_A	NMDG Radioligand Binding		
	Slack and Hall	pK_i Low	pK_i High	% High
Quinpirole (1)	6.87 ± 0.14*#			
Quinpirole (2)	6.97 ± 0.18*#	5.70 ± 0.09	7.71 ± 0.17	30.6 ± 3.0
Quinpirole (3)	7.06 ±0.18*#			
Dopamine	7.05 ± 0.16*#	5.45 ± 0.06	7.88 ± 0.19	38.4 ± 3.1
Bromocriptine	7.57 ± 0.12	7.90 ± 0.06	-	-
7OH-DPAT	7.21 ± 0.10*#	5.94 ± 0.04	8.37 ± 0.23	32.8 ± 2.9
Aripiprazole	8.64 ± 0.52	8.63 ± 0.17	-	-
(+)-3-PPP	6.29 ± 0.10*#	4.96 ± 0.09	7.29 ± 0.15	27.5 ± 1.1
(-)-3-PPP	6.34 ± 0.21*	5.46 ± 0.05	7.24 ± 0.30	28.6 ± 1.9
Apomorphine	8.40 ± 0.09*#	6.94 ± 0.09	8.97 ± 0.19	25.6 ± 2.9
Dihydroergocristine	8.09 ± 0.33	8.34 ± 0.06	-	-
Cabergoline	8.68 ± 0.19	8.75 ± 0.06	-	-
Pergolide	8.55 ± 0.12*	7.21 ± 0.20	8.64 ± 0.23	47.6 ± 9.4
Lisuride	9.31 ± 0.08	9.12 ± 0.04	-	-

Table 5.12:Comparison of modelling pK_A values with competition binding derived pK_i values from NMDG buffer experiments

Summary of derived affinities of agonists from both operational modelling and competition binding experiments. Data are pooled (mean ± SEM) of 4-5 independent experiments performed in duplicate.*P<0.05 c.f. pK_i low, # P<0.05 c.f. pK_i high; (Student's unpaired t-test)

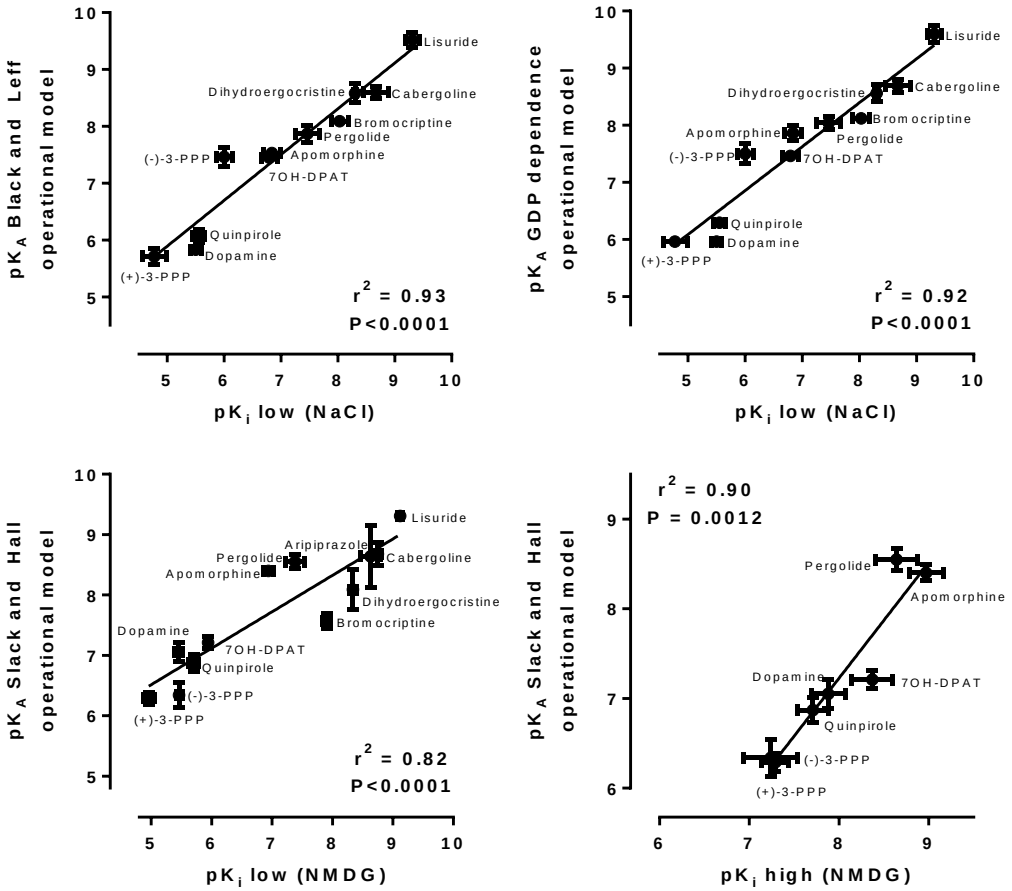


Figure 5.23: Correlation of affinities generated through competition binding and operational modelling

Correlation plots showing the relationship between pK_A derived through operational modelling of [^{35}S]-GTPγS binding data and the pK_i derived from competition binding against [^{3}H]-spiperone in both NaCl and NMDG containing buffers. Data are reproduced from **Table 5.11** and **Table 5.12** with data points representing pooled (mean ± SEM) of 4-5 independent experiments.

5.2.8 Comparison of operational model data fits between GraphPad Prism and Microsoft Excel

One of the disadvantages of the GraphPad Prism fits is that fitting data with shared parameters in this manner can only be achieved by simultaneous analysis of a maximum of six data sets. This required 3 separate data fits rather than a true 'global' fit of the data set as a whole. In order to examine whether the parameters derived through GraphPad Prism were an accurate representation of the data set as a whole, the GDP dependence and the Slack and Hall operational models were programmed into Microsoft Excel (David Hall; GSK, Stevenage) and the analysis repeated. As shown in the example data sets in **Figure 5.24**, the GDP dependence model in Microsoft Excel format allowed the simultaneous analysis of both the GDP concentration response curve and all 12 agonist data sets. Furthermore, no baseline correction of the agonist concentration response data was necessary as the Excel model uses the GDP concentration response curve to define the basal values at each GDP concentration. However, Microsoft Excel did fail to fit the model to one family of curves from both dihydroergocristine and (-)-3-PPP resulting in their exclusion from the final data set. As seen in **Table 5.13**, despite the restricted data sets in the GraphPad Prism fits, there were no significant differences in the derived parameters except for the dopamine pK_A ($P = 0.047$; Student's unpaired t-test).

In order to fit the GDP dependence operational model in GraphPad Prism, K_{GDP} and s were constrained to the IC_{50} and Hill slope from the concurrently performed GDP concentration response curve whereas Microsoft Excel allows the model to find the most suitable solution. There were no significant differences between the constraints applied in GraphPad Prism and the parameters derived in the Microsoft Excel fits; Microsoft Excel fits derived K_{GDP} as 6.87 ± 0.05 and s as 0.72 ± 0.01 whereas GraphPad Prism fits were constrained to the pEC_{50} 6.91 ± 0.06 and Hill slope of 0.73 ± 0.02.

As shown in the example data sets in **Figure 5.25**, the Slack and Hall operational model was also programmed into Microsoft Excel, allowing the simultaneous analysis of all 12 agonist data sets. Like the GDP dependence data sets, there were no significant differences between the derived parameters by each programme (**Table 5.14, Figure 5.26**).

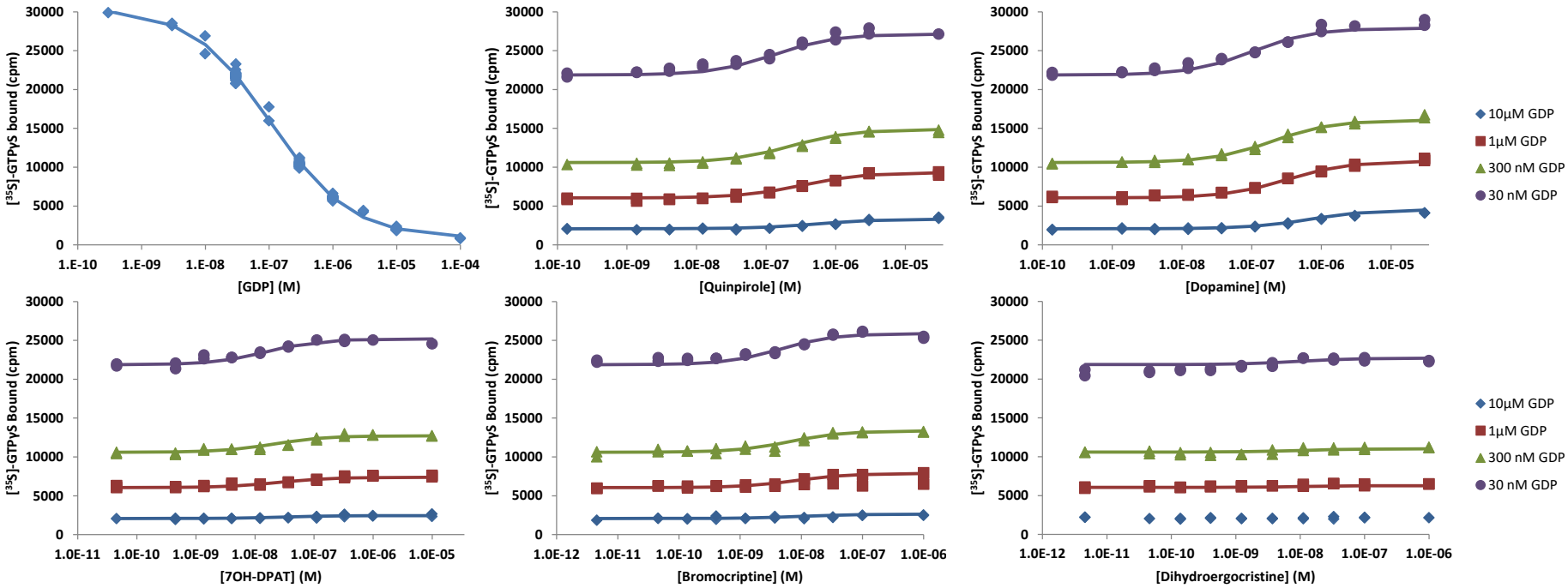


Figure 5.24: Fitting the GDP dependence operational model in Microsoft Excel

[^{35}S]-GTPγS binding NaCl buffer data were re-analysed using Microsoft Excel, simultaneously fitting the GDP and all 12 agonist data sets with data summarised in **Table 5.13**. Data shown are from an individual representative experiment, with data points from each replicate in the graphs, from 5 independent experiments performed in duplicate.

Ligand	pK_A Excel	$Log\tau_0$ Excel	pK_A GraphPad	$Log\tau_0$ GraphPad
Quinpirole	6.42 ± 0.10	0.83 ± 0.11	6.29 ± 0.09	0.80 ± 0.22
Dopamine	6.21 ± 0.11*	0.98 ± 0.10	5.96 ± 0.02	1.07 ± 0.19
Bromocriptine	8.15 ± 0.06	0.23 ± 0.09	8.12 ± 0.10	0.30 ± 0.13
7OH-DPAT	7.65 ± 0.19	0.06 ± 0.10	7.46 ± 0.05	0.09 ± 0.15
QP (PPP set)	-	-	*6.35 ± 0.07*	*0.71 ± 0.07*
(+)-3-PPP	6.23 ± 0.21	0.58 ± 0.08	5.96 ± 0.10	0.54 ± 0.06
(-)-3-PPP	7.38 ± 0.17	-0.33 ± 0.16	7.50 ± 0.18	-0.30 ± 0.04
Apomorphine	7.77 ± 0.05	0.68 ± 0.10	7.86 ± 0.13	0.56 ± 0.06
QP (DHEC set)	-	-	*6.36 ± 0.04*	*0.73 ± 0.08*
Dihydroergocristine	8.86 ± 0.92	-0.59 ± 0.15	8.56 ± 0.15	-0.45 ± 0.03
Cabergoline	8.65 ± 0.15	0.68 ± 0.17	8.69 ± 0.11	0.68 ± 0.10
Pergolide	7.85 ± 0.13	0.43 ± 0.17	8.04 ± 0.11	0.53 ± 0.09
Lisuride	9.38 ± 0.11	-0.01 ± 0.12	9.60 ± 0.15	0.02 ± 0.06

Table 5.13: Comparison of GDP dependence operational model fits in GraphPad Prism and Microsoft Excel

Summary of the parameters derived from the Microsoft Excel data fits, compared with the GraphPad Prism fits in **Table 5.5**. One set of dihydroergocristine and (-)-3-PPP data sets from the Excel fits were excluded due to a lack of fit. There were no significant differences between any of the derived parameters except for dopamine pK_A (Student's unpaired t-test, p=0.047). Data are pooled (mean ± SEM) of 5-6 independent experiments performed in duplicate; * P<0.05 c.f. pK_A GraphPad.

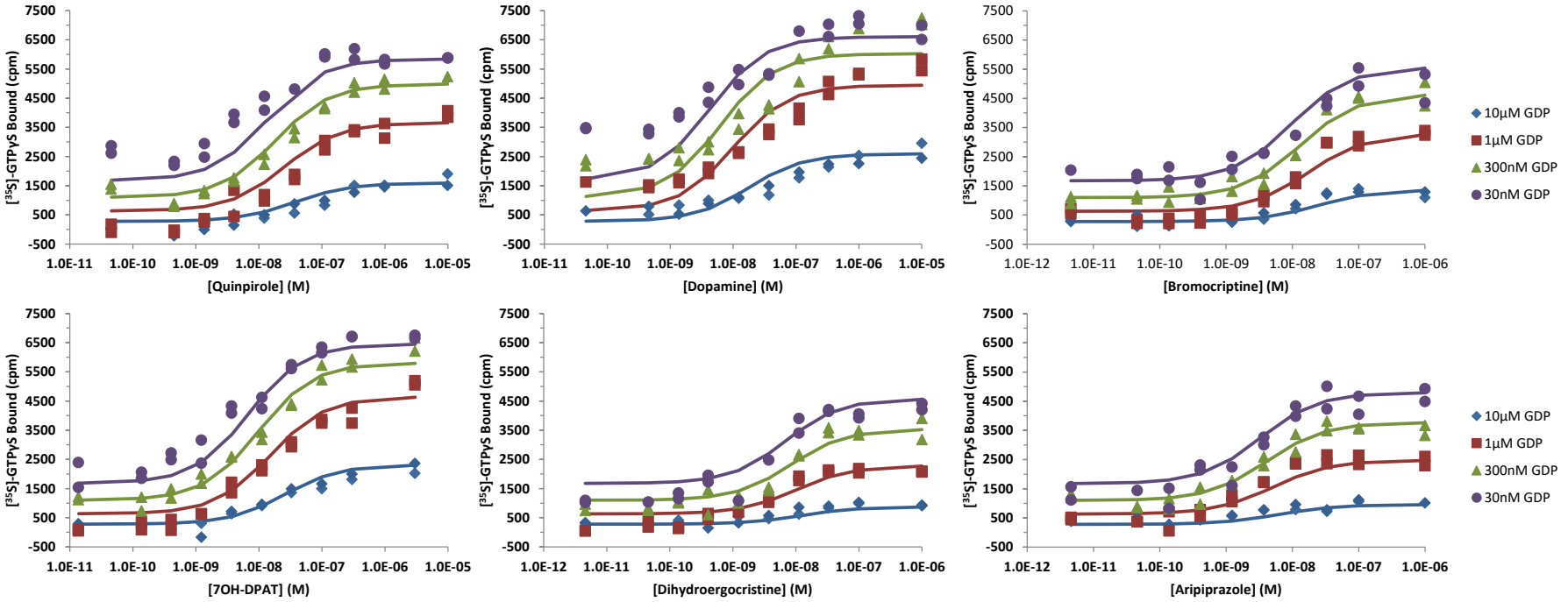


Figure 5.25: Fitting the Slack and Hall operational model in Microsoft Excel

[^{35}S]-GTPγS binding NMDG buffer data were re-analysed using Microsoft Excel, simultaneously analysing all 12 agonist data sets with data summarised in **Table 5.14.** Data shown are from an individual representative experiment, with data points from each replicate in the graphs, from 5 independent experiments performed in duplicate.

Ligand	pK_A excel	Logε excel	pK_A GraphPad	Logε GraphPad
Quinpirole	7.03 ± 0.12	1.40 ± 0.13	6.87 ± 0.14	1.36 ± 0.21
Dopamine	7.09 ± 0.19	1.64 ± 0.16	7.05 ± 0.16	1.52 ± 0.16
Bromocriptine	7.61 ± 0.09	1.38 ± 0.20	7.57 ± 0.12	1.28 ± 0.20
7OH-DPAT	7.24 ± 0.13	1.55 ± 0.19	7.21 ± 0.10	1.44 ± 0.20
Quinpirole (PPP set)	-	-	*6.97 ± 0.18*	*1.22 ± 0.08*
Aripiprazole	8.83 ± 0.62	0.78 ± 0.02	8.64 ± 0.52	0.74 ± 0.03
(+)-3-PPP	6.33 ± 0.07	1.26 ± 0.08	6.29 ± 0.10	1.24 ± 0.10
(-)-3-PPP	6.77 ± 0.15	1.01 ± 0.09	6.34 ± 0.21	1.06 ± 0.12
Apomorphine	8.54 ± 0.09	1.27 ± 0.03	8.40 ± 0.09	1.29 ± 0.07
Quinpirole (DHEC set)	-	-	*7.06 ± 0.18*	*1.24 ± 0.04*
Dihydroergocristine	8.11 ± 0.37	0.69 ± 0.09	8.09 ± 0.33	0.70 ± 0.04
Cabergoline	8.69 ± 0.21	1.37 ± 0.05	8.68 ± 0.19	1.40 ± 0.05
Pergolide	8.58 ± 0.13	1.21 ± 0.05	8.55 ± 0.12	1.23 ± 0.04
Lisuride	9.26 ± 0.08	1.19 ± 0.07	9.31 ± 0.08	1.20 ± 0.05

Table 5.14: Comparison of Slack and Hall operational model fits in GraphPad Prism and Microsoft Excel

Summary of the parameters derived from the Microsoft Excel data fits, compared with the GraphPad Prism fits in **Table 5.7**. There were no significant differences between any of the derived parameters (Student's unpaired t-test). Data are pooled (mean ± SEM) of 5 independent experiments performed in duplicate.

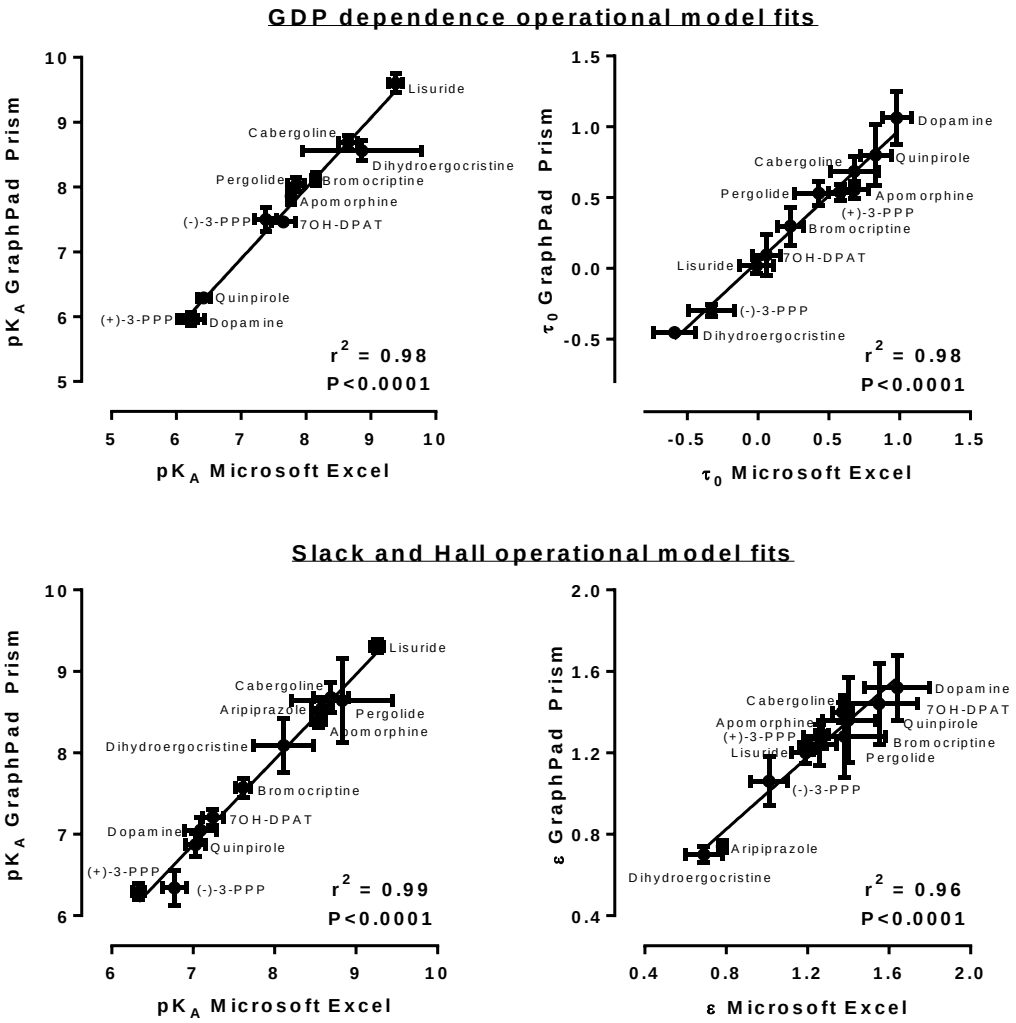


Figure 5.26: Correlation between Microsoft Excel and GraphPad Prism data fits

Relationship between the ligand affinities and efficacies derived through application of the GDP dependence and Slack and Hall operational models in GraphPad Prism and Microsoft Excel. Data are reproduced from **Table 5.13** and **Table 5.14** and expressed as mean ± SEM of 5-6 independent experiments performed in duplicate.

5.3 Discussion

Here, we have explored the use of different operational model approaches to determine agonist efficacy and affinity at the dopamine D2 receptor using [^{35}S]-GTPγS binding assays. When compared with the Black and Leff operational model, the GDP dependence model generated a single, global efficacy estimate whilst producing similar affinity estimations. The Slack and Hall operational model was applied to data within a constitutively active system to derive system independent ligand intrinsic efficacy values; however the necessary removal of buffer Na^+ limited agonist efficacy discriminations. For all models, functional affinities were generally matched with radioligand binding measurements although two-site binding for a number of agonists led to misaligned functional affinity estimations. Additionally, a comparison of analyses between GraphPad Prism and Microsoft Excel demonstrated good agreement between the different software packages.

5.3.1 Optimisation of [^{35}S]-GTPγS binding assays

As described in **5.1.1**, [^{35}S]-GTPγS binding assays allow the direct measurement of one of the initial stages of GPCR signal transduction – the activation of G proteins. For determination of agonist efficacy, this assay has a limited receptor reserve and offers the ability to equilibrate agonist binding prior to [^{35}S]-GTPγS addition (**5.3.3**). Initially, it was important to optimise assay conditions to ensure adequate signal window for subsequent measurements. In line with previous studies (Gardner *et al.*, 1996; Hilf *et al.*, 1989), [^{35}S]-GTPγS binding showed an initial, linear phase followed by saturation of the signal (**Figure 5.2**) therefore a time point (20min) was chosen to ensure the greatest signal window without signal saturation. Time course experiments also provided a preliminary examination of the ability of the different D2 receptors to induce [^{35}S]-GTPγS binding with the D2S displaying a much greater agonist stimulated [^{35}S]-GTPγS binding than D2L or D2L T6.34R. An early study noted that D2S was able to generate a larger [^{35}S]-GTPγS binding signal than D2L (Gardner *et al.*, 1996) which is in agreement with the results here. However both in that study and here, the D2S receptor

was expressed around twice as highly as D2L, which may account for this difference. D2L T6.34R membranes had the lowest signal window in this assay although that may be due to their much lower expression level (around one third and one fifth of D2L and D2S expression respectively (**3.2.5**, **4.2.2**)). A previous study with the equivalent mutation in D2S demonstrated that both D2S and D2S T343R could inhibit forskolin-stimulated cAMP production to the same extent when expressed at the same level (Wilson *et al.*, 2001), suggesting the lack of signal window here is not due to reduced coupling of the receptor to effector proteins but a reduced receptor expression.

Furthermore, as described in **5.1.2**, Na^+ buffer concentration can have significant effects on signal window. Na^+ has been shown to have biphasic effects on agonist response, with increasing Na^+ concentration increasing assay signal windows but decreasing it at high concentrations (Szekeres *et al.*, 1997). As shown in **Figure 5.4**, while increasing NaCl concentration from 100mM to 150mM appeared to increase assay window, there was a suppression of bound [^{35}S]-GTPγS. As such, 100mM NaCl was chosen as the optimal concentration for further assays.

5.3.2 Detection of constitutive activity at the D2 receptor

To allow the use of the Slack and Hall operational model, it was necessary to identify a constitutively active system to which the model could be applied. As there was little evidence from initial studies with the CHOcs ssD2L cell line for receptor constitutive activity (**3.3.3**), an attempt was made to create a constitutively active mutant. As described in **4.1.1**, T6.34R mutation of the D2S receptor leads to constitutive activity (Wilson *et al.*, 2001). It was hoped that the homologous mutation in D2L would render the receptor constitutively active. While evidence from initial CRE-SPAP reporter gene and receptor internalisation assays suggested the receptor was adopting a more active conformation, there was little evidence to suggest this led to receptor constitutive activity (**4.3.3**). As such, both D2L and D2L T6.34R receptors were examined in [^{35}S]-GTPγS binding assays to test their suitability for future operational modelling. The D2S receptor was also examined as a number of

reports on D2 ligand inverse agonism were from studies with the D2S receptor (Hall *et al.*, 1997; Roberts *et al.*, 2004; Roberts *et al.*, 2005; Wilson *et al.*, 2001).

As discussed in **5.1.1**, experimental conditions for [^{35}S]-GTPγS binding assays can be manipulated to favour either agonism or inverse agonism. Conditions for inverse agonism at the D2 receptor tend to be optimised in the absence of GDP in a Na^+ free buffer (Strange, 2010). It has been proposed that the removal of Na^+ renders the receptor more easily activated (Lin *et al.*, 2006). The allosteric effect of Na^+ on D2 receptor responses has been well documented with the Na^+ binding site identified from both mutagenesis studies and molecular dynamics simulations (Neve, 1991; Neve *et al.*, 1991; Neve *et al.*, 2001; Selent *et al.*, 2010). Molecular dynamic simulations suggest that the binding of Na^+ to residue D2.50 generates a conformational change in the receptor to an inactive state. Na^+ binding rotates W6.48 (the so-called 'toggle switch' (Schwartz *et al.*, 2006)) to its inactive conformation, which may also restrict agonist binding to the orthosteric site (Selent *et al.*, 2010). As such, the removal of Na^+ may increase agonist effects, and allow the detection of inverse agonists, by increasing the likelihood that the receptor adopts an active state. Interestingly this effect has been shown to be specific for NMDG substitution as replacement with K^+ or Li^+ did not have the same effect (Lin *et al.*, 2006).

The ability of reported inverse agonists to inhibit D2L, D2L T6.34R or D2S receptor constitutive activity was investigated in NaCl and NMDG containing buffers (**Figure 5.5**). Of the cell lines and conditions tested, only the D2S membranes with NMDG buffer substitution showed robust constitutive activity. No responses were seen with the D2L T6.34R line, even with buffer substitution, suggesting this mutation does not generate a constitutively active D2L receptor despite the evidence for constitutive activity in the homologous D2S mutation (Wilson *et al.*, 2001). This might be due to the reduced expression level in this cell line; high receptor expression is known to increase the detection of inverse agonism by increasing the absolute numbers

of receptors in the active state (Seifert *et al.*, 2002). However, the lack of robust constitutive activity in either D2L or D2L T6.34R expressing membranes suggests that overall, the D2S receptor is more prone to constitutive activity than the D2L receptor. Molecular dynamic simulations on an active state D2 receptor homology model have suggested that a number of residues in ICL3 (the location of the deletion in the D2S receptor) create contacts with the G protein (Kling *et al.*, 2013; Kling *et al.*, 2014). It is possible that the 29 amino acid deletion in the short isoform alters the ability of the receptor-G protein complex to form under basal conditions, increasing the likelihood that the receptor will adopt an active conformation capable of G protein stimulation in the absence of agonist occupancy.

5.3.3 The applicability of [^{35}S]-GTPγS binding assays to operational modelling

[^{35}S]-GTPγS binding assays should provide a good system for operational modelling whereby a number of its inherent assumptions can be fulfilled. One of the main assumptions of the operational model is that a dynamic equilibrium between ligand and receptor has been reached (Black *et al.*, 1983; Black *et al.*, 1985; Stott *et al.*, 2016). In many cellular assays, a number of signalling events are transient and as such, reaching equilibrium can be difficult, even impossible. This has been previously discussed in the context of calcium assays which often peak within seconds of agonist stimulation (Charlton *et al.*, 2010), before an agonist has had the chance to equilibrate with the receptor. More recently, this has been investigated in a study at the D2 receptor where the operational model was used in the calculation of ligand bias (Klein Herenbrink *et al.*, 2016). Measurements were initially taken at 5min as this equalled the shortest time to reach a peak measurement (ERK1/2 phosphorylation) for the readouts measured. However, further kinetic experiments revealed that some of the compounds with slower kinetics, aripiprazole and bifeprunox, would not have reached 50% occupancy by that time point and hence would not have reached equilibrium. When compounds were examined over increasing time points, bias profiles were

altered, demonstrating the importance of equilibrium and how pre-equilibrium measurements can significantly change obtained results (Klein Herenbrink *et al.*, 2016). With [^{35}S]-GTPγS binding assays detailed here, ligands were pre-incubated for 1h prior to addition of radioligand. Extending the ligand pre-incubation time had generally no effect on quinpirole, (+)-butaclamol or (-)-butaclamol responses at maximal concentrations (**Figure 5.3**), and therefore the measurements obtained after 1h should be at equilibrium for agonist binding to the receptor. It would be useful to verify this for a greater range of compounds and at lower concentrations (where the observed association rate is lower (Hulme *et al.*, 2010)), but recent agonist kinetic studies at the D2L receptor do suggest that after 1h, all compounds examined in this study are at equilibrium (DA Sykes, personal communication).

One of the main advantages of [^{35}S]-GTPγS binding assays over other downstream measurements of GPCR signalling is the relative lack of amplification inherent in the assay due to its early position in the signalling cascade. Studies at both the α_{2C}-adrenoceptor and μ-opioid receptor have confirmed using the methods of Furchgott (Furchgott, 1966) and the Black and Leff operational model respectively, that [^{35}S]-GTPγS binding assays have lower receptor reserve than downstream measures such as cAMP accumulation (Nickolls *et al.*, 2011; Umland *et al.*, 2001). As such, this assay tends to provide a greater definition of ligand efficacies from their R_{max} alone, due to a reduced system input to the response. Where there is no signal amplification in an assay, it has also been suggested that the operational model should not be applied to the derived data (Nickolls *et al.*, 2011). Under such conditions, the model simplifies; τ can be defined based on R_{max} and K_A on EC_{50}, which should not change with decreased system coupling efficiency (normally through receptor depletion) (Stott *et al.*, 2016). However, in the [^{35}S]-GTPγS binding assays in this study, the decreased agonist R_{max} with increasing GDP concentration is associated with a change in potency. This suggests there is at least a small level of receptor reserve in this system. As

discussed in **3.3.8**, there can be discrepancies in derived operational model parameters when transducers are far in excess of receptor, such as in reporter gene readouts (Leff *et al.*, 1989). [^{35}S]-GTPγS binding assays should therefore lie between these extremes of transducer:receptor ratios, whereby the model should provide more reliable estimations of efficacy and affinity.

5.3.4 Estimation of agonist affinity and efficacy using the Black and Leff operational model

While the lack of constitutive activity in the NaCl buffer precludes the use of the Slack and Hall operational model, it allows an exploration and comparison of the applicability of the Black and Leff operational model in a system whereby K_E is varied. Most studies which utilise the operational model of agonism apply the receptor depletion method (Black *et al.*, 1985) in which irreversible antagonists are used to decrease the active receptor population and thus reduce τ (via change in R_T) (**3.3.8**) (Giembycz, 2009; Navratilova *et al.*, 2007; Nickolls *et al.*, 2011; Simon *et al.*, 2009). If using a membrane-based assay, such as [^{35}S]-GTPγS binding, this requires additional irreversible antagonist pre-treated membranes. However, because agonist responses are dependent on GDP concentration, varying this can create a similar curve series with changing EC_{50} and R_{max} without the need for irreversible antagonism treatment (Slack *et al.*, 2012). These manipulations still alter the system dependent component of τ but in this case, K_E is varied rather than R_T, with the assumption that K_E is a simple function of GDP concentration which results in decreasing τ values with increasing GDP concentration as the GDP competes for [^{35}S]-GTPγS binding.

The Black and Leff operational model was applied to agonist [^{35}S]-GTPγS binding data in the presence of four GDP concentrations, deriving agonist affinity and efficacy estimations in the form of pK_A and τ values. Agonist efficacy estimations correlated well with the known pharmacology of the compounds under investigation when traditional R_{max} comparisons have been made in poorly amplified signalling endpoints e.g. β-arrestin recruitment,

[^{35}S]-GTPγS binding with a lower expressing cell line (Gardner *et al.*, 1998; Klewe *et al.*, 2008) or receptor internalisation assays (**3.2.4**). However, one outlying compound is 7OH-DPAT, which was a partial agonist in the [^{35}S]-GTPγS binding assay with a τ value significantly lower than quinpirole. Previous studies both within this thesis and in the literature suggest 7OH-DPAT is a full agonist (or at least a strong partial agonist) relative to quinpirole (**3.2**) or dopamine at the D2 receptor (Hall *et al.*, 1999; Payne *et al.*, 2002; Tadori *et al.*, 2011a). In the low reserve D2L receptor internalisation assay, in which ligand R_{max} should be a good indicator of efficacy, 7OH-DPAT is a full agonist (**3.2.4**). However there are some studies employing [^{35}S]-GTPγS binding assays that have demonstrated that 7OH-DPAT, like here, is a weak partial agonist. In an investigation of D2L-$G\alpha_{i/o}$ fusion proteins, it was shown that 7OH-DPAT was a partial agonist at inducing [^{35}S]-GTPγS binding at $G\alpha_{i1}$, $G\alpha_{i3}$ and $G\alpha_{o1}$ but not at $G\alpha_{i2}$ (Lane *et al.*, 2007). It is possible that signal amplification in other studies is obscuring the lower intrinsic efficacy of 7OH-DPAT. Alternatively, the involvement of other GPCR signalling partners such as β-arrestins (e.g. in receptor internalisation assays) may make 7OH-DPAT appear more efficacious than its true intrinsic efficacy for G protein mediated responses. However to date, no studies have examined the bias profile of 7OH-DPAT for G protein and β-arrestin responses.

When the functional affinities were compared with those derived through traditional radioligand binding experiments, there were significant differences for a number of compounds (**Table 5.11**). As described in **3.3.6**, it is thought that pK_A values derived from whole cell functional data should correspond with pK_i low due to the high cellular concentrations of guanine nucleotide (Strange, 2008). While [^{35}S]-GTPγS binding assays are performed on membranes, guanine nucleotides are added to the assay (principally GDP) which should result in the pK_A being more comparable with the pK_i low. However the presence of two-site binding for a number of compounds suggests that the pK_A derived from [^{35}S]-GTPγS binding assays may reflect a composite of both the high and low affinity binding sites. This discrepancy

might be resolved by including a high concentration of GDP in the radioligand binding buffer to more closely match the [^{35}S]-GTPγS binding assay conditions. It has been suggested that operational modelling of [^{35}S]-GTPγS binding can lead to overestimations of ligand pK_A values when compared with radioligand competition binding data. However, it was acknowledged that differences in guanine nucleotide concentrations between the assays conducted may account for these differences, similar to the data presented here (Nickolls *et al.*, 2011).

The only compounds which displayed single-site binding and a significantly higher pK_A than pK_i were 7OH-DPAT and (-)-3-PPP. The pK_A of (-)-3-PPP is of particular interest as it is much higher than may have been predicted from literature data (which is in agreement with the pK_i presented here) (Gardner *et al.*, 1997; Lin *et al.*, 2006). Normally classed as a low affinity, weak partial agonist, even in the highly amplified SPAP assay in CHOcs ssD2L cells, its EC_{50} was still nearly 10-fold lower than the functional affinity derived here (**3.2.3**). This is unusual because in highly amplified systems, EC_{50}s tend to be decreased compared to affinities, and only through reduction of system coupling does the EC_{50} approach the K_A (Stott *et al.*, 2016). Most studies which have examined (-)-3-PPP responses in [^{35}S]-GTPγS binding have used 1-10μM GDP to optimise signal window but at these GDP concentrations, responses to weak partial agonists are often small and can be difficult to detect (Gardner *et al.*, 1997; Koener *et al.*, 2012; Lin *et al.*, 2006). Decreasing the GDP concentration appears to have a similar effect to buffer Na^+ removal or increasing receptor density to improve partial agonist detection. At lower GDP concentrations, (-)-3-PPP was much more potent at inducing [^{35}S]-GTPγS binding than has been previously reported, leading to higher derived functional affinity. It has been suggested that (-)-3-PPP may be moderately biased towards $G\alpha_{i1}$ activation over cAMP production (Klein Herenbrink *et al.*, 2016) although earlier studies with fusion proteins suggested (-)-3-PPP could not activate $G\alpha_{i1}$ or $G\alpha_{i2}$ (Gazi *et al.*, 2003; Lane *et al.*, 2007).

5.3.5 Estimation of agonist affinity and efficacy using the GDP dependence operational model

While the Black and Leff operational model does provide a greater discrimination of ligand efficacies at a single signalling endpoint than traditional R_{max} comparisons, the inherent system dependence of τ means it is difficult to compare τ values across different signalling systems. As such, we explored approaches to reduce the system dependence of derived efficacy estimations. In our first alternative approach, a novel operational model was composed which incorporated a term to account for the effect of GDP on [^{35}S]-GTPγS binding. This model denotes ligand efficacy as τ_0, the τ value for the ligand in the absence of GDP. While it does not completely exclude system inputs as the effect of receptor-G protein coupling cannot be calculated, it does provide an alternative approach to analyse [^{35}S]-GTPγS binding data. As described in **5.1.5**, this model utilises a concurrently performed GDP concentration response curve to incorporate the effect of GDP on the system.

When compared to the data set generated by the application of the Black and Leff model, there were no differences in the derived affinities except for apomorphine and the quinpirole fits from data sets 2 and 3 (**Table 5.6**). The main difference between the data sets lies in the generated efficacy parameters. The Black and Leff model generates τ values for each condition whereas this model derives a single, global τ value. It is noted however that at the lowest GDP concentration used, the Black and Leff τ values are very similar to the τ_0 estimates derived with only apomorphine significantly different (**Table 5.6**). At 30nM GDP, the signal window between basal and agonist-stimulated [^{35}S]-GTPγS binding plateaus (**Figure 5.6**). As such, it would be expected that the level of agonist stimulation at 30nM GDP is very similar to that in the absence of GDP leading to comparable τ values.

One of the assumptions in this analysis is that, at a population level, the apparent affinity of the Gα subunit for GDP (K_{GDP}) does not change with

agonist binding to the receptor, and that this affinity is constant for all agonists. Furthermore, in the absence of a calculated K_D for [^{35}S]-GTPγS to perform the Cheng-Prusoff correction (Cheng *et al.*, 1973), we are assuming that the GDP IC_{50} approximates to K_{GDP}. When GDP concentration response curves were conducted in both buffers, there were small but significant decreases in GDP potency following treatment with 10μM quinpirole (**Table 5.3**) which could be indicative of agonists decreasing the affinity of GDP for the agonist-receptor complex. This is expected at the level of individual receptors because an activated agonist-receptor complex promotes GDP release from the Gα subunit by inducing a conformational change in the G protein that reduces its affinity for GDP (Dror *et al.*, 2015). These changes in potency were however small (less than 3-fold) which suggests at the population level measured in [^{35}S]-GTPγS binding assays, the effects are minor. Furthermore, the GDP concentration response curves also show that the majority of basal [^{35}S]-GTPγS binding measured is receptor independent suggesting that on the whole, a limited D2 receptor dependent effect of agonists on the system (K_{GDP}) would be expected. However, as only one agonist was investigated in this manner, it is impossible to know whether this small shift would be consistent across a panel of agonists, which may provide an insight into whether K_{GDP} would vary between agonists. Furthermore, the lack of effect of (+)-butaclamol on GDP potency in either buffer suggests this effect is specific to agonists and that inverse agonists have limited effect on K_{GDP}. There is some evidence in the literature that different compounds can have small variations in apparent affinity for guanine nucleotides. Selley *et al* (1997, 1998) used Scatchard analysis on [^{35}S]-GTPγS-binding assays to determine the apparent affinity of [^{35}S]-GTPγS for different μ-opioid receptor agonists. Small changes (less than 5-fold) in the apparent K_D of [^{35}S]-GTPγS were identified for a number of compounds in both rat striatal membranes and membranes from CHO cells stably expressing the μ-opioid receptor (Selley *et al.*, 1998; Selley *et al.*, 1997).

5.3.6 Toward estimations of ligand intrinsic efficacy using the Slack and Hall operational model

Following the identification of a constitutively active system, ligands were examined for their ability to induce [^{35}S]-GTPγS binding in NMDG buffer and the Slack and Hall operational model applied to the data. This model successfully provided ligand ε estimations, but only aripiprazole and dihydroergocristine showed significantly different ε from the reference compound quinpirole. Although the NMDG buffer was required to generate sufficient receptor constitutive activity, it increased the relative R_{max} of most compounds such that every compound except aripiprazole and dihydroergocristine became full agonists. A previous study examining the effect of NMDG substitution on agonist responses also demonstrated an increase in relative R_{max} compared to NaCl containing buffers. While that study was still able to obtain differences in R_{max} between ligands, it was using a lower expressing CHO cell line than here (Lin *et al.*, 2006). It is possible that the increased receptor expression in the cell line used in this study has amplified the signal such that the potential differences in maximal responses between agonists are lost. However, operational modelling should allow the differentiation of relative ligand efficacy despite equal maximal responses (**3.2.7**); the lack of ε differences between ligands therefore suggests that the buffer substitution has equalised the intrinsic efficacy of the ligands. An alternative reason might be a lack of power in the Slack and Hall model to differentiate between ligands. This was examined by re-analysing the data with both the Black and Leff and GDP dependence operational models with the data corrected such that only agonist stimulated [^{35}S]-GTPγS binding was fitted (**Figure 5.18, Figure 5.19, Figure 5.20, Table 5.9**). Again, only the τ values for aripiprazole and dihydroergocristine were significantly lower than quinpirole, supporting the view that buffer substitution has increased relative ligand efficacy.

One advantage of the increased relative R_{max} of compounds following NMDG substitution is the ability to detect weak partial agonists such as aripiprazole

which are not detectable with Na^+ containing buffer (Koener *et al.*, 2012; Lin *et al.*, 2006) allowing the determination of their efficacy and functional affinity. As described in **5.3.2**, Na^+ is an allosteric modulator of the D2 receptor and its removal from assay buffer is thought to create a receptor which more readily adopts an active conformation (Lin *et al.*, 2006; Selent *et al.*, 2010). This allows weak partial agonists, which alone would not normally induce sufficient receptor activation, to be identified.

This loss of ε differences does not reflect the normal range of relative efficacies normally seen with these compounds under more standard assay conditions (i.e. in media and buffers containing Na^+). This suggests a significant allosteric component in D2 receptor ligand responses from the presence of buffer Na^+ (discussed above in **5.3.2**). As such, this may limit the physiological relevance of the affinity and efficacy estimations derived with this model for the D2 receptor. However, there are a number of receptors that are constitutively active under physiological conditions (Meye *et al.*, 2014; Seifert *et al.*, 2002) to which the application of this model would generate desired efficacy and affinity measurements.

In theory, ε values should be a system independent measure because the system dependent component is described by the χ values. As seen in **Table 5.8**, χ values decreased with increasing concentration of GDP. This is expected as increased concentrations of GDP will lead to increased competition for [^{35}S]-GTPγS binding to the G protein and reduced effect of agonists (**Figure 5.6**). The small χ values generated suggest a general low level of coupling efficiency at this signalling endpoint, which is consistent with this assay's proximity to the receptor in the signalling cascade and its reported low receptor reserve (Nickolls *et al.*, 2011; Umland *et al.*, 2001). While it is expected that ligand ε values are system independent, it would be interesting to test that hypothesis. As previously described, there are two ways in which to modulate ligand responses for operational modelling; vary K_E as described here or by varying R_T with irreversible antagonists. While not all receptors have available irreversible antagonists, as described in **3.3.7**, two have been

described for the dopamine D2 receptor, one of which (PBz) appears irreversible over time periods of up to 7h. A comparison of the data here with a dataset under conditions of receptor alkylation would examine whether ε stays constant between different methods to modulate χ.

When the individual data fits are examined, it can be seen that a number of data sets appear poorly fit to the model, especially for the 30nM GDP data. At lower GDP concentrations, the increase in basal [^{35}S]-GTPγS binding is much higher, markedly reducing the assay signal window (**Figure 5.6**). When the data are baseline corrected to remove the contribution of constitutive activity, this large basal binding leads to poorly defined system basals at low GDP concentrations. One advantage of globally fitting multiple data sets is to give the model more information to more accurately define unknown parameters (Hall *et al.*, 2010). Therefore, while on an individual level some of the agonist curve fits look poor, they are more representative of the data set as a whole. When the data are pooled, it can be seen that these experimental deviations from the fits are lost (**Figure 5.17**). This supports the view that the individual fits best represent the global data set. The Slack and Hall operational model requires a good definition of constitutive activity to separate ligand from system contributions (Slack *et al.*, 2012) which is clearly better defined when the model incorporates as much information as possible.

5.3.7 Comparison of fitting operational models in GraphPad Prism and Microsoft Excel

GraphPad Prism was constrained to fitting a maximum of 6 data sets, and prevented simultaneous analysis of both the GDP and agonist concentration response curves. Both of these issues were overcome in a programmed Microsoft Excel model, and comparisons were made between the two methods. There were two reasons behind this: one, to investigate whether globally fitting the entire data set provided better estimations than fitting 4-5 data sets with the reference agonist quinpirole; and two, to examine whether the assumption that using the IC_{50} and Hill slope from the concurrently

performed GDP concentration response curve provided suitable K_{GDP} and s constraints in the GDP dependence model in the absence of the ability to simultaneously analyse the data sets.

As shown in **Table 5.13** and **Table 5.14**, there were no differences between the data fits in GraphPad Prism and Microsoft Excel demonstrating that fitting 4-5 data sets provides the model with enough information to suitably define parameters. Furthermore, as Excel provided the same values of K_{GDP} and s as the IC_{50} and n from GDP CRCs, it suggests the assumptions inherent in the GraphPad Prism fits of the GDP dependence operational model were not misplaced. There were some issues however with the data fits in Microsoft Excel, with a data set for both dihydroergocristine and (-)-3-PPP needing to be excluded due to a lack of fit.

While Microsoft Excel is more flexible in allowing the simultaneous analysis of two variables and can analyse much larger data sets, diagnostics on the data fits are not supplied, unlike GraphPad Prism. It was the ability of GraphPad Prism to provide parameter co-variances which led to all the operational modelling performed in this chapter to have n constrained to 1. Co-variance analysis revealed that when some modelling data sets had n shared rather than constrained to 1, the model found high co-variance (almost 1) between n, χ and ε. High co-variance between parameters signifies that the model is struggling separate two parameters, with infinite combinations of the two parameters resulting in the same model fit. This was alleviated by constraining n to 1. Reducing the number of parameters the model has to fit places extra constraints on the fit, allowing it to better resolve the other unknown parameters. Furthermore, reducing the number of parameters can also aid model fitting by reducing the chances of the model finding local curve minima which are not a representative fit (Hall *et al.*, 2010).

As a general rule, increasing the number of data sets in a global fit allows software to more easily find the optimal fit for the data (Hall *et al.*, 2010) which should make Microsoft Excel a better option. However, the ability of

GraphPad Prism to easily generate fit diagnostics, especially in models with large numbers of parameters where it can be more difficult to resolve individual parameters, makes it a preferable software package.

5.4 Conclusions

This chapter explored the application of operational models to [^{35}S]-GTPγS binding assay data to derive agonist affinity and efficacy estimations. While the D2L and D2L T6.34R receptors lacked the necessary constitutive activity for application of the Slack and Hall operational model, the D2S receptor was constitutively active following buffer substitution with NMDG. This however led to an increase in relative ligand efficacy for all compounds with only aripiprazole and dihydroergocristine showing lower efficacy than the reference compound quinpirole. This was not consistent with the data from modelling derived in the presence of buffer Na^+ and may reduce the overall physiological relevance of the data. An alternative operational model for the analysis of [^{35}S]-GTPγS binding data was also explored which provided estimations of both ligand affinity and efficacy that were consistent with literature reports of the ligand pharmacology.

Chapter Six: General Discussion

The Black and Leff operational model (Black *et al.*, 1983; Black *et al.*, 1985) was a milestone in quantitative pharmacology, allowing the derivation of agonist affinity and relative efficacy estimations directly from functional concentration response data for the first time. However, Black and Leff's measure of efficacy, τ, still remains fundamentally a system dependent parameter, which limits its use in comparisons across signalling systems or functional endpoints. The application of this model typically requires manipulation of the experimental system, for example, receptor depletion by irreversible antagonists to reduce agonist maximal responses, and globally fitting the data to isolate agonist parameters. The system dependence of current efficacy estimations makes determinations of true ligand intrinsic efficacy difficult to determine. This has become a particular problem following the identification of biased signalling in G protein coupled receptors, and potentially other transduction systems (Kenakin *et al.*, 2013b; Rajagopal *et al.*, 2010; Urban *et al.*, 2007a). The quantitative models currently described to identify ligand bias use ratiometric methods to normalise system contributions (Kenakin *et al.*, 2013b; Kenakin *et al.*, 2011; Rajagopal *et al.*, 2011), however these only provide a measure of relative bias referenced to a reference ligand. A system independent measure of ligand efficacy would overcome this limitation, and perhaps provide a more accurate way to distinguish true examples of ligand bias (in terms of the ability to select functionally distinct receptor conformations) from other confounding influences.

One receptor which has gained significant interest in this respect is the dopamine D2 receptor, which is targeted in the treatment of a number of diseases including schizophrenia and Parkinson's Disease (Beaulieu *et al.*, 2011). Studies have suggested that biased ligands for the D2 receptor may be of therapeutic value in the treatment of schizophrenia, with β-arrestin biased ligands promising antipsychotic efficacy with reduced EPS (Allen *et al.*, 2011)

and studies demonstrating signalling bias of the clinically used compound, aripiprazole (Klein Herenbrink *et al.*, 2016; Szabo *et al.*, 2014; Urban *et al.*, 2007b). However measuring and distinguishing the value of signalling bias of such compounds, compared to other drug properties such as receptor selectivity, remains a key challenge. This is especially true for in the treatment of schizophrenia, where drugs have complex therapeutic and side effect profiles (Mailman *et al.*, 2010). As an important pharmacological target, there are a wide range of ligands available for the D2 receptor with a broad range of structural classes. These different structural classes engage differentially with the receptor binding site (Kling *et al.*, 2014; Krogsgaard-Larsen *et al.*, 2014) and these interactions, particularly with TM5 serine residues, may govern downstream signalling (Fowler *et al.*, 2012; Wiens *et al.*, 1998).

Recently, a modification of the operational model has been described to derive system independent measures of ligand intrinsic efficacy (Slack *et al.*, 2012). This model utilises receptor constitutive activity to estimate the system contribution to ligand responses, separating the ligand and system dependent components of efficacy. Thus far, this model has been applied to determine the parameters of a limited number of agonists at the chemokine CCR4 and FFA2 receptors (Brown *et al.*, 2015; Slack *et al.*, 2012) but has not be applied to a wider data set.

This thesis explored the use of operational models in the derivation of agonist affinities and efficacies at the dopamine D2 receptor. In particular, we explored the applicability of the Slack and Hall model to derive intrinsic agonist efficacies. The dopamine D2 receptor was chosen as a model receptor as an important pharmacological target with well documented receptor constitutive activity (Hall *et al.*, 1997; Roberts *et al.*, 2004; Roberts *et al.*, 2005).

Chapter Three examined traditional concentration response analysis to derive ligand maximal responses and potencies at two representative functional assays with different levels of D2L receptor reserve. This highlighted the key

issue with traditional R_{max} comparisons, namely the ability of many compounds to elicit maximal responses at highly amplified signalling endpoints. While this is improved in low receptor reserve assays, such as receptor internalisation, this also presents a problem with the detection of very low efficacy agonists (Stott *et al.*, 2016). In the case of the dopamine D2 receptor, the low efficacy of aripiprazole, is often only detectable in either highly amplified signalling assays or following manipulation of experimental conditions, such as altered buffer compositions or increased D2 receptor expression (Koener *et al.*, 2012; Lin *et al.*, 2006). The use of the operational model to analyse the responses of four representative dopamine agonists allowed the derivation of estimations of ligand efficacy that more faithfully represented the known pharmacology of the compounds. This was only possible due to the availability of phenoxybenzamine as an irreversible antagonist for the D2 receptor (Hamblin *et al.*, 1982). However, these experiments provided no evidence for receptor constitutive activity of the D2L receptor in the current cellular system.

As such, attempts were made to generate a constitutively active mutant of the D2L receptor (D2L T6.34R; **Chapter Four**). The homologous mutation in the D2S receptor is reported to generate a receptor with measurable constitutive activity and an increased ability to detect inverse agonism (Wilson *et al.*, 2001). While the pharmacology of the D2L T6.34R receptor was generally consistent with a receptor with increased ability to adopt the active receptor state, ligand specific decreases in potency were observed for the ergo-derived compounds. It was hypothesised that these differences were down to differential engagement of the ergo-derived compounds with receptor binding site serine residues, which was altered following T6.34R mutation. A recent modelling study proposed that ergo-derived compounds bind deeper in the binding pocket, engaging preferentially with S5.46, whereas traditional catechol and hydroxyl containing compounds bound S5.42 (Krogsgaard-Larsen *et al.*, 2014). The examination of TM5 serine mutations revealed that, like previous studies (Coley *et al.*, 2000; Fowler *et*

al., 2012; Mansour *et al.*, 1992; Wiens *et al.*, 1998), serine mutations had different effects on structurally distinct compounds. With this dataset, we have expanded the range of compounds examined in this manner. In agreement with our hypothesis, the ergo-derived compounds, bromocriptine and dihydroergocristine, were most sensitive to S5.46A mutations; however contrasting effects were observed for the smaller, synthetic ergolines cabergoline and pergolide, whose binding appeared to be enhanced by the loss of the serine residues. These divergent effects for structurally related compounds were unexpected, and highlight how important structure-activity relationships are in terms of designing compounds that bind receptors in the desired manner. Expansion of the ligand data set to include more ergo-derived compounds may support this hypothesis, together with additional receptor mutants which retain only one of the three serine residues.

Since our results support different modes of agonist binding, and by implication the possibility of different receptor conformations, the use of a greater range of signalling assays might increase the evidence that such agonist bound states of the receptor produce functionally distinct, biased outcomes. For the dopamine D2 receptor, differential engagement of serine residues may play an important role in regulating the direction of downstream signalling events. For example, it has been proposed that dopamine interactions with S5.43 in the human D2L receptor may be necessary for arachidonic acid release but are not involved in cAMP or MAPK signalling (Fowler *et al.*, 2012), whereas for the rat D2S receptor, it was suggested that this residue was necessary for the inhibition of cAMP (Wiens *et al.*, 1998). This has important implications for the design and profiling of biased ligands of the D2 receptor. First, there might be species-specific requirements of serine residues in downstream signalling, that will need evaluation when profiling compounds in *in vitro* and *in vivo* settings. Even within a species, differences in receptor expression and system coupling efficiencies can lead to vastly different tissue responses (Kenakin *et al.*, 2013b). Second, the design of biased ligands for the D2 receptor might be

further improved by optimising ligand interactions with specific TM5 serine residues. There have been reports of SAR studies on ligand bias at the dopamine D2 receptors with subtle changes in ligand structure generating vastly different functional bias profiles (Shonberg *et al.*, 2013; Szabo *et al.*, 2014). Modelling of two structurally related compounds with different bias profiles revealed substantial differences in the orientation of TM5 serine residues, despite neither compound engaging these residues in hydrogen bond interactions (Shonberg *et al.*, 2013). This suggests that even for compounds which do not engage in hydrogen bond interactions with TM5 serines, these residues remain important in governing downstream signalling and bias. This is supported by our own observations that S5.42 and S5.46 mutations increased the relative efficacy of aripiprazole, a compound not believed to engage in hydrogen bond interactions with TM5 serines (Kling *et al.*, 2014).

The examination of these interactions in a proposed constitutively active receptor (D2L T6.34R) has also highlighted some issues surrounding the traditional assumptions associated with such mutants, namely that they solely represent a receptor more likely to adopt the active state (Seifert *et al.*, 2002). While the effects of the serine mutations in the T6.34R receptor were largely consistent with those in the WT background, there were some notable differences. This was highlighted with quinpirole responses in the CRE-SPAP reporter gene assay, where S5.42A mutation had opposing effects on potency. These opposing effects suggest different binding modes between the WT and T6.34R receptors, indicating potential conformational differences in the receptors. Future experiments to determine ligand affinities and receptor expression levels, and as well as profile other downstream signalling pathways, would provide more information on this mechanism.

Finally, the use of operational models to determine agonist affinities and efficacies at the dopamine D2 receptor was explored in **Chapter Five**. In order to generate a system with consistent, measureable constitutive activity for application of the Slack and Hall operational model, [^{35}S]-GTPγS binding

assays were conducted. This highly versatile assay allowed the manipulation of experimental conditions to favour both agonism and inverse agonism through variation of GDP and buffer Na^+ concentrations (Strange, 2010). Early assays revealed that there was either inconsistent or undetectable constitutive activity for the D2L and D2L T6.34R receptors respectively, and as such, the functionality of the D2S receptor was further examined. In agreement with published reports (Hall *et al.*, 1997; Roberts *et al.*, 2004; Roberts *et al.*, 2005), the D2S receptor was found to be constitutively active, although it was only detectable following the removal of buffer Na^+.

Following the identification of a constitutively active system, we were able to successfully apply the Slack and Hall operational model to agonist functional responses, deriving agonist affinities and intrinsic efficacies. Constitutive activity allows application of this model to agonist functional response curves without the need for an irreversible antagonist, which are not available for all GPCRs. Inverse agonists can be fitted simultaneously with agonist data to define the receptor constitutive activity (Brown *et al.*, 2015) or alternatively, as in this study, the concentration of GDP in [^{35}S]-GTPγS binding assays can be varied (Slack *et al.*, 2012). Changing GDP concentration varies the level of constitutive activity in the system and allowed the generation of a large agonist data set which could be globally fit to improve the accuracy of the derived parameters (Hall *et al.*, 2010).

The difficulties in detecting constitutive activity at the D2 receptor were unexpected and highlights a potential problem with the application of the Slack and Hall operational model. While receptor constitutive activity is detectable at physiological concentrations for some GPCRs, for many others it requires high receptor expression or constitutively activating mutations (Seifert *et al.*, 2002), limiting the applicability of the model. In the case of the dopamine D2S receptor system studied here, the necessary buffer substitution to detect constitutive activity increased ligand efficacies such that the range of ligand efficacies observed in the Na^+-containing buffer were lost. The buffer substitution however did allow the detection of low efficacy

agonism. This highlights a common problem with GPCR functional assays – the difficulty in finding an optimal functional response and assay window whereby ligand responses are detectable, but not saturated by the system. This is particularly difficult in the detection of constitutive activity where assays need to be sensitive enough to detect the potentially limited number of receptors spontaneously adopting the receptor active state, but not too highly coupled or constitutively active to lose the agonist dependent signal. While the Slack and Hall offers the potential to identify biased ligands based on their intrinsic efficacies for different signalling pathways, it may be difficult to find a receptor system with measureable constitutive activity across multiple pathways, particularly for poorly coupled assays such as β-arrestin recruitment. Nonetheless, for GPCRs with robust constitutive activity, this model offers the opportunity for the first time to derive ligand intrinsic efficacies. The applicability of this model could be further explored using GPCRs with well characterised, high levels of constitutive activity, such as β2AR or 5-HT_{2C} receptors (Meye *et al.*, 2014; Seifert *et al.*, 2002).

For all the operational models explored in this thesis, there were an increased number of parameters that needed to be unambiguously defined by the fit, in comparison to simple concentration response curve analysis. This necessitated large, robust data sets and globally fitting multiple agonist data sets to reduce the co-variance of parameters and more accurately define parameters. For larger ligand sets, for example when drug screening, this may not provide a practical approach. The nature of agonism, and whether there truly is an empirical separation of affinity and efficacy, has been widely discussed (Colquhoun, 1998; Strange, 2008). It may not always be necessary to individually define agonist parameters and it is now more common, especially in the consideration of ligand bias, to define τ/K_A ratios as a single parameter, R (Reinartz *et al.*, 2015; van der Westhuizen *et al.*, 2014). Furthermore, there is an increasing focus on the use of allosteric ligands as effective therapeutics. For these compounds, the properties of both the allosteric and orthosteric ligand, as well as their interactions at the target

receptor, must be considered. As such, allosteric operational models contain even more parameters than standard operational models of agonism (Christopoulos, 2014; Keov *et al.*, 2011). While there is a need for models that fully describe ligand behaviour, this must be balanced by practical application to obtain measurements that are unambiguous and still useful in ranking compounds.

Furthermore, while operational models provide a view of receptor signalling at equilibrium, the role of ligand kinetics in functional responses is becoming increasingly appreciated (Klein Herenbrink *et al.*, 2016; Rosethorne *et al.*, 2016; Sykes *et al.*, 2009). For some signalling endpoints, such as calcium mobilisation, the transient nature of the response makes reaching a dynamic equilibrium difficult, particularly for compounds with slow kinetics (Charlton *et al.*, 2010). While kinetics has not been explored in this thesis, there have been suggestions that kinetics may play an important role in the improved side effect profile of atypical antipsychotics (Kapur *et al.*, 2001). While the effect of antagonist kinetics under hemi-equilibrium conditions has been incorporated into the operational model (Kenakin *et al.*, 2006; Mould *et al.*, 2014), as yet there are no reports of the incorporation of agonist kinetics into operational model fitting. Until such time, equilibrium based operational models provide the most accessible methods to generate estimations of agonist affinity and efficacy. For a constitutively active system, the Slack and Hall operational model provides the best model to estimate intrinsic efficacy values.

Chapter Seven: References

Ahn S, Shenoy SK, Wei H, Lefkowitz RJ (2004). Differential Kinetic and Spatial Patterns of β-Arrestin and G Protein-mediated ERK Activation by the Angiotensin II Receptor. *J Biol Chem.* **279**(34)**:** 35518-35525.

Ajram L, Begg M, Slack R, Cryan J, Hall D, Hodgson S*, et al.* (2014). Internalization of the chemokine receptor CCR4 can be evoked by orthosteric and allosteric receptor antagonists. *European journal of pharmacology* **729:** 75-85.

Alewijnse AE, Timmerman H, Jacobs EH, Smit MJ, Roovers E, Cotecchia S*, et al.* (2000). The Effect of Mutations in the DRY Motif on the Constitutive Activity and Structural Instability of the Histamine H2Receptor. *Molecular pharmacology* **57**(5)**:** 890-898.

Allen JA, Yost JM, Setola V, Chen X, Sassano MF, Chen M*, et al.* (2011). Discovery of β-Arrestin–Biased Dopamine D2 Ligands for Probing Signal Transduction Pathways Essential for Antipsychotic Efficacy. *Proc. Natl. Acad. Sci. USA* **108**(45)**:** 18488-18493.

Allen M, Hall D, Collins B, Moore K (2002). A homogeneous high throughput nonradioactive method for measurement of functional activity of Gs-coupled receptors in membranes. *J Biomol Screen* **7**(1)**:** 35-44.

Alt A, Clark MJ, Woods JH, Traynor JR (2002). Mu and Delta opioid receptors activate the same G proteins in human neuroblastoma SH-SY5Y cells. *British journal of pharmacology* **135**(1)**:** 217-225.

Angrist BM, Gershon S (1970). The phenomenology of experimentally induced amphetamine psychosis: Preliminary observations. *Biol. Psychiatry* **2**(2)**:** 95-107.

Ariens EJ, De Groot WM (1954). Affinity and intrinsic-activity in the theory of competitive inhibition. III. Homologous decamethonium-derivatives and succinyl-choline-esters. *Archives internationales de pharmacodynamie et de therapie* **99**(2)**:** 193-205.

Arinami T, Hamaguchi H, Itokawa M, Enguchi H, Tagaya H, Yano S*, et al.* (1994). Association of dopamine D2 receptor molecular variant with schizophrenia. *The Lancet* **343**(8899)**:** 703-704.

Arunlakshana O, Schild HO (1959). Some quantitative uses of drug antagonists. *British journal of pharmacology and chemotherapy* **14**(1)**:** 48-58.

Baker JG, Adams LA, Salchow K, Mistry SN, Middleton RJ, Hill SJ*, et al.* (2011). Synthesis and Characterization of High-Affinity 4,4-Difluoro-4-bora-3a,4a-diaza-s-indacene-Labeled Fluorescent Ligands for Human β-Adrenoceptors. *Journal of medicinal chemistry* **54**(19)**:** 6874-6887.

Baker JG, Hall IP, Hill SJ (2003). Agonist and Inverse Agonist Actions of β-Blockers at the Human β2-Adrenoceptor Provide Evidence for Agonist-Directed Signaling. *Molecular pharmacology* **64**(6)**:** 1357-1369.

Baker JG, Hall IP, Hill SJ (2002). Pharmacological characterization of CGP 12177 at the human β_2-adrenoceptor. *British journal of pharmacology* **137**(3)**:** 400-408.

Baker JG, Hall IP, Hill SJ (2004). Temporal Characteristics of cAMP Response Element-Mediated Gene Transcription: Requirement for Sustained cAMP Production. *Molecular pharmacology* **65**(4)**:** 986-998.

Ballesteros JA, Jensen AD, Liapakis G, Rasmussen SG, Shi L, Gether U*, et al.* (2001). Activation of the β_2-adrenergic receptor involves disruption of an ionic lock between the cytoplasmic ends of transmembrane segments 3 and 6. *The Journal of biological chemistry* **276**(31)**:** 29171-29177.

Ballesteros JA, Weinstein H (1995). Integrated methods for the construction of three-dimensional models and computational probing of structure-function relations in G protein-coupled receptors. In: Stuart CS (ed)^(eds). *Methods Neurosci*, edn, Vol. 25: Academic Press. p^pp 366-428.

Beaulieu J-M, Sotnikova TD, Marion S, Lefkowitz RJ, Gainetdinov RR, Caron MG (2005). An Akt/β-Arrestin 2/PP2A Signaling Complex Mediates Dopaminergic Neurotransmission and Behavior. *Cell* **122**(2)**:** 261-273.

Beaulieu JM, Gainetdinov RR (2011). The physiology, signaling, and pharmacology of dopamine receptors. *Pharmacological reviews* **63**(1)**:** 182-217.

Beaulieu JM, Sotnikova TD, Yao WD, Kockeritz L, Woodgett JR, Gainetdinov RR*, et al.* (2004). Lithium antagonizes dopamine-dependent behaviors mediated by an AKT/glycogen synthase kinase 3 signaling cascade. *Proceedings of the National Academy of Sciences of the United States of America* **101**(14)**:** 5099-5104.

Belleau B, DiTullio V, Godin D (1969). The mechanism of irreversible adrenergic blockade by N-carbethoxydihydroquinolines—model studies with typical serine hydrolases. *Biochemical pharmacology* **18**(5)**:** 1039-1044.

Berk M, Dodd S, Kauer-Sant'Anna M, Malhi GS, Bourin M, Kapczinski F*, et al.* (2007). Dopamine dysregulation syndrome: implications for a dopamine hypothesis of bipolar disorder. *Acta Psychiatr Scand* **116:** 41-49.

Bhattacharyya S, Puri S, Miledi R, Panicker MM (2002). Internalization and recycling of 5-HT2A receptors activated by serotonin and protein kinase C-mediated mechanisms. *Proc. Natl. Acad. Sci. USA* **99**(22)**:** 14470-14475.

Bjarnadóttir TK, Fredriksson R, Schiöth HB (2005). The gene repertoire and the common evolutionary history of glutamate, pheromone (V2R), taste(1) and other related G protein-coupled receptors. *Gene* **362:** 70-84.

Bjarnadottir TK, Gloriam DE, Hellstrand SH, Kristiansson H, Fredriksson R, Schioth HB (2006). Comprehensive repertoire and phylogenetic analysis of the G protein-coupled receptors in human and mouse. *Genomics* **88**(3)**:** 263-273.

Black JB, Premont RT, Daaka Y (2016). Feedback regulation of G protein-coupled receptor signaling by GRKs and arrestins. *Semin Cell Dev Biol* **50:** 95-104.

Black JW, Leff P (1983). Operational models of pharmacological agonism. *Proc. R. Soc. Lond. B: Biol. Sci.* **220**(1219)**:** 141-162.

Black JW, Leff P, Shankley NP, Wood J (1985). An operational model of pharmacological agonism: the effect of E/[A] curve shape on agonist dissociation constant estimation. *British journal of pharmacology* **84**(2)**:** 561-571.

Brostrom CO, Corbin JD, King CA, Krebs EG (1971). Interaction of the Subunits of Adenosine 3′:5′-Cyclic Monophosphate-Dependent Protein Kinase of Muscle. *Proceedings of the National Academy of Sciences of the United States of America* **68**(10)**:** 2444-2447.

Brown AJ, Tsoulou C, Ward E, Gower E, Bhudia N, Chowdhury F*, et al.* (2015). Pharmacological properties of acid N-thiazolylamide FFA2 agonists. *Pharmacol Res Perspect.* **3**(3)**:** e00141.

Bruins Slot LA, De Vries L, Newman-Tancredi A, Cussac D (2006). Differential profile of antipsychotics at serotonin 5-HT1A and dopamine D2S receptors coupled to extracellular signal-regulated kinase. *European journal of pharmacology* **534**(1-3)**:** 63-70.

Brust TF, Hayes MP, Roman DL, Burris KD, Watts VJ (2015a). Bias Analyses of Preclinical and Clinical D2 Dopamine Ligands: Studies with Immediate and Complex Signaling Pathways. *J. Pharm. Exp. Ther.* **352**(3)**:** 480-493.

Brust TF, Hayes MP, Roman DL, Watts VJ (2015b). New functional activity of aripiprazole revealed: Robust antagonism of D2 dopamine receptor-stimulated Gβγ signaling. *Biochemical pharmacology* **93**(1)**:** 85-91.

Bubeníková-Valešová V, Horáček J, Vrajová M, Höschl C (2008). Models of schizophrenia in humans and animals based on inhibition of NMDA receptors. *Neurosci. Biobehav. Rev.* **32**(5)**:** 1014-1023.

Buchsbaum MS, Ingvar DH, Kessler R, et al. (1982). Cerebral glucography with positron tomography: Use in normal subjects and in patients with schizophrenia. *Arch. Gen. Psychiatry* **39**(3)**:** 251-259.

Burris KD, Molski TF, Xu C, Ryan E, Tottori K, Kikuchi T*, et al.* (2002). Aripiprazole, a novel antipsychotic, is a high-affinity partial agonist at human dopamine D2 receptors. *The Journal of pharmacology and experimental therapeutics* **302**(1)**:** 381-389.

Carlsson A, Lindqvist M, Magnusson TOR (1957). 3,4-Dihydroxyphenylalanine and 5-Hydroxytryptophan as Reserpine Antagonists. *Nature* **180**(4596)**:** 1200-1200.

Carpenter B, Nehmé R, Warne T, Leslie AGW, Tate CG (2016). Structure of the adenosine A2A receptor bound to an engineered G protein. *Nature* **advance online publication**.

Carrillo JJ, Stevens PA, Milligan G (2002). Measurement of Agonist-Dependent and -Independent Signal Initiation of α1b-Adrenoceptor Mutants by Direct Analysis of Guanine Nucleotide Exchange on the G Protein Gα11. *J. Pharm. Exp. Ther.* **302**(3)**:** 1080-1088.

Charlton SJ, Vauquelin G (2010). Elusive equilibrium: the challenge of interpreting receptor pharmacology using calcium assays. *British journal of pharmacology* **161**(6)**:** 1250-1265.

Cheng Y-C, Prusoff WH (1973). Relationship between the inhibition constant (K_I) and the concentration of inhibitor which causes 50 per cent inhibition (I_{50}) of an enzymatic reaction. *Biochemical pharmacology* **22**(23)**:** 3099-3108.

Chien EY, Liu W, Zhao Q, Katritch V, Han GW, Hanson MA*, et al.* (2010). Structure of the human dopamine D3 receptor in complex with a D2/D3 selective antagonist. *Science* **330**(6007)**:** 1091-1095.

Cho D, Zheng M, Kim K-M (2010a). Current perspectives on the selective regulation of dopamine D2 and D3 receptors. *Arch. Pharm. Res.* **33**(10)**:** 1521-1538.

Cho D, Zheng M, Min C, Ma L, Kurose H, Park JH*, et al.* (2010b). Agonist-Induced Endocytosis and Receptor Phosphorylation Mediate Resensitization of Dopamine D2 Receptors. *Mol. Endocrinol.* **24**(3)**:** 574-586.

Cho DI, Zheng M, Min C, Kwon KJ, Shin CY, Choi HK*, et al.* (2013). ARF6 and GASP-1 are post-endocytic sorting proteins selectively involved in the intracellular trafficking of dopamine D2 receptors mediated by GRK and PKC in transfected cells. *British journal of pharmacology* **168**(6)**:** 1355-1374.

Christopoulos A (2014). Advances in G Protein-Coupled Receptor Allostery: From Function to Structure. *Molecular pharmacology* **86**(5)**:** 463-478.

Cimino M, Weiss B (1988). Characteristics of the binding of phenoxybenzamine to calmodulin. *Biochemical pharmacology* **37**(14)**:** 2739-2745.

Clark AJ (1926a). The antagonism of acetyl choline by atropine. *J Physiol* **61**(4)**:** 547-556.

Clark AJ (1933). *The mode of action of drugs on cells*. edn. Edward Arnold.

Clark AJ (1926b). The reaction between acetyl choline and muscle cells. *J Physiol* **61**(4)**:** 530-546.

Clayton CC, Donthamsetti P, Lambert NA, Javitch JA, Neve KA (2014). Mutation of three residues in the third intracellular loop of the dopamine D2 receptor creates an internalization-defective receptor. *The Journal of biological chemistry* **289**(48)**:** 33663-33675.

Coley C, Woodward R, Johansson AM, Strange PG, Naylor LH (2000). Effect of multiple serine/alanine mutations in the transmembrane spanning region V of the D2 dopamine receptor on ligand binding. *Journal of neurochemistry* **74**(1)**:** 358-366.

Colquhoun D (1998). Binding, gating, affinity and efficacy: the interpretation of structure-activity relationships for agonists and of the effects of mutating receptors. *British journal of pharmacology* **125**(5)**:** 924-947.

Costa T, Herz A (1989). Antagonists with negative intrinsic activity at delta opioid receptors coupled to GTP-binding proteins. *Proc. Natl. Acad. Sci. USA* **86**(19)**:** 7321-7325.

Costa T, Lang J, Gless C, Herz A (1990). Spontaneous association between opioid receptors and GTP-binding regulatory proteins in native membranes:

specific regulation by antagonists and sodium ions. *Molecular pharmacology* **37**(3)**:** 383-394.

Creese I, Burt DR, Snyder SH (1976). Dopamine receptor binding predicts clinical and pharmacological potencies of antischizophrenic drugs. *Science* **192**(4238)**:** 481-483.

Cullen BR, Malim MH (1992). [31] Secreted placental alkaline phosphatase as a eukaryotic reporter gene. In: (ed)^(eds). *Methods Enzymol.*, edn, Vol. Volume 216: Academic Press. p^pp 362-368.

Davis KL, Kahn RS, Ko G, Davidson M (1991). Dopamine in schizophrenia: a review and reconceptualization. *Am. J. Psychiatry* **148**(11)**:** 1474-1486.

De Lean A, Stadel JM, Lefkowitz RJ (1980). A ternary complex model explains the agonist-specific binding properties of the adenylate cyclase-coupled β-adrenergic receptor. *The Journal of biological chemistry* **255**(15)**:** 7108-7117.

Del Castillo J, Katz B (1957). Interaction at end-plate receptors between different choline derivatives. *Proceedings of the Royal Society of London. Series B, Containing papers of a Biological character. Royal Society (Great Britain)* **146**(924)**:** 369-381.

Dennis D, Jacobson K, Belardinelli L (1992). Evidence of spare A1-adenosine receptors in guinea pig atrioventricular node. *Am. J. Physiol. Heart Circ. Physiol.* **262**(3)**:** H661-H671.

DeWire SM, Yamashita DS, Rominger DH, Liu G, Cowan CL, Graczyk TM*, et al.* (2013). A G Protein-Biased Ligand at the μ-Opioid Receptor Is Potently Analgesic with Reduced Gastrointestinal and Respiratory Dysfunction Compared with Morphine. *J. Pharm. Exp. Ther.* **344**(3)**:** 708-717.

Dong C, Filipeanu CM, Duvernay MT, Wu G (2007). Regulation of G protein-coupled receptor export trafficking. *Biochim Biophys Acta.* **1768**(4)**:** 853-870.

Dror RO, Arlow DH, Maragakis P, Mildorf TJ, Pan AC, Xu H*, et al.* (2011). Activation mechanism of the β2-adrenergic receptor. *Proc. Natl. Acad. Sci. USA* **108**(46)**:** 18684-18689.

Dror RO, Mildorf TJ, Hilger D, Manglik A, Borhani DW, Arlow DH*, et al.* (2015). SIGNAL TRANSDUCTION. Structural basis for nucleotide exchange in heterotrimeric G proteins. *Science* **348**(6241)**:** 1361-1365.

Eaves S, Rey JA (2016). Brexpiprazole (Rexulti): A New Monotherapy for Schizophrenia and Adjunctive Therapy for Major Depressive Disorder. *P T* **41**(7)**:** 418-422.

Ebersole BJ, Visiers I, Weinstein H, Sealfon SC (2003). Molecular Basis of Partial Agonism: Orientation of Indoleamine Ligands in the Binding Pocket of the Human Serotonin 5-HT2A Receptor Determines Relative Efficacy. *Molecular pharmacology* **63**(1)**:** 36-43.

Ellisdon Andrew M, Halls Michelle L (2016). Compartmentalization of GPCR signalling controls unique cellular responses. *Biochemical Society transactions* **44**(2)**:** 562-567.

Emamian ES, Hall D, Birnbaum MJ, Karayiorgou M, Gogos JA (2004). Convergent evidence for impaired AKT1-GSK3β signaling in schizophrenia. *Nat Genet* **36**(2)**:** 131-137.

Engström M, Närvänen A, Savola J-M, Wurster S (2004). Assessing activation of the human neuropeptide FF2 receptor with a non-radioactive GTP binding assay. *Peptides* **25**(12)**:** 2099-2104.

Fenalti G, Giguere PM, Katritch V, Huang X-P, Thompson AA, Cherezov V*, et al.* (2014). Molecular control of δ-opioid receptor signalling. *Nature* **506**(7487)**:** 191-196.

Feng W, Song ZH (2003). Effects of D3.49A, R3.50A, and A6.34E mutations on ligand binding and activation of the cannabinoid-2 (CB2) receptor. *Biochemical pharmacology* **65**(7)**:** 1077-1085.

Fowler JC, Bhattacharya S, Urban JD, Vaidehi N, Mailman RB (2012). Receptor conformations involved in dopamine D(2L) receptor functional selectivity induced by selected transmembrane-5 serine mutations. *Molecular pharmacology* **81**(6)**:** 820-831.

Fradkov AF, Chen Y, Ding L, Barsova EV, Matz MV, Lukyanov SA (2000). Novel fluorescent protein from Discosoma coral and its mutants possesses a unique far-red fluorescence. *FEBS letters* **479**(3)**:** 127-130.

Frang H, Cockcroft V, Karskela T, Scheinin M, Marjamäki A (2001). Phenoxybenzamine Binding Reveals the Helical Orientation of the Third Transmembrane Domain of Adrenergic Receptors. *J Biol Chem.* **276**(33)**:** 31279-31284.

Fredriksson R, Lagerström MC, Lundin L-G, Schiöth HB (2003). The G-Protein-Coupled Receptors in the Human Genome Form Five Main Families. Phylogenetic Analysis, Paralogon Groups, and Fingerprints. *Molecular pharmacology* **63**(6)**:** 1256-1272.

Furchgott RF (1966). The use of beta-haloalkylamines in the differentiation of receptors and in the determination of dissociation constants of receptor-agonist complexes. *Adv. Drug Res.* **3:** 21-25.

Gaddum JH (1926). The action of adrenalin and ergotamine on the uterus of the rabbit. *J. Physiol.* **61**(1)**:** 141-150.

Gaddum JH (1937). The quantitative effects of antagonist drugs. *J Physiol* **89:** 7P-9P.

Gao K, Calabrese JR (2005). Newer treatment studies for bipolar depression. *Bipolar disorders* **7 Suppl 5:** 13-23.

Gardner B, Hall DA, Strange PG (1996). Pharmacological analysis of dopamine stimulation of [35S]-GTPγS binding via human D2short and D2long dopamine receptors expressed in recombinant cells. *British journal of pharmacology* **118**(6)**:** 1544-1550.

Gardner B, Strange PG (1998). Agonist action at D2(long) dopamine receptors: ligand binding and functional assays. *British journal of pharmacology* **124**(5)**:** 978-984.

Gardner BR, Hall DA, Strange PG (1997). Agonist action at D2(short) dopamine receptors determined in ligand binding and functional assays. *Journal of neurochemistry* **69**(6)**:** 2589-2598.

Garland SL (2013). Are GPCRs still a source of new targets? *J Biomol Screen* **18**(9)**:** 947-966.

Gautier A, Juillerat A, Heinis C, Corrêa Jr IR, Kindermann M, Beaufils F*, et al.* (2008). An Engineered Protein Tag for Multiprotein Labeling in Living Cells. *Chem. Biol.* **15**(2)**:** 128-136.

Gazi L, Nickolls SA, Strange PG (2003). Functional coupling of the human dopamine D2 receptor with $G\alpha_{i1}$, $G\alpha_{i2}$, $G\alpha_{i3}$ and $G\alpha_{o}$ G proteins: evidence for agonist regulation of G protein selectivity. *British journal of pharmacology* **138**(5)**:** 775-786.

Geddes J, Freemantle N, Harrison P, Bebbington P (2000). Atypical antipsychotics in the treatment of schizophrenia: systematic overview and meta-regression analysis. *BMJ* **321**(7273)**:** 1371-1376.

George SE, Bungay PJ, Naylor LH (1998). Functional analysis of the D2L dopamine receptor expressed in a cAMP-responsive luciferase reporter cell line. *Biochemical pharmacology* **56**(1)**:** 25-30.

George SE, Bungay PJ, Naylor LH (1997). Functional Coupling of Endogenous Serotonin (5-HT1B) and Calcitonin (C1a) Receptors in CHO Cells to a Cyclic AMP-Responsive Luciferase Reporter Gene. *Journal of neurochemistry* **69**(3)**:** 1278-1285.

Ghanouni P, Gryczynski Z, Steenhuis JJ, Lee TW, Farrens DL, Lakowicz JR*, et al.* (2001). Functionally different agonists induce distinct conformations in the G protein coupling domain of the β2 adrenergic receptor. *The Journal of biological chemistry* **276**(27)**:** 24433-24436.

Giembycz MA (2009). An estimation of β2-adrenoceptor reserve on human bronchial smooth muscle for some sympathomimetic bronchodilators. *British journal of pharmacology* **158**(1)**:** 287-299.

Giros B, Sokoloff P, Martres MP, Riou JF, Emorine LJ, Schwartz JC (1989). Alternative splicing directs the expression of two D2 dopamine receptor isoforms. *Nature* **342**(6252)**:** 923-926.

Glatt SJ, Jönsson EG (2006). The Cys allele of the DRD2 Ser311Cys polymorphism has a dominant effect on risk for schizophrenia: Evidence from fixed- and random-effects meta-analyses. *Am. J. Med. Genet. Part B* **141B**(2)**:** 149-154.

Goggi JL, Sardini A, Egerton A, Strange PG, Grasby PM (2007). Agonist-dependent internalization of D2 receptors: Imaging quantification by confocal microscopy. *Synapse (New York, N.Y.)* **61**(4)**:** 231-241.

Grandy DK, Marchionni MA, Makam H, Stofko RE, Alfano M, Frothingham L*, et al.* (1989). Cloning of the cDNA and gene for a human D2 dopamine receptor. *Proc. Natl. Acad. Sci. USA* **86**(24)**:** 9762-9766.

Greengard P (2001). The Neurobiology of Slow Synaptic Transmission. *Science* **294**(5544)**:** 1024-1030.

Griffin BA, Adams SR, Tsien RY (1998). Specific Covalent Labeling of Recombinant Protein Molecules Inside Live Cells. *Science* **281**(5374)**:** 269-272.

Griffin MT, Figueroa KW, Liller S, Ehlert FJ (2007). Estimation of Agonist Activity at G Protein-Coupled Receptors: Analysis of M2 Muscarinic Receptor Signaling through Gi/o,Gs, and G15. *J. Pharm. Exp. Ther.* **321**(3)**:** 1193-1207.

Hall DA, Langmead CJ (2010). Matching models to data: a receptor pharmacologist's guide. *British journal of pharmacology* **161**(6)**:** 1276-1290.

Hall DA, Strange PG (1999). Comparison of the ability of dopamine receptor agonists to inhibit forskolin-stimulated adenosine 3'5'-cyclic monophosphate (cAMP) accumulation via D2L (long isoform) and D3 receptors expressed in Chinese hamster ovary (CHO) cells. *Biochemical pharmacology* **58**(2)**:** 285-289.

Hall DA, Strange PG (1997). Evidence that antipsychotic drugs are inverse agonists at D2 dopamine receptors. *British journal of pharmacology* **121**(4)**:** 731-736.

Hamblin MW, Creese I (1983). Behavioral and radioligand binding evidence for irreversible dopamine receptor blockade by N-ethoxycarbonyl-2-ethoxy-1,2-dihydroquinoline. *Life sciences* **32**(19)**:** 2247-2255.

Hamblin MW, Creese I (1982). Phenoxybenzamine treatment differentiates dopaminergic 3H-ligand binding sites in bovine caudate membranes. *Molecular pharmacology* **21**(1)**:** 44-51.

Harrison C, Traynor JR (2003). The [35S]GTPγS binding assay: approaches and applications in pharmacology. *Life sciences* **74**(4)**:** 489-508.

Henkel JG, Portoghese PS, Miller JW, Lewis P (1976). Synthesis and adrenoreceptor blocking action of aziridinium ions derived from phenoxybenzamine and dibenamine. *Journal of medicinal chemistry* **19**(1)**:** 6-10.

Heusler P, Newman-Tancredi A, Loock T, Cussac D (2008). Antipsychotics differ in their ability to internalise human dopamine D2S and human serotonin 5-HT1A receptors in HEK293 cells. *European journal of pharmacology* **581**(1-2)**:** 37-46.

Hilf G, Gierschik P, Jakobs KH (1989). Muscarinic acetylcholine receptor-stimulated binding of guanosine 5′ -O-(3-thiotriphosphate) to guanine-nucleotide-binding proteins in cardiac membranes. *European journal of biochemistry / FEBS* **186**(3)**:** 725-731.

Hill AV (1909). The mode of action of nicotine and curari, determined by the form of the contraction curve and the method of temperature coefficients. *J. Physiol.* **39**(5)**:** 361-373.

Hill AV (1910). The possible effects of the aggregation of the molecules of haemoglobin on its dissociation curve. *J. Physiol.* **40**(Suppl)**:** iv-vii.

Hill SJ, Baker JG, Rees S (2001). Reporter-gene systems for the study of G-protein-coupled receptors. *Current opinion in pharmacology* **1**(5)**:** 526-532.

Hill SJ, Williams C, May LT (2010). Insights into GPCR pharmacology from the measurement of changes in intracellular cyclic AMP; advantages and pitfalls of differing methodologies. *British journal of pharmacology* **161**(6)**:** 1266-1275.

Hoffmann C, Gaietta G, Zurn A, Adams SR, Terrillon S, Ellisman MH*, et al.* (2010). Fluorescent labeling of tetracysteine-tagged proteins in intact cells. *Nat. Protocols* **5**(10)**:** 1666-1677.

Hoffmann C, Ziegler N, Reiner S, Krasel C, Lohse MJ (2008). Agonist-selective, Receptor-specific Interaction of Human P2Y Receptors with β-Arrestin-1 and -2. *J Biol Chem.* **283**(45)**:** 30933-30941.

Howes OD, Kapur S (2009). The dopamine hypothesis of schizophrenia: version III--the final common pathway. *Schizophrenia bulletin* **35**(3)**:** 549-562.

Huang P, Li J, Chen C, Visiers I, Weinstein H, Liu-Chen L-Y (2001). Functional Role of a Conserved Motif in TM6 of the Rat μ Opioid Receptor: Constitutively Active and Inactive Receptors Result from Substitutions of Thr6.34(279) with Lys and Asp. *Biochemistry* **40**(45)**:** 13501-13509.

Huang P, Visiers I, Weinstein H, Liu-Chen L-Y (2002). The Local Environment at the Cytoplasmic End of TM6 of the μ Opioid Receptor Differs from Those of Rhodopsin and Monoamine Receptors: Introduction of an Ionic Lock between the Cytoplasmic Ends of Helices 3 and 6 by a L6.30(275)E Mutation Inactivates the μ Opioid Receptor and Reduces the Constitutive Activity of Its T6.34(279)K Mutant. *Biochemistry* **41**(40)**:** 11972-11980.

Huang W, Manglik A, Venkatakrishnan AJ, Laeremans T, Feinberg EN, Sanborn AL*, et al.* (2015). Structural insights into μ-opioid receptor activation. *Nature* **524**(7565)**:** 315-321.

Hulme EC, Trevethick MA (2010). Ligand binding assays at equilibrium: validation and interpretation. *British journal of pharmacology* **161**(6)**:** 1219-1237.

Ingvar DH, Franzen G (1974). Abnormalities of cerebral blood flow distribution in patients with chronic schizophrenia. *Acta Psychiatr Scand* **50**(4)**:** 425-462.

Iravani MM, McCreary AC, Jenner P (2012). Striatal plasticity in Parkinson's disease and L-dopa induced dyskinesia. *Parkinsonism & related disorders* **18 Suppl 1:** S123-125.

Isogai S, Deupi X, Opitz C, Heydenreich FM, Tsai C-J, Brueckner F*, et al.* (2016). Backbone NMR reveals allosteric signal transduction networks in the β1-adrenergic receptor. *Nature* **530**(7589)**:** 237-241.

Ito K, Haga T, Lameh J, Sadee W (1999). Sequestration of dopamine D2 receptors depends on coexpression of G-protein-coupled receptor kinases 2 or 5. *European journal of biochemistry / FEBS* **260**(1)**:** 112-119.

Itokawa M, Toru M, Ito K, Tsuga H, Kameyama K, Haga T*, et al.* (1996). Sequestration of the short and long isoforms of dopamine D2 receptors expressed in Chinese hamster ovary cells. *Molecular pharmacology* **49**(3)**:** 560-566.

Iwami G, Kawabe J-i, Ebina T, Cannon PJ, Homcy CJ, Ishikawa Y (1995). Regulation of Adenylyl Cyclase by Protein Kinase A. *J Biol Chem.* **270**(21)**:** 12481-12484.

Iwamoto T, Okumura S, Iwatsubo K, Kawabe J-I, Ohtsu K, Sakai I*, et al.* (2003). Motor Dysfunction in Type 5 Adenylyl Cyclase-null Mice. *J Biol Chem.* **278**(19)**:** 16936-16940.

Javitch JA, Fu D, Chen J, Karlin A (1995). Mapping the binding-site crevice of the dopamine D2 receptor by the substituted-cysteine accessibility method. *Neuron* **14**(4)**:** 825-831.

Javitch JA, Fu D, Liapakis G, Chen J (1997). Constitutive Activation of the β2 Adrenergic Receptor Alters the Orientation of Its Sixth Membrane-spanning Segment. *J Biol Chem.* **272**(30)**:** 18546-18549.

Jenkinson DH (2003). Classical Approaches to the Study of Drug–Receptor Interactions. In: Foreman JC, Johansen, T.J. (ed)^(eds). *Textbook of Receptor Pharmacology*, edn. Boca Raton, Florida: CRC Press LLC. p^pp 4-72.

Jensen DD, Halls ML, Murphy JE, Canals M, Cattaruzza F, Poole DP*, et al.* (2014). Endothelin-converting Enzyme 1 and β-Arrestins Exert Spatiotemporal Control of Substance P-induced Inflammatory Signals. *J Biol Chem.* **289**(29)**:** 20283-20294.

Jentsch JD, Redmond DE, Elsworth JD, Taylor JR, Youngren KD, Roth RH (1997). Enduring Cognitive Deficits and Cortical Dopamine Dysfunction in Monkeys After Long-Term Administration of Phencyclidine. *Science* **277**(5328)**:** 953-955.

Johnson FH, Shimomura O, Saiga Y, Gershman LC, Reynolds GT, Waters JR (1962). Quantum efficiency of Cypridina luminescence, with a note on that of Aequorea. *Journal of cellular and comparative physiology* **60**(1)**:** 85-103.

Jordan S, Johnson JL, Regardie K, Chen R, Koprivica V, Tadori Y*, et al.* (2007). Dopamine D2 receptor partial agonists display differential or contrasting characteristics in membrane and cell-based assays of dopamine D2 receptor signaling. *Prog. Neuropsychopharmacol. Biol. Psychiatry* **31**(2)**:** 348-356.

Kalani MY, Vaidehi N, Hall SE, Trabanino RJ, Freddolino PL, Kalani MA*, et al.* (2004). The predicted 3D structure of the human D2 dopamine receptor and the binding site and binding affinities for agonists and antagonists. *Proceedings of the National Academy of Sciences of the United States of America* **101**(11)**:** 3815-3820.

Kalsner S (1973). Mechanism of potentiation by amines of non-equilibrium blockade of the α-adrenoceptor. *British journal of pharmacology* **47**(2)**:** 386-397.

Kang Y, Zhou XE, Gao X, He Y, Liu W, Ishchenko A*, et al.* (2015). Crystal structure of rhodopsin bound to arrestin by femtosecond X-ray laser. *Nature* **523**(7562)**:** 561-567.

Kapur S, Seeman P (2001). Does fast dissociation from the dopamine d(2) receptor explain the action of atypical antipsychotics?: A new hypothesis. *The American journal of psychiatry* **158**(3)**:** 360-369.

Karam CS, Ballon JS, Bivens NM, Freyberg Z, Girgis RR, Lizardi-Ortiz JE*, et al.* (2010). Signaling pathways in schizophrenia: emerging targets and therapeutic strategies. *Trends in pharmacological sciences* **31**(8)**:** 381-390.

Karlsson P, Farde L, Halldin C, Sedvall G (2002). PET study of D(1) dopamine receptor binding in neuroleptic-naive patients with schizophrenia. *The American journal of psychiatry* **159**(5)**:** 761-767.

Katritch V, Fenalti G, Abola EE, Roth BL, Cherezov V, Stevens RC (2014). Allosteric sodium in class A GPCR signaling. *Trends Biochem Sci* **39**(5)**:** 233-244.

Kemp DM, George SE, Bungay PJ, Naylor LH (1999). Partial agonism at serotonin 5-HT1B and dopamine D2L receptors using a luciferase reporter gene assay. *European journal of pharmacology* **373**(2–3)**:** 215-222.

Kenakin T (2014a). What is pharmacological 'affinity'? Relevance to biased agonism and antagonism. *Trends in pharmacological sciences* **35**(9)**:** 434-441.

Kenakin T, Christopoulos A (2013a). Measurements of ligand bias and functional affinity. *Nature reviews. Drug discovery* **12**(6)**:** 483-483.

Kenakin T, Christopoulos A (2013b). Signalling bias in new drug discovery: detection, quantification and therapeutic impact. *Nature reviews. Drug discovery* **12**(3)**:** 205-216.

Kenakin T, Jenkinson S, Watson C (2006). Determining the potency and molecular mechanism of action of insurmountable antagonists. *The Journal of pharmacology and experimental therapeutics* **319**(2)**:** 710-723.

Kenakin T, Miller LJ (2010). Seven Transmembrane Receptors as Shapeshifting Proteins: The Impact of Allosteric Modulation and Functional Selectivity on New Drug Discovery. *Pharmacological reviews* **62**(2)**:** 265-304.

Kenakin T, Watson C, Muniz-Medina V, Christopoulos A, Novick S (2011). A Simple Method for Quantifying Functional Selectivity and Agonist Bias. *ACS Chem. Neurosci.* **3**(3)**:** 193-203.

Kenakin T, Williams M (2014). Defining and characterizing drug/compound function. *Biochemical pharmacology* **87**(1)**:** 40-63.

Kenakin TP (2012). Biased signalling and allosteric machines: new vistas and challenges for drug discovery. *British journal of pharmacology* **165**(6)**:** 1659-1669.

Kenakin TP (2014b). *A Pharmacology Primer: Techniques for More Effective and Strategic Drug Discovery*. 4th Edition edn. Academic Press: San Diego.

Keov P, Sexton PM, Christopoulos A (2011). Allosteric modulation of G protein-coupled receptors: A pharmacological perspective. *Neuropharmacol.* **60**(1)**:** 24-35.

Keppler A, Gendreizig S, Gronemeyer T, Pick H, Vogel H, Johnsson K (2003). A general method for the covalent labeling of fusion proteins with small molecules in vivo. *Nat Biotech* **21**(1)**:** 86-89.

Keppler A, Pick H, Arrivoli C, Vogel H, Johnsson K (2004). Labeling of fusion proteins with synthetic fluorophores in live cells. *Proceedings of the National Academy of Sciences of the United States of America* **101**(27)**:** 9955-9959.

Kilpatrick LE, Briddon SJ, Hill SJ, Holliday ND (2010). Quantitative analysis of neuropeptide Y receptor association with β-arrestin2 measured by bimolecular fluorescence complementation. *British journal of pharmacology* **160**(4)**:** 892-906.

Kilpatrick LE, Humphrys LJ, Holliday ND (2015). A g protein-coupled receptor dimer imaging assay reveals selectively modified pharmacology of neuropeptide y y1/y5 receptor heterodimers. *Molecular pharmacology* **87**(4)**:** 718-732.

Kilts JD, Connery HS, Arrington EG, Lewis MM, Lawler CP, Oxford GS*, et al.* (2002). Functional selectivity of dopamine receptor agonists. II. Actions of dihydrexidine in D2L receptor-transfected MN9D cells and pituitary lactotrophs. *The Journal of pharmacology and experimental therapeutics* **301**(3)**:** 1179-1189.

Kim JH, Cho EY, Min C, Park JH, Kim KM (2008). Characterization of functional roles of DRY motif in the 2nd intracellular loop of dopamine D2 and D3 receptors. *Arch Pharm Res* **31**(4)**:** 474-481.

Kim KM, Valenzano KJ, Robinson SR, Yao WD, Barak LS, Caron MG (2001). Differential regulation of the dopamine D2 and D3 receptors by G protein-coupled receptor kinases and beta-arrestins. *The Journal of biological chemistry* **276**(40)**:** 37409-37414.

Kim SJ, Kim MY, Lee EJ, Ahn YS, Baik JH (2004). Distinct regulation of internalization and mitogen-activated protein kinase activation by two isoforms of the dopamine D2 receptor. *Molecular endocrinology (Baltimore, Md.)* **18**(3)**:** 640-652.

Kjelsberg MA, Cotecchia S, Ostrowski J, Caron MG, Lefkowitz RJ (1992). Constitutive activation of the alpha 1B-adrenergic receptor by all amino acid substitutions at a single site. Evidence for a region which constrains receptor activation. *J Biol Chem.* **267**(3)**:** 1430-1433.

Klein Herenbrink C, Sykes DA, Donthamsetti P, Canals M, Coudrat T, Shonberg J*, et al.* (2016). The role of kinetic context in apparent biased agonism at GPCRs. *Nat Commun* **7**.

Klewe IV, Nielsen SM, Tarpø L, Urizar E, Dipace C, Javitch JA*, et al.* (2008). Recruitment of β-arrestin2 to the dopamine D2 receptor: Insights into anti-psychotic and anti-parkinsonian drug receptor signaling. *Neuropharmacol.* **54**(8)**:** 1215-1222.

Kling RC, Clark T, Gmeiner P (2016). Comparative MD Simulations Indicate a Dual Role for Arg132$^{3.50}$ in Dopamine-Dependent D2R Activation. *PloS one* **11**(1)**:** e0146612.

Kling RC, Lanig H, Clark T, Gmeiner P (2013). Active-State Models of Ternary GPCR Complexes: Determinants of Selective Receptor-G-Protein Coupling. *PloS one* **8**(6)**:** e67244.

Kling RC, Tschammer N, Lanig H, Clark T, Gmeiner P (2014). Active-State Model of a Dopamine D_2 Receptor - $G\alpha_i$ Complex Stabilized by Aripiprazole-Type Partial Agonists. *PloS one* **9**(6)**:** e100069.

Koener B, Focant MC, Bosier B, Maloteaux JM, Hermans E (2012). Increasing the density of the D2L receptor and manipulating the receptor environment are required to evidence the partial agonist properties of aripiprazole. *Progress in neuro-psychopharmacology & biological psychiatry* **36**(1)**:** 60-70.

Kofuku Y, Ueda T, Okude J, Shiraishi Y, Kondo K, Maeda M*, et al.* (2012). Efficacy of the β2-adrenergic receptor is determined by conformational equilibrium in the transmembrane region. *Nat Commun* **3:** 1045.

Koval A, Kopein D, Purvanov V, Katanaev VL (2010). Europium-labeled GTP as a general nonradioactive substitute for [35S]GTPγS in high-throughput G protein studies. *Anal. Biochem.* **397**(2)**:** 202-207.

Krogsgaard-Larsen N, Harpsoe K, Kehler J, Christoffersen CT, Brosen P, Balle T (2014). Revision of the classical dopamine D2 agonist pharmacophore based on an integrated medicinal chemistry, homology modelling and computational docking approach. *Neurochemical research* **39**(10)**:** 1997-2007.

Kruse AC, Hu J, Pan AC, Arlow DH, Rosenbaum DM, Rosemond E*, et al.* (2012). Structure and dynamics of the M3 muscarinic acetylcholine receptor. *Nature* **482**(7386)**:** 552-556.

Küffer A, Lakkaraju AKK, Mogha A, Petersen SC, Airich K, Doucerain C*, et al.* (2016). The prion protein is an agonistic ligand of the G protein-coupled receptor Adgrg6. *Nature* **advance online publication**.

Labrecque J, Wong RS, Fricker SP (2009). A time-resolved fluorescent lanthanide (Eu)-GTP binding assay for chemokine receptors as targets in drug discovery. *Methods in molecular biology (Clifton, N.J.)* **552:** 153-169.

Lambright DG, Sondek J, Bohm A, Skiba NP, Hamm HE, Sigler PB (1996). The 2.0 A crystal structure of a heterotrimeric G protein. *Nature* **379**(6563)**:** 311-319.

Lan H, Liu Y, Bell MI, Gurevich VV, Neve KA (2009). A Dopamine D2 Receptor Mutant Capable of G Protein-Mediated Signaling but Deficient in Arrestin Binding. *Molecular pharmacology* **75**(1)**:** 113-123.

Lane JR, Powney B, Wise A, Rees S, Milligan G (2007). Protean agonism at the dopamine D2 receptor: (S)-3-(3-hydroxyphenyl)-N-propylpiperidine is an agonist for activation of Go1 but an antagonist/inverse agonist for Gi1,Gi2, and Gi3. *Molecular pharmacology* **71**(5)**:** 1349-1359.

Lawler CP, Prioleau C, Lewis MM, Mak C, Jiang D, Schetz JA*, et al.* (1999). Interactions of the novel antipsychotic aripiprazole (OPC-14597) with dopamine and serotonin receptor subtypes. *Neuropsychopharmacology : official publication of the American College of Neuropsychopharmacology* **20**(6)**:** 612-627.

Lee K-W, Hong J-H, Choi IY, Che Y, Lee J-K, Yang S-D*, et al.* (2002). Impaired D2 Dopamine Receptor Function in Mice Lacking Type 5 Adenylyl Cyclase. *J. Neurosci.* **22**(18)**:** 7931-7940.

Lee M-H, Appleton KM, Strungs EG, Kwon JY, Morinelli TA, Peterson YK*, et al.* (2016). The conformational signature of β-arrestin2 predicts its trafficking and signalling functions. *Nature* **531**(7596)**:** 665-668.

Lee S-M, Booe JM, Pioszak AA (2015). Structural insights into ligand recognition and selectivity for classes A, B, and C GPCRs. *European journal of pharmacology* **763, Part B:** 196-205.

Leff P, Dougall IG, Harper D (1993). Estimation of partial agonist affinity by interaction with a full agonist: a direct operational model-fitting approach. *British journal of pharmacology* **110**(1)**:** 239-244.

Leff P, Harper D (1989). Do pharmacological methods for the quantification of agonists work when the ternary complex mechanism operates? *J Theor Biol* **140**(3)**:** 381-397.

Leucht S, Corves C, Arbter D, Engel RR, Li C, Davis JM (2009). Second-generation versus first-generation antipsychotic drugs for schizophrenia: a meta-analysis. *The Lancet* **373**(9657)**:** 31-41.

Lew M (2007). Overview of Parkinson's disease. *Pharmacotherapy* **27**(12 Pt 2)**:** 155S-160S.

Li J, Huang P, Chen C, de Riel JK, Weinstein H, Liu-Chen L-Y (2001). Constitutive Activation of the μ Opioid Receptor by Mutation of D3.49(164), but Not D3.32(147): D3.49(164) Is Critical for Stabilization of the Inactive Form of the Receptor and for Its Expression. *Biochemistry* **40**(40)**:** 12039-12050.

Li X, Rosborough KM, Friedman AB, Zhu W, Roth KA (2007). Regulation of mouse brain glycogen synthase kinase-3 by atypical antipsychotics. *Int. J. Neuropsychopharmacol.* **10**(1)**:** 7-19.

Liapakis G, Ballesteros JA, Papachristou S, Chan WC, Chen X, Javitch JA (2000). The Forgotten Serine: A Critical Role for Ser-$203^{5.42}$ in Ligand Binding to and Activation of the β2-adrenergic Receptor. *J Biol Chem.* **275**(48)**:** 37779-37788.

Lin H, Saisch SG, Strange PG (2006). Assays for enhanced activity of low efficacy partial agonists at the D(2) dopamine receptor. *British journal of pharmacology* **149**(3)**:** 291-299.

Lindgren N, Usiello A, Goiny M, Haycock J, Erbs E, Greengard P*, et al.* (2003). Distinct roles of dopamine D2L and D2S receptor isoforms in the regulation of protein phosphorylation at presynaptic and postsynaptic sites. *Proceedings of the National Academy of Sciences of the United States of America* **100**(7)**:** 4305-4309.

Liu W, Chun E, Thompson AA, Chubukov P, Xu F, Katritch V*, et al.* (2012). Structural Basis for Allosteric Regulation of GPCRs by Sodium Ions. *Science* **337**(6091)**:** 232-236.

Lohse M, Benovic J, Codina J, Caron M, Lefkowitz R (1990). β-Arrestin: A protein that regulates β-adrenergic receptor function. *Science* **248**(4962)**:** 1547-1550.

Los GV, Encell LP, McDougall MG, Hartzell DD, Karassina N, Zimprich C*, et al.* (2008). HaloTag: A Novel Protein Labeling Technology for Cell Imaging and Protein Analysis. *ACS Chem. Biol.* **3**(6)**:** 373-382.

Luo R, Jeong S-J, Jin Z, Strokes N, Li S, Piao X (2011). G protein-coupled receptor 56 and collagen III, a receptor-ligand pair, regulates cortical development and lamination. *Proc. Natl. Acad. Sci. USA* **108**(31)**:** 12925-12930.

Maeda K, Sugino H, Akazawa H, Amada N, Shimada J, Futamura T*, et al.* (2014). Brexpiprazole I: In Vitro and In Vivo Characterization of a Novel Serotonin-Dopamine Activity Modulator. *J. Pharm. Exp. Ther.* **350**(3)**:** 589-604.

Mailman RB, Murthy V (2010). Third generation antipsychotic drugs: partial agonism or receptor functional selectivity? *Current pharmaceutical design* **16**(5)**:** 488-501.

Majumdar A, Mangal NS (2013). Hyperprolactinemia. *Journal of human reproductive sciences* **6**(3)**:** 168-175.

Malmberg A, Nordvall G, Johansson AM, Mohell N, Hacksell U (1994). Molecular basis for the binding of 2-aminotetralins to human dopamine D2A and D3 receptors. *Molecular pharmacology* **46**(2)**:** 299-312.

Manglik A, Kim Tae H, Masureel M, Altenbach C, Yang Z, Hilger D*, et al.* (2015). Structural Insights into the Dynamic Process of β2-Adrenergic Receptor Signaling. *Cell* **161**(5)**:** 1101-1111.

Manglik A, Kruse AC, Kobilka TS, Thian FS, Mathiesen JM, Sunahara RK*, et al.* (2012). Crystal structure of the μ-opioid receptor bound to a morphinan antagonist. *Nature* **485**(7398)**:** 321-326.

Mangmool S, Kurose H (2011). G(i/o) Protein-Dependent and -Independent Actions of Pertussis Toxin (PTX). *Toxins* **3**(7)**:** 884-899.

Mannoury la Cour C, Salles MJ, Pasteau V, Millan MJ (2011). Signaling pathways leading to phosphorylation of Akt and GSK-3β by activation of cloned human and rat cerebral D_2 and D_3 receptors. *Molecular pharmacology* **79**(1)**:** 91-105.

Mansour A, Meng F, Meador-Woodruff JH, Taylor LP, Civelli O, Akil H (1992). Site-directed mutagenesis of the human dopamine D2 receptor. *European journal of pharmacology* **227**(2)**:** 205-214.

Masri B, Salahpour A, Didriksen M, Ghisi V, Beaulieu JM, Gainetdinov RR*, et al.* (2008). Antagonism of dopamine D2 receptor/β-arrestin 2 interaction is a common property of clinically effective antipsychotics. *Proceedings of the National Academy of Sciences of the United States of America* **105**(36)**:** 13656-13661.

Massink A, Gutiérrez-de-Terán H, Lenselink EB, Ortiz Zacarías NV, Xia L, Heitman LH*, et al.* (2015). Sodium Ion Binding Pocket Mutations and Adenosine A2A Receptor Function. *Molecular pharmacology* **87**(2)**:** 305-313.

Matz MV, Fradkov AF, Labas YA, Savitsky AP, Zaraisky AG, Markelov ML*, et al.* (1999). Fluorescent proteins from nonbioluminescent Anthozoa species. *Nat Biotech* **17**(10)**:** 969-973.

Maurel D, Comps-Agrar L, Brock C, Rives M-L, Bourrier E, Ayoub MA*, et al.* (2008). Cell-surface protein-protein interaction analysis with time-resolved FRET and snap-tag technologies: application to GPCR oligomerization. *Nat Meth* **5**(6)**:** 561-567.

McLean AJ, Zeng F-Y, Behan D, Chalmers D, Milligan G (2002). Generation and Analysis of Constitutively Active and Physically Destabilized Mutants of the Human β1-Adrenoceptor. *Molecular pharmacology* **62**(3)**:** 747-755.

McLoughlin DJ, Strange PG (2000). Mechanisms of Agonism and Inverse Agonism at Serotonin 5-HT1A Receptors. *Journal of neurochemistry* **74**(1)**:** 347-357.

Meller E, Puza T, Diamond J, Lieu HD, Bohmaker K (1992). Comparative effects of receptor inactivation, 17 beta-estradiol and pertussis toxin on dopaminergic inhibition of prolactin secretion in vitro. *The Journal of pharmacology and experimental therapeutics* **263**(2)**:** 462-469.

Meller E, Puza T, Miller JC, Friedhoff AJ, Schweitzer JW (1991). Receptor reserve for D2 dopaminergic inhibition of prolactin release in vivo and in vitro. *The Journal of pharmacology and experimental therapeutics* **257**(2)**:** 668-675.

Meltzer HY, Li Z, Kaneda Y, Ichikawa J (2003). Serotonin receptors : their key role in drugs to treat schizophrenia. *Prog. Neuropsychopharmacol. Biol. Psychiatry* **27**(7)**:** 1159-1172.

Meltzer HY, Massey BW (2011). The role of serotonin receptors in the action of atypical antipsychotic drugs. *Current opinion in pharmacology* **11**(1)**:** 59-67.

Meltzer HY, Matsubara S, Lee JC (1989). Classification of typical and atypical antipsychotic drugs on the basis of dopamine D-1, D-2 and serotonin2 pKi values. *J. Pharm. Exp. Ther.* **251**(1)**:** 238-246.

Meye FJ, Ramakers GMJ, Adan RAH (2014). The vital role of constitutive GPCR activity in the mesolimbic dopamine system. *Transl Psychiatry* **4:** e361.

Meyer-Lindenberg A, Miletich RS, Kohn PD, Esposito G, Carson RE, Quarantelli M*, et al.* (2002). Reduced prefrontal activity predicts exaggerated striatal dopaminergic function in schizophrenia. *Nature neuroscience* **5**(3)**:** 267-271.

Millan MJ, Maiofiss L, Cussac D, Audinot V, Boutin J-A, Newman-Tancredi A (2002). Differential Actions of Antiparkinson Agents at Multiple Classes of Monoaminergic Receptor. I. A Multivariate Analysis of the Binding Profiles of 14 Drugs at 21 Native and Cloned Human Receptor Subtypes. *J. Pharm. Exp. Ther.* **303**(2)**:** 791-804.

Milligan G (2003). Principles: extending the utility of [35S]GTP gamma S binding assays. *Trends in pharmacological sciences* **24**(2)**:** 87-90.

Milligan G, Kostenis E (2006). Heterotrimeric G-proteins: a short history. *British journal of pharmacology* **147**(S1)**:** S46-S55.

Miyake N, Thompson J, Skinbjerg M, Abi-Dargham A (2011). Presynaptic dopamine in schizophrenia. *CNS Neurosci Ther* **17**(2)**:** 104-109.

Mohn AR, Gainetdinov RR, Caron MG, Koller BH (1999). Mice with Reduced NMDA Receptor Expression Display Behaviors Related to Schizophrenia. *Cell* **98**(4)**:** 427-436.

Monsma FJ, Jr., McVittie LD, Gerfen CR, Mahan LC, Sibley DR (1989). Multiple D2 dopamine receptors produced by alternative RNA splicing. *Nature* **342**(6252)**:** 926-929.

Morey TE, Belardinelli L, Dennis DM (1998). Validation of Furchgott's method to determine agonist-dependent A1-adenosine receptor reserve in guinea-pig atrium. *British journal of pharmacology* **123**(7)**:** 1425-1433.

Morris SJ, Van H, II, Daigle M, Robillard L, Sajedi N, Albert PR (2007). Differential desensitization of dopamine D2 receptor isoforms by protein kinase C: the importance of receptor phosphorylation and pseudosubstrate sites. *European journal of pharmacology* **577**(1-3)**:** 44-53.

Mottola DM, Kilts JD, Lewis MM, Connery HS, Walker QD, Jones SR*, et al.* (2002). Functional selectivity of dopamine receptor agonists. I. Selective activation of postsynaptic dopamine D2 receptors linked to adenylate cyclase. *The Journal of pharmacology and experimental therapeutics* **301**(3)**:** 1166-1178.

Moukhametzianov R, Warne T, Edwards PC, Serrano-Vega MJ, Leslie AGW, Tate CG*, et al.* (2011). Two distinct conformations of helix 6 observed in antagonist-bound structures of a β1-adrenergic receptor. *Proc. Natl. Acad. Sci. USA* **108**(20)**:** 8228-8232.

Mould R, Brown J, Marshall FH, Langmead CJ (2014). Binding kinetics differentiates functional antagonism of orexin-2 receptor ligands. *British journal of pharmacology* **171**(2)**:** 351-363.

Namkung Y, Sibley DR (2004). Protein kinase C mediates phosphorylation, desensitization, and trafficking of the D2 dopamine receptor. *The Journal of biological chemistry* **279**(47)**:** 49533-49541.

Navratilova E, Waite S, Stropova D, Eaton MC, Alves ID, Hruby VJ*, et al.* (2007). Quantitative evaluation of human delta opioid receptor desensitization using the operational model of drug action. *Molecular pharmacology* **71**(5)**:** 1416-1426.

Neve KA (1991). Regulation of dopamine D2 receptors by sodium and pH. *Molecular pharmacology* **39**(4)**:** 570-578.

Neve KA, Cox BA, Henningsen RA, Spanoyannis A, Neve RL (1991). Pivotal role for aspartate-80 in the regulation of dopamine D2 receptor affinity for drugs and inhibition of adenylyl cyclase. *Molecular pharmacology* **39**(6)**:** 733-739.

Neve KA, Cumbay MG, Thompson KR, Yang R, Buck DC, Watts VJ*, et al.* (2001). Modeling and Mutational Analysis of a Putative Sodium-Binding Pocket on the Dopamine D2 Receptor. *Molecular pharmacology* **60**(2)**:** 373-381.

Neve KA, Ford CP, Buck DC, Grandy DK, Neve RL, Phillips TJ (2013). Normalizing dopamine D2 receptor-mediated responses in D2 null mutant mice by virus-mediated receptor restoration: Comparing D2L and D2S. *Neuroscience* **248:** 479-487.

Neve KA, Neve RL (1997). Molecular Biology of Dopamine Receptors. In: Neve KA, Neve RL (ed)^(eds). *The Dopamine Receptors*, edn. New York: Humana Press. p^pp 27-76.

Nevo I, Avidor-Reiss T, Levy R, Bayewitch M, Heldman E, Vogel Z (1998). Regulation of Adenylyl Cyclase Isozymes on Acute and Chronic Activation of Inhibitory Receptors. *Molecular pharmacology* **54**(2)**:** 419-426.

Newman-Tancredi A, Kleven MS (2011). Comparative pharmacology of antipsychotics possessing combined dopamine D2 and serotonin 5-HT1A receptor properties. *Psychopharmacology* **216**(4)**:** 451-473.

Nickolls SA, Strange PG (2004). The influence of G protein subtype on agonist action at D2 dopamine receptors. *Neuropharmacol.* **47**(6)**:** 860-872.

Nickolls SA, Waterfield A, Williams RE, Kinloch RA (2011). Understanding the effect of different assay formats on agonist parameters: a study using the μ-opioid receptor. *J Biomol Screen* **16**(7)**:** 706-716.

Nikolaev VO, Bunemann M, Hein L, Hannawacker A, Lohse MJ (2004). Novel single chain cAMP sensors for receptor-induced signal propagation. *The Journal of biological chemistry* **279**(36)**:** 37215-37218.

Nord M, Farde L (2011). Antipsychotic occupancy of dopamine receptors in schizophrenia. *CNS Neurosci Ther* **17**(2)**:** 97-103.

Nuber S, Zabel U, Lorenz K, Nuber A, Milligan G, Tobin AB*, et al.* (2016). β-Arrestin biosensors reveal a rapid, receptor-dependent activation/deactivation cycle. *Nature* **531**(7596)**:** 661-664.

Oakley RH, Laporte SA, Holt JA, Barak LS, Caron MG (2001). Molecular Determinants Underlying the Formation of Stable Intracellular G Protein-coupled Receptor-β-Arrestin Complexes after Receptor Endocytosis*. *J Biol Chem.* **276**(22)**:** 19452-19460.

Oakley RH, Laporte SA, Holt JA, Caron MG, Barak LS (2000). Differential Affinities of Visual Arrestin, βArrestin1, and βArrestin2 for G Protein-coupled Receptors Delineate Two Major Classes of Receptors. *J Biol Chem.* **275**(22)**:** 17201-17210.

Odagaki Y, Toyoshima R (2006). Dopamine D2 receptor-mediated G protein activation assessed by agonist-stimulated [35S]guanosine 5′-O-(γ-thiotriphosphate) binding in rat striatal membranes. *Prog. Neuropsychopharmacol. Biol. Psychiatry* **30**(7)**:** 1304-1312.

Okubo Y, Suhara T, Suzuki K, Kobayashi K, Inoue O, Terasaki O*, et al.* (1997). Decreased prefrontal dopamine D1 receptors in schizophrenia revealed by PET. *Nature* **385**(6617)**:** 634-636.

Oldham WM, Hamm HE (2008). Heterotrimeric G protein activation by G-protein-coupled receptors. *Nat Rev Mol Cell Biol* **9**(1)**:** 60-71.

Palczewski K, Kumasaka T, Hori T, Behnke CA, Motoshima H, Fox BA*, et al.* (2000). Crystal structure of rhodopsin: A G protein-coupled receptor. *Science* **289**(5480)**:** 739-745.

Pauwels PJ, Gouble A, Wurch T (1999). Activation of constitutive 5-hydroxytryptamine(1B) receptor by a series of mutations in the BBXXB motif: positioning of the third intracellular loop distal junction and its G(o)alpha protein interactions. *The Biochemical journal* **2:** 435-442.

Payne SL, Johansson AM, Strange PG (2002). Mechanisms of ligand binding and efficacy at the human D2(short) dopamine receptor. *Journal of neurochemistry* **82**(5)**:** 1106-1117.

Perez-Aso M, Segura V, Montó F, Barettino D, Noguera MA, Milligan G*, et al.* (2013). The three α1-adrenoceptor subtypes show different spatio-temporal mechanisms of internalization and ERK1/2 phosphorylation. *Biochim Biophys Acta.* **1833**(10)**:** 2322-2333.

Platania CBM, Salomone S, Leggio GM, Drago F, Bucolo C (2012). Homology Modeling of Dopamine D2 and D3 Receptors: Molecular Dynamics Refinement and Docking Evaluation. *PloS one* **7**(9)**:** e44316.

Podder A, Pandey D, Latha N (2016). Investigating the structural impact of S311C mutation in DRD2 receptor by molecular dynamics & docking studies. *Biochimie* **123:** 52-64.

Pou C, Mannoury la Cour C, Stoddart LA, Millan MJ, Milligan G (2012). Functional Homomers and Heteromers of Dopamine D2L and D3 Receptors Co-exist at the Cell Surface. *J Biol Chem.* **287**(12)**:** 8864-8878.

Premont RT, Gainetdinov RR (2007). Physiological roles of G protein-coupled receptor kinases and arrestins. *Annual review of physiology* **69:** 511-534.

Purohit A, Herrick-Davis K, Teitler M (2003). Creation, expression, and characterization of a constitutively active mutant of the human serotonin 5-HT6 receptor. *Synapse (New York, N.Y.)* **47**(3)**:** 218-224.

Quan W, Kim J-H, Albert PR, Choi H, Kim K-M (2008). Roles of G protein and β-arrestin in dopamine D2 receptor-mediated ERK activation. *Biochem. Biophys. Res. Commun.* **377**(2)**:** 705-709.

Quirk K, Roberts DJ, Strange PG (2007). Mechanisms of G protein activation via the D2 dopamine receptor: evidence for persistent receptor/G protein interaction after agonist stimulation. *British journal of pharmacology* **151**(1)**:** 125-133.

Racioppi L, Means AR (2012). Calcium/Calmodulin-dependent Protein Kinase Kinase 2: Roles in Signaling and Pathophysiology. *Journal of Biological Chemistry* **287**(38)**:** 31658-31665.

Rajagopal S (2013). Quantifying biased agonism: understanding the links between affinity and efficacy. *Nature reviews. Drug discovery* **12**(6)**:** 483-483.

Rajagopal S, Ahn S, Rominger DH, Gowen-MacDonald W, Lam CM, Dewire SM*, et al.* (2011). Quantifying ligand bias at seven-transmembrane receptors. *Molecular pharmacology* **80**(3)**:** 367-377.

Rajagopal S, Rajagopal K, Lefkowitz RJ (2010). Teaching old receptors new tricks: biasing seven-transmembrane receptors. *Nature reviews. Drug discovery* **9**(5)**:** 373-386.

Raote I, Bhattacharyya S, Panicker MM (2013). Functional Selectivity in Serotonin Receptor 2A (5-HT2A) Endocytosis, Recycling, and Phosphorylation. *Molecular pharmacology* **83**(1)**:** 42-50.

Rasmussen SG, DeVree BT, Zou Y, Kruse AC, Chung KY, Kobilka TS*, et al.* (2011a). Crystal structure of the β2 adrenergic receptor-Gs protein complex. *Nature* **477**(7366)**:** 549-555.

Rasmussen SG, Jensen AD, Liapakis G, Ghanouni P, Javitch JA, Gether U (1999). Mutation of a highly conserved aspartic acid in the β_2 adrenergic receptor: constitutive activation, structural instability, and conformational rearrangement of transmembrane segment 6. *Molecular pharmacology* **56**(1)**:** 175-184.

Rasmussen SGF, Choi H-J, Fung JJ, Pardon E, Casarosa P, Chae PS*, et al.* (2011b). Structure of a nanobody-stabilized active state of the β_2 adrenoceptor. *Nature* **469**(7329)**:** 175-180.

Reinartz M, Kälble S, Littmann T, Ozawa T, Dove S, Kaever V*, et al.* (2015). Structure-bias relationships for fenoterol stereoisomers in six molecular and cellular assays at the β2-adrenoceptor. *Naunyn-Schmiedeberg's Arch Pharmacol* **388**(1)**:** 51-65.

Ren Q, Kurose H, Lefkowitz RJ, Cotecchia S (1993). Constitutively active mutants of the alpha 2-adrenergic receptor. *The Journal of biological chemistry* **268**(22)**:** 16483-16487.

Roberts DJ, Lin H, Strange PG (2004). Investigation of the mechanism of agonist and inverse agonist action at D2 dopamine receptors. *Biochemical pharmacology* **67**(9)**:** 1657-1665.

Roberts DJ, Strange PG (2005). Mechanisms of inverse agonist action at D2 dopamine receptors. *British journal of pharmacology* **145**(1)**:** 34-42.

Robinson SW, Caron MG (1997). Selective Inhibition of Adenylyl Cyclase Type V by the Dopamine D3 Receptor. *Molecular pharmacology* **52**(3)**:** 508-514.

Roettger BF, Ghanekar D, Rao R, Toledo C, Yingling J, Pinon D*, et al.* (1997). Antagonist-Stimulated Internalization of the G Protein-Coupled Cholecystokinin Receptor. *Molecular pharmacology* **51**(3)**:** 357-362.

Root-Bernstein R, Dillon PF (2014). A Common Molecular Motif Characterizes Extracellular Allosteric Enhancers of GPCR Aminergic Receptors and Suggests Enhancer Mechanism of Action. *Current medicinal chemistry* **21**(32)**:** 3673-3686.

Rosethorne EM, Bradley ME, Gherbi K, Sykes DA, Sattikar A, Wright JD*, et al.* (2016). Long Receptor Residence Time of C26 Contributes to Super Agonist Activity at the Human β2 Adrenoceptor. *Molecular pharmacology* **89**(4)**:** 467-475.

Rovati GE, Capra V, Neubig RR (2007). The highly conserved DRY motif of class A G protein-coupled receptors: beyond the ground state. *Molecular pharmacology* **71**(4)**:** 959-964.

Sadana R, Dessauer CW (2009). Physiological Roles for G Protein-Regulated Adenylyl Cyclase Isoforms: Insights from Knockout and Overexpression Studies. *Neurosignals* **17**(1)**:** 5-22.

Samama P, Cotecchia S, Costa T, Lefkowitz RJ (1993). A mutation-induced activated state of the β2-adrenergic receptor. Extending the ternary complex model. *J Biol Chem.* **268**(7)**:** 4625-4636.

Sample V, Newman RH, Zhang J (2009). The structure and function of fluorescent proteins. *Chem. Soc. Rev.* **38**(10)**:** 2852-2864.

Sartania N, Strange PG (1999). Role of Conserved Serine Residues in the Interaction of Agonists with D3 Dopamine Receptors. *Journal of neurochemistry* **72**(6)**:** 2621-2624.

Sato T, Baker J, Warne T, Brown GA, Leslie AGW, Congreve M*, et al.* (2015). Pharmacological Analysis and Structure Determination of 7-Methylcyanopindolol–Bound β1-Adrenergic Receptor. *Molecular pharmacology* **88**(6)**:** 1024-1034.

Scheer A, Fanelli F, Costa T, De Benedetti PG, Cotecchia S (1996). Constitutively active mutants of the alpha 1B-adrenergic receptor: role of highly conserved polar amino acids in receptor activation. *The EMBO journal* **15**(14)**:** 3566-3578.

Schild HO (1949). pAx and competitive drug antagonism. *British journal of pharmacology and chemotherapy* **4**(3)**:** 277-280.

Schiöth HB, Nordström KJV, Fredriksson R (2010). The Adhesion GPCRs; Gene Repertoire, Phylogeny and Evolution. In: Yona S, Stacey M (ed)^(eds). *Adhesion-GPCRs: Structure to Function*, edn. Boston, MA: Springer US. p^pp 1-13.

Schizophrenia Working Group of the Psychiatric Genomics C (2014). Biological insights from 108 schizophrenia-associated genetic loci. *Nature* **511**(7510)**:** 421-427.

Schrage R, De Min A, Hochheiser K, Kostenis E, Mohr K (2015). Superagonism at G protein-coupled receptors and beyond. *British journal of pharmacology*.

Schwartz TW, Frimurer TM, Holst B, Rosenkilde MM, Elling CE (2006). Molecular mechanism of 7TM receptor activation--a global toggle switch model. *Annual review of pharmacology and toxicology* **46:** 481-519.

Seamon KB, Padgett W, Daly JW (1981). Forskolin: unique diterpene activator of adenylate cyclase in membranes and in intact cells. *Proceedings of the National Academy of Sciences of the United States of America* **78**(6)**:** 3363-3367.

Seeman P, Lee T (1975). Antipsychotic drugs: direct correlation between clinical potency and presynaptic action on dopamine neurons. *Science* **188**(4194)**:** 1217-1219.

Seifert R, Wenzel-Seifert K (2002). Constitutive activity of G-protein-coupled receptors: cause of disease and common property of wild-type receptors. *Naunyn-Schmiedeberg's Arch Pharmacol* **366**(5)**:** 381-416.

Selent J, Sanz F, Pastor M, De Fabritiis G (2010). Induced Effects of Sodium Ions on Dopaminergic G-Protein Coupled Receptors. *PLoS Comput Biol* **6**(8)**:** e1000884.

Selley DE, Cao CC, Liu Q, Childers SR (2000). Effects of sodium on agonist efficacy for G-protein activation in mu-opioid receptor-transfected CHO cells and rat thalamus. *British journal of pharmacology* **130**(5)**:** 987-996.

Selley DE, Liu Q, Childers SR (1998). Signal Transduction Correlates of Mu Opioid Agonist Intrinsic Efficacy: Receptor-Stimulated [^{35}S]GTPγS Binding in mMOR-CHO Cells and Rat Thalamus. *J. Pharm. Exp. Ther.* **285**(2)**:** 496-505.

Selley DE, Sim LJ, Xiao R, Liu Q, Childers SR (1997). μ-Opioid Receptor-Stimulated Guanosine-5′-O-(γ-thio)-triphosphate Binding in Rat Thalamus and Cultured Cell Lines: Signal Transduction Mechanisms Underlying Agonist Efficacy. *Molecular pharmacology* **51**(1)**:** 87-96.

Shapiro DA, Renock S, Arrington E, Chiodo LA, Liu LX, Sibley DR*, et al.* (2003). Aripiprazole, a novel atypical antipsychotic drug with a unique and robust pharmacology. *Neuropsychopharmacology : official publication of the American College of Neuropsychopharmacology* **28**(8)**:** 1400-1411.

Shenoy SK, Drake MT, Nelson CD, Houtz DA, Xiao K, Madabushi S*, et al.* (2006). β-Arrestin-dependent, G Protein-independent ERK1/2 Activation by the β2 Adrenergic Receptor. *J Biol Chem.* **281**(2)**:** 1261-1273.

Shi L, Javitch JA (2002). THE BINDING SITE OF AMINERGIC G PROTEIN–COUPLED RECEPTORS: The Transmembrane Segments and Second

Extracellular Loop. *Annual review of pharmacology and toxicology* **42**(1)**:** 437-467.

Shimomura O, Johnson FH, Saiga Y (1962). Extraction, purification and properties of aequorin, a bioluminescent protein from the luminous hydromedusan, Aequorea. *Journal of cellular and comparative physiology* **59:** 223-239.

Shnerb T, Lin N, Shurki A (2007). What Is the Role of the Helical Domain of Gsα in the GTPase Reaction? *Biochemistry* **46**(38)**:** 10875-10885.

Shonberg J, Herenbrink CK, Lopez L, Christopoulos A, Scammells PJ, Capuano B*, et al.* (2013). A structure-activity analysis of biased agonism at the dopamine D2 receptor. *Journal of medicinal chemistry* **56**(22)**:** 9199-9221.

Siehler S (2009). Regulation of RhoGEF proteins by G(12/13)-coupled receptors. *British journal of pharmacology* **158**(1)**:** 41-49.

Simon S, Young TJ, Nickolls SA (2009). The effect of assay formats on the estimation of melanocortin agonist affinity and efficacy using the operation model of agonism. *European journal of pharmacology* **615**(1-3)**:** 33-39.

Slack RJ, Hall DA (2012). Development of operational models of receptor activation including constitutive receptor activity and their use to determine the efficacy of the chemokine CCL17 at the CC chemokine receptor CCR4. *British journal of pharmacology* **166**(6)**:** 1774-1792.

Smit MJ, Vischer HF, Bakker RA, Jongejan A, Timmerman H, Pardo L*, et al.* (2007). Pharmacogenomic and Structural Analysis of Constitutive G Protein–Coupled Receptor Activity. *Annual review of pharmacology and toxicology* **47**(1)**:** 53-87.

Smith JS, Rajagopal S (2016). The β-Arrestins: Multifunctional Regulators of G Protein-coupled Receptors. *J Biol Chem.* **291**(17)**:** 8969-8977.

Smith PK, Krohn RI, Hermanson GT, Mallia AK, Gartner FH, Provenzano MD*, et al.* (1985). Measurement of protein using bicinchoninic acid. *Anal. Biochem.* **150**(1)**:** 76-85.

Snyder SH (1976). The dopamine hypothesis of schizophrenia: focus on the dopamine receptor. *Am. J. Psychiatry* **133**(2)**:** 197-202.

Soergel DG, Subach RA, Burnham N, Lark MW, James IE, Sadler BM*, et al.* (2014). Biased agonism of the mu-opioid receptor by TRV130 increases analgesia and reduces on-target adverse effects versus morphine: A randomized, double-blind, placebo-controlled, crossover study in healthy volunteers. *Pain* **155**(9)**:** 1829-1835.

Sorkin A, von Zastrow M (2009). Endocytosis and signalling: intertwining molecular networks. *Nat Rev Mol Cell Biol* **10**(9)**:** 609-622.

Spalding TA, Burstein ES, Wells JW, Brann MR (1997). Constitutive activation of the m5 muscarinic receptor by a series of mutations at the extracellular end of transmembrane 6. *Biochemistry* **36**(33)**:** 10109-10116.

Staus DP, Strachan RT, Manglik A, Pani B, Kahsai AW, Kim TH*, et al.* (2016). Allosteric nanobodies reveal the dynamic range and diverse mechanisms of G-protein-coupled receptor activation. *Nature* **535**(7612)**:** 448-452.

Steegborn C (2014). Structure, mechanism, and regulation of soluble adenylyl cyclases — similarities and differences to transmembrane adenylyl cyclases. *Biochim Biophys Acta.* **1842**(12, Part B)**:** 2535-2547.

Stephenson RP (1956). A modification of receptor theory. *British journal of pharmacology and chemotherapy* **11**(4)**:** 379-393.

Stip E, Tourjman V (2010). Aripiprazole in schizophrenia and schizoaffective disorder: A review. *Clinical therapeutics* **32 Suppl 1:** S3-20.

Stoddart LA, Kellam B, Briddon SJ, Hill SJ (2014). Effect of a toggle switch mutation in TM6 of the human adenosine A(3) receptor on Gi protein-dependent signalling and Gi-independent receptor internalization. *British journal of pharmacology* **171**(16)**:** 3827-3844.

Stott LA, Hall DA, Holliday ND (2016). Unravelling intrinsic efficacy and ligand bias at G protein coupled receptors: A practical guide to assessing functional data. *Biochemical pharmacology* **101:** 1-12.

Strader CD, Candelore MR, Hill WS, Sigal IS, Dixon RA (1989). Identification of two serine residues involved in agonist activation of the β-adrenergic receptor. *J Biol Chem.* **264**(23)**:** 13572-13578.

Strange PG (2008). Agonist binding, agonist affinity and agonist efficacy at G protein-coupled receptors. *British journal of pharmacology* **153**(7)**:** 1353-1363.

Strange PG (2010). Use of the GTPγS ([35S]GTPγS and Eu-GTPγS) binding assay for analysis of ligand potency and efficacy at G protein-coupled receptors. *British journal of pharmacology* **161**(6)**:** 1238-1249.

Sukalovic V, Soskic V, Sencanski M, Andric D, Kostic-Rajacic S (2013). Determination of key receptor-ligand interactions of dopaminergic arylpiperazines and the dopamine D2 receptor homology model. *J Mol Model* **19**(4)**:** 1751-1762.

Sunahara RK, Tesmer JJG, Gilman AG, Sprang SR (1997). Crystal Structure of the Adenylyl Cyclase Activator Gsα. *Science* **278**(5345)**:** 1943-1947.

Swaminath G, Deupi X, Lee TW, Zhu W, Thian FS, Kobilka TS*, et al.* (2005). Probing the β2 Adrenoceptor Binding Site with Catechol Reveals Differences in Binding and Activation by Agonists and Partial Agonists. *J Biol Chem.* **280**(23)**:** 22165-22171.

Sykes DA, Dowling MR, Charlton SJ (2009). Exploring the Mechanism of Agonist Efficacy: A Relationship between Efficacy and Agonist Dissociation Rate at the Muscarinic M3 Receptor. *Molecular pharmacology* **76**(3)**:** 543-551.

Szabo M, Klein Herenbrink C, Christopoulos A, Lane JR, Capuano B (2014). Structure-activity relationships of privileged structures lead to the discovery of novel biased ligands at the dopamine D(2) receptor. *Journal of medicinal chemistry* **57**(11)**:** 4924-4939.

Szekeres PG, Traynor JR (1997). Delta Opioid Modulation of the Binding of Guanosine-5′-O-(3-[^{35}S]thio)triphosphate to NG108‐15 Cell Membranes: Characterization of Agonist and Inverse Agonist Effects. *J. Pharm. Exp. Ther.* **283**(3)**:** 1276-1284.

Tadori Y, Forbes RA, McQuade RD, Kikuchi T (2011a). Functional potencies of dopamine agonists and antagonists at human dopamine D(2) and D(3) receptors. *European journal of pharmacology* **666**(1-3)**:** 43-52.

Tadori Y, Forbes RA, McQuade RD, Kikuchi T (2011b). In vitro pharmacology of aripiprazole, its metabolite and experimental dopamine partial agonists at human dopamine D2 and D3 receptors. *European journal of pharmacology* **668**(3)**:** 355-365.

Tadori Y, Miwa T, Tottori K, Burris KD, Stark A, Mori T*, et al.* (2005). Aripiprazole's low intrinsic activities at human dopamine D2L and D2S receptors render it a unique antipsychotic. *European journal of pharmacology* **515**(1-3)**:** 10-19.

Taylor SS, Ilouz R, Zhang P, Kornev AP (2012). Assembly of allosteric macromolecular switches: lessons from PKA. *Nat Rev Mol Cell Biol* **13**(10)**:** 646-658.

Tehan BG, Bortolato A, Blaney FE, Weir MP, Mason JS (2014). Unifying Family A GPCR Theories of Activation. *Pharmacol. Ther.* **143**(1)**:** 51-60.

Thompson GL, Lane JR, Coudrat T, Sexton PM, Christopoulos A, Canals M (2015). Biased Agonism of Endogenous Opioid Peptides at the μ-Opioid Receptor. *Molecular pharmacology* **88**(2)**:** 335-346.

Thompson GL, Lane JR, Coudrat T, Sexton PM, Christopoulos A, Canals M (2016). Systematic analysis of factors influencing observations of biased agonism at the mu-opioid receptor. *Biochemical pharmacology* **113:** 70-87.

Tolbert LC, Morris PE, Spollen JJ, Ashe SC (1992). Stereospecific effects of ascorbic acid and analogues on D1 and D2 agonist binding. *Life sciences* **51**(12)**:** 921-930.

Tran TM, Friedman J, Qunaibi E, Baameur F, Moore RH, Clark RB (2004). Characterization of Agonist Stimulation of cAMP-Dependent Protein Kinase and G Protein-Coupled Receptor Kinase Phosphorylation of the β2-Adrenergic Receptor Using Phosphoserine-Specific Antibodies. *Molecular pharmacology* **65**(1)**:** 196-206.

Trzaskowski B, Latek D, Yuan S, Ghoshdastider U, Debinski A, Filipek S (2012). Action of molecular switches in GPCRs--theoretical and experimental studies. *Current medicinal chemistry* **19**(8)**:** 1090-1109.

Tschammer N, Bollinger S, Kenakin T, Gmeiner P (2011). Histidine 6.55 Is a Major Determinant of Ligand-Biased Signaling in Dopamine D2L Receptor. *Molecular pharmacology* **79**(3)**:** 575-585.

Tsien RY (1998). The Green Fluorescent Protein. *Annu Rev Biochem* **67**(1)**:** 509-544.

Umland SP, Wan Y, Shah H, Billah M, Egan RW, Hey JA (2001). Receptor reserve analysis of the human α2C-adrenoceptor using [35S]GTPγS and cAMP functional assays. *European journal of pharmacology* **411**(3)**:** 211-221.

Urban JD, Clarke WP, von Zastrow M, Nichols DE, Kobilka B, Weinstein H*, et al.* (2007a). Functional selectivity and classical concepts of quantitative pharmacology. *The Journal of pharmacology and experimental therapeutics* **320**(1)**:** 1-13.

Urban JD, Vargas GA, von Zastrow M, Mailman RB (2007b). Aripiprazole has functionally selective actions at dopamine D2 receptor-mediated signaling pathways. *Neuropsychopharmacology : official publication of the American College of Neuropsychopharmacology* **32**(1)**:** 67-77.

Usiello A, Baik J-H, Rouge-Pont F, Picetti R, Dierich A, LeMeur M*, et al.* (2000). Distinct functions of the two isoforms of dopamine D2 receptors. *Nature* **408**(6809)**:** 199-203.

van der Westhuizen ET, Breton B, Christopoulos A, Bouvier M (2014). Quantification of Ligand Bias for Clinically Relevant β2-Adrenergic Receptor Ligands: Implications for Drug Taxonomy. *Molecular pharmacology* **85**(3)**:** 492-509.

Van Eps N, Preininger AM, Alexander N, Kaya AI, Meier S, Meiler J*, et al.* (2011). Interaction of a G protein with an activated receptor opens the interdomain interface in the alpha subunit. *Proc. Natl. Acad. Sci. USA* **108**(23)**:** 9420-9424.

van Koppen CJ, Jakobs KH (2004). Arrestin-Independent Internalization of G Protein-Coupled Receptors. *Molecular pharmacology* **66**(3)**:** 365-367.

van Os J, Kapur S (2009). Schizophrenia. *The Lancet* **374**(9690)**:** 635-645.

Vickery RG, von Zastrow M (1999). Distinct dynamin-dependent and -independent mechanisms target structurally homologous dopamine receptors to different endocytic membranes. *The Journal of cell biology* **144**(1)**:** 31-43.

Violin JD, Crombie AL, Soergel DG, Lark MW (2014). Biased ligands at G-protein-coupled receptors: promise and progress. *Trends in pharmacological sciences* **35**(7)**:** 308-316.

Violin JD, Ren X-R, Lefkowitz RJ (2006). G-protein-coupled Receptor Kinase Specificity for β-Arrestin Recruitment to the β2-Adrenergic Receptor Revealed by Fluorescence Resonance Energy Transfer. *J Biol Chem.* **281**(29)**:** 20577-20588.

Wall MA, Coleman DE, Lee E, Iñiguez-Lluhi JA, Posner BA, Gilman AG*, et al.* (1995). The structure of the G protein heterotrimer $G_{i\alpha1}\beta_1\gamma_2$. *Cell* **83**(6)**:** 1047-1058.

Wang C, Jiang Y, Ma J, Wu H, Wacker D, Katritch V*, et al.* (2013). Structural Basis for Molecular Recognition at Serotonin Receptors. *Science* **340**(6132)**:** 610-614.

Warne T, Moukhametzianov R, Baker JG, Nehme R, Edwards PC, Leslie AGW*, et al.* (2011). The structural basis for agonist and partial agonist action on a β1-adrenergic receptor. *Nature* **469**(7329)**:** 241-244.

Watson SJ, Brown AJ, Holliday ND (2012). Differential signaling by splice variants of the human free fatty acid receptor GPR120. *Molecular pharmacology* **81**(5)**:** 631-642.

Weiss JM, Morgan PH, Lutz MW, Kenakin TP (1996). The Cubic Ternary Complex Receptor–Occupancy Model I. Model Description. *J. Theor. Biol.* **178**(2)**:** 151-167.

Wenzel-Seifert K, Seifert R (2000). Molecular Analysis of β2-Adrenoceptor Coupling to Gs-, Gi-, and Gq-Proteins. *Molecular pharmacology* **58**(5)**:** 954-966.

Westfield GH, Rasmussen SGF, Su M, Dutta S, DeVree BT, Chung KY*, et al.* (2011). Structural flexibility of the Gαs α-helical domain in the β2-adrenoceptor Gs complex. *Proc. Natl. Acad. Sci. USA* **108**(38)**:** 16086-16091.

Wiens BL, Nelson CS, Neve KA (1998). Contribution of serine residues to constitutive and agonist-induced signaling via the D2S dopamine receptor: evidence for multiple, agonist-specific active conformations. *Molecular pharmacology* **54**(2)**:** 435-444.

Wilden U, Wüst E, Weyand I, Kühn H (1986). Rapid affinity purification of retinal arrestin (48 kDa protein) via its light-dependent binding to phosphorylated rhodopsin. *FEBS letters* **207**(2)**:** 292-295.

Wilson J, Lin H, Fu D, Javitch JA, Strange PG (2001). Mechanisms of inverse agonism of antipsychotic drugs at the D(2) dopamine receptor: use of a mutant D(2) dopamine receptor that adopts the activated conformation. *Journal of neurochemistry* **77**(2)**:** 493-504.

Zaccolo M, De Giorgi F, Cho CY, Feng L, Knapp T, Negulescu PA*, et al.* (2000). A genetically encoded, fluorescent indicator for cyclic AMP in living cells. *Nat Cell Biol* **2**(1)**:** 25-29.

Zhang Q, Okamura M, Guo Z-D, Niwa S, Haga T (2004). Effects of Partial Agonists and Mg2+ Ions on the Interaction of M2 Muscarinic Acetylcholine Receptor and G Protein Gαi1 Subunit in the M2-Gαi1 Fusion Protein. *J. Biochem.* **135**(5)**:** 589-596.

Zürn A, Zabel U, Vilardaga J-P, Schindelin H, Lohse MJ, Hoffmann C (2009). Fluorescence Resonance Energy Transfer Analysis of α2a-Adrenergic Receptor Activation Reveals Distinct Agonist-Specific Conformational Changes. *Molecular pharmacology* **75**(3)**:** 534-541.

Zwier JM, Roux T, Cottet M, Durroux T, Douzon S, Bdioui S*, et al.* (2010). A Fluorescent Ligand-Binding Alternative Using Tag-lite® Technology. *J. Biomol. Screen.* **15**(10)**:** 1248-1259.